frontiers | Research Topics

Hydrobiogeochemistry of major asian rivers

Edited by
Shafi Mohammad Tareq, Xixi Lu, Mashura Shammi and Masahiro Maruo

Published in
Frontiers in Earth Science
Frontiers in Environmental Science

ISSN 1664-8714
ISBN 978-2-8325-2746-7
DOI 10.3389/978-2-8325-2746-7

About Frontiers

Frontiers is more than just an open access publisher of scholarly articles: it is a pioneering approach to the world of academia, radically improving the way scholarly research is managed. The grand vision of Frontiers is a world where all people have an equal opportunity to seek, share and generate knowledge. Frontiers provides immediate and permanent online open access to all its publications, but this alone is not enough to realize our grand goals.

Frontiers journal series

The Frontiers journal series is a multi-tier and interdisciplinary set of open-access, online journals, promising a paradigm shift from the current review, selection and dissemination processes in academic publishing. All Frontiers journals are driven by researchers for researchers; therefore, they constitute a service to the scholarly community. At the same time, the *Frontiers journal series* operates on a revolutionary invention, the tiered publishing system, initially addressing specific communities of scholars, and gradually climbing up to broader public understanding, thus serving the interests of the lay society, too.

Dedication to quality

Each Frontiers article is a landmark of the highest quality, thanks to genuinely collaborative interactions between authors and review editors, who include some of the world's best academicians. Research must be certified by peers before entering a stream of knowledge that may eventually reach the public - and shape society; therefore, Frontiers only applies the most rigorous and unbiased reviews. Frontiers revolutionizes research publishing by freely delivering the most outstanding research, evaluated with no bias from both the academic and social point of view. By applying the most advanced information technologies, Frontiers is catapulting scholarly publishing into a new generation.

What are Frontiers Research Topics?

Frontiers Research Topics are very popular trademarks of the *Frontiers journals series*: they are collections of at least ten articles, all centered on a particular subject. With their unique mix of varied contributions from Original Research to Review Articles, Frontiers Research Topics unify the most influential researchers, the latest key findings and historical advances in a hot research area.

Find out more on how to host your own Frontiers Research Topic or contribute to one as an author by contacting the Frontiers editorial office: frontiersin.org/about/contact

Hydrobiogeochemistry of major asian rivers

Topic editors

Shafi Mohammad Tareq — Jahangirnagar University, Bangladesh
Xixi Lu — National University of Singapore, Singapore
Mashura Shammi — Jahangirnagar University, Bangladesh
Masahiro Maruo — University of Shiga Prefecture, Japan

Citation

Tareq, S. M., Lu, X., Shammi, M., Maruo, M., eds. (2023). *Hydrobiogeochemistry of major asian rivers*. Lausanne: Frontiers Media SA. doi: 10.3389/978-2-8325-2746-7

Table of contents

frontiers | Frontiers in Earth Science

TYPE Editorial
PUBLISHED 18 November 2022
DOI 10.3389/feart.2022.1065133

OPEN ACCESS

EDITED AND REVIEWED BY
Eliot Atekwana,
University of California, Davis,
United States

*CORRESPONDENCE
Shafi M. Tareq,
smtareq@juniv.edu

SPECIALTY SECTION
This article was submitted to Hydrosphere, a section of the journal Frontiers in Earth Science

RECEIVED 09 October 2022
ACCEPTED 11 November 2022
PUBLISHED 18 November 2022

CITATION
Tareq SM, Lu XX, Shammi M and Maruo M (2022), Editorial: Hydrobiogeochemistry of major Asian rivers.
Front. Earth Sci. 10:1065133.
doi: 10.3389/feart.2022.1065133

Editorial: Hydrobiogeochemistry of major Asian rivers

Shafi M. Tareq [1]*, Xi Xi Lu[2], Mashura Shammi[1] and Masahiro Maruo[3]

[1]Hydrobiogeochemistry and Pollution Control Laboratory, Department of Environmental Sciences, Jahangirnagar University, Dhaka, Bangladesh, [2]Department of Geography, National University of Singapore, Singapore, Singapore, [3]Department of Ecosystem Studies, School of Environmental Science, The University of Shiga Prefecture, Hikone, Shiga, Japan

KEYWORDS

water pollution, carbon cyle, dissolved organic matter, greenhouse gas emission, anthropogenic activities, ecological risk

Editorial on the Research Topic
Hydrobiogeochemistry of major Asian rivers

The Asian continent is home to many large rivers, such as the Ganges, Brahmaputra, Mekong, and Yellow, which provide abundant freshwater resources. Many rivers in the Asian continent are transboundary in nature, and their tributaries and distributaries flow in different countries or regions. These rivers support millions of people and their livelihoods through diverse landscapes. The hydrobiogeochemistry of these rivers plays a crucial role in water quality, nutrient dynamics, carbon cycle, and aquatic ecology. The hydrobiogeochemistry of these Asian rivers is highly sensitive to natural disturbances and human perturbations because of rapid socioeconomic and environmental changes. Diverse hydrobiogeochemical research from various parts of the Asian continent and their status are gathered in this particular issue to support policy decisions on global carbon dynamics, nutrient and pollution dynamics, and greenhouse gas emissions. We have received eight unique articles for this Research Topic.

One common problem related to hydrobiogeochemistry of rivers in the Asian continent is water pollution (Begum et al., 2021; Nayna et al.). In this Research Topic, we have four articles from South Asia. South Asia has the largest Ganges-Brahmaputra-Meghna (GBM) Delta situated in Bangladesh and part of India. The comparative study on Ganges-Brahmaputra by Niloy et al. described the concentrations, origins, availability, and seasonal variation of dissolved organic matter (DOM) in Bangladesh's major river systems. It was critical to understand biogeochemical cycles, destiny, and ecological and environmental factors before discharging into the Bay of Bengal. This study also showed that sewage discharge was the second highest contributor to DOM in river water after natural sources, indicating unsustainable anthropogenic activities in the river systems.

We have two articles that deal with the estuarine systems and distributaries of the lower Ganges. The Ganges River distributaries feed their discharges to the most extensive mangrove forests in the world-the Sundarbans. The Sundarbans mangrove ecosystem is a hotspot for

biogeochemical studies in the tropical estuarine environment due to its high productivity and extensive organic matter cycling. Spatial and temporal dynamics of the biogenic gases (CO_2, CH_4, and N_2O), also known as radiatively active gases, were measured in mangrove-dominated estuaries (Acharya et al.). The Acharya et al. study showed that CH_4 and N_2O fluxes were positively associated (p 0. 05), with organic matter decomposition. Furthermore, water-air CO_2, CH_4, and N_2O fluxes demonstrate that estuaries are a minor source of CH_4 but oscillate between sources and sinks for CO_2 and N_2O gases. In addition, CO_2 fluxes were ~10 times higher in the monsoon season than in both the pre-monsoon and the post-monsoon seasons.

Another article relevant to the Ganges is "*Pollution level of trace metals (As, Pb, Cr, and Cd) in the sediment of Rupsha River, Bangladesh: assessment of ecological and human health risks*" (Kubra et al.). The Rupsha River is a distributary of the Ganges and an important River in South-west Bangladesh. Trace metal concentrations of As, Pb, Cd, and Cr, along with biological effects and potential ecological and human health hazards for adults and children, were identified from sediment samples. The metals in the sediments were attributed to natural sources and anthropogenic industrial activities.

The fourth article is on "*Intersectoral competition for water between users and uses in Tamil Nadu-India*" (Suresh). Water demands for household potable water, agricultural food production, aquaculture, and industry rise as the population increases. Furthermore, urbanization will demand a large share of common water resources for household purposes, thereby increasing intersectional conflicts. Conflict resolution needs investment in the water sector and state-of-the-art technological measures, and diplomacy for water reuse, recycling, and treatment.

Given the growing interest in evaluating the contribution of riverine CO_2 emissions to the global C budget, field measurements of pCO_2 have increased (Haque et al., 2022). We have two articles from East Asia on the measurements of pCO_2. Direct field measurements of pCO_2 using manual headspace equilibration or sensor-based instrumental measurements will provide increasingly more reliable field-based data (Nayna et al.). The first article on the method study of this Research Topic is "*Improving carbonate equilibria-based estimation of pCO_2 in anthropogenically impacted river systems*" (Nayna et al.). Across the five Asian rivers (Ganges, Mekong, Yangtze, Yellow, and Han rivers), calculated and measured pCO_2 values exhibited more significant discrepancies during the monsoon season, particularly in the low pH range. The authors urged using carbonate equilibria-based models to complement the corrective measures for calculating pCO_2.

The second East Asian article is on "*Rapid loss of dissolved CO_2 from a subtropical steep headwater stream*" (Chan et al.). The study was conducted in the Pokf ulam catchment (area: 1.7 km^2) in subtropical Hong Kong. CO_2 emissions have been largely overlooked in the steep headwater streams due to their limited water surface areas and the difficulty in measuring them due to narrow channel widths and severe turbulence. This study suggests that high-gradient headwater streams are hotspots of CO_2 emissions. The omission of these systems may introduce significant biases in estimating catchment scale and regional CO_2 flux from aquatic ecosystems, The third paper from East Asia is on the heterotrophic bacteria in rivers that depend on dissolved organic nitrogen (DON) as an essential energy source and/or organic nutrients. Takaki et al. identified factors controlling the spatial distribution of DOM with changes in the C/N ratio from the upper to lower reaches of the Ishikari River, Japan (Takaki et al.). Although several variables influence the quantity and quality of DOM in rivers, DON was less explored than dissolved organic carbon (DOC). The C/N ratio of bulk DOM decreased continuously from the upper reaches to lower reaches due to *in situ* microbiological degradation.

The last article on this Research Topic is from Northeastern Siberia-the Asian Taiga. The article is about "*Stable water isotope assessment of tundra wetland hydrology as a potential source of Arctic Riverine dissolved organic carbon in the Indigirka River Lowland, Northeastern Siberia*" (Takano et al.). The wetlands exhibited higher $\delta^{18}O$ and greater DOC concentrations than the Indigirka River's tributaries and main channel. There was a link between the two parameters in the wetlands, tributaries, and mainstream, indicating that the wetlands can be a source of DOC for the mainstream *via* the tributaries.

What's next? The hydrobiogeochemistry of rivers and the causes of river water deterioration can only be demonstrated and recognized by systematic monitoring and assessment of water interchange processes between rivers and catchments. This understanding is critical for protecting and managing significant water resources and obtaining ecological services from rivers. As a result, river hydrobiogeochemistry research is essential to ensuring enough excellent quality water supplies for future generations and sustainable development. The special Research Topic is broadly related to hydrochemistry, carbon transport mechanisms, and analytical methods of hydrobiogeochemical analysis in Asian rivers. The future stresses focusing the hydrobiogeochemistry of the rivers on maintaining a healthy water ecosystem while simultaneously strengthening the focus on minimizing anthropogenic and climate stressors.

Author contributions

All authors listed have made a substantial, direct, and intellectual contribution to the work and approved it for publication.

Conflict of interest

The authors declare that the research was conducted in the absence of any commercial or financial relationships that could be construed as a potential conflict of interest.

Publisher's note

References

Begum, M. S., Bogard, M. J., Butman, D. E., Chea, E., Kumar, S., Lu, X., et al. (2021). Localized pollution impacts on greenhouse gas dynamics in three anthropogenically modified Asian river systems. *J. Geophys. Res. Biogeosci.* 126, e2020JG006124. doi:10.1029/2020JG006124

Haque, M. M., Begum, M. S., Nayna, O. K., Tareq, S. M., and Park, J-H. (2022). Seasonal shifts in diurnal variations of $p\,CO_2$ and O_2 in the lower Ganges River. *Limnol. Oceanogr. Lett.* 7, 191–201. doi:10.1002/lol2.10246

frontiers in Earth Science

ORIGINAL RESEARCH
published: 06 July 2021
doi: 10.3389/feart.2021.699365

Stable Water Isotope Assessment of Tundra Wetland Hydrology as a Potential Source of Arctic Riverine Dissolved Organic Carbon in the Indigirka River Lowland, Northeastern Siberia

Shinya Takano[1,2,3]*, *Youhei Yamashita*[1,2], *Shunsuke Tei*[4,5], *Maochang Liang*[1,6], *Ryo Shingubara*[1,7], *Tomoki Morozumi*[1,5,8], *Trofim C. Maximov*[9] and *Atsuko Sugimoto*[2,5,10]

[1]Graduate School of Environmental Science, Hokkaido University, Sapporo, Japan, [2]Faculty of Environmental Earth Science, Hokkaido University, Sapporo, Japan, [3]Research Institute for Humanity and Nature, Kyoto, Japan, [4]Department of Forest Management, Forestry and Forest Products Research Institute, Tsukuba, Japan, [5]Arctic Research Center, Hokkaido University, Sapporo, Japan, [6]College of Horticulture and Gardening, Yangtze University, Jingzhou, China, [7]Graduate School of Environmental Studies, Nagoya University, Nagoya, Japan, [8]Research Faculty of Agriculture, Hokkaido University, Sapporo, Japan, [9]Institute for Biological Problem of Cryolithozone, Siberian Division of Russian Academy of Science, Yakutsk, Russia, [10]Global Station for Arctic Research, Global Institution for Collaborative Research and Education, Hokkaido University, Sapporo, Japan

OPEN ACCESS

Edited by:
Shafi Mohammad Tareq, Jahangirnagar University, Bangladesh

Reviewed by:
Mohammad Mohinuzzaman, Noakhali Science and Technology University, Bangladesh
Thibault Lambert, University of Lausanne, Switzerland

***Correspondence:**
Shinya Takano
hawk-field@ees.hokudai.ac.jp

Specialty section:
This article was submitted to Geochemistry, a section of the journal Frontiers in Earth Science

Received: *23 April 2021*
Accepted: *21 June 2021*
Published: *06 July 2021*

Citation:
Takano S, Yamashita Y, Tei S, Liang M, Shingubara R, Morozumi T, Maximov TC and Sugimoto A (2021) Stable Water Isotope Assessment of Tundra Wetland Hydrology as a Potential Source of Arctic Riverine Dissolved Organic Carbon in the Indigirka River Lowland, Northeastern Siberia. Front. Earth Sci. 9:699365. doi: 10.3389/feart.2021.699365

Arctic tundra wetlands may be an important source of dissolved organic carbon (DOC) in Arctic rivers and the Arctic Ocean under global warming. We investigated stable water isotopes and DOC concentration in wetlands, tributaries, and the mainstream at the lower reaches of the Indigirka River in northeastern Siberia during the summers of 2010–2014 to assess the complex hydrology and role of wetlands as sources of riverine DOC. The wetlands had higher values of $\delta^{18}O$ and DOC concentration than the tributaries and mainstream of the Indigirka River. A relationship between the two parameters was observed in the wetlands, tributaries, and mainstream, suggesting the wetlands can be a source of DOC for the mainstream through the tributaries. The combined temporal variations in riverine $\delta^{18}O$ and DOC concentration indicate the mainstream water flowed into the tributaries during relatively high river-level periods in summer, whereas high DOC water in the downstream wetlands could be discharged to the mainstream through the tributaries during the low river-level periods. A minor fraction (7–13%) of riverine and wetland DOC was degraded during 40 days of dark incubation. Overall, the downstream wetlands potentially provide relatively less biodegradable DOC to the Arctic river and costal ecosystem during the low river-level periods—from late summer to autumn.

Keywords: Arctic tundra wetland, riverine dissolved organic carbon, wetland hydrology, stable water isotopes, Northeastern siberia

INTRODUCTION

The pedosphere of the Arctic has substantial stocks of organic carbon and plays an important role in the global carbon cycle as sources and sinks of CO_2 and CH_4, which are affected by global warming (McGuire et al., 2009; McGuire et al., 2010b). Arctic rivers transport large amounts of organic carbon, mostly in the form of dissolved organic carbon (DOC), from the Arctic pedosphere to the Arctic Ocean (Gordeev et al., 1996; Dittmar and Kattner, 2003; Rachold et al., 2004; Raymond et al., 2007; McClelland et al., 2012). Although the Arctic Ocean corresponds to only 1% of the global ocean volume, it receives more than 10% of both global river discharge and DOC, namely 25–36 $TgCyr^{-1}$ (Lobbes, 2000; Lammers et al., 2001; Raymond et al., 2007; Holmes et al., 2012). In the future, riverine DOC concentration and flux are predicted to increase due to Arctic warming (Frey and Smith, 2005); yet, some proportion of the DOC in Arctic rivers is known to be degraded by microbes (e.g., Köhler et al., 2002; Holmes et al., 2012; Stanley et al., 2016). Thus, the transport of DOC from the Arctic pedosphere to the Arctic Ocean by rivers is possibly an important process controlling not only organic carbon stocks in soil but also marine ecosystems, in particular microbial loops.

The transport of DOC from the pedosphere to the river networks of Arctic watersheds is unique because of the presence of permafrost. The terrestrial runoff carries DOC derived from organic-rich surface soil and fresh vegetation in boreal forests (Finlay et al., 2006; Amon et al., 2012) to rivers during the spring because the frozen ground limits the infiltration of rain and snowmelt. Therefore, the river discharge and riverine DOC concentration generally reach their maxima during the snowmelt season in Arctic rivers (Cooper et al., 2008; Prokushkin et al., 2009, 2011; Holmes et al., 2008, 2012). After the peak of river discharge, the DOC concentration generally decreases correspondingly with the decrease in discharge (Cooper et al., 2008; Prokushkin et al., 2009, 2011; Holmes et al., 2008, 2012), a phenomenon which can be attributed to the longer flow path of the infiltration water, created by seasonal deepening of the active layer. This longer flow path allows DOC decomposition and/or adsorption onto mineral particles in the soil before leaching into the stream (MacLean et al., 1999; Striegl et al., 2005; Petrone et al., 2006; Prokushkin et al., 2007).

This mechanism of decrease in DOC concentration after snowmelt is possibly less effective in the downstream tundra wetlands, which have a shallower active layer than the upstream boreal forests. In fact, Amon et al. (2012) reported that the contribution of mosses and peat bogs to Arctic river DOC significantly increased after spring (i.e., after thawing of the active layer). It has also been pointed out that the degradation of permafrost in the subsurface of the downstream peatland probably releases DOC from the permafrost into rivers, thereby increasing the DOC concentration and flux in Arctic rivers (Frey and Smith, 2005; Frey and McClelland, 2009). Therefore, knowledge regarding DOC leaching from downstream tundra wetlands to rivers is crucial for a better estimation of the DOC flux in Arctic rivers under global warming. However, downstream tundra wetlands have not received considerable attention as a DOC source, because previous studies have focused mostly on major Arctic rivers (e.g., Kattner et al., 1999; Amon et al., 2012; Holmes et al., 2012; Kicklighter et al., 2013; Pokrovsky et al., 2015) for which the watersheds cover extensive regions of boreal forests.

In this study, we evaluated the DOC concentration in the mainstream, tributaries, and wetlands at the lower reaches of the Indigirka River in summer to assess the role of the wetlands as a source of riverine DOC. The Indigirka River basin, located in northeastern Siberia, is relatively small compared with other major Arctic river basins in the continuous permafrost zone, and tundra wetlands are widely distributed in the middle and lower reaches. Therefore, the study region is suitable for evaluating the potential of wetlands as DOC sources for Arctic rivers. In addition, we used stable isotopes of water to assess the complex hydrology in the study region (Woo, 2012), that is, the occupation of tributaries by water from the mainstream during snowmelt, as well as the contribution of water from downstream tundra wetlands to tributaries after the snowmelt.

MATERIALS AND METHODS

Study Sites

The study area is located in the downstream region of the Indigirka River near Chokurdakh (70°37′N, 147°53′E), Republic of Sakha (Yakutia), Russia (**Figure 1**). The upper and middle reaches of the Indigirka River basin mostly consist of taiga forest, alpine desert, and mountain tundra landscapes with an altitude of up to 2,800 m, whereas the lower reaches consist of the forest tundra and tundra landscapes with a relatively low altitude (Geodesy and Cartography Bureau of Soviet Council of Ministers, 1989; Gusev et al., 2013; Tei et al., 2020).

Observation and sampling were conducted in four sites (V: Verkhny Khatistakha; K: Kodac; CKH: Chokurdakh; B: Boydom), which are adjacent to the Indigirka River or its tributary. The study area is located on the taiga–tundra boundary, and tree density decreases from site V to site B, which is relatively close to the tundra landscape. Trees/shrubs and wetlands are distributed in patches in the area. The only tree species present is Siberian larch (*Larix cajanderi*; syn *L. gmelinii*) and the dominant shrubs are dwarf birches (*Betula nana*), dwarf willows (*Salix spp.*), and dwarf alders (*Alnus fruticosa*; syn *Deschekia fruticosa*). The area where the trees/shrubs grow is covered by green-mosses (including *Tomentypnum nitens*, *Hylocomium splendens*, and *Aulacomnium turgidum*), and the vegetation of the wetlands includes sedges (*Eriophorum spp.* and *Carex spp.*) and sphagnum-mosses (including *Sphagnum balticum*, *S. squarrosum*, and *S. angustifolium*). The mainstream and tributaries are surrounded by bare-ground/shrub and wetland-dominant (>50%) land cover, respectively, in the Indigirka lowland (Morozumi et al., 2019a). More details of the vegetation and dominant species in the study area are described in Morozumi et al. (2019b).

The observation area is located in the Russian Arctic and underlain by continuous permafrost with the mean annual air temperature and precipitation of −13.9°C and 208 mm,

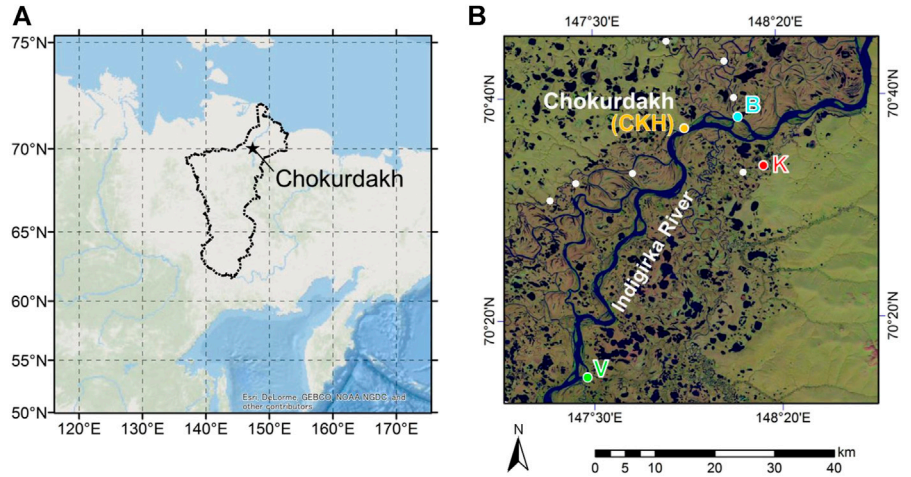

FIGURE 1 | Location of the study area. **(A)** Location of the study region in northeastern Siberia (ArcGIS ESRI, Redland, CA, United States) modified by Takano et al. (2019). The Indigirka River basin boundaries are shown with a black line. **(B)** Satellite image of the Indigirka River lowland around the village of Chokurdakh from Landsat 8 modified by Shingubara et al. (2019). Observation points of the mainstream (CKH, B, and V) and one tributary (K) of the Indigirka River are shown. Those of the other tributaries are shown by closed white circles.

respectively, for the period of 1950–2008 according to the Baseline Meteorological Data in Siberia (BMDS) Version 5.0 (Yabuki et al., 2011). Snowmelt and active layer thawing usually start in late May to early June. The growing season is from late June to early August, with a thaw depth of approximately 20–30 cm (Shingubara et al., 2019; Takano et al., 2019). The maximum thaw depth (more than 50 cm in depth) typically occurs in the first half of September, whereas the depth of the surface organic layer is approximately 30 cm (Takano et al., 2019). Active layer freezing usually starts in the second half of September to October and freezes completely from November to December.

Field Observations

Field observations and sample collection were conducted during 14–July 24, 2010, 9–July 28, 2011, 25 June–August 11, 2012, 17 June–July 25, 2013, 23–April 26, 2014, and 30 June–August 2, 2014. The observation team traveled to each sampling site by motorboat in summer and snowmobile in spring.

River water samples from the Indigirka mainstream and tributaries, wetland water, precipitation, and snow cover were mainly collected in the four observation sites (**Figure 1**). The sampling points of river water adjacent to sites B, K, V, and CKH are hereinafter referred to as points B, K, V, and CKH, respectively. Time-series observations of the mainstream and tributary water were conducted at intervals of 2 or 3 days for isotope analysis sampling and 1 week for DOC analysis sampling. Those of the tributary water were conducted at point K, and the sampling points of the other tributary waters are shown in **Figure 1B**. Wetland water was collected from the surface water of the wetlands, whereas bulk snow was obtained as a core of diameter 10 cm and placed in a plastic bag to melt. The water samples for isotope analysis were stored in 3- or 6-ml glass vials. For this study, the isotopic compositions of the Indigirka mainstream and tributaries in 2011 and 2012, summer precipitation in 2012–2014, and snow cover were obtained from Takano et al. (2019).

Samples for the DOC analysis were collected in a 60 ml plastic syringe after three consecutive rinses with the sample water in each sampling point and passed through polyvinylidene difluoride (PVDF) filters (Durapore, Millipore) of pore size 0.45 μm. After three consecutive rinses with the filtrates, the final filtrates were stored in 50 ml polyethylene bottles, which were wrapped with aluminum foil and maintained frozen in dark until analysis. The syringes and bottles were pre-washed by soaking in 0.1 mol l^{-1} HCl for 24 h and then rinsed with Milli-Q water.

To evaluate the biodegradability of DOC, bottle incubation experiments were performed as described by Yamashita et al. (2013). Water samples were passed through PVDF filter of pore size 0.45 μm and collected in 50 ml polyethylene bottles, which were wrapped with aluminum foil; then, the samples were incubated in dark at room temperature (16–25°C). After 40 days of incubation, the samples were stored frozen in dark until analysis without any filtration. The incubation experiment was carried out with a single sample.

Analysis

Stable isotope ratios of water have long been used in studies on the water cycle (e.g., Craig, 1961; Dansgaard, 1964; Craig and Gordon, 1965). They are considered to be a useful tool for determining source water and assessing hydrological processes in Arctic rivers (Welp et al., 2005; Cooper et al., 2008; Yi et al., 2010, 2012; Sugimoto and Maximov, 2012). The stable isotopic compositions of water (oxygen and hydrogen) were determined using the $CO_2/H_2/H_2O$ equilibration method with a mass spectrometer (MAT 253; Thermo Fisher Scientific, United States, manufactured in Germany) with a gas bench

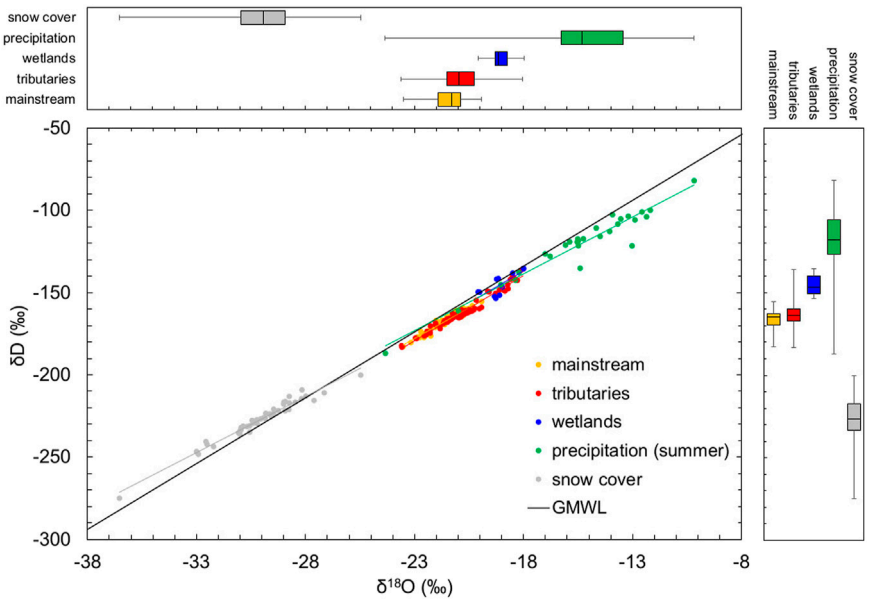

FIGURE 2 | δD–δ^{18}O plot grouping Indigirka mainstream and tributaries, wetlands, precipitation in summer, and snow cover with different colors and showing distributions as boxplots on the top and side panels. The Global Meteoric Water Line (GMWL; $\delta D = 8 \times \delta^{18}O + 10$) is shown as a black solid line. These data were obtained during summer in 2010–2014, and the data of snow cover were obtained in April 2014. The isotopic compositions of Indigirka mainstream and tributaries in 2011 and 2012, summer precipitation in 2012–2014, and snow cover are cited from Takano et al. (2019).

(Thermo Fisher Scientific, United States, manufactured in Germany). The isotopic compositions are expressed in delta notation relative to Vienna Standard Mean Ocean Water (VSMOW), defined as follows:

$$\delta^{18}O \text{ or } \delta D = \left(R_{sample}/R_{VSMOW} - 1\right) \times 1000\ (‰), \quad (1)$$

where R_{sample} and R_{VSMOW} are the isotopic ratios of water ($^{18}O/^{16}O$ or D/H) of the samples and VSMOW, respectively. The precision of the analysis was within ±0.2‰ for $\delta^{18}O$ and ±2‰ for δD.

The concentration of DOC was determined by high-temperature catalytic oxidation using a total organic carbon analyzer (TOC-V_{CSH}, Shimadzu, Japan). The DOC concentration was calculated from the standard curve with 0, 3.6, 7.2, and 12 mg C L^{-1} potassium hydrogen phthalate solution, which was determined daily.

RESULTS

Isotopic Composition of Water Samples

Figure 2 shows the δD – $\delta^{18}O$ diagram for water from the Indigirka mainstream, Indigirka tributaries, wetlands, lakes, precipitation in summer, and snow cover. The summer precipitation had the highest delta values, with $\delta^{18}O$ values ranging from −24.3‰ to −10.2‰ (median of −15.3‰), whereas the snow cover had the lowest delta values, with $\delta^{18}O$ values ranging from −36.5‰ to −25.5‰ (median of −29.9‰). The $\delta^{18}O$ values of Indigirka mainstream water ranged from −23.5‰ to −19.9‰ (median of −21.3‰), and they were between the values of summer precipitation and snow cover. The $\delta^{18}O$ values of the Indigirka tributary water ranged from −23.6‰ to −18.0‰ (median of −20.9‰), and they were slightly higher than the values of the mainstream ($p < 0.05$, student's *t*-test). The wetlands mostly had higher $\delta^{18}O$ values than the river water, ranging from −20.1‰ to −18.0‰ (median of −19.2‰).

Temporal Variations in the $\delta^{18}O$ Values of River Water

The $\delta^{18}O$ values of river water in both mainstream and tributary at point K generally increased with time during the summer, irrespective of the difference in the observation year (**Figure 3**). In 2011, the mainstream and tributary showed the same $\delta^{18}O$ values until day-of-year (DOY) 203, and the tributary on DOY 212 showed a 1‰ higher value than the mainstream on DOY 210. In 2012, the $\delta^{18}O$ of the mainstream observed at three points (CKH, B, and V) showed almost the same values, but only at point B on DOY 195, the value was −20.3‰, which was higher than that of the mainstream predicted from the variation trend. The $\delta^{18}O$ of the tributary was always approximately 2‰ higher than that of the mainstream since the start of the observation, and the difference between them gradually increased with time. The $\delta^{18}O$ of the tributary showed a unique variation in 2013. The values were almost the same as those of the mainstream until DOY 183, and then gradually increased and reached −20.5‰, which was 1.5‰ higher than those of the mainstream on DOY 199. Thereafter, the $\delta^{18}O$ value of the tributary dropped

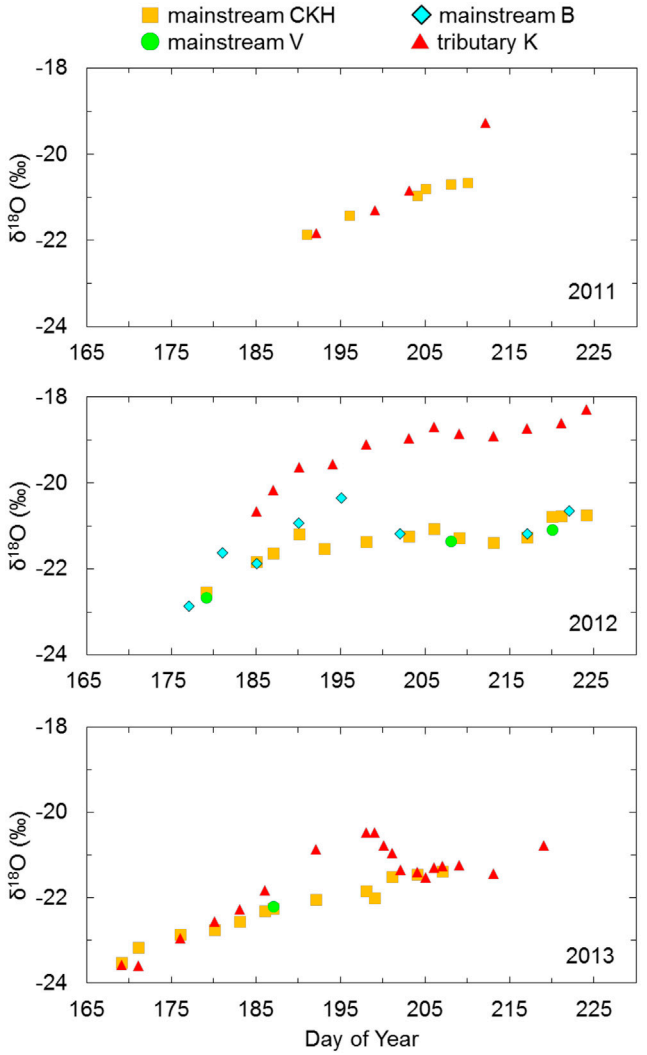

FIGURE 3 | Time series for $\delta^{18}O$ grouped to the Indigirka mainstream and tributary during summer in 2011–2013. The mainstream samples were observed at sampling points CKH, B, and V, and the tributary samples were observed at point K.

sharply and reached almost the same values as those of the mainstream by DOY 202.

Dissolved Organic Carbon Concentration

Figure 4 shows the box plots of DOC concentration in the Indigirka mainstream, Indigirka tributaries, and wetlands. The DOC concentration in the tributaries tended to be higher, ranging from 4.42 to 23.46 mg C L^{-1} (median of 9.19 mg C L^{-1}), than that in the mainstream, which ranged from 4.20 to 9.04 mg C L^{-1} (median of 6.84 mg C L^{-1}). Overall, the DOC concentration range of the tributaries was wider than that of the mainstream. The wetlands had the highest DOC concentration with the range from 12.04 to 44.43 mg C L^{-1} (median of 18.60 mg C L^{-1}).

Temporal Variations in the Dissolved Organic Carbon Concentration in the River Water

The DOC concentration in the mainstream did not largely change during the observation periods of 2011 and 2012, but it showed a gradual decrease from 8.63 to 4.89 mg C L^{-1} during 2013 (**Figure 5**). The DOC concentration in the three other mainstream points CKH, B, and V was similar. However, at point B, the value was 8.47 mg C L^{-1} on DOY 195, and it was higher than the value of mainstream predicted from the variation trend. In 2011, the DOC concentration in the tributary observed at point K was almost the same as that in the mainstream until DOY 203, whereas the tributary showed approximately 5 mg C L^{-1} higher value than the mainstream on DOY 212. The DOC concentration in the tributary, ranging from 9.06 to 12.50 mg C L^{-1}, was consistently higher than that in the mainstream, at approximately 5 mg C L^{-1} in 2012. In 2013, the DOC concentration in the tributary was similar to that in the mainstream until DOY 183, after which it was 9.12 mg C L^{-1}, which was approximately 4 mg C L^{-1} higher than that in the mainstream, on DOY 192. Subsequently, it decreased again to a value similar to that of the mainstream by DOY 207.

Biodegradation of Dissolved Organic Carbon

The DOC loss (%) after 40 days of dark incubation of the water samples was compared with the initial concentration (**Figure 6**). The loss in the Indigirka mainstream, ranging from 7.1 to 8.6%, was slightly lower than that in the tributaries, ranging from 7.8 to 12.6%. A plot of tributaries showed the highest initial DOC concentration of 21.3 mg C L^{-1}; nevertheless, the DOC loss (7.8%) was not significantly different from that in the other sites. The DOC loss in one wetland water sample with a high

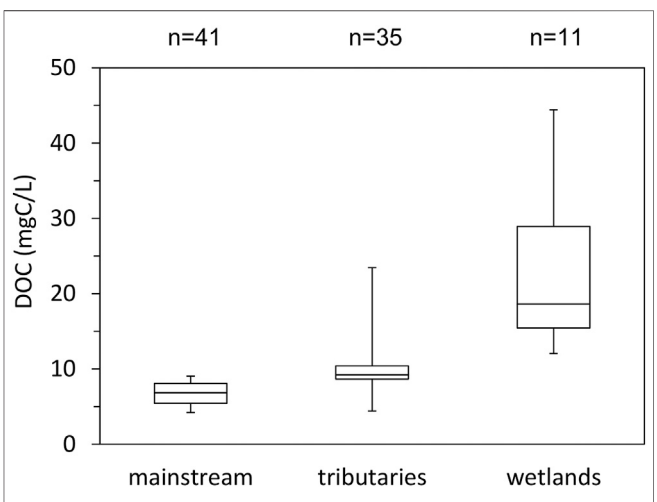

FIGURE 4 | Boxplots showing the distribution of DOC concentration during summer in the Indigirka mainstream and tributaries in 2010–2013, and wetlands in 2010–2012.

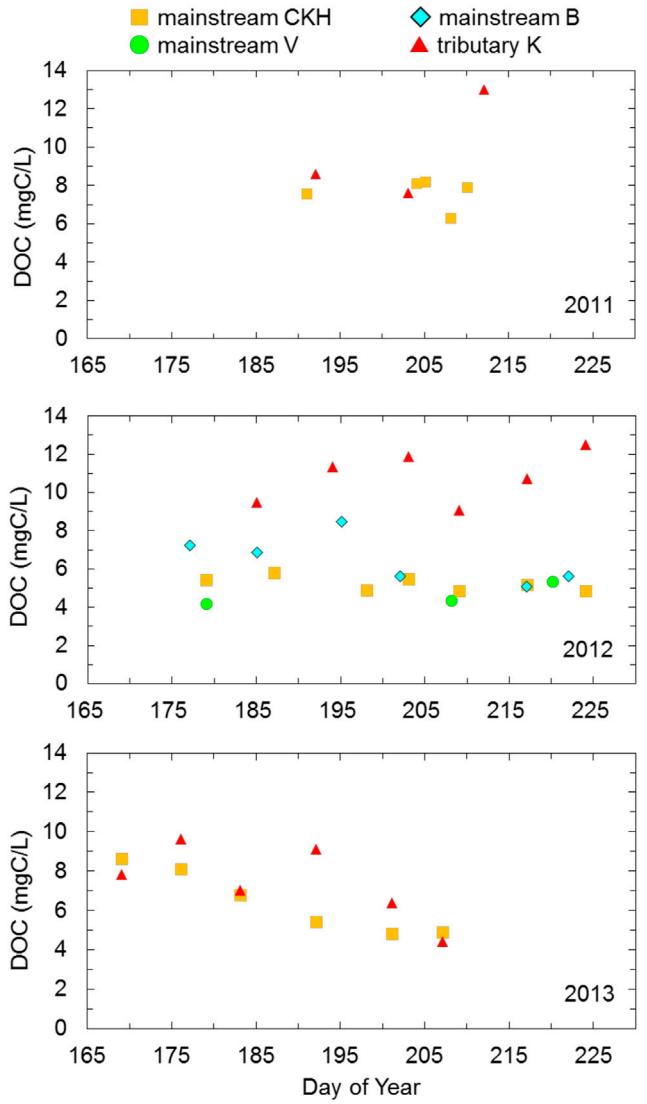

FIGURE 5 | Time series of DOC concentration grouped to the Indigirka mainstream and one tributary for summer observation periods in 2011–2013. The mainstream samples were observed at sampling points CKH, B, and V, and the tributary samples were observed at point K.

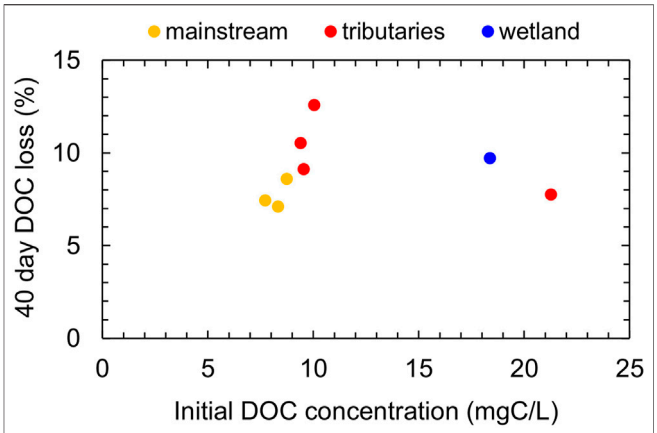

FIGURE 6 | DOC loss in the water of the Indigirka mainstream, tributaries, and wetlands observed in 2011 after 40 days of lab incubation at room temperature, compared with the initial DOC concentration.

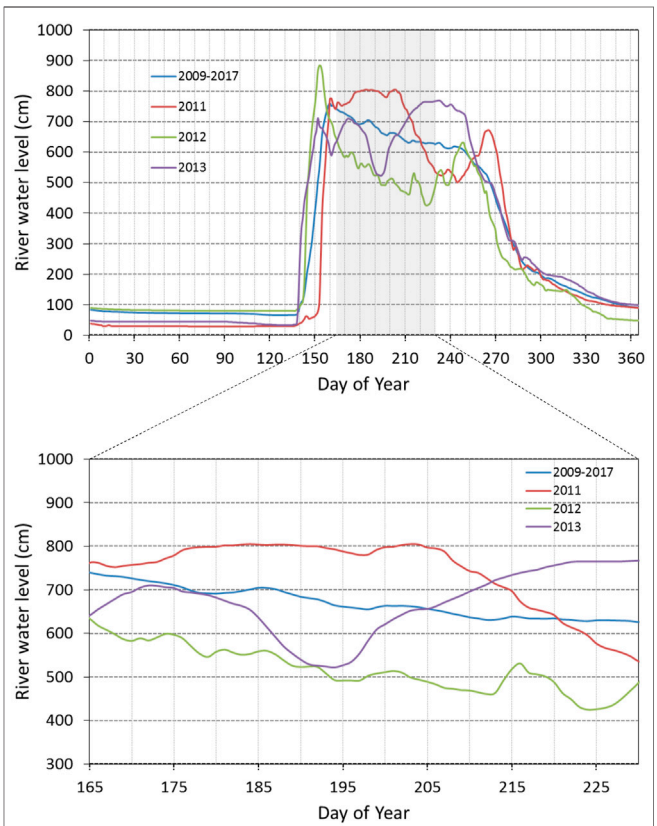

FIGURE 7 | Seasonal and interannual variations in the river water level of Indigirka mainstream at CKH during 2009–2017. The data are from Tei et al. (2020). The blue line denotes the temporal average of the river water level during 2009–2017, and the red, green, and purple lines show the river water level in 2011, 2012, and 2013, respectively.

initial DOC concentration of 18.4 mg C L^{-1} was 9.7%. Based on these findings, there appears to be no relationship between DOC loss and initial DOC concentration.

DISCUSSIONS

Hydrological Processes in the Downstream Region of the Indigirka River

Generally, the $\delta^{18}O$ of Arctic rivers rapidly decrease in spring with the highest discharge due to the inflow of snowmelt water, followed by an increase in summer due to the recession of the snowmelt water and the contribution of runoff of summer precipitation (Welp et al., 2005; Cooper et al., 2008; Yi et al., 2010, 2012; Sugimoto and Maximov, 2012). Similarly, in the Indigirka River, the water level reaches the maximum during the snowmelt season, and then gradually decreases in summer

(**Figure 7**). For this study area, snow cover and summer precipitation with the lowest (median of −29.9‰) and highest (median of −15.3‰) $\delta^{18}O$ values, respectively, can be considered as end-members of the surface water of the Indigirka River and its catchment (**Figure 2**). This is because the $\delta^{18}O$ of the Indigirka mainstream and tributary water increased in summer (**Figure 3**), and it was between the value of summer precipitation and that of snow cover (**Figure 2**). These results indicate that the increasing trends of the riverine $\delta^{18}O$ in summer are due to the recession of snowmelt water and the contribution of summer precipitation runoff to riverine water, as is typically observed for other Arctic rivers (Welp et al., 2005; Cooper et al., 2008; Yi et al., 2010; Sugimoto and Maximov, 2012).

In the permafrost zone, precipitation and snowmelt water are generally limited infiltrating to the subsurface by the frozen ground during spring (Sugimoto et al., 2003), whereas during summer, they flow into the river through the subsurface owing to deepening of the seasonal thawed active layer. Therefore, wetlands and soil water in summer are assumed to be mixtures of residual snowmelt water, summer precipitation, and soil water remaining from the previous year. In this study, the $\delta^{18}O$ of wetlands was between the $\delta^{18}O$ of summer precipitation and snow cover, and closer to that of summer precipitation (**Figure 2**), suggesting slightly more contribution from the summer precipitation. This indicates that drainage from wetlands may contribute to the increasing trends of riverine $\delta^{18}O$ in summer (**Figure 3**).

The high $\delta^{18}O$ of the tributary compared with that of the mainstream suggests the drainage of wetland water, whereas the same delta values of the tributary and mainstream may show inflow from the mainstream to the tributary. The temporal variation in $\delta^{18}O$ of the tributary in 2012 was approximately 2‰ higher than that of the mainstream (**Figure 3**), indicating the contribution of drainage from the wetlands into the tributary and thus probably into the mainstream. On the contrary, both mainstream and tributary showed the same delta values and variations up until DOY 183 and after DOY 202 in 2013 (**Figure 3**), implying the possibility that the mainstream water was flowing into the tributary at these times.

Flooding commonly occurs during the snowmelt season in Arctic river lowlands (Woo, 2012). The flooding of the Indigirka River mainstream probably extends and contributes to the tributaries, as the water level of the tributary has been observed to suddenly increase even though snow melting had not yet progressed sufficiently in the tributary basin (Morozumi et al., 2020). The same trend of variation in the $\delta^{18}O$ of the mainstream and tributary until DOY 183 in 2013 (**Figure 3**) indicates that this contribution of the mainstream water continued until early summer when the flooding had already ended. In fact, the $\delta^{18}O$ of the tributary became higher than that of the mainstream after DOY 183 in 2013 (**Figure 3**), indicating that the contribution of drainage from the wetlands into the tributary was increased due to the decrease in river level in summer (**Figure 7**). A similar variation in the $\delta^{18}O$ of the tributary was observed before this at the end of the observation period in 2011 (**Figure 3**) when the river level began to decrease (**Figure 7**). Thus, in 2013, the mainstream and tributary showed renewed $\delta^{18}O$ values after DOY 202 (**Figure 3**), indicating that the mainstream water again contributed to the tributary, possibly due to an increase in the water level of the mainstream (**Figure 7**).

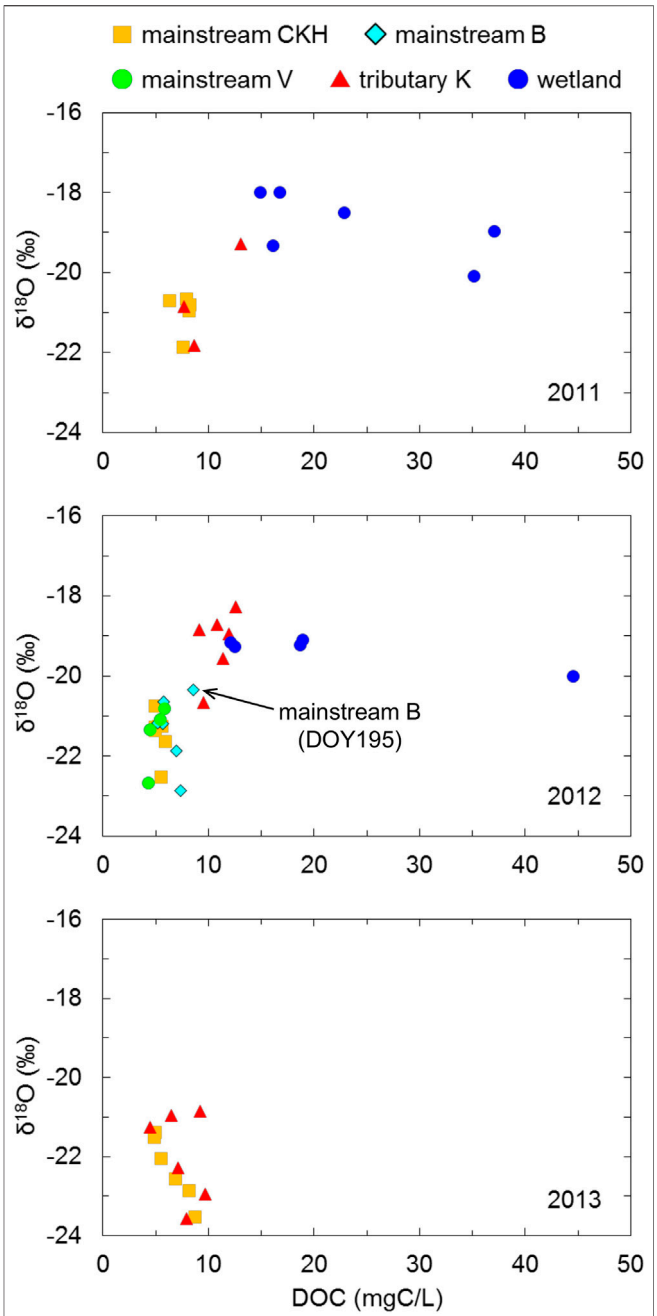

FIGURE 8 | Relationship of $\delta^{18}O$ and DOC concentration in the Indigirka mainstream, one tributary, and the wetlands. The mainstream samples were observed at sampling points CKH, B, and V, and the tributary samples were observed at point K.

According to these results, it can be considered that the mainstream water flowed into the tributaries during both flooding period and relatively high river-level period in summer. On the contrary, water in the downstream wetlands

can discharge to the tributaries and mainstream when the river level is lowered, thereby contributing as a source. Namely, the contribution of drainage from the wetlands to the river becomes the largest after summer.

Downstream Wetlands as the Source of Dissolved Organic Carbon in Arctic Rivers

Overall, the wetlands showed obviously higher DOC concentration than the rivers (**Figure 4**). The DOC concentration in wetlands was also higher than that of the six largest Arctic rivers (Ob', Yenisey, Lena, Kolyma, Yukon and Mackenzie), which ranged from 4.39 to 10.14 mg C L^{-1} in summer (from 4.35 to 11.37 mg C L^{-1} annual average) (Cooper et al., 2008; Amon et al., 2012; Holmes et al., 2012). Furthermore, the organic layer of the surface soil is known to store large amounts of organic carbon in the Arctic region (Hugelius et al., 2014), and in this study area, the surface organic layer is relatively thick, with a depth of approximately 30 cm (Takano et al., 2019). Therefore, the high DOC concentration in the wetlands is considered to be the result of sufficient dissolution from the soil organic carbon stored in the organic layer.

The $\delta^{18}O$ and DOC concentration in the tributary showed similar or higher value than those of the mainstream, and the timing of the temporal variations in the DOC concentration accorded with that of the $\delta^{18}O$ (**Figures 3**, **5**). These temporal variations indicate the degree of hydrological control of the DOC concentration in the tributary. Based on this, the $\delta^{18}O$ and DOC concentration were directly compared to further evaluate the hydrological effect as a factor controlling the DOC concentration (**Figure 8**). From this comparison, the relationship between the $\delta^{18}O$ and DOC concentration showed that the wetlands had the highest values, whereas the mainstream had the lowest values. Furthermore, the tributary was plotted between the mainstream and the wetlands, indicating that the wetland water drains into the mainstream through the tributaries. For 2012, a plot of mainstream point B (DOY195) was close to the tributary plots (**Figure 8**), indicating that the sample was more strongly affected by the tributary water because sampling point B was closer to the confluence with the tributaries than mainstream points CKH and V (**Figure 1**). Therefore, it can be concluded that wetland water in this study area (i.e., the downstream region) can be the source of DOC in the Indigirka River mainstream.

The DOC concentration in the mainstream tended to decrease during the summer observation period in 2013 (**Figure 5**). This decreasing trend was also observed for other Arctic rivers after the snowmelt season (Cooper et al., 2008; Prokushkin et al., 2009, Prokushkin er al., 2011; Holmes et al., 2008, Holmes et al., 2012). This was possibly caused by a longer flow path of the infiltration water created by seasonal deepening of the active layer in boreal forests; the longer flow path allows DOC decomposition and/or adsorption onto mineral particles in the soil before leaching into the stream (MacLean et al., 1999; Striegl et al., 2005; Petrone et al., 2006; Prokushkin et al., 2007). The subarctic taiga distributed in the upper and middle reaches of the Indigirka River basin could be considered to cause a decreasing trend in the DOC concentration in the mainstream. Additionally, the wetland water with a high DOC concentration in the downstream region could not drain to the tributaries and mainstream due to the relatively high river level (**Figure 7**), as described for the temporal variation in $\delta^{18}O$. The combination of these two factors is possibly the reason of the decrease in DOC concentration in the mainstream and tributary in the summer of 2013.

From a previous study, Amon et al. (2012) reported that the proportion of DOC derived from wetlands in Arctic riverine DOC increased after the high-flow season. Yet, in 2012, the DOC concentration in the mainstream was relatively uniform during the entire observation period (**Figure 5**). During that period, both $\delta^{18}O$ and DOC concentration of the tributary were consistently higher than those of the mainstream (**Figures 3**, **5**), indicating the wetland water drained to the tributary and probably to the mainstream. This was consistent with the relatively low river level during the period (**Figure 7**). Therefore, it can be considered that the relatively uniform DOC concentration of the mainstream in 2012 may be due to the drainage from the downstream wetlands with high DOC concentration through the tributaries.

In 2011, the DOC concentration in the mainstream was also relatively uniform at approximately 8 mg C L^{-1} during the observation period, except on DOY 208 with 6.26 mg C L^{-1} DOC (**Figure 5**). Although it is not certain because the amount of data was small and the period was short, the recovery of DOC concentration from the depression on DOY 208 might have been caused by the drainage from the downstream wetlands through the tributaries due to a decrease in the river level (**Figure 7**). On the basis of this finding, it can be considered that the drainage from the downstream wetlands likely increases with a decrease in the river level; therefore, the effect of the downstream wetland water on mainstream DOC concentration potentially increases from late summer (i.e., after the decrease in river level) to autumn.

The limitation of drainage due to high river levels not only disturbs DOC release but also maintains high soil moisture during the growing season. This may have several effects such as an increase in methane emissions (Shingubara et al., 2019; Murase et al., 2020), the withering of trees at the taiga-tundra boundary (Liang et al., 2014), and thickening of the seasonally thawed active layer (Takano et al., 2019). Such biogeochemical changes can affect the overall carbon cycle in the Arctic region (McGuire et al., 2010a). For example, the thickening of the active layer (i.e., thawing of surface permafrost), in which an estimated 1,000 ± 150 Pg of organic carbon could be stored at 0–3 m depth (Hugelius et al., 2014), potentially causes not only an increase in carbon emission to the atmosphere (Turetsky et al., 2020), but also an increase in the DOC concentration in soil water and wetlands (Fouché et al., 2020). This in turn causes an increase in the Arctic riverine DOC concentration in late summer to autumn (Frey and Smith, 2005; Frey and McClelland, 2009).

Regarding the loss of riverine DOC from the river system, such a loss may be caused by photochemical and microbial degradation within the system during transport (Wiegner and Seitzinger, 2001; Yang et al., 2021). For example, in the Alaskan and Kolyma Rivers, a substantial fraction of DOC in spring freshet water (20–40%) has been found to be biodegradable, whereas only a minor fraction (less than 10%) has been found

to be degraded during summer by microbes (Holmes et al., 2008; Mann et al., 2012). The high DOC lability of spring freshet water has been attributed to less degraded recently formed (<5–10 years) DOC (Neff et al., 2006; Raymond et al., 2007), derived from the organic-rich surface soil and fresh vegetation (Finlay et al., 2006; Amon et al., 2012). Additionally, a limitation of microbial processing due to cold temperatures and a relatively short residence time in the flow path may contribute to a less degraded DOC. Contrarily, the lower lability of summer riverine DOC is considered to be due to the component of a relatively old DOC (Neff et al., 2006; Raymond et al., 2007), which originates from the deeper part of the active layer where DOC decomposition and/or adsorption onto mineral particles occur during the thawing season of active layer (MacLean et al., 1999; Striegl et al., 2005; Petrone et al., 2006; Prokushkin et al., 2007). In this study, a minor fraction (7–13%) of DOC was degraded during the 40 days of dark incubation of riverine and wetland DOC observed in summer (**Figure 6**). This is comparable with the lability of Arctic river DOC in summer (Holmes et al., 2008; Mann et al., 2012), implying that downstream wetlands supply relatively less biodegradable DOC. Meanwhile, the predicted release of highly biodegradable DOC due to permafrost thawing has been generally established (Abbott et al., 2014; Fouché et al., 2020). Furthermore, the photochemical degradation of DOC has known to be the other important degradation process of Arctic terrestrial DOC, which in turn affects biodegradation (Mann et al., 2012; Cory et al., 2014; Ward and Cory, 2016; Ward et al., 2017). As riverine DOC affects Arctic coastal ecosystems, such as primary production, food webs, and elemental cycles (Dittmar and Kattner, 2003; Dunton et al., 2006), changes in the chemical characteristics and bio- and photo-reactivity of DOC from downstream wetlands with ongoing climatic change need to be further clarified.

CONCLUSION

We investigated the DOC concentration and stable isotopes of water in the lower reaches of the Indigirka River in northeastern Siberia during summer to assess the complex hydrology and role of wetlands as a source of Arctic riverine DOC. The $\delta^{18}O$ and DOC concentration in wetlands were higher (medians of −19.2‰ and 18.60 mg C L^{-1}, respectively) than those of the mainstream (medians of −21.3‰ and 6.84 mg C L^{-1}, respectively) and tributaries (medians of −20.9‰ and 9.19 mg C L^{-1}, respectively) of the Indigirka River. The relationship between $\delta^{18}O$ and DOC concentration indicated that the downstream wetland water could be a source of DOC in the Indigirka River mainstream through the tributaries. The temporal and seasonal variations in riverine $\delta^{18}O$ showed the nature of complex hydrological processes in this region; the mainstream water flows into the tributaries during relatively high river-level periods in summer, whereas the water in the downstream wetlands can drain into the mainstream through the tributaries when the river level decreases. The temporal variations in the DOC concentration were coupled with those in $\delta^{18}O$ in one tributary, indicating the apparent hydrological control of DOC concentration in the tributaries. These results imply that the downstream wetland water potentially affects the Arctic riverine DOC concentration as one of the major sources after the decrease in river level (i.e., from late summer to autumn). Biodegradation in riverine and wetland waters collected in summer indicates that a major fraction of DOC was less labile, that is, less than 13% of the initial DOC was degraded during 40 days of incubation. Because riverine DOC affects the Arctic coastal ecosystems, changes in flux and chemical characteristics (bioavailability) of DOC from the downstream wetlands controlled by hydrology with ongoing climatic change need to be further clarified.

DATA AVAILABILITY STATEMENT

The original contributions presented in the study are included in the article/Supplementary Material, further inquiries can be directed to the corresponding author.

AUTHOR CONTRIBUTIONS

Conceptualization: STa, YY Data curation: STa, STe, ML, RS, and TM Formal analysis: STa Funding acquisition: AS Investigation: STa, YY, ST, ML, RS, TM, and AS Methodology: STa, YY Project administration: TM, AS Resources: TM, AS Supervision: TM, AS Validation: STa, TM, and AS Visualization: STa. Writing—original draft: STa, YY Writing—review and editing: STa, YY, STe, ML, RS, TM, TM, and AS.

FUNDING

This research was supported by a Grantin-Aid from the Global Center of Excellence Program "Establishment of Center for Integrated Field Environmental Science" (IFES-GCOE) funded by the Ministry of Education, Culture, Sports, Science and Technology–Japan (MEXT), Japan Science and Technology Agency (JST, Strategic International Collaborative Research Program: SICORP) EU cooperative research project "Dynamics of permafrost and methane emission in Arctic terrestrial ecosystem in Eastern Siberia," the Green Network of Excellence (GRENE) program funded by MEXT, the COPERA (C budget of Ecosystems, Cities and Villages on Permafrost in Eastern Russian Arctic) project funded by the Belmont Forum through JST, and KAKENHI JP19H04249 by the Japan Society for the Promotion of Science.

ACKNOWLEDGMENTS

We sincerely thank Alexander Kononov, Roman Petrov, Egor Starostin, Alexandra Alexeeva, and other members of the Institute for Biological Problems of Cryolithozone Siberian Branch of the Russian Academy of Science, Tatiana Stryukova,

Sergey Ianygin, and other staff at the Allikhovsky Ulus Inspectorate of Nature Protection for supporting our fieldwork in the vicinity of Chokurdakh. We also acknowledge the help of Yumi Hoshino, Satori Nunohashi, Kanako Tanaka, Kayoko Saito, Hanae Kudo, Ruslan Shakhmatov, Aleksandr Nogovitcyn, Yuka Sazuka, and Shuji Goto in our research group at Hokkaido University. We would like to thank Editage (www.editage.com) for English language editing.

REFERENCES

Abbott, B. W., Larouche, J. R., Jones, J. B., Bowden, W. B., and Balser, A. W. (2014). Elevated Dissolved Organic Carbon Biodegradability from Thawing and Collapsing Permafrost. *J. Geophys. Res. Biogeosci.* 119 (10), 2049–2063. doi:10.1002/2014jg002678

Amon, R. M. W., Rinehart, A. J., Duan, S., Louchouarn, P., Prokushkin, A., Guggenberger, G., et al. (2012). Dissolved Organic Matter Sources in Large Arctic Rivers. *Geochim. Cosmochi. Acta* 94, 217–237. doi:10.1016/j.gca.2012.07.015

Cooper, L. W., McClelland, J. W., Holmes, R. M., Raymond, P. A., Gibson, J. J., Guay, C. K., et al. (2008). Flow-weighted Values of Runoff Tracers (δ18O, DOC, Ba, Alkalinity) from the Six Largest Arctic Rivers. *Geophys. Res. Lett.* 35 (18). Article L18606. doi:10.1029/2008gl035007

Cory, R. M., Ward, C. P., Crump, B. C., and Kling, G. W. (2014). Sunlight Controls Water Column Processing of Carbon in Arctic Fresh Waters. *Science* 345, 925–928. doi:10.1126/science.1253119

Craig, H., and Gordon, L. I. (1965). "Deuterium and Oxygen 18 Variations in the Ocean and the marine Atmosphere," in Proceedings of a Conference on Stable Isotopes in Oceanographic Studies and Paleotemperatures, Lischi and Figli; Pisa, Italy. Editor E. Tongiorgi (Pisa: Laboratory of Geology and Nuclear Science), 9–130.

Craig, H. (1961). ISOTOPIC VARIATIONS IN METEORIC WATERS. *Science* 133 (346), 1702–1703. doi:10.1126/science.133.3465.1702

Dansgaard, W. (1964). STABLE ISOTOPES IN PRECIPITATION. *Tellus* 16 (4), 436–468. doi:10.3402/tellusa.v16i4.8993

Dittmar, T., and Kattner, G. (2003). The Biogeochemistry of the River and Shelf Ecosystem of the Arctic Ocean: a Review. *Mar. Chem.* 83 (3-4), 103–120. doi:10.1016/s0304-4203(03)00105-1

Dunton, K. H., Weingartner, T., and Carmack, E. C. (2006). The Nearshore Western Beaufort Sea Ecosystem: Circulation and Importance of Terrestrial Carbon in Arctic Coastal Food Webs. *Prog. Oceanography* 71 (2-4), 362–378. doi:10.1016/j.pocean.2006.09.011

Finlay, J., Neff, J., Zimov, S., Davydova, A., and Davydov, S. (2006). Snowmelt Dominance of Dissolved Organic Carbon in High-Latitude Watersheds: Implications for Characterization and Flux of River DOC. *Geophys. Res. Lett.* 33 (10). Article L10401. doi:10.1029/2006gl025754

Fouché, J., Christiansen, C. T., Lafrenière, M. J., Grogan, P., and Lamoureux, S. F. (2020). Canadian Permafrost Stores Large Pools of Ammonium and Optically Distinct Dissolved Organic Matter. *Nat. Commun.* 11 (1). Article 4500. doi:10.1038/s41467-020-18331-w

Frey, K. E., and McClelland, J. W. (2009). Impacts of Permafrost Degradation on Arctic River Biogeochemistry. *Hydrol. Process.* 23 (1), 169–182. doi:10.1002/hyp.7196

Frey, K. E., and Smith, L. C. (2005). Amplified Carbon Release from Vast West Siberian Peatlands by 2100. *Geophys. Res. Lett.* 32 (9). doi:10.1029/2004gl022025), Article L09401

Geodesy and Cartography Bureau of Soviet Council of Ministers (1989). *Atlas of Yakutia*. Moscow: Geodesy and Cartography Bureau of Soviet Council of Ministers.

Gordeev, V. V., Martin, J. M., Sidorov, I. S., and Sidorova, M. V. (1996). A Reassessment of the Eurasian River Input of Water, Sediment, Major Elements, and Nutrients to the Arctic Ocean. *Am. J. Sci.* 296 (6), 664–691. doi:10.2475/ajs.296.6.664

Gusev, E. M., Nasonova, O. N., Dzhogan, L. Y., and Aizel', G. V. (2013). Modeling Streamflow of the Olenek and Indigirka Rivers Using Land Surface Model SWAP. *Water Resour.* 40 (5), 535–543. doi:10.1134/S0097807813030056

Holmes, R. M., McClelland, J. W., Peterson, B. J., Tank, S. E., Bulygina, E., Eglinton, T. I., et al. (2012). Seasonal and Annual Fluxes of Nutrients and Organic Matter from Large Rivers to the Arctic Ocean and Surrounding Seas. *Estuaries Coasts* 35 (2), 369–382. doi:10.1007/s12237-011-9386-6

Holmes, R. M., McClelland, J. W., Raymond, P. A., Frazer, B. B., Peterson, B. J., and Stieglitz, M. (2008). Lability of DOC Transported by Alaskan Rivers to the Arctic Ocean. *Geophys. Res. Lett.* 35 (3). Article L03402 doi:10.1029/2007gl032837

Hugelius, G., Strauss, J., Zubrzycki, S., Harden, J. W., Schuur, E. A. G., Ping, C.-L., et al. (2014). Estimated Stocks of Circumpolar Permafrost Carbon with Quantified Uncertainty Ranges and Identified Data Gaps. *Biogeosciences* 11 (23), 6573–6593. doi:10.5194/bg-11-6573-2014

Kattner, G., Lobbes, J. M., Fitznar, H. P., Engbrodt, R., Nothig, E. M., and Lara, R. J. (1999). Tracing Dissolved Organic Substances and Nutrients from the Lena River through Laptev Sea (Arctic). *Mar. Chem.* 65 (1-2), 25–39. doi:10.1016/s0304-4203(99)00008-0

Kicklighter, D. W., Hayes, D. J., McClelland, J. W., Peterson, B. J., McGuire, A. D., and Melillo, J. M. (2013). Insights and Issues with Simulating Terrestrial DOC Loading of Arctic River Networks. *Ecol. Appl.* 23 (8), 1817–1836. doi:10.1890/11-1050.1

Köhler, S., Buffam, I., Jonsson, A., and Bishop, K. (2002). Photochemical and Microbial Processing of Stream and Soil Water Dissolved Organic Matter in a Boreal Forested Catchment in Northern Sweden. *Aquat. Sci.* 64 (3), 269–281. doi:10.1007/s00027-002-8071-z

Lammers, R. B., Shiklomanov, A. I., Vörösmarty, C. J., Fekete, B. M., and Peterson, B. J. (2001). Assessment of Contemporary Arctic River Runoff Based on Observational Discharge Records. *J. Geophys. Res.* 106 (D4), 3321–3334. doi:10.1029/2000jd900444

Liang, M., Sugimoto, A., Tei, S., Bragin, I. V., Takano, S., Morozumi, T., et al. (2014). Importance of Soil Moisture and N Availability to Larch Growth and Distribution in the Arctic Taiga-Tundra Boundary Ecosystem, Northeastern Siberia. *Polar Sci.* 8 (4), 327–341. doi:10.1016/j.polar.2014.07.008

Lobbes, J. M., Fitznar, H. P., and Kattner, G. (2000). Biogeochemical Characteristics of Dissolved and Particulate Organic Matter in Russian Rivers Entering the Arctic Ocean. *Geochimica Et Cosmochimica Acta* 64 (17), 2973–2983. doi:10.1016/s0016-7037(00)00409-9

Mann, P. J., Davydova, A., Zimov, N., Spencer, R. G. M., Davydov, S., Bulygina, E., et al. (2012). Controls on the Composition and Lability of Dissolved Organic Matter in Siberia's Kolyma River basin. *J. Geophys. Res.* 117. Article G01028. doi:10.1029/2011jg001798

McClelland, J. W., Holmes, R. M., Dunton, K. H., and Macdonald, R. W. (2012). The Arctic Ocean Estuary. *Estuaries Coasts* 35 (2), 353–368. doi:10.1007/s12237-010-9357-3

McGuire, A. D., Anderson, L. G., Christensen, T. R., Dallimore, S., Guo, L., Hayes, D. J., et al. (2009). Sensitivity of the Carbon Cycle in the Arctic to Climate Change. *Ecol. Monogr.* 79 (4), 523–555. doi:10.1890/08-2025.1

McGuire, A. D., Hayes, D. J., Kicklighter, D. W., Manizza, M., Zhuang, Q., Chen, M., et al. (2010a). An Analysis of the Carbon Balance of the Arctic Basin from 1997 to 2006. *Tellus B: Chem. Phys. Meteorology* 62 (5), 455–474. doi:10.1111/j.1600-0889.2010.00497.x

McGuire, A. D., Macdonald, R. W., Schuur, E. A., Harden, J. W., Kuhry, P., Hayes, D. J., et al. (2010b). The Carbon Budget of the Northern Cryosphere Region. *Curr. Opin. Environ. Sustainability* 2 (4), 231–236. doi:10.1016/j.cosust.2010.05.003

Morozumi, T., Shingubara, R., Murase, J., Nagai, S., Kobayashi, H., Takano, S., et al. (2019a). Usability of Water Surface Reflectance for the Determination of Riverine Dissolved Methane during Extreme Flooding in Northeastern Siberia. *Polar Sci.* 21, 186–194. doi:10.1016/j.polar.2019.01.005

Morozumi, T., Shingubara, R., Suzuki, R., Kobayashi, H., Tei, S., Takano, S., et al. (2019b). Estimating Methane Emissions Using Vegetation Mapping in the Taiga-Tundra Boundary of a north-eastern Siberian lowland. *Tellus B: Chem. Phys. Meteorol.* 71. Article 1581004. doi:10.1080/16000889.2019.1581004

Morozumi, T., Sugimoto, A., Suzuki, R., Nagai, S., Kobayashi, H., Tei, S., et al. (2020). Photographic Records of Plant Phenology and spring River Flush Timing in a River lowland Ecosystem at the Taiga-Tundra Boundary, Northeastern Siberia. *Ecol. Res.* 35 (5), 717–723. doi:10.1111/1440-1703.12107

Murase, J., Sugimoto, A., Shingubara, R., Liang, M., Morozumi, T., Takano, S., et al. (2020). Methane Oxidation Potential of the Arctic Wetland Soils of a Taiga-Tundra Ecotone in Northeastern Siberia. *Soil Sci. Plant Nutr.* 66 (4), 645–652. doi:10.1080/00380768.2020.1786343

Neff, J. C., Finlay, J. C., Zimov, S. A., Davydov, S. P., Carrasco, J. J., Schuur, E. A. G., et al. (2006). Seasonal Changes in the Age and Structure of Dissolved Organic Carbon in Siberian Rivers and Streams. *Geophys. Res. Lett.* 33 (23). Article L23401. doi:10.1029/2006gl028222

Pokrovsky, O. S., Manasypov, R. M., Loiko, S., Shirokova, L. S., Krickov, I. A., Pokrovsky, B. G., et al. (2015). Permafrost Coverage, Watershed Area and Season Control of Dissolved Carbon and Major Elements in Western Siberian Rivers. *Biogeosciences* 12 (21), 6301–6320. doi:10.5194/bg-12-6301-2015

Prokushkin, A. S., Kawahigashi, M., and Tokareva, I. V. (2009). "Global Warming and Dissolved Organic Carbon Release from Permafrost Soils," in *Permafrost Soils. Series Soil Biology 16*. Editor R. Margesin (Berlin, Germany: Springer-Verlag), 237–250.

Prokushkin, A. S., Pokrovsky, O. S., Shirokova, L. S., Korets, M. A., Viers, J., Prokushkin, S. G., et al. (2011). Sources and the Flux Pattern of Dissolved Carbon in Rivers of the Yenisey basin Draining the Central Siberian Plateau. *Environ. Res. Lett.* 6 (4), 045212. doi:10.1088/1748-9326/6/4/045212

Rachold, V., Eicken, H., Gordeev, V. V., Grigoriev, M. N., Hubberten, H.-W., Lisitzin, A. P., et al. (2004). "Modern Terrigenous Organic Carbon Input to the Arctic Ocean," in *The Organic Carbon Cycle in the Arctic Ocean*. Editors R. S. Stein and R. W. Macdonald (New York: Springer), 33–55. doi:10.1007/978-3-642-18912-8_2

Raymond, P. A., McClelland, J. W., Holmes, R. M., Zhulidov, A. V., Mull, K., Peterson, B. J., et al. (2007). Flux and Age of Dissolved Organic Carbon Exported to the Arctic Ocean: A Carbon Isotopic Study of the Five Largest Arctic Rivers. *Glob. Biogeochem. Cycles* 21 (4). Article Gb4011. doi:10.1029/2007gb002934

Shingubara, R., Sugimoto, A., Murase, J., Iwahana, G., Tei, S., Liang, M., et al. (2019). Multi-year Effect of Wetting on CH4 Flux at Taiga-Tundra Boundary in Northeastern Siberia Deduced from Stable Isotope Ratios of CH4. *Biogeosciences* 16 (3), 755–768. doi:10.5194/bg-16-755-2019

Stanley, E. H., Casson, N. J., Christel, S. T., Crawford, J. T., Loken, L. C., and Oliver, S. K. (2016). The Ecology of Methane in Streams and Rivers: Patterns, Controls, and Global Significance. *Ecol. Monogr.* 86 (2), 146–171. doi:10.1890/15-1027

Sugimoto, A., and Maximov, T. C. (2012). "Study on Hydrological Processes in Lena River Basin Using Stable Isotope Ratios of River Water (IAEA-TECDOC–1673)," in Monitoring Isotopes in Rivers: Creation of the Global Network of Isotopes in Rivers, Vienna (Vienna: IAEA), 41–49. Available at: https://www.osti.gov/etdeweb/biblio/21570990.

Sugimoto, A., Naito, D., Yanagisawa, N., Ichiyanagi, K., Kurita, N., Kubota, J., et al. (2003). Characteristics of Soil Moisture in Permafrost Observed in East Siberian Taiga with Stable Isotopes of Water. *Hydrol. Process.* 17 (6), 1073–1092. doi:10.1002/hyp.1180

Takano, S., Sugimoto, A., Tei, S., Liang, M., Shingubara, R., Morozumi, T., et al. (2019). Isotopic Compositions of Ground Ice in Near-Surface Permafrost in Relation to Vegetation and Microtopography at the Taiga-Tundra Boundary in the Indigirka River Lowlands, Northeastern Siberia. *Plos One* 14 (10). Article0223720. doi:10.1371/journal.pone.0223720

Tei, S., Morozumi, T., Nagai, S., Takano, S., Sugimoto, A., Shingubara, R., et al. (2020). An Extreme Flood Caused by a Heavy Snowfall over the Indigirka River basin in Northeastern Siberia. *Hydrological Process.* 34 (3), 522–537. doi:10.1002/hyp.13601

Turetsky, M. R., Abbott, B. W., Jones, M. C., Anthony, K. W., Olefeldt, D., Schuur, E. A. G., et al. (2020). Carbon Release through Abrupt Permafrost Thaw. *Nat. Geosci.* 13(2), 138, 143. doi:10.1038/s41561-019-0526-0

Ward, C. P., and Cory, R. M. (2016). Complete and Partial Photo-Oxidation of Dissolved Organic Matter Draining Permafrost Soils. *Environ. Sci. Technol.* 50 (7), 3545–3553. doi:10.1021/acs.est.5b05354

Ward, C. P., Nalven, S. G., Crump, B. C., Kling, G. W., and Cory, R. M. (2017). Photochemical Alteration of Organic Carbon Draining Permafrost Soils Shifts Microbial Metabolic Pathways and Stimulates Respiration. *Nat. Commun.* 8 (1), 1–7. doi:10.1038/s41467-017-00759-2

Welp, L. R., Randerson, J. T., Finlay, J. C., Davydov, S. P., Zimova, G. M., Davydova, A. I., et al. (2005). A High-Resolution Time Series of Oxygen Isotopes from the Kolyma River: Implications for the Seasonal Dynamics of Discharge and basin-scale Water Use. *Geophys. Res. Lett.* 32 (14). Article L14401. doi:10.1029/2005gl022857

Wiegner, T., and Seitzinger, S. (2001). Photochemical and Microbial Degradation of External Dissolved Organic Matter Inputs to Rivers. *Aquat. Microb. Ecol.* 24 (1), 27–40. doi:10.3354/ame024027

Woo, M.-K. (2012). *Permafrost Hydrology*. Berlin, Germany: Springer. doi:10.1007/978-3-642-23462-0

Yabuki, H., Park, H., Kawamoto, H., Suzuki, R., Razuvaev, V. N., Bulygina, O. N., et al. (2011). Baseline Meteorological Data in Siberia (BMDS) Version 5.0. RIGC, JAMSTEC, Yokosuka, Japan Distributed by CrDAP, Digital Media. Available at: https://ads.nipr.ac.jp/dataset/A20131107-002. (Accessed June 2020).

Yamashita, Y., Nosaka, Y., Suzuki, K., Ogawa, H., Takahashi, K., and Saito, H. (2013). Photobleaching as a Factor Controlling Spectral Characteristics of Chromophoric Dissolved Organic Matter in Open Ocean. *Biogeosciences* 10 (11), 7207–7217. doi:10.5194/bg-10-7207-2013

Yang, X., Yuan, J., Yue, F.-J., Li, S.-L., Wang, B., Mohinuzzaman, M., et al. (2021). New Insights into Mechanisms of Sunlight- and Dark-Mediated High-Temperature Accelerated Diurnal Production-Degradation of Fluorescent DOM in lake Waters. *Sci. Total Environ.* 760, 143377. doi:10.1016/j.scitotenv.2020.143377

Yi, Y., Gibson, J. J., Cooper, L. W., Hélie, J.-F., Birks, S. J., McClelland, J. W., et al. (2012). Isotopic Signals (18O,2H,3H) of Six Major Rivers Draining the Pan-Arctic Watershed. *Glob. Biogeochem. Cycles* 26. Article Gb1027. doi:10.1029/2011gb004159

Yi, Y., Gibson, J. J., Hélie, J.-F., and Dick, T. A. (2010). Synoptic and Time-Series Stable Isotope Surveys of the Mackenzie River from Great Slave Lake to the Arctic Ocean, 2003 to 2006. *J. Hydrol.* 383 (3-4), 223–232. doi:10.1016/j.jhydrol.2009.12.038

Conflict of Interest: The authors declare that the research was conducted in the absence of any commercial or financial relationships that could be construed as a potential conflict of interest.

frontiers in Earth Science

ORIGINAL RESEARCH
published: 08 September 2021
doi: 10.3389/feart.2021.663198

Intersectoral Competition for Water Between Users and Uses in Tamil Nadu-India

S. Suresh *

Department of Civil Engineering, Sona College of Technology, Salem, India

Water is a manageable asset for drinking, food creation, and industry, and demand increases as the population increases. Water for irrigated agriculture, industry and domestic needs in India will go up to 1,072, 130, and 102 billion m^3 (BCM) by the year 2050. In the state of Tamil Nadu in 2025, water needs for irrigation, domestic, livestock, and industrial sectors will be 52.7, 1.5, 1, and 2 billion m^3, respectively, against the available supply of 24.6 BCM of surface water and 23 BCM of groundwater during the same period. A balance between need and supply is often difficult to achieve. By the year 2050, some 60 per cent of the world's population will live in cities. In India and Tamil Nadu, 38 and 48 per cent of people will live in cities. Tamil Nadu is the second most urbanized state in India with 48 per cent of its population living in cities. This urban push will demand a large share of common water resources and most of the reservoir systems will face increased water demand for non-agricultural purposes, bringing in imbalances with other sectors, namely agriculture. Contrary to mounting demand, it will be difficult to facilitate the growing need for water. Furthermore, there are social and environmental costs in terms of the diversion of water from agriculture to urban uses. The discharge of sewage and industrial effluents also pollutes surface and groundwater, affecting not only human health but also the entire ecosystem. This paper examines the water management challenges in Tamil Nadu, India with respect to meeting future water demands across competing sectors.

Keywords: intersectoral competition, ground water, anicut, river basin, fresh water

OPEN ACCESS

Edited by:
Shafi Mohammad Tareq, Jahangirnagar University, Bangladesh

Reviewed by:
Venkatramanan Senapathi, Ton Duc Thang University, Vietnam
Parvin Fahmida, Jahangirnagar University, Bangladesh

***Correspondence:**
S. Suresh
sansuresh86@yahoo.co.in
sankarsuresh86@gmail.com

Specialty section:
This article was submitted to Hydrosphere, a section of the journal Frontiers in Earth Science

Received: *02 February 2021*
Accepted: *30 June 2021*
Published: *08 September 2021*

Citation:
Suresh S (2021) Intersectoral Competition for Water Between Users and Uses in Tamil Nadu-India. Front. Earth Sci. 9:663198. doi: 10.3389/feart.2021.663198

Abbreviations: BOT, built operate and transfer; BCM, billion cubic metre; BOD, biochemical oxygen demand; CCWR, climate crop water requirement; CGWB, central ground water board; CPCB, central pollution control board; DFID, DFID engineering knowledge and research programme; GDP, gross domestic product; GWEC, groundwater estimation committee; IPCC, intergovernmental panel on climate change; LPCD, liters per capita per day; KM, kilometre; NWP, national water policy of india; MSMEs, micro, small and medium enterprises department; Mm^3, million cubic metre; Mg/l, milligram per litre; MHA, million hectare; Mld, million litres per day; NABARD, national bank for agriculture and rural development; PWD, public works department; TDS, total dissolved solids; TMC, thousand million cubic feet; TIIC, tamil nadu industrial investment corporation Ltd.; TWAD Board, tamil nadu water supply and drainage board; RTPs, rural town panchayats; RWH, rain water harvesting; UTPs, urban town panchayats.

INTRODUCTION

The Indian irrigation sector utilizes about ninety-three percent of total water withdrawn and the remaining seven percent is shared between domestic and industrial sectors. At the time of Indian independence (1947), the irrigation facilities available were one-sixth of the cropped area. The government's main concern was to expand the irrigation infrastructure. Reservoirs, barrages, and diversion structures were constructed without thinking about environmental issues. In the late seventies, the importance of ecological balance was realized and attention turned to improving the performance of existing systems. In the eighties, it focused on institutional and social constraints. By 1987, a National Water Policy of India (NWP) was formulated and provided guidelines for acquiring, conserving, and utilizing water resources and the need to ensure equity and equality. The policy recommends the involvement of farmers in irrigation management. At the beginning of the 21st century, it was thought that the integrated land, water, and human resource management

FIGURE 1 | Location map of Tamil Nadu State. Source: Maps of India.

was ideal for sustainable development and safeguarding the water resources for the future generation.

Tamil Nadu is the southernmost state of India, delimited by the Indian Ocean on the south, the Bay of Bengal to the east, and on the west, north, and east by the states of Kerala, Karnataka, and Andhra Pradesh, respectively (**Figure 1**). With a spatial extent of 1,30,058 km^2, this state covers 4 percent of the total area of India, 7 percent of the population of India, and 3 percent of the water resources of India (Census of India 2011). Tamil Nadu has a fairly high average population density of 429 per km^2 and is also the second most urbanized state of India with 48.45% of the population living in urban areas (Chitra and Laxmi, 2017). The state has a tropical climate with a temperature of 43°C in summer and a minimum of a little lower than 18°C during winter (Statistical Hand Book 2016-2017). The average rainfall of the state is 925 mm against the average rainfall of 1,170 mm in India. Tamil Nadu receives its rainfall from the north east as well as south west monsoons. A variation in the monsoon has a serious impact on the economic life and livelihood hood of people, especially in rural areas. Thus, Tamil Nadu is a deficit state from the point of view of water resources both for irrigation and drinking water and is dependent on the monsoons very heavily.

The intersectoral competition for water between the users and uses involves varied resources, including 1) water, 2) land, 3) human, and 4) livestock. Thus, integrated water, land, human, and livestock resources management is necessary to avoid conflicts and ensure rational and sustainable utilization of water resources. Tamil Nadu is one of the more progressive states in India, and has already achieved more than 95 per cent of its total water potential, and has implemented several inter- and intra-state water transfer diversions from existing irrigation projects (the water transfer from Veeranam tank to Chennai city by a 250 KM pipeline is the second longest ever and the longest intra state transfer in India (DFID, 2005)). Tamil Nadu also undertakes ground water extraction, desalination of sea water, and cloud seeding, etc., to augment water for domestic sectors. The crux of the entire problem lies in the successful implementation and successive follow-up. A host of other factors are responsible for non-implementation or improper implementation of meeting the water requirement. These include a lack of coordination, unimodal, multiple jurisdictions, mutual exclusiveness, and political motivations. Vairavamoorthy et al. (2007) outline guidelines for the design of the urban water distribution systems, especially developing countries with equitable distribution when the resources are scarce.

A climate crop water requirement (CCWR) integrated framework (Mohan and Ramsundram, 2014) has been developed. The project studied the influence of climate variability on irrigation water requirements in an arid region, the Manimuthar river basin in India, and found that the irrigation water requirement is likely to increase by 5% in the time period from 2010 to 2020. Bitterman et al. (2016) present a conceptual framework for measuring water security in the context of rainwater harvesting tanks. Glendenning et al. (2012) focus on the hydrological impact of rainwater harvesting (RWH) on the ground water recharge in rural areas of India and emphasize remote sensing methods and modeling for better assessment and policy to RWH. Sivasankar et al. (2012) studied the various physical and chemical characteristics of groundwater samples from Ramanathapuram, a coastal district of Tamil Nadu, and the aquifer are severely affected, with a fluoride content more than 1.5 mg/L. Therefore, this paper investigates the various water management challenges in Tamil Nadu, India with respect to meeting future water demands across competing sectors.

WATER RESOURCES OF TAMIL NADU

Major Surface Water Resources

The state is drained by 34 river basins with about 54 major reservoirs and more than 300 medium and small anicuts, barrages, and diversion structures. Construction of dams, diversion structures, and barrages are centuries old. The Grand Anicut (called Kallanai in Tamil, kall = stone: Anai = dam) was constructed by the chola dynasty of King Karikalan during the second century BC. It is possibly the oldest existing structure on earth still in operation. At present, for convenience, the 34 river basins are grouped into 17 major river basins (Figure-2). Thus, almost 95 percent of the surface water potential is brought into human control by way of the construction of dams and anicuts. While major dams were constructed during British rule, medium projects were commissioned after independence. Most of the major rivers like Cauvery, Pennar, Palar are interstate rivers (**Figure 2**) and their flows in the state are dependent on certain mutual agreements with the neighboring states like Karnataka, Andhra Pradesh, and Kerala. Rivers are state subjects and therefore there are often disputes about sharing waters between the states. This problem is further aggravated when the political party in power in a state is different from the party that rules at the center. Moreover, since states have been divided on a linguistic basis, there are a number of reasons for disagreement.

Groundwater Resources

Having utilized more than 90% of the available surface water resources, it is necessary for Tamil Nadu to develop its own groundwater resources, including a more judicious conjunctive use of its own surface and groundwater. The groundwater estimation committee (GWEC) constituted by the National Bank for Agriculture and Rural Development (NABARD) with the Central Ground Water Board (CGWB, 2000) and Groundwater wing of the public works department (PWD), estimated that the groundwater potential in Tamil Nadu is 22,432 Mm^3, of which 1,022 Mm^3 is earmarked for domestic and industrial water supply requirements (CGWB 2017). The actual requirement of water supply schemes is 1,057 Mm^3 both for the urban and rural populations. However, these figures, although indicative of the overall water balance, should be taken with a great deal of caution, particularly as regards domestic water supply where spot-specific availability is as critical as sheer availability. At present, only 61% of the groundwater has been harnessed and it is still the most economical, individually managed (private) resource. Traditionally well irrigation was practiced in the eastern part

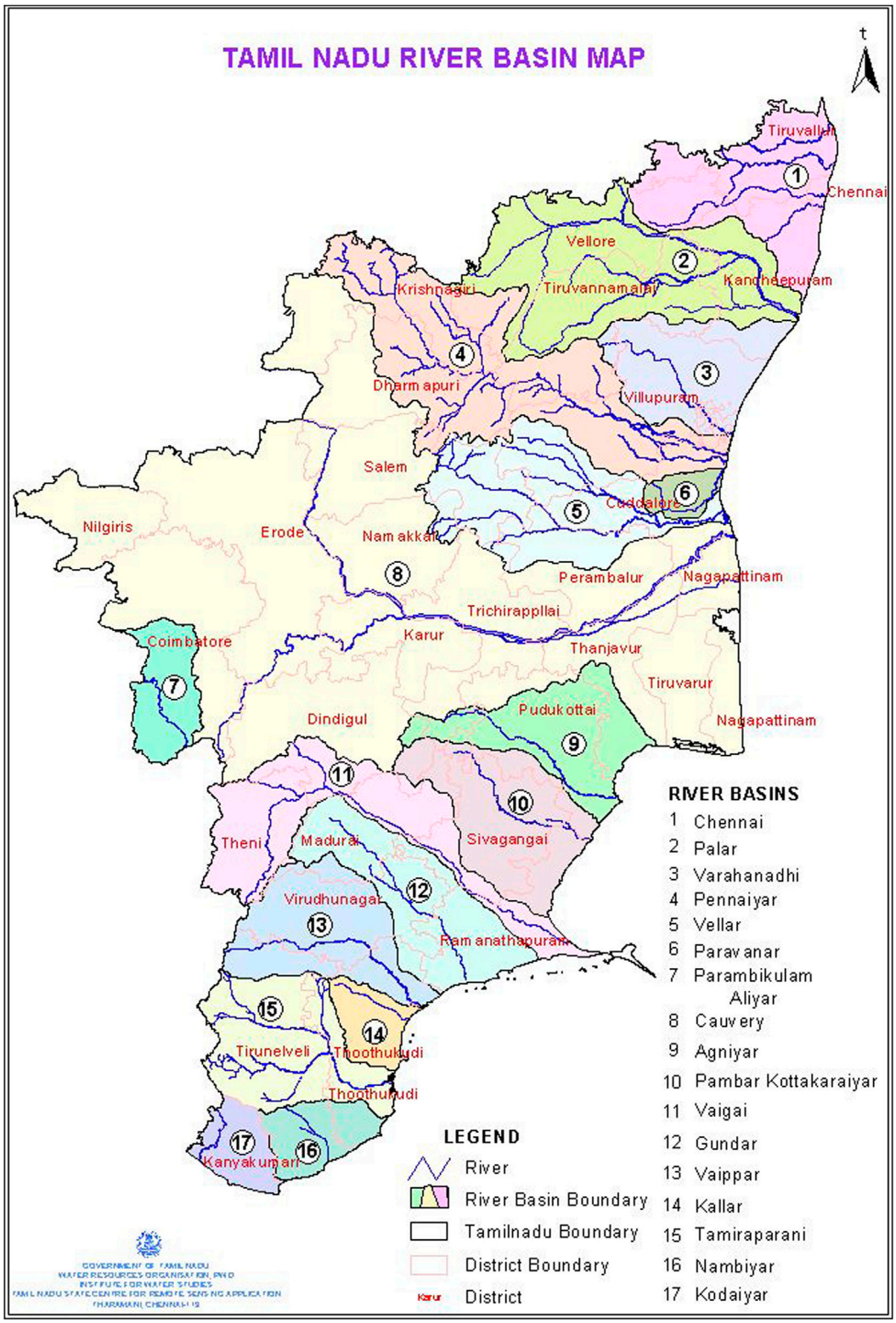

FIGURE 2 | River basin of Tamil Nadu. Source: PWD, Chennai, Tamil Nadu.

of the state. There were open wells and the water was drawn by draught powered by bullocks. The depth and drawing of groundwater are directly related to the length and duration of travel by the bullocks, which helped in sustaining the groundwater without depriving groundwater from neighbors. The advent of electrification and use of high-powered pump sets, improvements in drilling technology, and the subsequent supply of free electricity for agricultural uses had led to the large-scale mining of groundwater, leading to dwindling quantities and deteriorating quality. It should be understood that the availability of an irreproachable standard constitutes part of the very quality of human life. The difficulties and cost of treating polluted water and the impossibility, even in the medium term, of rehabilitating polluted groundwater systems should encourage us to understand the vital need for maintaining good quality groundwater resources. The overexploitation of groundwater beyond the annual recharge into aquifers has already led to this resource being classified as exploited (CGWB 2017).

From the **Table 1** it can be observed that 23 percent of total blocks experience heavy groundwater extraction, over and above the recharge, resulting in depletion and seawater ingress in the coastal aquifer system. By adapting spot-specific artificial groundwater recharge techniques continuously for more than a decade in Tamil Nadu, it is possible to recharge 3 and 4m thick sedimentary and hard rock terrains aquifers, respectively, and additionally, recharge about 375 TMC (Thousand Million Cubic feet) of groundwater.

TABLE 1 | Groundwater exploitation level in Tamil Nadu. Source: CGWB 2017.

S. No	Classification	Exploitation level	No of blocks
1	Dark	85–100%	89
2	Grey	65–85%	86
3	White	Less than 65%	211
Total Number of Blocks in Tamil Nadu		386	

DEMAND FOR WATER

The demand pattern of water among the various sectors (agriculture, industrial, and domestic) has changed (**Figure 3**) considerably over the past 100 years. For instance, in 2010 out of the total water supplied, 90% was utilized in the irrigation sector as compared to 6% in industry and 4% in the domestic water sector (Natarajan et al., 2017). In 2020, the water utilized by the irrigation sector reduced to 60% whereas the water diverted to the industrial sector was 26%, and in the domestic sector 14%. **Figure 4** represents water demand in Tamil Nadu for 2010, 2020, and includes the projection for 2025 to 2050 (PWD, Chennai, India).

Agricultural Sector

India tops the list of countries with a large extent of the area brought under irrigation (total gross irrigated area of 62 MHA) (ICID, 2018). The state of Tamil Nadu with its limited resources ranks sixth in India and irrigates about 3.5 MHA (State of Indian Agriculture, 2016). By 2022 the total potential created under major and medium irrigation projects is reported at 1.34 MHA (90% of the assessed ultimate potential of 1.5 MHA) and minor irrigation potential of 2.20 MHA (91% of the ultimate potential of 2.4 MHA). The net sown area accounts for 42.6% of the total geographical area of which the net and gross irrigated areas as per the recent statistics were of the order of 2.4 and 2.9 MHA, respectively. It is estimated that rice crop consumes more than 45% of the total water that goes into agriculture. The major sources for irrigation are canals/rivers, tanks, and groundwater. The traditional utilization pattern of the water resources was one third each from reservoirs, tanks, and groundwater. Recently, the pattern transformed and the utilization at present is around 30 percent of reservoir water, 20 percent of tank water, and 50 percent of groundwater, respectively. Agriculture performance (Ruttan 1965; Gollin et al., 2002) is fundamental to India's future economic and social development. Agriculture contributes 30% of GDP, 60% of employment, and is the primary source of livelihood in rural areas, which account for 75% of India's

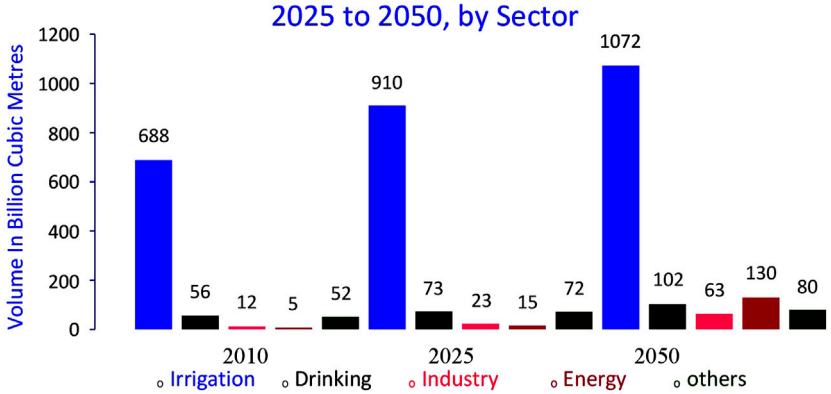

FIGURE 3 | Water demand in India for 2010 and the projection for 2025 to 2050, by Sector. Source: Ministry of Water Resources, India.

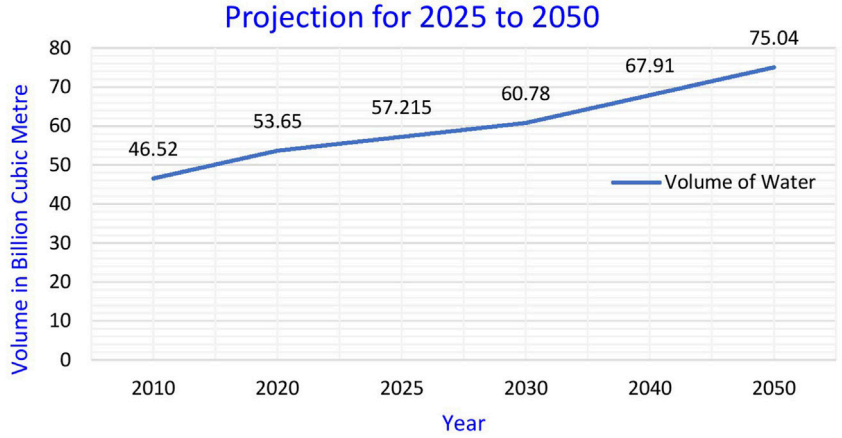

FIGURE 4 | Water demand in Tamil Nadu for 2010, 2020, and the projection for 2025 to 2050. Source: PWD, Chennai, India.

population and 80% of its poor and low-income population. The performance of irrigated agriculture, which contributes 55% of agricultural output, will be the most important influence on these objectives. Therefore, the largest irrigated area in the world is in India (ICID, 2018).

Domestic Water Sectors

There are 146 Municipalities and 15 Municipal Corporations in Tamil Nadu (Corporation of Tamil Nadu, 2020; Municipality of Tamil Nadu 2020). The metro water and the Tamil Nadu Water supply and Drainage Board (TWAD Board) are responsible for providing drinking water to the city of Chennai and the rest of the state, respectively. The drinking water requirement by the total population of Tamil Nadu by 2020 A.D is only 4.5% (1,055 Mm^3 both for urban and rural population) of the total assessed groundwater resource, but every year the city of Chennai and most other towns face acute water scarcity (Vairavamoorthy et al., 2007). As the population has grown, freshwater (IPCC et al., 2014) has become increasingly less available where and when it is needed. Acute water shortages already have required extraordinary measures in Chennai, where water was transported from neighboring places by all modes of transport ranging from bicycles and trucks to railway tankers, with distances ranging from a few kilometers to 200 km. In certain parts of the city, people are forced to pay water tax and water charges to the government and at the same time, make daily purchases of drinking water from private vendors for drinking purposes.

Industrial Water Sectors

Industry in Tamil Nadu

Tamil Nadu is the second-largest state economy following Maharashtra state, which has a much larger area and population. Tamil Nadu is also ranked first among Indian states in terms of exports from the special economic zone. Vision Tamil Nadu 2023 anticipates that an investment of 230 billion United States dollars (Rs. 15 lakhs core) will be invested in the state before the year 2023 (ENVIS 2020). This includes investment in projects falling under the manufacturing, infrastructure, and services sectors. At present, out of 217 infrastructure projects listed in vision Tamil Nadu 2023, 88 projects are under various stages of implementation, with the implementation of the remaining projects, the milestones envisaged in vision Tamil Nadu 2023 will be achieved.

Tamil Nadu Industrial Investment Corporation Ltd. (TIIC) is the first state-level financial corporation in the country catering to the needs of MSMEs. TIIC provides financial support to major industrial units such as the sugar, cement, textile, and aluminum industries. TIIC also has a role in the promotion of industrial clusters like hosiery in Tirupur textiles and foundries in Coimbatore, Sericulture and Sago factory in Salam and Dharmapuri, wind mills in Tirunelveli, Palladam, and Udumalper, etc. The major industries in Tamil Nadu are information technology, manufacturing, and engineering industry, automobile industry, leather industry, paper industry, chemical, and plastic industry, textile industry, handloom and power loom industry, sugar industry, and chemical industry.

Industrial Water Demand

In Tamil Nadu, industry is the second-highest consumer of water. Groundwater has emerged as a preferred source to meet the water requirement of industries since the surface water supply from municipal sources is not sufficiently guaranteed. The industrial water demand of Tamil Nadu has been increasing with the pace of industrial development. Furthermore, the growth of water-intensive industries is constantly putting pressure on the industrial demand for water, while the annual growth of the chemical and construction industry is been 8 percent, the textile and food industry is 6 percent, and the paper industry is 4 percent.

Quantity Dimension

In India, there are no accurate estimates of water consumption by the industrial sector, but different agencies are recommending the

water use value. For instance, according to the Ministry of Water Resources, India, the industrial sector accounts for six percent of the total freshwater abstraction while the Central Pollution Control Board (CPCB) recommends 8 percent (Suresh and Surender, 2011). However, the world bank estimates that the current industrial use in India is about 13 percent of the total freshwater withdrawal in the country and predicts the water demand for industrial uses and energy production will grow at a rate of 4.2 percent per year in coming years. The estimates of sectoral water demand in Tamil Nadu are given in **Table 2**. The industrial water demand in the city of Chennai is estimated at around 326 Mld. These estimates reveal that the industrial water demand is not negligible and will constantly grow in the coming years.

COMPETITION AMONG USER SECTORS

Rising demand for urban and industrial water supplies poses a serious threat to irrigated agriculture. Irrigated agriculture faces two significant challenges, water shortages and dwindling financial resources, in the coming decades. In India, irrigation investments in the past amount to about 30% of total public investments after independence. In Tamil Nadu, irrigation projects have taken 18 percent of total/agricultural investments. The investment pattern of plan outlays for the irrigation sector in India during 2020–21 was 230 million and it rose to 275 million during 2029–30 but the percentage allocation for the same period was 18 and 16 percent, respectively. Despite these challenges, irrigated agriculture will provide 70 to 75 percent of additional food grain requirements to developing countries. This will not be possible without 1) substantial improvements in the productivity of existing irrigation schemes, and 2) investment in new irrigation projects.

TABLE 2 | Estimates of sectoral water demand in Tamil Nadu, India.

Category	2010	2020	2025	2030	2040	2050
	Volume in billion cubic meters (BCM)					
Irrigation	43.22	49.85	52.7	55.78	60.44	65.6
Domestic	1.0	1.2	1.5	2	3	4
Industry	1.5	1.7	2	2.5	3.5	4.5
Live stocks	0.8	0.9	1.015	1	0.97	0.94
Total	46.52	53.65	57.215	60.78	67.91	75.04

WATER DEMAND AND SUPPLY PROJECTIONS

Population Trends and Explosive Urban Growth

The population of Tamil Nadu as per the 2011 census is 72.1 million (Census of India 2011) and the total population is expected to reach 85 million in the year 2021AD, out of which 32 million comprise the urban population and 53 million comprise the rural population (**Figure 5**). On a happy note, the substantial decline in the birth rate could fall further during the coming years. It was 28 per 1,000 during 2012 and 19.2 in 2022 and is expected to reach 15 per 1,000 during the year 2032. The water demand and supply projections have been made for agriculture, domestic, industrial and livestock requirements basin wise (as it would be an appropriate unit for planning any water resources system). For agriculture demand the cropping pattern, area sown, and water requirements are taken into account. For domestic purposes, the existing population in urban areas with a supply of 90 L per capita per day (lpcd) and rural with a supply of 40 L per capita per day has been taken (National Water Mission 2017). For industrial consumption, the yardstick fixed by the industries department is taken into account and for the livestock the number of cattle on each river basin is taken and an average consumption of 80 L per capita per day per cattle. The projection for future requirements for agriculture is made based on future schemes to be implemented in the river basins. For the assessment of domestic water supply, the population projections have been

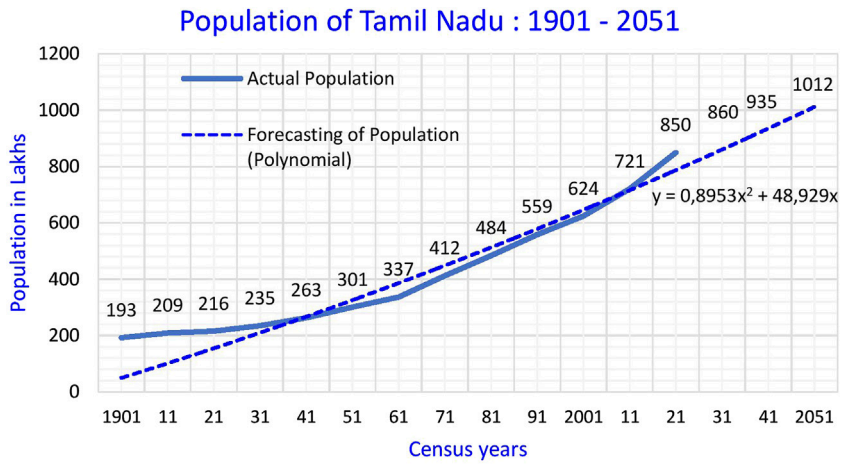

FIGURE 5 | Population of Tamil Nadu: 1901–2021, source: Census of India.

made for urban and rural areas. For urban areas, a 30 years 100% increase is taken. For rural areas, 30% was taken. For industrial projections, the annual increase of 8% was taken into consideration. As far as the livestock are concerned no norms for the increase have been fixed and as per the present requirement are taken for the projection also. From research studies, it was revealed that water needs during 2025 for irrigation, domestic, livestock, and industrial sectors are 55.28, 2, 1, and 2.5 billion m^3, respectively.

WATER AND CONFLICT

Resource's scarcity can exacerbate preexisting tensions or invite new ones (Tamas. Pal 2003), and water is no exception. Like the oil shock which the world experienced during the nineteen eighties it would be water shock for the developing countries in the near future, as the population increases steadily bringing down the per capita availability of fresh water as the fresh water resources that are renewed through the global water cycle is a finite natural resource in each country (IPCC, 2014). Access to water is further complicated by conflicts arising over rights to water in river basins shared by countries or by states within a country (Williams et al., 2015). In India the river is still a state subject even though many rivers pass through different states. Coupled with the political process in which a state ruled by a party can be different from the party in power at the Center (India) further complicates river basin management. It would be much prudent to shift the management of the renewable water resources that exist within administrative and political borders, as water is more of a regional resource than a global resource.

WATER RESOURCES DEVELOPMENT: PROJECT PLANNING ON A REGIONAL SCALE

The central purpose of water resource development is to meet demand and supply. This process involves a detailed assessment of demand both for the present and the future. The natural unit of water resources development is the river basin. Water resources systems were created for the task of matching the supply to the demand for water, in basins or in their sub units. Their traditional form is a group of structures connected through information links; these connect all aspects of supply with all aspects of water demand.

Organizations for Irrigation Management

Normally, dual-management irrigation systems are developed in a top-down approach. The water users in their "tertiary units" have to follow the technical and institutional innovations made by technicians. Recent rehabilitation programs have not improved irrigation as expected, and water users have not yet become "partners in irrigation management". Good irrigation management appears to be difficult, as conflicting interests are normal in irrigation, and different parties have their own responsibilities.

Management Strategies

Management strategies must be multifaceted rather than unimodel. It should have macro, micro, and grassroots level planning followed by effective management of catchment (on the upstream side) reservoir and the command (downstream side). The illegal felling of trees and excessive grazing over the catchment besides increasing runoff brings in silt and sediment which ends in surpluses to sea. Optimal catchment treatment would help in a great way in the proper upkeep of the structures created.

The experience in many developing countries has shown that the "fragmented, command-and-control" approach to the management of water resources has failed, both economically and environmentally. Hence, there is a need to use economic incentives and fiscal instruments in achieving economic efficiency in the use of the resource. Furthermore, it is necessary to show that better economic management of this resource will greatly assist in improving the environment. Thus, a policy package is urgently required with a judicious mix of legislation and regulation, including water tariffs, pollution taxes, effluent charges, and groundwater extraction charges, and providing tax benefits or investment support for water conservation and effluent treatment plants.

Water Management Techniques

Surface water is utilized by scientific methods to the extent possible. Even then, the entire surface water available as surplus is not effectively and economically used, the surplus water (Suresh and Somasundaram, 1996; Suresh 2002) flows into the sea. The T.S. Vijaya Raghavan Committee (The Hindu, 2014) has estimated that from the seven river basins (**Figure 2**) of Tamil Nadu State, about 76.94 TMC of floodwater is let into the Bay of Bengal in the normal monsoon years. (**Figure 6**).

To improve the groundwater potential and quality it has been suggested that check dams be constructed across the rivers or surplus waters that could enable water to be diverted to areas in need, where the groundwater table is lower than the sea level. Traditional water management techniques have been neglected or fallen into disuse and are heading to a further decline in water storage capacity and consequently surface water flow into the sea. At present, the coordination between user departments is not up to the required level. The available water sources may be grouped for a river basin and various activities may be monitored. Nothing appreciable is being done to economize water use at present. The difficulties encountered in protecting the installed capacities and loopholes in the system. Tampering by the public, unwillingness to pay for water supply, insufficient qualified staff, paucity of funds, and delegation of powers at various levels may be considered conducive to the present reality.

Rain Water Harvesting in Chennai City, Tamil Nadu

Chennai is a coastal city, meaning it is always under threat from seawater intrusion along the coast if more freshwater is extracted. For instance, in the Minjure and Mouthambedu well fields located north of Chennai City the fresh groundwater aquifer has been salinized to a length of about 20 KM from the coast with a seawater migration rate of 427 m per annum-(Natarajan et al., 2017) (**Figure 7**). Indiscriminate extraction in Minjur, the coastal

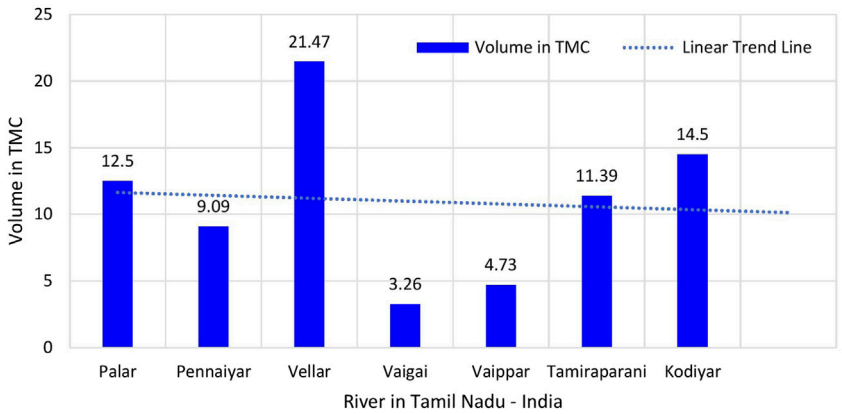

FIGURE 6 | Surplus water from Tamil Nadu river basin. Source: The Hindu (June 23, 2014).

area along the North Sea coast of Chennai has spoiled water because of overexploitation (CGWB 2017).

NATIONAL WATER DEVELOPMENT AGENCY

This agency has identified that the performance of the existing schemes is insufficient and that the current state of affairs can be improved by modernizing the existing irrigation system, which is dilapidated due to neglect and a lack of maintenance over the years. In most of the systems, the typical problems are an unrealistic and poor distribution of water with tail-enders frequently not getting water and even farmers in the upper reaches getting only unpredictable supply, and that too does not necessarily correspond to the agricultural calendar.

Increasing New Investments in Irrigation

Although improving the efficiency of existing irrigation schemes is a must, it is still not sufficient to meet the additional requirement for food and fiber in the next 2 decades. Large-scale new investments in irrigation schemes will be required for providing adequate food and fiber to meet the objectives of poverty alleviation and development. During the last decade, real investment in irrigation schemes has declined as the cost of new schemes has increased, while the international price of food grains has declined. Given the large contributions required from new schemes, concerted efforts are needed, both at national and international levels, to increase real investments in new irrigation schemes. Many of the delays in the completion of water resource projects often become costly and by the time a revised estimate is sanctioned another price escalation has already taken place.

Water Resources Consolidation Projects

The prestigious Water Resources Consolidation Project was carried out at an estimated cost of Rs.1400 crores for remedying the situation. Its main focus is on institutional arrangements, operation and maintenance, planning and management of farmer's participation in water conservation and management, and environmental impact assessment. This project was also undertaken as part of a major revamping of the organizational structure of the Public Works Department (PWD).

CONSERVATION AND RECYCLING-REUSE

In the domestic sector, the use of water for flushing, bathing, washing, and cleaning can be minimized greatly when conventional taps are replaced by pressure taps where air at relatively high pressure is mixed with water to reduce the quantum water needed. In the industrial sector, a change in the process from water intensive to less water-intensive and finally to cent percent recycling of water could make a difference. In the agriculture sector, efforts to encourage water conservation face special challenges not encountered with other natural resources. In much of the world, water is not controlled by market mechanisms because it is either free or unmetered. Now water is a global resource that can be traded like coal or petroleum. Often, wasting water in one river basin is seen as irrelevant to those who live in another. There is significant scope for water conservation in irrigated agriculture. Higher water rates for water intensive crops such as rice and sugarcane could also encourage farmers a shift towards other crops such as maize, wheat, and barley, etc. Since irrigation charges are generally much lower than the value of water in alternative uses, these low prices do not encourage efficient water use on the farm. Furthermore, efficiency will improve by a more equitable distribution of water between farmers at the head of the distribution system and those at its tail end.

Recycling (desalination) had been tried in coastal districts of Tamilnadu and could be used only for domestic needs (drinking water) in the absence of alternate sources, but the technology available at this date is cost-intensive with the unit cost including depreciation and debt servicing reported from a pilot plant study in 2018–19 of (Rs. 100) $ 1.3 per 1,000 L Moreover, the disposal of

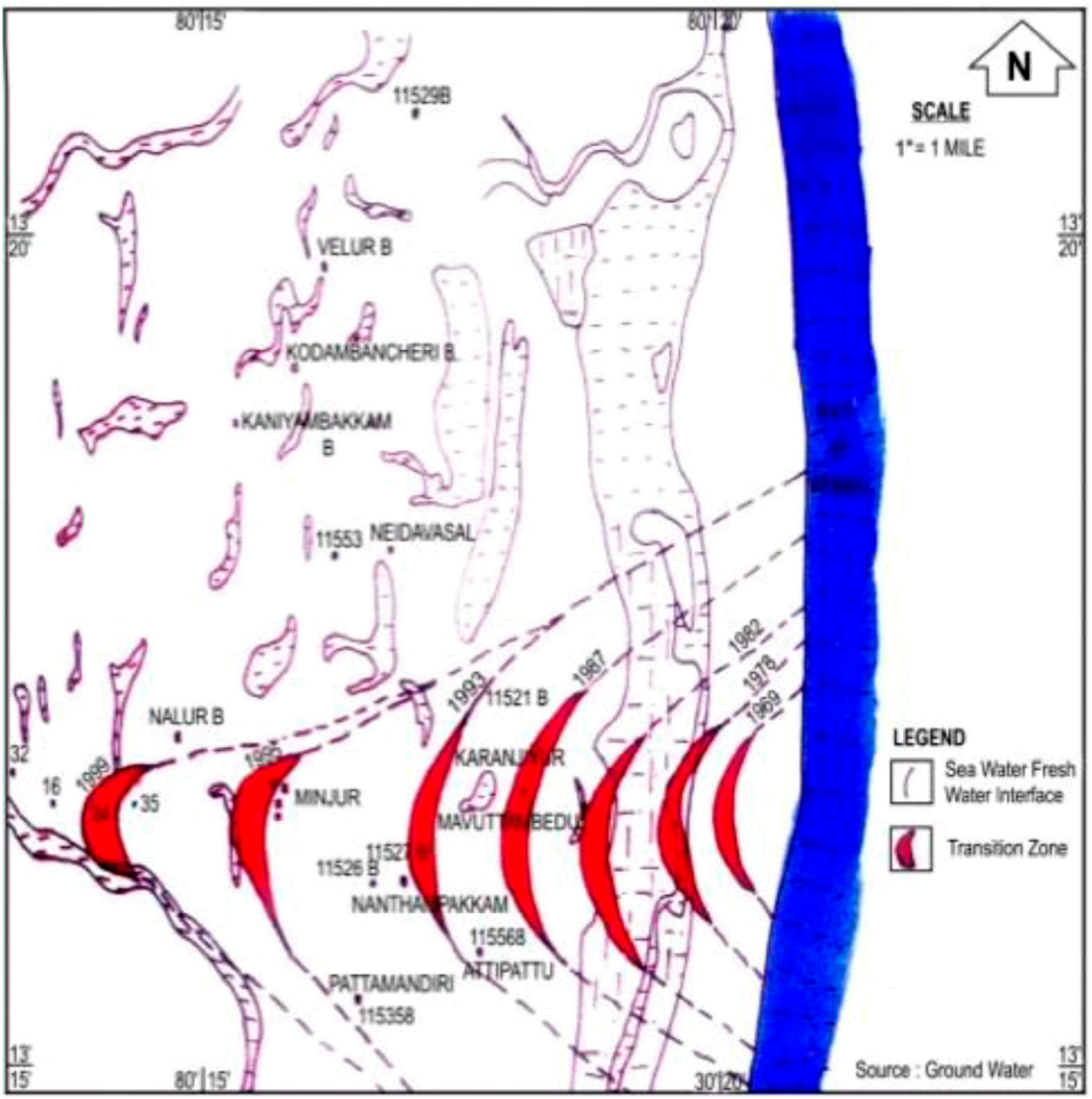

FIGURE 7 | Sea Water Intrusion North Sea coast of Chennai-Tamil Nadu. Source (CGWB 2017).

reject water from the desalination plants is a major problem for these plants.

WATER QUALITY–GENERAL OVERVIEW

Tamil Nadu has limited water resources and draws much for its drinking water schemes from surface, subsurface in riverbeds, and groundwater sources. A large number of water supply schemes draw water from infiltration wells located in major riverbeds. A number of water supply schemes, particularly as regards Urban Town Panchayats (UTPs) and Rural Town Panchayats (RTPs), draw water from groundwater sources. Approximately 0.15 million bore wells fitted with hand pumps also supply water to the rural public.

Status of Water Quality in Major Municipal Water Supply Schemes

An analysis of data reveals that fluoride, nitrate, iron, and Total Dissolved Solids (TDS) are the critical chemical parameters that noticeably influence water quality (Sivasankar et al., 2012). The Tamil Nadu districts of Dharmapuri, Salem, and Periyar are severely affected by fluoride. The districts of Coimbatore,

Madurai, Virudhunagar, and Tuticorin are also affected to some level. In Dharmapuri District about 54% of the sources are found to be not potable either in one season or another season. High seasonal variation renders the same water sources as potable in one season and not potable in another season. Approximately 10% of the sources in Dharmapuri, Salem, and Erode have high fluoride levels of greater than 3 mg/L. Special attention is needed in these districts to avoid the problem of skeletal flourish. Cases of skeletal flourish have already been reported in Salem District. The level of Nitrate in most of the groundwater sources is becoming a problem and it has been noted in most of the districts. In the northwestern parts of Tamilnadu, it is above 60%. Increased agriculture activities and the application of fertilizers may be attributed to this phenomenon. Parts of the northern districts are affected by the high level of iron in the water. It has been observed that the iron content in any source generally decreases with continuous use.

High seasonal variation is noted in the level of TDS in groundwater sources in Tamilnadu. In Coimbatore about 90% of the water sources become non-potable for no specific season. With respect to groundwater sources, it is difficult to separately demarcate the saline areas in the state. The level of TDS depends on the water level and the depth of the well in various places. Certain pockets in the districts of Ramanathapuram (Sivasankar et al., 2012), Tuticorin, Pudukottai, and Coimbatore have a TDS of more than 3,000 mg/L. In these areas where water quality is a limiting factor, a change of source or treatment of water to bring it into a form suited for drinking purposes is required. Rainwater harvesting on rooftops and construction of percolation ponds (**Figure 8**) would result in diluting the groundwater by direct recharge and thus result in the portability of water.

Factors Affecting Water Quality in Tamilnadu

In Tamil Nadu, there are about 4,820 highly polluting industries, which are called RED category industries. It has also been reported that out of the 5,059 industries listed as requiring effluent treatment plants, only 1,114 industries have provided the same type of effluent treatment plant. The impact of tannery pollution in the Palar river basin is in alarming proportion. The tannery effluent having high BOD, Sodium chloride, and chromium are let into the Palar river which takes water from infiltration wells is having high TDS, contrary to the expected quality for subsurface water in the river bed. High salinity is also noted in open well and bore well sources in Vaniyabadi, Ambur, Ranipet, Wallajah, and other towns in Tiruvannamalai, Vellore, Ranipet, and Tirupathur district. Dindigul is another district, which is severely affected by tannery pollution. Due to the depletion of present water sources and lowering of water levels in many of the bore wells, it is noted that the groundwater quality is severely affected. It is natural that when the groundwater level decreases the traveling time and contact time of water through soil increases and thus carries more salt with it.

FIGURE 8 | Percolation pond–artificial recharge technique. Source: DFID, 2005.

CONCLUSION

Over exploitation of groundwater, which is frequently used and transported for urban uses indiscriminately can be easily checked if land policies are framed for fragmentation and subdivision, pricing of electricity, limiting the use and spacing of deep bore rigs, and the long-awaited groundwater legislation. From the research study, it was revealed that an increase in 10–15 per cent of water use efficiency in the agriculture sector would result in sufficient water availability for urban and industrial uses without sacrificing food production. Drinking water (less than 4 per cent of agriculture water use), which is of the highest priority, should be supplied through pipelines to the tail and reaches of the river basins (Ramanathapuram district in Vaigai basin) from existing reservoir schemes rather than using the local groundwater beyond the recharging limits.

Livestock reared by almost every household in rural areas are slowly disappearing as many of the cattle are sent to neighboring Kerala state for slaughter (cow slaughtering is banned in the Hindu region). Furthermore, several commercial ventures have come up recently adding to the concentration of livestock population, commercial cultivation of fodder, and thereby bringing in pressures on scarce water resources. This is of serious note, as a pair of bullocks/cows/goats form a symbiotic and synergistic relationship with the farming community leading to sustainable agriculture, but commercialization has resulted in a greater shift from the existing practices. Efforts in the form of loans and other incentives should be given to encourage small livestock holdings.

Increased investment in wastewater treatment and reuse could yield good returns as the marginal cost of treatment, storage, and conveyance of purified wastewater for agriculture use will be only $\$0.13/m^3$. The introduction of tradable water rights will help move the water from less productive to more productive use. Farmers could also sell their water rights to the non-agriculture sector thus making the irrigation systems more competitive and challenging. Recently a neighboring Kerala state had ventured into an issue of bonds to raise capital for

implementing water projects. Such a venture could help to boost the morale of the public and encourage them to invest in developmental projects.

To increase the level of coordination between various sectors and implement projects in time and full commitment, a hierarchy of irrigation cooperatives should be formed at different levels with user participation for the operation and maintenance of systems. The placement of water issues in the top five of their manifestos to choose a political party to form the government is also a welcome sign in raising the water consciousness of people. In this regard, the concept of Built Operate and Transfer (BOT) or the Turn over the system, has already proved successful in minor irrigation schemes (Tank projects) and could present a solution for conflicts between users as opposed to uses. If minor changes are made in improving irrigation efficiency, reducing effluent discharges, and increasing the reuse of water in all sectors, they could help solve water problems and bring prosperity in the foreseeable future.

DATA AVAILABILITY STATEMENT

The datasets presented in this study can be found in online repositories. The names of the repository/repositories and accession number(s) can be found in the article/**Supplementary Material**.

ETHICS STATEMENT

Ethical review and approval was not required for the study on human participants in accordance with the local legislation and institutional requirements. Written informed consent to participate in this study was provided by the participants' legal guardian/next of kin.

AUTHOR CONTRIBUTIONS

The author confirms being the sole contributor of this work and has approved it for publication.

ACKNOWLEDGMENTS

The author sincerely thanks the reviewers and Professor Shafi Mohammad Tareq for reviewing this manuscript. The author thank his daughter Akshaya Suresh, XII Class student, Cluny Matriculation Higher Secondary School, Salem-7, Tamil Nadu and his wife K. Sathia Meena, Assistant Professor, Government College of Arts, Salem-7, Tamil Nadu for their support to write this manuscript. This paper is dedicated to the fond memory of the author's Master degree guide, (Late) Dr. M.V. Somasundaram, Professor and Scientist 'F' and his master degree professor in-charge (Late) Dr. S. Thayumanavan at Centre for Water Resources, College of Engineering, Guindy, Anna University, Chennai-600025, Tamil Nadu, India.

SUPPLEMENTARY MATERIAL

The Supplementary Material for this article can be found online at: https://www.frontiersin.org/articles/10.3389/feart.2021.663198/full#supplementary-material

REFERENCES

Bitterman., P., Eric., T., Itimberly, J., Van, M., and Nandita, B. B. (2016). Water Security and Rainwater Harvesting: A Conceptual Framework and Candidate Indicators. *Appl. Geogr.* 76, 75–84.

Chitra, M., and Laxmi, K. B. (2017). An Analysis on Supply of Water in Tamil Nadu. *Shanlax Int. J. Econ.* 5 (3), 48–54. Available at: https://www.researchgate.net/publication/331772076_An_Analysis_on_Supply_of_Water_in_Tamil_Nadu.

Census of India (2011). Census of India. Available at: https://censusindia.gov.in/2011-prov-results/data_files/tamilnadu/3.Tamil%20Nadu_PPT_2011-BOOK%20FINAL.pdf.

Cgwb (2000). CGWB. Available at: http://cgwb.gov.in/documents/ArtificialRecharge-Guide.pdf.

Cgwb (2017). CGWB. Available at: http://cgwb.gov.in/AQM/NAQUIM_REPORT/TAMILNADU/chennai%20Aquifer%20system.pdf.

Corporation of Tamil Nadu (2020). Corporation of Tamil Nadu. Available at: https://en.wikipedia.org/wiki/List_of_municipal_corporations_in_Tamil_Nadu.

DFID (2005). Engineering Knowledge and Research Programme: Water Demand Management in the Areas of Ground Water over Exploitation, A Report on Case Studies. Available at: https://assets.publishing.service.gov.uk/media/57a08c6b40f0b652dd0012fe/R8332-CaseStud.pdf.173

ENVIS (2020). Envis center: Tamil Nadu State Environmental and Related Issues. Available at: http://tnenvis.nic.in/Database/Industries_1167.aspx.

Glendenning, C. J., van Ogtrop, F. F., Mishra, A. K., and Vervoort, R. W. (2012). Balancing Watershed and Local Scale Impacts of Rain Water Harvesting in India-A Review. *Agric. Water Management* 107, 1–13. doi:10.1016/j.agwat.2012.01.011

Gollin, D., Parente, S., and Rogerson, R. (2002). The Role of Agriculture in Development. *Am. Econ. Rev.* 92 (2), 160–164. doi:10.1257/000282802320189177

ICID (2018). *International Commission of Irrigation and Drainage (ICID), 48 Nyaya Marg*. New Delhi: Chanakyapuri, 110021. Available at: https://www.icid.org/world-irrigated-area.pdf.

Municipality of Tamil Nadu (2020). Municipality of Tamil Nadu. Available at: https://tnrd.gov.in/databases/tn_municipality_details.pdf.

Natarajan, P. M., Ponnavaiko, M., Kalloikar, S., Rangaraju, G., and Ganesh, S. (2017). Sustainable Water Resources Development in Tamil Nadu India through Water Security Pathways. XVI World Water Congress, 1–19. Available at: https://iwra.org/member/congress/resource/ABSID139_ABSID139_WWC_1.pdf.

National Water Mission (20172017). State/UT Specific Action Plans (SSAP) on Water: Towards Water Security, Safety and Sustainability. Available at: http://nwm.gov.in/sites/default/files/SSAP%2029.10.2017%20with%20headnote.pdf.443445

Pal Tamas (2003). Water Resource Scarcity and Conflict: Review of Applicable Indicators and Systems of referenceTechnical Documents in Hydrology: PC-CP Series, SC.2003/WS/49, 1–37. Available at: https://unesdoc.unesco.org/ark:/48223/pf0000133307.

IPCC (2014). in *Climate Change 2014: Synthesis Report, Contribution of Working Groups, I, II and III to the Fifth Assessment Report of Intergovernmental Panel on Climate Change [Core Writing Team*. Editors R. K. Pachauri and L. A. Meyer (Geneva, Switzerland: IPCC), 1–151. Available at: https://www.ipcc.ch/site/assets/uploads/2018/05/SYR_AR5_FINAL_full_wcover.pdf

Ruttan, V. W. (1965). Growth Stage Theories and Agricultural Development Policy*. *Aust. J. Agric. Econ.* 9, 17–32. doi:10.1111/j.1467-8489.1965.tb00327.x

S, M., and N, R. (2014). Climate Change and its Impact on Irrigation Water Requirements on Temporal Scale. *Irrigat Drainage Sys Eng.* 03 (118), 2–10. doi:10.4172/2168-9768.1000118

Sivasankar, V., Ramachandramoorthy, T., and Chandramohan, A. (2012). Deterioration of Coastal Groundwater Quality in Island and mainland Regions of Ramanathapuram District-Southern India. *Environ. Monit. Assess.* 185, 931–944. doi:10.1007/s10661-012-2604-2

State of Indian Agriculture (2016). State of Indian Agriculture. Available at: https://agricoop.nic.in/sites/default/files/State_of_Indian_Agriculture%2C2015-16.pdf.

Statistical Hand Book (2016). Statistical Hand Book. Availableat: https://cdn.s3waas.gov.in/s313f3cf8c531952d72e5847c4183e6910/uploads/2018/06/2018062923.pdf.

Suresh, C. A., and Surender, K. (2011). "Challenges and Implications for Water Pricing Industrial Water Demand in India," in the India Infrastructure Report 2011, 274–281. Available at: https://www.idfc.com/pdf/report/2011/Chp-18-Industrial-Water-Demand-in-India-Challenges.pdf.

Suresh, S., and Somasundaram, M. V. (1996). *Towards a Comprehensive Water Policy for India with Special Reference to Tamil Nadu*. Sixth Stockholm Water Symposium, Stockholm, Sweden 277–279. Available at: https://www.ircwash.org/resources/safeguarding-water-resources-tomorrow-new-solutions-old-problems-proceedings-sixth.

Suresh, S. (2002). Sustainability of Integrated Water Resources Management in Indian River Basin with Special Reference to Flood. *Second Int. Symp. Flood Defence (Isfd'2002) Beijing* 1, 382–388. Available at: http://www.irtces.org/nszx/zt/isshhu/isfd10.htm#Volume%20I.

The Hindu (2014). The Hindu. Available at: https://www.thehindu.com/archive/web/2014/06/23/.

Vairavamoorthy, K., Gorantiwar, S. D., and Mohan, S. (2007). Intermittent Water Supply under Water Scarcity Situations. *Water Int.* 32 (1), 121–132. doi:10.1080/02508060708691969

Williams, R. B., and Al-Hmoud, R. (2015). Virtual Water on the Southern High Plains of Texas: The Case of a Nonrenewable Blue Water Resource. *Nr* 06 (1), 27–36. doi:10.4236/nr.2015.61004

Conflict of Interest: The author declares that the research was conducted in the absence of any commercial or financial relationships that could be construed as a potential conflict of interest.

frontiers in Earth Science

ORIGINAL RESEARCH
published: 01 November 2021
doi: 10.3389/feart.2021.741678

Rapid Loss of Dissolved CO_2 From a Subtropical Steep Headwater Stream

*Chun Ngai Chan[1], Cheuk Lam Tsang[1], Frederick Lee[2], Boyi Liu[1] and Lishan Ran[1]**

[1]Department of Geography, The University of Hong Kong, Pokfulam, Hong Kong, SAR China, [2]Centre for Water Technology and Policy, The University of Hong Kong, Pokfulam, Hong Kong, SAR China

High-gradient headwater streams are major participants in the carbon (C) cycle because of their capabilities of emitting a significant amount of carbon dioxide (CO_2). Notwithstanding, their CO_2 emissions have been largely overlooked in previous studies owing to their small water surface area and are sometimes strenuous to be measured because of their narrow channel widths and strong turbulence. This study examined the spatial and seasonal variabilities of CO_2 dynamics of a subtropical steep headwater stream fed by groundwater. Our study found that the pH and dissolved oxygen exhibited a general increasing trend away from the source of the headwater whereas the partial pressure of carbon dioxide (pCO_2) showed a downward trend. The stream water pCO_2 in the upper reach was found to be higher than the ambient level by 19–114 times, with an average drop of >70% at just 9.2 m from the groundwater source, demonstrating the potentially large emission of CO_2 into the atmosphere within this short distance. Additionally, the sampling works conducted further downstream revealed that the CO_2 derived from groundwater could almost completely dissipate within approximately half a kilometer downstream of the source. The concentrations of dissolved organic carbon and pCO_2 were also lower during the period with lower air temperatures in the headwater stream, indicating temperature-dependent metabolism and decomposition of organic matter in soil might modulate the C dynamics in the headwater stream, although the rapid gas exchange along the stream remained the determinative factor. Our findings reassert that headwater streams are an essential source of CO_2 and disregarding them from the studies of greenhouse gas emissions of inland waters would underestimate their potency to influence the global C cycle.

Keywords: carbon dioxide, carbon dioxide emissions, groundwater, carbon cycle, headwater streams

OPEN ACCESS

Edited by:
Shafi Mohammad Tareq, Jahangirnagar University, Bangladesh

Reviewed by:
Youhei Yamashita, Hokkaido University, Japan
Siyue Li, Southern Cross University, Australia

****Correspondence:***
Lishan Ran
lsran@hku.hk

Specialty section:
This article was submitted to Biogeoscience, a section of the journal Frontiers in Earth Science

Received: *15 July 2021*
Accepted: *11 October 2021*
Published: *01 November 2021*

Citation:
Chan CN, Tsang CL, Lee F, Liu B and Ran L (2021) Rapid Loss of Dissolved CO_2 From a Subtropical Steep Headwater Stream. Front. Earth Sci. 9:741678. doi: 10.3389/feart.2021.741678

INTRODUCTION

There has been a growing number of studies showing that carbon dioxide (CO_2) emissions from inland waters into the atmosphere have substantial repercussions on the regional and global carbon (C) cycle. Headwater streams are a crucial component of the water cycle because they dominate the riparian interface in the world and account for approximately 80% of the Earth's perennial channels (Downing et al., 2012; Schneider et al., 2020). Headwater streams are also important players in the global C cycle as they receive different forms of C from surrounding environments, with running waters as the "vehicles" that transport these C downstream (Duvert et al., 2018). They can also provide an environment for the development of metabolic processes such as respiration that lead to gaseous C emissions, while aquatic sediments do not typically store substantial amounts of terrestrial

C (Bernal et al., 2013; Argerich et al., 2016; Schneider et al., 2020). Studies that analyzed rivers and streams worldwide also showed that greenhouse gas (GHG) emissions decrease with increasing Strahler stream orders, and the amount of annual GHG emission from first order headwater streams is the highest, highlighting they are a hotspot for GHG emissions (Ran et al., 2021a; Li et al., 2021). A regional study on the CO_2 emissions from inland waters also observed 61% of the flux is attributable to first and second order streams in China (Ran et al., 2021a). Additionally, past research on the partial pressure of CO_2 (pCO_2) of stream networks in boreal regions revealed a general decreasing trend of pCO_2 and CO_2 evasion flux with stream order (Crawford et al., 2013; Wallin et al., 2013). It has been suggested that approximately 36% of the global CO_2 emitted from lotic systems is sourced from headwaters (Marx et al., 2017). During the high-flow period when the hydrological connectivity is the highest in a year, CO_2 evasion from headwater streams can even dominate the aquatic CO_2 loss (Gómez-Gener et al., 2016). These studies unequivocally demonstrated that headwater streams have a significant role to contribute to the global C cycle. In addition, when a headwater stream is connected to a CO_2-enriched groundwater source, the rapid evasion of CO_2 along the stream may also enable it to serve as an important conduit for terrestrially-respired C (Johnson et al., 2008; Duvert et al., 2018). For determining the extent to which a system is affected by groundwater input, measurement of radon-222 concentration has been identified to be one of the promising solutions (Wu et al., 2004; Mullinger et al., 2007).

Despite the prominence of headwater streams in the C cycle, they have largely been overlooked in C cycle studies because of their narrow width and strong turbulence, making them difficult to use traditional methods, including floating chamber or tracer gas, to estimate the GHG emissions. Furthermore, their water surface area is subject to significant seasonal variations which is the underlying cause of the huge uncertainties in documenting the length and area of streams on both regional and global scales (Benstead and Leigh, 2012; Wallin et al., 2013; Horgby et al., 2019b). These systems can have particularly high emission rates due to their common associations with steep slopes, high flow velocities, and rough riverbeds (Schelker et al., 2016; Maurice et al., 2017; Aho and Raymond, 2019; Horgby et al., 2019b; Ulseth et al., 2019). The substantial differences in the CO_2 concentration between headwater streams and the ambient air is another factor that elevates the emission rate of CO_2. Headwater streams are typically supersaturated in CO_2 owing to a number of factors, such as the mobilization of organic C arising from the degradation of organic matters, the input of CO_2-enriched groundwater, as well as the influence of carbonate-dominated catchment lithology (Davidson et al., 2010; Marx et al., 2017; Duvert et al., 2018). It has also been postulated previous studies might have underestimated the magnitude of catchment-scale CO_2 degassing flux because samples were collected distant from the groundwater source, thereby having a great potential of underestimating the contribution of groundwater inputs and obscuring the impacts of CO_2 evasion (Johnson et al., 2008; Duvert et al., 2018).

Although the relatively small water surface area covered by a single headwater stream signifies that the GHG emissions from an individual headwater stream may not be significant, they are still likely to make a substantial contribution to the global C budget due to their sheer numbers on a global scale. It has been estimated that first—third order systems comprise nearly 48% of the surface area of all rivers and streams globally (Li et al., 2021), implying a substantial fraction of GHG emissions from lotic systems are contributed by low-order headwater streams. Furthermore, the CO_2 dynamics (i.e., pCO_2 and CO_2 emission rate) of headwater streams are spatially and temporally heterogeneous, adding to the difficulty in the accurate quantification of their roles in the global C cycle (Crawford et al., 2017). Although the difficulty of this task cannot be understated, given the above factors, there is a genuine need to better characterize and quantify GHG emissions from headwater streams in order to render greater accuracy to relevant studies in the future. When these studies are more accurately reflective of the actual scale of the GHG emissions, a more comprehensive understanding of the factors contributing to climate change may be gained.

In this study, the spatio-temporal patterns of pCO_2 of a high-gradient forested headwater stream fed by groundwater in subtropical Hong Kong were analyzed. We paid particular attention to the rate of CO_2 degassing from this headwater stream into the atmosphere. The relationships of pCO_2 with selected environmental and hydrological variables, such as pH, dissolved oxygen (DO), and dissolved organic carbon (DOC), were also investigated to identify the potential drivers that have regulated the C dynamics in the studied headwater stream.

MATERIALS AND METHODS

Study Site

This study was conducted in a headwater stream in the Pokfulam catchment (area: 1.7 km^2) in subtropical Hong Kong (22°16′00″N—22°16′08″N, 114°08′25″E—114°08′41″E, **Figure 1**). The bedrock geology of the study area is dominated by early Cretaceous volcanic rocks (Fletcher, 1997). The annual precipitation is approximately 2,400 mm and the climate is classified as Cwa (monsoon-influenced humid subtropical climate) according to the Köppen climate classification (Cheung et al., 2019). The altitude of the groundwater resurgence is 258 m above the sea level (m.a.s.l.) (**Figure 1C**). It was fed by groundwater and the groundwater resurgence was visible. A total of nine sampling campaigns were conducted at a monthly interval from June 2020 to February 2021 at the beginning of each month and 7 water samples were taken from the first 520 m of the headwater stream at the sampling sites of 0 m (Site A, the groundwater resurgence), 1.3 m (Site B), 3.3 m (Site C), 5.1 m (Site D), 6.7 m (Site E), 9.2 m (Site F), and 520 m (Site G) from the headwater stream respectively during each field campaign (**Figures 1C,D**). Sites A—F and site G are defined as the upper reach and lower reach of the headwater stream, respectively. The average slope of the stream reach from site A to F and site F to G is 24.7 and 7.8%, respectively. There is a

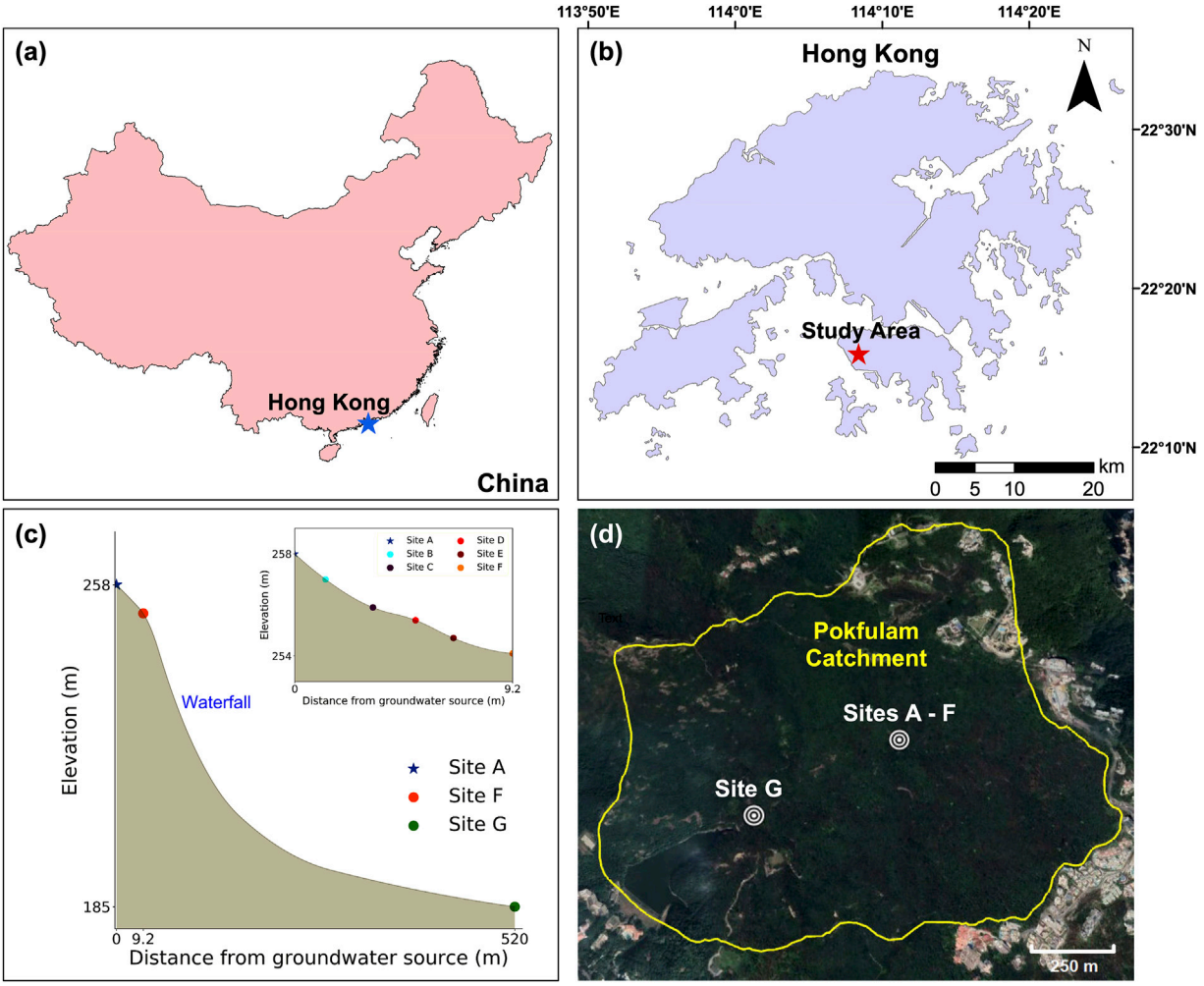

FIGURE 1 | Location map of the study area **(A,B)**, the schematic diagram showing the changes in elevation from site A to G (not scaled) **(C)**, and the enlarged satellite image obtained from Google Earth showing the locations of the study sites, i.e., sites A—F and site G and the boundary of the Pokfulam catchment **(D)**.

waterfall immediately downstream of site F and site G is located downstream of the waterfall (**Figure 1C**). The sampling sites were selected to characterize the potential evasion of CO_2 along the reach and for illustrating the longitudinal changes in water chemistry and C properties. Based on the climatic characteristics of Hong Kong, June to October is defined as the "wet season" and November to February as the "dry season" in this study. The meteorological data from the Hong Kong Observatory suggested that June to October on average account for >70% of the annual precipitation whereas this figure is only around 5% for November to February (Hong Kong Observatory, 2021).

Sampling Procedures and Laboratory Analysis

At each site, approximately 500 ml of stream water was collected by using a polyethylene bottle. All the polyethylene bottles were thoroughly cleaned and sterilized prior to each field campaign and were filled completely with stream water without headspace. At Sites A and G, an additional 9 L of water was collected without headspace for analyzing the radon-222 concentration in the laboratory.

The basic water quality parameters, including pH, electroconductivity (EC), and DO at each sampling site was measured by using a ProDSS Multiparameter water quality meter (YSI, Yellow Springs, Ohio, United States). The water quality meter was calibrated with two pH buffer solutions (pH = 4.00 and 7.00) prior to each sampling work to ensure the accuracy of pH measurement. The water collected in the polyethylene bottle was filtered using 47 mm GF/C filter paper with a pore size of 1.2 μm (Whatman, Maidstone, United Kingdom), and alkalinity and dissolved organic carbon (DOC) were subsequently measured in the laboratory. 20 ml of sample was titrated with 0.05 M hydrochloric acid (HCl) to determine the alkalinity, using methyl orange as the indicator. A 60 ml subsample was prepared from the filtered water and acidified by concentrated sulfuric acid to pH < 2 for the measurement of DOC concentration. The determination of

alkalinity and acidification of the subsample were carried out immediately upon the return of the laboratory and within the same day of the sampling. The acidified subsamples were then preserved in a refrigerator at 4°C until analysis, usually for 1 week. The DOC concentration was assessed by a TOC-L TOC analyzer (Shimadzu, Kyoto, Japan) using high-temperature combustion method with triple injections and an error of <2%. The standard used was 10 mg C L^{-1} potassium hydrogen phthalate. The stream discharge has been measured at sites A and G by using salt dilution gauging as reported in Moore (2004).

The pCO_2 of the stream water at each site was measured by the headspace equilibrium method *in-situ* immediately after sampling (Campeau et al., 2014; Ran et al., 2021b). Briefly, 400 ml of water sample was collected in a reagent bottle with a capacity of 610 ml, while the remaining space was filled with ambient air, thus giving a water to headspace ratio of 1.91:1. The bottle was subsequently closed with a lid and shaken vigorously for at least 2 min for equilibrating the pCO_2 between water and the headspace prior to the connection of a Li-850 CO_2 analyzer (LI-COR, Lincoln, Nebraska, United States). The measurements of the headspace pCO_2 were done in duplicate with repeatability better than 5%, and the values of original stream water pCO_2 were accordingly computed from the headspace ratio, solubility constant of CO_2, and temperature (Koschorreck et al., 2021). The calculation of average areal evasion flux of CO_2 within the headwater stream was done in two steps. Firstly, the total amount of CO_2 loss along the reach was estimated by the differences in the pCO_2 between sites A and F and then multiply by the discharge at site A. Secondly, the average areal evasion flux of CO_2 was calculated by dividing the total amount of CO_2 loss along the reach by the estimated surface area of the reach.

The water collected at sites A and G was analyzed for radon-222 concentration with a RAD7 radon detector (Durridge, Billerica, Massachusetts, United States) in laboratory within 2 h after collection to determine the groundwater signature at sites A and G. It usually took approximately 30–45 min for the reading of radon-222 to reach equilibrium. The gap between the time of water collection and radon-222 measurement was considered unlikely to have a substantial effect on the experimental results because of the relatively short half-life of radon-222, which is about 3.8 days (Dimova et al., 2013).

Statistical Analyses

The statistical analyses were executed by IBM SPSS Statistics (Version 27). Apart from pH, the mean values of the parameters were presented as mean ± standard deviation. The two-sample independent *t*-test was conducted to test for the differences in the mean of variables between the dry season and wet season. The Pearson correlation coefficient (r) was selected to assess the strength of a linear association between two variables. The threshold of the *p*-value to be regarded as statistically significant was 0.05.

RESULTS

Patterns of General Water Chemistry

The mean EC ranged from 43.9 to 50.4 μS cm^{-1}, with a mean of 47.2 ± 1.4 μS cm^{-1} and exhibited a slight downward trend downstream from site A to F (**Figure 2A**). The mean EC at site F was 2.8 μS cm^{-1} lower than that of site A. The DO was always undersaturated with a range from 68.4 to 95.1% and a mean of 85.9 ± 6.3%, exhibiting a significant increasing trend downstream (**Figure 2B**). The mean DO at site F was 14.2% higher than that of site A, and stream water with DO < 80% was observed mainly at sites A and B. The stream water was acidic with pH ranging from 4.53 to 5.63 and a mean of 5.07, exhibiting a significant increasing trend downstream (**Figure 2C**). The mean pH value at site F was approximately on average 0.32 units higher than site A, and stream water with pH < 5 was mostly found at sites A, B, and C. The alkalinity did not display significant spatial differences along the reach, ranging from 125 to 206 μmol L^{-1}, with a mean of 159 ± 22 μmol L^{-1} (**Figure 2D**). The DOC varied between 0.40 and 5.73 mg C L^{-1} with a mean of 1.38 ± 1.10 mg C L^{-1}. There was a generally decreasing trend in DOC downstream during the dry season, with the mean DOC concentration decreased progressively from 1.15 mg C L^{-1} at site A to 0.48 mg C L^{-1} at site F, but this tendency was not observed during the wet season (**Figure 2E**). The discharge measured at site A ranged from 0.23 to 0.63 L s^{-1} with a mean of 0.37 ± 0.13 L s^{-1}, and the average stream width was 0.2 m. The mean discharge during the wet and dry seasons was 0.42 ± 0.18 and 0.33 ± 0.04 L s^{-1}, respectively (**Figure 2F**). Radon-222 concentrations at site A often reached high levels, exceeding 100,000 Bq m^{-3} in most sampling months with a mean of 101,720 ± 18,880 Bq m^{-3} (**Figure 2G**). The mean DOC was significantly lower in the dry season than in the wet season (p < 0.05, Two-sample *t*-test, **Figure 2E**), while no significant differences in EC, DO, pH, and alkalinity between the dry and wet seasons were found (p > 0.05, Two-sample *t*-test, **Figures 2A–D**).

For site G, the mean EC, DO, pH, alkalinity, and DOC were 92.6 ± 12.9 μS cm^{-1}, 100.5 ± 0.8%, 7.13, 211 ± 21 μmol L^{-1}, and 1.15 ± 0.31 mg C L^{-1}, respectively (**Figures 3A–E**). DO and DOC were significantly higher in the wet season than the dry season (p < 0.05, Two-sample *t*-test) while the seasonal differences of the remaining variables were not statistically significant (p > 0.05, Two-sample *t*-test). The mean EC, DO, pH, and alkalinity at site G were significantly higher than that of sites A—F (p < 0.05, Two-sample *t*-test). The mean radon-222 concentration at site G was 562 ± 168 Bq m^{-3}.

Temporal and Spatial Variations of Partial Pressure of Carbon Dioxide

The atmospheric pCO_2 was determined to be 410 μatm based on the average value in 2020. The stream water at sites A—F was significantly supersaturated with CO_2 with the pCO_2 ranging from 7,890 to 46,750 μatm (mean: 22,940 ± 9,840 μatm), which was equal to supersaturation of 19–114 times with respect to atmospheric equilibrium (**Figure 4**). Concerning the temporal variability of the pCO_2, the mean pCO_2 during the wet season and dry season were 23,680 ± 9,810 and 22,010 ± 10,000 μatm, respectively, with the highest values in September and the lowest values in January (**Figure 4**). The mean pCO_2 at sites A and F were 38,590 ± 5,780 and 10,820 ± 1,880 μatm, respectively, implying approximately 72% of

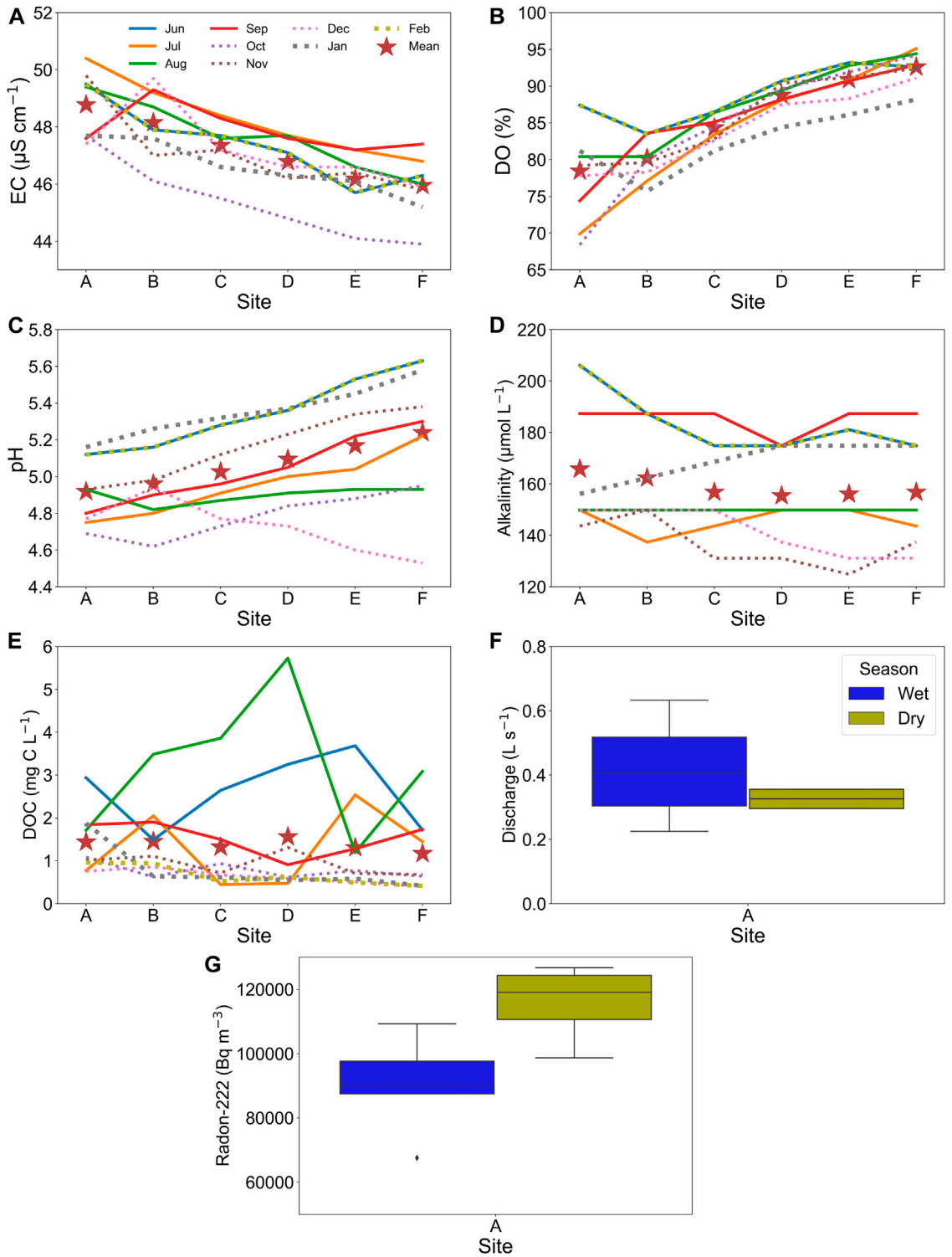

FIGURE 2 | Plots summarizing the monthly water quality variables, including EC **(A)**, DO **(B)**, pH **(C)**, alkalinity **(D)**, and DOC **(E)** of sites A—F, and discharge **(F)** and radon-222 **(G)** of site A between wet and dry seasons in the headwater stream.

the stream CO_2 has been lost over the 9.2-m distance along the headwater stream (**Figure 4**). The pCO_2 recorded at site G was significantly lower than that of sites A—F with the range of 533–1,590 µatm (mean: 778 ± 317 µatm) (**Figure 4**). The mean pCO_2 at site G during the dry and wet seasons were 674 ± 114 and 861 ± 414 µatm, respectively.

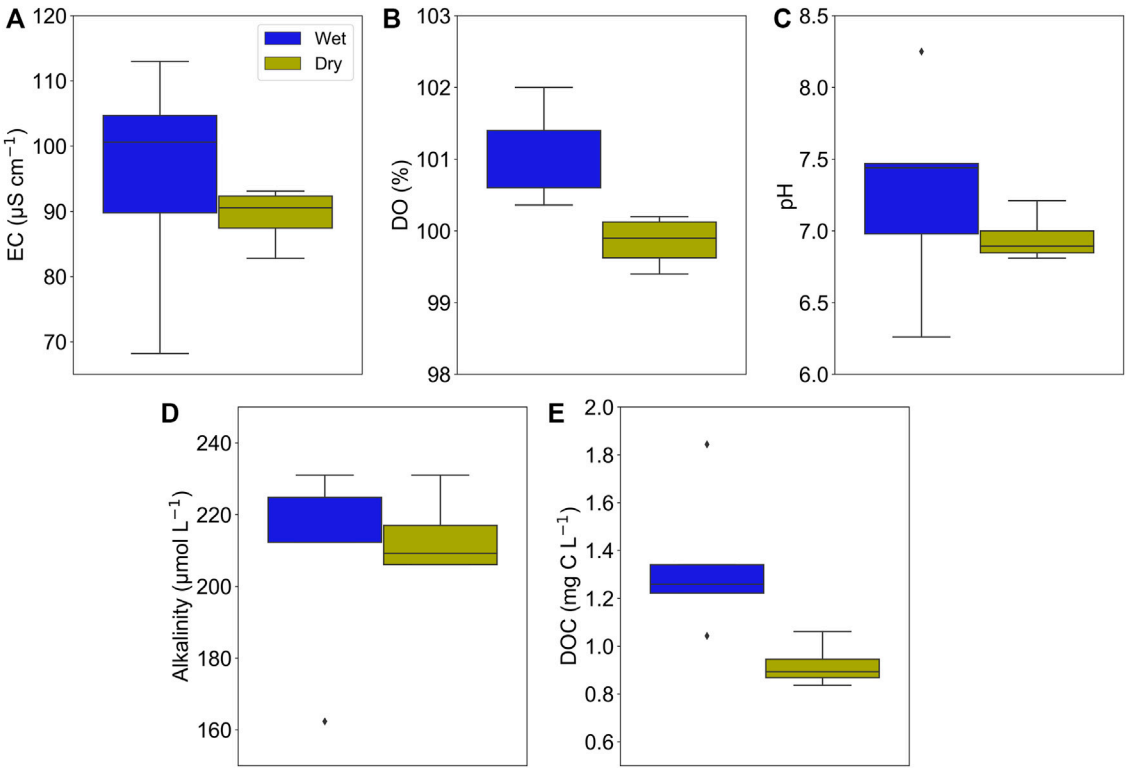

FIGURE 3 | Boxplots summarizing the water quality variables (EC, DO, pH, alkalinity, and DOC) of site G between wet and dry season.

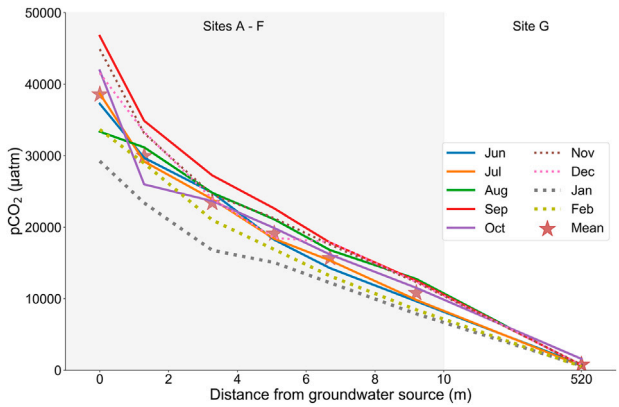

FIGURE 4 | The longitudinal changes in pCO_2 as a function of distance downstream from the groundwater source.

TABLE 1 | The monthly values of Pearson correlation coefficient (r) of pCO_2 with water quality variables in the headwater stream at sites A—F.

	DO	pH	DOC
June	−0.80	−0.97[a]	−0.07
July	−1.00[a]	−0.96[a]	−0.27
August	−0.99[a]	−0.50	−0.05
September	−0.99[a]	−0.95[a]	0.47
October	−0.99[a]	−0.76	0.74
November	−0.90[a]	−0.96[a]	0.44
December	−0.96[a]	0.74	0.88[a]
January	−0.77	−0.97[a]	0.82[a]
February	−0.82[a]	−0.97[a]	0.94[a]

[a]*Correlation is significant at the* $\alpha = 0.05$ *level (2-tailed).*

Relationship of Partial Pressure of Carbon Dioxide With Water Quality Parameters

For sites A—F, the pCO_2 always exhibited a negative relationship with DO, and the correlations of pCO_2 with DO and pH were significant in six out of 9 months with the magnitude of r higher than 0.9 (**Table 1**). The relationship of DOC with pCO_2 was less prominent and consistent compared to that of DO and pH since the r ranged from −0.27 to 0.94, and the relationship was only significant during the dry season from December to February. The values of r of pCO_2 with radon-222 and discharge were 0.33 and 0.01, respectively at site A, and both relationships were not statistically significant. For site G, the pCO_2 had a positive significant relationship with discharge ($p < 0.05$, **Table 2**) while the relationships with DO, pH, DOC, and radon-222 were not statistically significant ($p > 0.05$, **Table 2**).

DISCUSSION

General Chemistry of the Stream Water

Our measurements on the water quality parameters suggested that the chemistry of the headwater stream is heavily influenced

TABLE 2 | The values of Pearson correlation coefficient (r) of pCO_2 with water quality variables at site G of the headwater stream.

Parameters	Correlation Coefficients
DO	−0.03
pH	−0.56
DOC	−0.16
Discharge	0.90[a]
Radon	0.25

[a]*Correlation is significant at the α = 0.05 level (2-tailed).*

by groundwater. Since the EC values remained fairly constant and low under all months of sampling, this indicated that the headwater stream had no signs of saltwater intrusion from the surrounding environment.

The general increase in pH along the downstream direction was a manifestation of the decrease in CO_2 concentration due to degassing (Johnson et al., 2008). There was an occasion in which the pH at sites C—F remained low with the value lower than 5, and this might be attributable to the introduction of anthropogenic acidic substances into the stream or soil which resulted in a drop in the pH value (**Figure 2C**). As the concentration of DO also increased downstream owing to intense gas exchange (Dick et al., 2016), this was likely the reason for the significant positive association between pH and DO in the headwater stream. However, there have been a couple of instances with DO showing a slight decrease from site A to site B, and we suggest that the decomposition of OC along this distance may be a possible reason for this trend. Our measurements were consistent with the theoretical correlation between alkalinity and pH since an increase in pH leads to the production of chemically sequestered bicarbonate ions, a component of alkalinity (Piñol and Avila, 1992; Abril et al., 2015). There was also a general decreasing trend in the DOC concentration within sites A—F of the headwater stream during the dry season (**Figure 2E**), potentially due to in-stream metabolic processes such as mineralization of organic carbon (OC) and by the dilution of DOC-depleted water downstream (Duan et al., 2017). However, this decreasing trend was obscured in the wet season likely because of the capability of heavy rainfall events displacing terrestrially derived OC from the upstream catchment and riparian areas along the reach, which also led to up to more than twofold higher levels of DOC in the headwater stream during the wet season (**Figure 2E**) (Pumpanen et al., 2014; Panton et al., 2020). The generally higher discharge during the wet season might also reduce the water residence time which had the potential to impact the duration of OC mineralization that occurred along the reach (Wickland et al., 2007). Additionally, the variabilities of DOC were higher in the wet season than in the dry season (**Figure 2E**), especially at sites A—F, potentially owing to the sporadic and incidental nature of heavy rainfall events that brought about an increase in DOC levels.

Carbon Dioxide Exchange Dynamics

The pCO_2 was mostly two orders of magnitude higher than the ambient air at sites A—F along the headwater stream, and it was even >100 times higher at sites immediately adjacent to the groundwater source (**Figure 4**), indicating the reach was a consistent source of CO_2. This observation was consistent with the pCO_2 values obtained from headwater stream networks elsewhere in the world (Dawson et al., 2002; Crawford et al., 2013; Winterdahl et al., 2016; Crawford et al., 2017; Li et al., 2021). Because the mean pCO_2 value recorded at site A was in good agreement with the mean value (51,900 ± 1,600 ppmv) of Amazonian deep soil for emergent groundwater reported previously (Johnson et al., 2008) and fell within the range of the groundwater pCO_2 in Swiss mountain catchments and Ganges River catchment (Horgby et al., 2019b; Manaka et al., 2019), it is of high confidence that the high pCO_2 in the headwater stream is contributed by the CO_2-enriched groundwater. The elevated pCO_2 level in groundwater was likely the result of root respiration as well as the microbial respiration of organic matter and its decomposition in surrounding soils (Crawford et al., 2013; Deirmendjian and Abril, 2018; Horgby et al., 2019a; Manaka et al., 2019). The C dynamics of headwater streams located in upper reaches are more profoundly influenced by terrestrially sourced C when compared with large rivers, and therefore they are less sensitive to in-stream metabolism (Johnson et al., 2008; Hotchkiss et al., 2015; Argerich et al., 2016; Deirmendjian and Abril, 2018; Wang et al., 2021). Furthermore, a larger proportion of stream water was in contact with adjacent soil horizons, allowing a stronger hydrological connection between CO_2-rich soils and surface water, contributing to high pCO_2 values in groundwater (Crawford et al., 2013; Schneider et al., 2020). Because the study area is dominated by volcanic rocks without extensive coverage of carbonate rocks, the dissolution of carbonate rocks is highly unlikely to occur and thus cannot be the underlying cause of the elevated pCO_2 in the groundwater (Duvert et al., 2018; Wang et al., 2021).

The rate of decline in pCO_2 along the reach was analogous to the Johnson et al. (2008) study, which developed a model showing a 77% reduction in dissolved CO_2 at 9.2 m from the groundwater spring and was even more rapid than a headwater stream in southwestern France, which exhibited a 70% loss of pCO_2 at 40 m downstream of the groundwater resurgence (Deirmendjian and Abril, 2018). The median percentage of CO_2 loss in the first 100 m from groundwater sources in 15 streams worldwide covering tropical, temperate, and boreal catchments was 76% (Duvert et al., 2018). Our pCO_2 measurement unequivocally indicated the evasion of CO_2 along the reach was very substantial and occurred immediately upon entry of the groundwater into the surface stream (Pu et al., 2019). This observation was particularly salient because it reflected the presence of very active gas exchange triggered by strong turbulence in this high gradient headwater stream fed by groundwater and illustrated that groundwater with exceptionally high CO_2 content had a diminishing effect on stream pCO_2 values with increasing distance downstream (Duvert et al., 2018).

Additionally, our fieldwork results indicated the evasion of CO_2 along the stream via outgassing was responsible for the gradual equilibration of CO_2 in the stream with the atmosphere (Duvert et al., 2018; Schneider et al., 2020). The simultaneous increase in the DO concentrations downstream further

corroborated the strong and rapid gas exchange in this headwater stream since its turbulent nature allowed oxygen to seep and dissolve into the stream water (Dick et al., 2016), and also permitted CO_2 to be released into the atmosphere, yielding the aforementioned pCO_2 and DO trend. In addition, DO and pCO_2 measurements at site G further confirm that water-air gas exchange to reach equilibrium, and complete evasion of groundwater CO_2, was likely to be achieved within 520 m of the groundwater source since the DO consistently reached saturation regardless of the sampling month, while pCO_2 fell to the level similar to the ambient level. This distance was even shorter than that of a previous study which suggested that a majority of the CO_2 in headwater streams sourced from groundwater might be degassed within a few kilometers (Davidson et al., 2010). We argue that this exceptionally large decline in the pCO_2 level might be attributed to the presence of a waterfall between sites F and G. Several previous studies have elaborated on the importance of waterfalls in the emission of CO_2 from freshwater ecosystems due to their abilities in triggering turbulence and favoring gaseous exchange through bubble-mediated transfer, which in turn produced a significant decrease (>50%) in pCO_2 after the stream water passing through waterfalls (Teodoru et al., 2015; Leibowitz et al., 2017; Looman et al., 2021). Because the CO_2 dynamics at downstream locations could be driven by interactions of multiple biogeochemical processes, such as community respiration, primary production, precipitation of minerals, and input of nutrients and CO_2 from immediate surroundings (Davidson et al., 2010; Atkins et al., 2013; Peter et al., 2014; Duvert et al., 2018), the precise quantification of the fraction of groundwater-derived CO_2 remained at site G remains an arduous task. Yet, the enormous decrease in radon-222 concentration by > 99% from site A to G as well as the observed DO and pCO_2 longitudinal trends at least demonstrated that the stream water has lost most of its groundwater signature over this distance.

Our longitudinal pCO_2 results were consistent with the findings observed by Schneider et al. (2020) study, who showed a higher pCO_2 in the upper portion of the stream and declined in the lower reaches, although our study reach was even shorter than the study and the pCO_2 at the source of groundwater was an order of magnitude higher. Another similar study also reported that the significant drop of the differences between the concentration of CO_2 in the stream water and the ambient air in first order streams could be ascribed to highly efficient gas exchange resulting in significant CO_2 loss along the reach (Schelker et al., 2016). Based on the above comparisons, our research data revealed that the evasion of CO_2 along the headwater stream is governed by groundwater input and extremely likely to play a pivotal role in the C dynamics (Deirmendjian et al., 2018). Assuming the decline in pCO_2 derived from groundwater along the reach was solely attributable to the evasion of CO_2 with the contribution of in-stream metabolism being negligible, our measurements on pCO_2 and discharge data estimated that the average areal evasion flux of CO_2 from site A to F and from site F to G amounted to 19,000 and 140 mmol m^{-2} d^{-1}, respectively. The former flux was two orders of magnitude higher than previous CO_2 emission fluxes in stream networks that range from 180 to 920 mmol m^{-2} d^{-1} (Butman and Raymond, 2011; Crawford et al., 2013; Crawford et al., 2014; Wang et al., 2017). Therefore, our measurement indicated the water surface of the upstream region of a catchment is capable of emitting significantly more CO_2 per unit area, in agreement with a groundwater study conducted in an alpine stream network which highlighted the CO_2 emissions from mountainous streams in zones of local groundwater upwelling can outweigh those located in lowland areas (Horgby et al., 2019a). Despite the small water surface area, the CO_2 emission from the first few tens of meters of a groundwater-fed headwater stream is potentially huge and must be considered for obtaining an accurate estimation of the reach-scale CO_2 flux. Waterfalls and cascades along stream reach, on the other hand, may also facilitate the outgassing of CO_2 and their contributions to reach- and catchment-scale CO_2 emissions merit further investigation.

Environmental Factors Affecting Carbon Dioxide Dynamics

The CO_2 dynamics within the headwater stream were found to be statistically correlated with a few water quality and environmental parameters. Firstly, the significant negative correlation between the DO and pCO_2 level in most sampling months (**Table 1**) at sites A—F was consistent with the Li et al. (2021) study covering global rivers, and we anticipated this negative correlation was likely a consequence of rapid gas exchange since the turbulent nature of this headwater stream permits outgassing of a significant amount of CO_2, causing a large decrease in the pCO_2 within a short distance. At the same time, the intense turbulence triggered by steep slopes also resulted in a high rate of reaeration along the stream which led to the rapid replenishment of oxygen from the ambient air and thus a significant increase in DO levels (Huang et al., 2017). At site G, the DO levels were approximately similar regardless of the sampling month, so this could be a potential explanation for the lack of association between dissolved oxygen and pCO_2 levels (**Table 2**). As anticipated, the significant negative pH-pCO_2 relationship (**Table 1**) is likely to be attributed to the dissolution of CO_2 in water lowering the pH.

The lack of strong and consistent association between pCO_2 with the DOC concentration in the headwater stream (**Tables 1** and **2**) has also been documented in previous studies conducted in different parts of the world with varying climate conditions (Nydahl et al., 2017; Horgby et al., 2019a; Luo et al., 2019), and this reflected the mineralization of organic C is unlikely to be the primary source of pCO_2 in this headwater stream (Winterdahl et al., 2016). Although DOC concentration has been hypothesized to be positively associated with pCO_2 level in riverine systems owing to the *in-situ* oxidation of organic matter (Nydahl et al., 2017), the rapid outgassing of CO_2 in this system may attenuate the strength of the pCO_2—DOC relationship along the reach, reflecting the fact that the level of DOC concentration might play an auxiliary role in modulating pCO_2 while the intense gas exchange was still the fundamental factor in controlling the C dynamics. In addition, the increase in DOC is occasionally

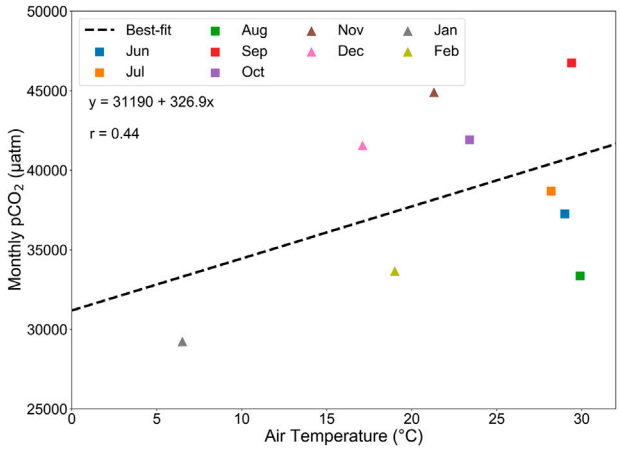

FIGURE 5 | The relationship between monthly pCO_2 at site A and ambient temperature. The dashed line represents the best-fit line of the regression.

associated with an increase in precipitation, but the dilution of stream water CO_2 is possible when precipitation increases, thus obscuring the relationship between the two variables (Luo et al., 2019). Our results support the existence of this precipitation-induced dilution effect since significant positive pCO_2—DOC relationships were only recorded during dry season when the precipitation was low (**Table 1**). Apart from the quantity of DOC, it has also been suggested the chemical properties and degradability of DOC had a role to play in determining the pCO_2 level, while these properties could be impacted by changes in vegetation type and water residence time (Wickland et al., 2007; Dinsmore et al., 2013; Luo and Li, 2021). Thus, a more specific chemical analysis on the properties of DOC in streams is likely to better constrain the processes leading to pCO_2 variabilities in headwater streams. Nonetheless, the results of our current study do not unambiguously preclude the possibility of organic C mineralization in influencing pCO_2 level within the headwater stream, though its effect should be appreciably less influential than that of longitudinal evasive CO_2 loss.

Furthermore, we also found that the CO_2 dynamics of the headwater stream might be influenced by the ambient air temperature since there was a positive relationship between the monthly pCO_2 at site A and air temperature ($r = 0.44$, **Figure 5**). In addition, January and September were the 2 months with the lowest and highest average pCO_2 values in the stream, while the air temperature was the lowest and second highest (**Figure 5**). Thus, we suggested that the observed seasonal variabilities in pCO_2 could be ascribable to the temperature-dependent metabolic activities because the higher temperature in summer months might have facilitated heterotrophic and root respiration in soil, and the downward diffusion of soil CO_2 will lead to a surge in pCO_2 values within the studied headwater stream (Jones and Mulholland, 1998; Deirmendjian and Abril, 2018). This has also been observed in a regional stream study that reported significantly higher pCO_2 levels in summer than spring in headwaters (Jones and Mulholland, 1998). Although the effect of stormwater dilution on groundwater CO_2 has been reported previously (Deirmendjian and Abril, 2018), it might not be a significant factor in regulating the pCO_2 levels in the section of the headwater stream close to the groundwater source because of an absence of the relationships between the discharge and pCO_2 at site A. In contrast, there was a significant positive correlation of pCO_2 with discharge at site G (**Table 2**), and the cause of this relationship might be independent of DOC input since there was no significant relationship between discharge and DOC. Thus, it is hypothesized that such a relationship in the lower reach could be attributable to the increased runoff from the upper catchment area that was enriched in CO_2 (Dinsmore et al., 2013).

Implications for Quantifying Carbon Dioxide Emissions From Stream Networks

Based on our sampling efforts, a close linkage was found between the groundwater and stream networks (Duvert et al., 2018), and the contribution of CO_2 from groundwater and outgassing of CO_2 along the reach was considered to be the primary determinants of C dynamics in this headwater stream. Although other environmental variables including DOC concentration and ambient air temperature might also be capable of regulating pCO_2 levels in the studied headwater stream, the changes were substantially more modest as compared to the longitudinal changes in pCO_2, even at distances of less than 10 m. Additionally, the influence of groundwater in pCO_2 within the catchment was almost varnished at a distance of up to 520 m. This finding is prominent and highlights the necessity of future works focusing on exploring the possibility of other high-gradient headwater streams fed by groundwater having similarly high outgassing rates. On top of that, our study demonstrated that the upstream section of headwaters fed by groundwater are conceivable hotspots of CO_2 emission since the flux can be several orders of magnitude higher than the previously reported stream networks with varying topography and climatic conditions. Because of the rapid gas exchange in high-gradient headwater streams, strong spatial heterogeneities in C dynamics are also occasionally detectable within a catchment. Therefore, the resulting estimates are likely to underestimate the true C flux if these headwater systems are not duly and adequately accounted for when quantifying the landscape-scale C budget (Deirmendjian and Abril, 2018; Aho and Raymond, 2019). The geomorphological characteristics of headwater streams, such as stream bed roughness and slope, are also subject to spatial heterogeneities that result in localized zones with strong turbulence and hence evasion (Duvert et al., 2018), and our results emphatically showed that the physical and biochemical processes controlling pCO_2 may differ in headwater streams fed by groundwater and its downstream section. Therefore, a more intensive study of the variations of these processes and mechanisms with respect to changes in location within a headwater stream is a promising direction for future research on the C dynamics.

CONCLUSION

Our sampling on a high-gradient headwater stream fed by groundwater in Hong Kong indicated that headwater streams are prominent emitters of CO_2. The pCO_2 levels of the upper reaches of the headwater stream were 19–114 times higher than the atmosphere and dropped by approximately 72% over a distance shorter than 10 m from the groundwater resurgence, indicating that a substantial share of the CO_2 derived from groundwater has been outgassed into the atmosphere within such a short distance. We also found that the groundwater signature and the effect of elevated CO_2 from groundwater could be completely dissipated at a distance of up to 520 m based on the pCO_2, DO, and radon-222 measurements at the lower reach of the headwater stream. Meanwhile, other water quality parameters, such as DO, DOC, EC, and pH, also exhibited longitudinal changes within the headwater stream, and pCO_2 was found to be significantly associated with several water quality parameters including pH and DO. Although other environmental drivers, for example, the ambient temperature and the availability of DOC for metabolic activities may also modulate the pCO_2 pattern, the intense gas exchange triggered by turbulence remains the overriding factor controlling the C dynamics in this headwater stream. The existence of waterfalls and cascades within a stream network may also influence the C dynamics since they could exert an accelerating effect in CO_2 outgassing. Despite the generally small water surface area covered by a single headwater stream, this study suggests that high-gradient headwater streams are hotspots of CO_2 emissions. The omission of these systems may introduce significant biases in estimating catchment-scale and regional CO_2 flux from aquatic ecosystems, thus illustrating the importance of sampling in the immediate vicinity of groundwater emergence. We hope this work offers new knowledge that will lead to more accurate and comprehensive assessments of CO_2 emissions from headwater streams in the humid subtropical region and render the potential of upscaling the estimates to broader regions with similar climatic and land cover features.

DATA AVAILABILITY STATEMENT

The original contributions presented in the study are included in the article/Supplementary Material, further inquiries can be directed to the corresponding author.

AUTHOR CONTRIBUTIONS

CC, FL, and LR contributed to conceptualization and design of the study. CC, CT, and BL performed the fieldworks and experiments. CC performed the statistical analysis and wrote the manuscript with inputs from all authors. LR supervised the project. All authors contributed to manuscript revision.

FUNDING

This study was financially supported by the Research Grants Council of Hong Kong (Grants: 17300619 and 27300118), the National Natural Science Foundation of China (Grant: 41807318), and the Hui Oi-Chow Trust Fund (Grant: 263690564).

ACKNOWLEDGMENTS

Special thanks are also given to Jeannette Liu, Yu Ching Ip, and Fong Ching Ma for their contributions to the fieldwork.

REFERENCES

Abril, G., Bouillon, S., Darchambeau, F., Teodoru, C. R., Marwick, T. R., Tamooh, F., et al. (2015). Technical Note: Large Overestimation of pCO_2 Calculated from pH and Alkalinity in Acidic, Organic-Rich Freshwaters. *Biogeosciences* 12 (1), 67–78. doi:10.5194/bg-12-67-2015

Aho, K. S., and Raymond, P. A. (2019). Differential Response of Greenhouse Gas Evasion to Storms in Forested and Wetland Streams. *J. Geophys. Res. Biogeosci.* 124 (3), 649–662. doi:10.1029/2018JG004750

Argerich, A., Haggerty, R., Johnson, S. L., Wondzell, S. M., Dosch, N., Corson-Rikert, H., et al. (2016). Comprehensive Multiyear Carbon Budget of a Temperate Headwater Stream. *J. Geophys. Res. Biogeosci.* 121 (5), 1306–1315. doi:10.1002/2015JG003050

Atkins, M. L., Santos, I. R., Ruiz-Halpern, S., and Maher, D. T. (2013). Carbon Dioxide Dynamics Driven by Groundwater Discharge in a Coastal Floodplain Creek. *J. Hydrol.* 493, 30–42. doi:10.1016/j.jhydrol.2013.04.008

Benstead, J. P., and Leigh, D. S. (2012). An Expanded Role for River Networks. *Nat. Geosci* 5 (10), 678–679. doi:10.1038/ngeo1593

Bernal, S., von Schiller, D., Sabater, F., and Martí, E. (2013). Hydrological Extremes Modulate Nutrient Dynamics in Mediterranean Climate Streams across Different Spatial Scales. *Hydrobiologia* 719 (1), 31–42. doi:10.1007/s10750-012-1246-2

Butman, D., and Raymond, P. A. (2011). Significant Efflux of Carbon Dioxide from Streams and Rivers in the United States. *Nat. Geosci* 4 (12), 839–842. doi:10.1038/ngeo1294

Campeau, A., Lapierre, J.-F., Vachon, D., and del Giorgio, P. A. (2014). Regional Contribution of CO_2 and CH_4 fluxes from the Fluvial Network in a lowland Boreal Landscape of Québec. *Glob. Biogeochem. Cycles* 28 (1), 57–69. doi:10.1002/2013GB004685

Cheung, P. K., Hung, P. L., and Fok, L. (2019). River Microplastic Contamination and Dynamics upon a Rainfall Event in Hong Kong, China. *Environ. Process.* 6 (1), 253–264. doi:10.1007/s40710-018-0345-0

Crawford, J. T., Lottig, N. R., Stanley, E. H., Walker, J. F., Hanson, P. C., Finlay, J. C., et al. (2014). CO_2 and CH_4 emissions from Streams in a lake-rich Landscape: Patterns, Controls, and Regional Significance. *Glob. Biogeochem. Cycles* 28 (3), 197–210. doi:10.1002/2013gb004661

Crawford, J. T., Stanley, E. H., Dornblaser, M. M., and Striegl, R. G. (2017). CO_2 Time Series Patterns in Contrasting Headwater Streams of North America. *Aquat. Sci.* 79 (3), 473–486. doi:10.1007/s00027-016-0511-2

Crawford, J. T., Striegl, R. G., Wickland, K. P., Dornblaser, M. M., and Stanley, E. H. (2013). Emissions of Carbon Dioxide and Methane from a Headwater Stream Network of interior Alaska. *J. Geophys. Res. Biogeosci.* 118 (2), 482–494. doi:10.1002/jgrg.20034

Davidson, E. A., Figueiredo, R. O., Markewitz, D., and Aufdenkampe, A. K. (2010). Dissolved CO_2 in Small Catchment Streams of Eastern Amazonia: A Minor Pathway of Terrestrial Carbon Loss. *J. Geophys. Res.* 115 (G4). doi:10.1029/2009JG001202

Dawson, J. J. C., Billett, M. F., Neal, C., and Hill, S. (2002). A Comparison of Particulate, Dissolved and Gaseous Carbon in Two Contrasting upland Streams in the UK. *J. Hydrol.* 257 (1), 226–246. doi:10.1016/S0022-1694(01)00545-5

Deirmendjian, L., and Abril, G. (2018). Carbon Dioxide Degassing at the Groundwater-Stream-Atmosphere Interface: Isotopic Equilibration and Hydrological Mass Balance in a sandy Watershed. *J. Hydrol.* 558, 129–143. doi:10.1016/j.jhydrol.2018.01.003

Deirmendjian, L., Loustau, D., Augusto, L., Lafont, S., Chipeaux, C., Poirier, D., et al. (2018). Hydro-ecological Controls on Dissolved Carbon Dynamics in Groundwater and export to Streams in a Temperate pine forest. *Biogeosciences* 15 (2), 669–691. doi:10.5194/bg-15-669-2018

Dick, J. J., Soulsby, C., Birkel, C., Malcolm, I., and Tetzlaff, D. (2016). Continuous Dissolved Oxygen Measurements and Modelling Metabolism in Peatland Streams. *PLOS ONE* 11 (8), e0161363. doi:10.1371/journal.pone.0161363

Dimova, N. T., Burnett, W. C., Chanton, J. P., and Corbett, J. E. (2013). Application of Radon-222 to Investigate Groundwater Discharge into Small Shallow Lakes. *J. Hydrol.* 486, 112–122. doi:10.1016/j.jhydrol.2013.01.043

Dinsmore, K. J., Wallin, M. B., Johnson, M. S., Billett, M. F., Bishop, K., Pumpanen, J., et al. (2013). Contrasting CO_2 concentration Discharge Dynamics in Headwater Streams: A Multi-Catchment Comparison. *J. Geophys. Res. Biogeosci.* 118 (2), 445–461. doi:10.1002/jgrg.20047

Downing, J., Cole, J. J., Duarte, C. M., Middelburg, J. J., Melack, J. M., Prairie, Y. T., et al. (2012). Global Abundance and Size Distribution of Streams and Rivers. *Iw* 2 (4), 229–236. doi:10.5268/IW-2.4.502

Duan, S., He, Y., Kaushal, S. S., Bianchi, T. S., Ward, N. D., and Guo, L. (2017). Impact of Wetland Decline on Decreasing Dissolved Organic Carbon Concentrations along the Mississippi River Continuum. *Front. Mar. Sci.* 3 (280). doi:10.3389/fmars.2016.00280

Duvert, C., Butman, D. E., Marx, A., Ribolzi, O., and Hutley, L. B. (2018). CO_2 Evasion along Streams Driven by Groundwater Inputs and Geomorphic Controls. *Nat. Geosci* 11, 813–818. doi:10.1038/s41561-018-0245-y

Fletcher, C. J. N. (1997). The Geology of Hong Kong. *J. Geol. Soc.* 154 (6), 999–1000. doi:10.1144/gsjgs.154.6.0999

Gómez-Gener, L., von Schiller, D., Marcé, R., Arroita, M., Casas-Ruiz, J. P., Staehr, P. A., et al. (2016). Low Contribution of Internal Metabolism to Carbon Dioxide Emissions along Lotic and Lentic Environments of a Mediterranean Fluvial Network. *J. Geophys. Res. Biogeosci.* 121 (12), 3030–3044. doi:10.1002/2016jg003549

Hong Kong Observatory (2021). Daily Data for Single Element. [Online]. Available: http://www.hko.gov.hk/en/cis/dailyElement.htm [Accessed] .

Horgby, Å., Boix Canadell, M., Ulseth, A. J., Vennemann, T. W., and Battin, T. J. (2019a). High-Resolution Spatial Sampling Identifies Groundwater as Driver of CO_2 Dynamics in an Alpine Stream Network. *J. Geophys. Res. Biogeosci.* 124 (7), 1961–1976. doi:10.1029/2019JG005047

Horgby, Å., Segatto, P. L., Bertuzzo, E., Lauerwald, R., Lehner, B., Ulseth, A. J., et al. (2019b). Unexpected Large Evasion Fluxes of Carbon Dioxide from Turbulent Streams Draining the World's Mountains. *Nat. Commun.* 10 (1), 4888. doi:10.1038/s41467-019-12905-z

Hotchkiss, E. R., Hall Jr, R. O., Jr, Sponseller, R. A., Butman, D., Klaminder, J., Laudon, H., et al. (2015). Sources of and Processes Controlling CO_2 Emissions Change with the Size of Streams and Rivers. *Nat. Geosci* 8 (9), 696–699. doi:10.1038/ngeo2507

Huang, J., Yin, H., Chapra, S., and Zhou, Q. (2017). Modelling Dissolved Oxygen Depression in an Urban River in China. *Water* 9 (7), 520. doi:10.3390/w9070520

Johnson, M. S., Lehmann, J., Riha, S. J., Krusche, A. V., Richey, J. E., Ometto, J. P. H. B., et al. (2008). CO_2 efflux from Amazonian Headwater Streams Represents a Significant Fate for Deep Soil Respiration. *Geophys. Res. Lett.* 35 (17). doi:10.1029/2008GL034619

Jones, J. B., and Mulholland, P. J. (1998). Influence of Drainage basin Topography and Elevation on Carbon Dioxide and Methane Supersaturation of Stream Water. *Biogeochemistry* 40 (1), 57–72. doi:10.1023/A:1005914121280

Koschorreck, M., Prairie, Y. T., Kim, J., and Marcé, R. (2021). Technical Note: CO_2 Is Not like CH_4 - Limits of and Corrections to the Headspace Method to Analyse pCO_2 in Fresh Water. *Biogeosciences* 18 (5), 1619–1627. doi:10.5194/bg-18-1619-2021

Leibowitz, Z. W., Brito, L. A. F., De Lima, P. V., Eskinazi-Sant'Anna, E. M., and Barros, N. O. (2017). Significant Changes in Water pCO_2 Caused by Turbulence from Waterfalls. *Limnologica* 62, 1–4. doi:10.1016/j.limno.2016.09.008

Li, M., Peng, C., Zhang, K., Xu, L., Wang, J., Yang, Y., et al. (2021). Headwater Stream Ecosystem: an Important Source of Greenhouse Gases to the Atmosphere. *Water Res.* 190, 116738. doi:10.1016/j.watres.2020.116738

Looman, A., Maher, D. T., and Santos, I. R. (2021). Carbon Dioxide Hydrodynamics along a wetland-lake-stream-waterfall Continuum (Blue Mountains, Australia). *Sci. Total Environ.* 777, 146124. doi:10.1016/j.scitotenv.2021.146124

Luo, J., Li, S., Ni, M., and Zhang, J. (2019). Large Spatiotemporal Shifts of CO_2 Partial Pressure and CO_2 Degassing in a Monsoonal Headwater Stream. *J. Hydrol.* 579, 124135. doi:10.1016/j.jhydrol.2019.124135

Luo, J., and Li, S. (2021). Optical Properties of Dissolved Organic Matter in a Monsoonal Headwater Stream, China: Insights for Structure, Source and Riverine pCO_2. *J. Clean. Prod.* 282, 124545. doi:10.1016/j.jclepro.2020.124545

Manaka, T., H. M. Zakir Hossain, H. M. Z., Yoshimura, T., Suzuki, A., and Kawahata, H. (2019). Monthly Changes in pCO_2 in the Ganges River: Implications for Carbon Release from Soil to the Atmosphere via Inland Waters. *J. Agric. Meteorol.* 75 (1), 47–55. doi:10.2480/agrmet.D-18-00007

Marx, A., Dusek, J., Jankovec, J., Sanda, M., Vogel, T., van Geldern, R., et al. (2017). A Review of CO_2 and Associated Carbon Dynamics in Headwater Streams: A Global Perspective. *Rev. Geophys.* 55 (2), 560–585. doi:10.1002/2016rg000547

Maurice, L., Rawlins, B. G., Farr, G., Bell, R., and Gooddy, D. C. (2017). The Influence of Flow and Bed Slope on Gas Transfer in Steep Streams and Their Implications for Evasion of CO_2. *J. Geophys. Res. Biogeosci.* 122 (11), 2862–2875. doi:10.1002/2017jg004045

Moore, R. D. (2004). Introduction to Salt Dilution Gauging for Streamflow Measurement Part 2: Constant-Rate Injection. *Streamline Watershed Manage. Bull.* 8 (1), 11–15.

Mullinger, N. J., Binley, A. M., Pates, J. M., and Crook, N. P. (2007). Radon in Chalk Streams: Spatial and Temporal Variation of Groundwater Sources in the Pang and Lambourn Catchments, UK. *J. Hydrol.* 339 (3), 172–182. doi:10.1016/j.jhydrol.2007.03.010

Nydahl, A. C., Wallin, M. B., and Weyhenmeyer, G. A. (2017). No Long-Term Trends in pCO_2 Despite Increasing Organic Carbon Concentrations in Boreal Lakes, Streams, and Rivers. *Glob. Biogeochem. Cycles* 31 (6), 985–995. doi:10.1002/2016GB005539

Panton, A., Couceiro, F., Fones, G. R., and Purdie, D. A. (2020). The Impact of Rainfall Events, Catchment Characteristics and Estuarine Processes on the export of Dissolved Organic Matter from Two lowland Rivers and Their Shared Estuary. *Sci. Total Environ.* 735, 139481. doi:10.1016/j.scitotenv.2020.139481

Peter, H., Singer, G. A., Preiler, C., Chifflard, P., Steniczka, G., and Battin, T. J. (2014). Scales and Drivers of temporal pCO_2 dynamics in an Alpine Stream. *J. Geophys. Res. Biogeosci.* 119 (6), 1078–1091. doi:10.1002/2013JG002552

Piñol, J., and Avila, A. (1992). Streamwater pH, Alkalinity, pCO_2 and Discharge Relationships in Some Forested Mediterranean Catchments. *J. Hydrol.* 131 (1), 205–225. doi:10.1016/0022-1694(92)90218-K

Pu, J., Li, J., Zhang, T., Xiong, X., and Yuan, D. (2019). High Spatial and Seasonal Heterogeneity of pCO_2 and CO_2 Emissions in a Karst Groundwater-Stream Continuum, Southern China. *Environ. Sci. Pollut. Res.* 26 (25), 25733–25748. doi:10.1007/s11356-019-05820-9

Pumpanen, J., Lindén, A., Miettinen, H., Kolari, P., Ilvesniemi, H., Mammarella, I., et al. (2014). Precipitation and Net Ecosystem Exchange Are the Most Important Drivers of DOC Flux in upland Boreal Catchments. *J. Geophys. Res. Biogeosci.* 119 (9), 1861–1878. doi:10.1002/2014JG002705

Ran, L., Butman, D. E., Battin, T. J., Yang, X., Tian, M., Duvert, C., et al. (2021a). Substantial Decrease in CO_2 Emissions from Chinese Inland Waters Due to Global Change. *Nat. Commun.* 12 (1), 1730. doi:10.1038/s41467-021-21926-6

Ran, L., Shi, H., and Yang, X. (2021b). Magnitude and Drivers of CO_2 and CH_4 Emissions from an Arid/semiarid River Catchment on the Chinese Loess Plateau. *J. Hydrol.* 598, 126260. doi:10.1016/j.jhydrol.2021.126260

Schelker, J., Singer, G. A., Ulseth, A. J., Hengsberger, S., and Battin, T. J. (2016). CO_2 Evasion from a Steep, High Gradient Stream Network: Importance of Seasonal and Diurnal Variation in Aquatic pCO_2 and Gas Transfer. *Limnol. Oceanogr.* 61 (5), 1826–1838. doi:10.1002/lno.10339

Schneider, C. L., Herrera, M., Raisle, M. L., Murray, A. R., Whitmore, K. M., Encalada, A. C., et al. (2020). Carbon Dioxide (CO_2) Fluxes from Terrestrial and Aquatic Environments in a High-Altitude Tropical Catchment. *J. Geophys. Res. Biogeosci.* 125 (8), e2020JG005844. doi:10.1029/2020JG005844

Teodoru, C. R., Nyoni, F. C., Borges, A. V., Darchambeau, F., Nyambe, I., and Bouillon, S. (2015). Dynamics of Greenhouse Gases (CO_2, CH_2, N_2O) along the Zambezi River and Major Tributaries, and Their Importance in the Riverine Carbon Budget. *Biogeosciences* 12 (8), 2431–2453. doi:10.5194/bg-12-2431-2015

Ulseth, A. J., Hall, R. O., Boix Canadell, M., Madinger, H. L., Niayifar, A., and Battin, T. J. (2019). Distinct Air-Water Gas Exchange Regimes in Low- and High-Energy Streams. *Nat. Geosci.* 12, 259–263. doi:10.1038/s41561-019-0324-8

Wallin, M. B., Grabs, T., Buffam, I., Laudon, H., Ågren, A., Öquist, M. G., et al. (2013). Evasion of CO_2 from Streams - the Dominant Component of the Carbon export through the Aquatic Conduit in a Boreal Landscape. *Glob. Change Biol.* 19 (3), 785–797. doi:10.1111/gcb.12083

Wang, C., Xie, Y., Liu, S., McCallum, J. L., Li, Q., and Wu, J. (2021). Effects of Diffuse Groundwater Discharge, Internal Metabolism and Carbonate Buffering on Headwater Stream CO_2 Evasion. *Sci. Total Environ.* 777, 146230. doi:10.1016/j.scitotenv.2021.146230

Wang, X., He, Y., Yuan, X., Chen, H., Peng, C., Zhu, Q., et al. (2017). pCO_2 and CO_2 fluxes of the Metropolitan River Network in Relation to the Urbanization of Chongqing, China. *J. Geophys. Res. Biogeosci.* 122 (3), 470–486. doi:10.1002/2016JG003494

Wickland, K. P., Neff, J. C., and Aiken, G. R. (2007). Dissolved Organic Carbon in Alaskan Boreal Forest: Sources, Chemical Characteristics, and Biodegradability. *Ecosystems* 10 (8), 1323–1340. doi:10.1007/s10021-007-9101-4

Winterdahl, M., Wallin, M. B., Karlsen, R. H., Laudon, H., Öquist, M., and Lyon, S. W. (2016). Decoupling of Carbon Dioxide and Dissolved Organic Carbon in Boreal Headwater Streams. *J. Geophys. Res. Biogeosci.* 121 (10), 2630–2651. doi:10.1002/2016JG003420

Wu, Y., Wen, X., and Zhang, Y. (2004). Analysis of the Exchange of Groundwater and River Water by Using Radon-222 in the Middle Heihe Basin of Northwestern China. *Environ. Geology.* 45 (5), 647–653. doi:10.1007/s00254-003-0914-y

Conflict of Interest: The authors declare that the research was conducted in the absence of any commercial or financial relationships that could be construed as a potential conflict of interest.

The handling Editor declared a past co-authorship with one of the authors (LR).

Publisher's Note: All claims expressed in this article are solely those of the authors and do not necessarily represent those of their affiliated organizations, or those of the publisher, the editors, and the reviewers. Any product that may be evaluated in this article, or claim that may be made by its manufacturer, is not guaranteed or endorsed by the publisher.

frontiers in Earth Science

ORIGINAL RESEARCH
published: 20 December 2021
doi: 10.3389/feart.2021.778215

Improving Carbonate Equilibria-Based Estimation of pCO_2 in Anthropogenically Impacted River Systems

*Omme K. Nayna[1], Most Shirina Begum[1], Lishan Ran[2] and Ji-Hyung Park[1]**

[1]Department of Environmental Science and Engineering, Ewha Womans University, Seoul, South Korea, [2]Department of Geography, The University of Hong Kong, Pokfulam, Hong Kong, China

Estimating riverine carbon dioxide (CO_2) emissions has been constrained by lacking field measurements of the partial pressure of CO_2 (pCO_2) and inaccuracies in calculating pCO_2 using carbonate equilibria-based models such as CO2SYS. To evaluate potential errors in applying the carbonate equilibria-based pCO_2 calculation to river systems affected by monsoon rainfall and water pollution, we compared pCO_2 values calculated using CO2SYS and those measured by headspace equilibration in five Asian rivers (Ganges, Mekong, Yangtze, Yellow, and Han rivers) undergoing various water pollution stages. Across the five rivers, calculated and measured pCO_2 values exhibited larger discrepancies during the monsoon season, particularly in the low pH range, while in the Han River mismatches were also noticeable during the dry season. In the Han River, pH was negatively correlated with dissolved organic carbon (DOC) during the monsoon, indicating organic acids flushed from soils during rainfalls as a key factor for overestimated pCO_2 at sites with low pH and alkalinity, whereas dry-season overestimation of pCO_2 may be ascribed to non-carbonate alkalinity including organic acids and inorganic anions delivered by wastewater effluents or sporadic rainfalls. The four large rivers exhibited a positive correlation between pH and DOC in tributaries during the monsoon season, indicating that DOC flushed from soils may be diluted by monsoonal floods to such a degree as to exert little influence on pH and hence pCO_2. Therefore, the monsoonal overestimation of pCO_2 at sites with low pH and alkalinity warrants further investigation of other factors than non-carbonate alkalinity to explain the increased sensitivity of pCO_2 to subtle changes in acidity and buffering. These results illustrate the importance of direct measurements of pCO_2 in highly polluted rivers, especially during the monsoon season. For river systems lacking pCO_2 measurements, we suggest that carbonate equilibria-based models be complemented with corrective measures: 1) presenting pCO_2 values calculated from low pH values (pH < 6.5 for monsoon and pH < 6.3 for dry season) together with the pH range to warn potential overestimation; 2) using pre-established regressions between measured pCO_2 and environmental variables to correct pCO_2

OPEN ACCESS

Edited by:
Xixi Lu,
National University of Singapore, Singapore

Reviewed by:
Ronny Lauerwald,
Université Paris-Saclay, France
Manab Kumar Dutta,
National Centre for Earth Science Studies, India
Ping Yang,
Fujian Normal University, China

***Correspondence:**
Ji-Hyung Park
jhp@ewha.ac.kr

Specialty section:
This article was submitted to Biogeoscience, a section of the journal Frontiers in Earth Science

Received: *16 September 2021*
Accepted: *17 November 2021*
Published: *20 December 2021*

Citation:
Nayna OK, Begum MS, Ran L and Park J-H (2021) Improving Carbonate Equilibria-Based Estimation of pCO_2 in Anthropogenically Impacted River Systems. Front. Earth Sci. 9:778215. doi: 10.3389/feart.2021.778215

Abbreviations: DIC, dissolved inorganic carbon; DOC, dissolved organic carbon; DOM, dissolved organic matter; DO, dissolved oxygen; OM, organic matter; pCO_2, Partial pressure of CO_2; TA, total alkalinity.

values, particularly during wet periods when large changes in pH and acid buffering are expected.

Keywords: Asian rivers, carbonate equilibria, monsoon, partial pressure of CO_2 (pCO_2), urban tributary, wastewater

1 INTRODUCTION

Inland waters have been recognized as important sources of carbon dioxide (CO_2) and other greenhouse gases (GHGs), as highlighted by recent regional and global syntheses (Raymond et al., 2013; Borges et al., 2015; Lauerwald et al., 2015; Park et al., 2018). Inland waters play a crucial role in the global carbon cycle by storing, transporting, or transforming carbon (C) in the form of inorganic or organic C in the terrestrial-aquatic-atmosphere continuum (Cole et al., 2007); however, these synthesis efforts have been limited by the lack of spatially resolved datasets (Raymond et al., 2013; Lauerwald et al., 2015; Park et al., 2018). Various direct and indirect methods have been employed to measure or calculate the aquatic partial pressure of CO_2 (pCO_2) (Park, 1969; Smethie et al., 1985; Kling et al., 1992; Pierrot et al., 2006; Yoon et al., 2016). Due to the lack of direct measurements of pCO_2, many studies on CO_2 emissions from inland waters depend on calculated pCO_2 using carbonate equilibria (Butman and Raymond, 2011; Raymond et al., 2013; Lauerwald et al., 2015; Park et al., 2018). Although this carbonate equilibria-based pCO_2 calculation has been widely used to estimate regional and global CO_2 emissions from inland waters, considerable concerns exist about potential errors associated with such calculations. The estimation accuracy of pCO_2 and CO_2 emissions needs to be improved by employing proper corrective measures under specific conditions, for instance, where large changes in pH and acid buffering are expected (Liu et al., 2020).

Direct measurements of pCO_2 are based on the gas equilibration between the water and air phases (headspace equilibration method) or continuous measurements using various systems and devices, including membrane-enclosed CO_2 sensors and automated equilibrators (Yoon et al., 2016). Carbonate equilibria-based methods for estimating pCO_2 use combinations of related water quality parameters, including pH, total alkalinity (TA), dissolved inorganic carbon (DIC), and water temperature (Park, 1969; Lewis and Wallace, 1998). Constants used for pCO_2 calculation in freshwater systems include those for the carbonic acid dissociation (Millero, 1979) and CO_2 solubility (Weiss, 1974), both of which are dependent on temperature.

The potential bias in the calculated pCO_2 relative to the measured one may arise from inaccuracies of these multiple parameters. Frankignoulle and Borges (2001) provided the first comparison between the pCO_2 calculated from pH and TA and pCO_2 measured by an equilibrator coupled to an IR analyzer in an estuary in Belgium. They observed a relatively good agreement between the two approaches under the conditions of high TA (2,500–4,800 μeq L^{-1}) and pH (>7.4). The concomitant measurements of pH, TA, and pCO_2 in acidic and organic-rich waters of the Sinnamary River in French Guiana exhibited extremely high values of estimated pCO_2 under the conditions of pH at 5 and TA at 200 μeq L^{-1}, compared to pCO_2 values directly measured using the headspace equilibration technique (Abril et al., 2005; Abril et al., 2006). This overestimation in pCO_2 indicates the contribution of organic acids to TA. Organic acids in DOC can significantly contribute to TA not only in the polluted rivers, but also in the organic-rich, unpolluted rivers, resulting in overestimation of calculated pCO_2 (Hunt et al., 2011; Wang et al., 2013). Abril et al. (2015) warned that in acidic, poorly buffered,and organic-rich freshwaters pCO_2 can be overestimated by 50–300% when compared to direct pCO_2 measurements. Recently, Golub et al. (2017) have also reported potential biases in pCO_2 calculated using carbonate equilibria (pH-TA), due to influences of organic acids and ionic strengths in freshwater systems. While the calculation method works well in systems with typical pH range (e.g., pH > 7) and alkalinity (e.g., TA>1,000 μeq L^{-1}) (Abril et al., 2015; Liu et al., 2016), potential overestimation of pCO_2 has been found in systems with low pH and alkalinity (Hunt et al., 2011; Abril et al., 2015; Liu et al., 2020). Calculated and measured pCO_2 values exhibited larger discrepancies during floods, particularly in the low pH range (e.g., pH < 8), resulting in overestimation of pCO_2 (Abril et al., 2015). In the large rivers across Asia, seasonal variations in carbonate equilibria regimes have been associated with the monsoon climate, because heavy monsoonal rainfalls can dilute river water TA and decrease pH, resulting in overestimation of pCO_2 under conditions of low pH and alkalinity (Li et al., 2013; Manaka et al., 2015; Ran et al., 2015).

The calculation of pCO_2 from water quality data could not only provide useful data for estimating regional and global riverine CO_2 emissions but also help to reconstruct long-term changes in pCO_2, as conducted for a large number of rivers in China (Ran et al., 2021). This study aimed to improve the prediction capability of the carbonate equilibria-based pCO_2 model by comparing calculated and measured pCO_2 with associated water quality measurements in the mainstem, tributaries, and/or wastewater drains of the Ganges, Mekong, Yangtze, Yellow, and Han River during both monsoon and dry seasons. We compared the values of pCO_2 calculated using CO2SYS with pCO_2 measurements from seasonal field measurements across various locations in the five river basins. In the case of the Han River in Korea, more frequent measurements in the mainstem, tributaries, and wastewater effluents during both dry and monsoon seasons were separately analyzed to evaluate the effects of both monsoon and sporadic, dry-season rainfalls on seasonal differences in pCO_2 and associated water quality components. This study provides the first comprehensive comparison of the calculated and measured pCO_2 values between monsoon and dry seasons in multiple Asian river basins under elevating anthropogenic pressures (**Figure 1**). We postulate that riverine CO_2

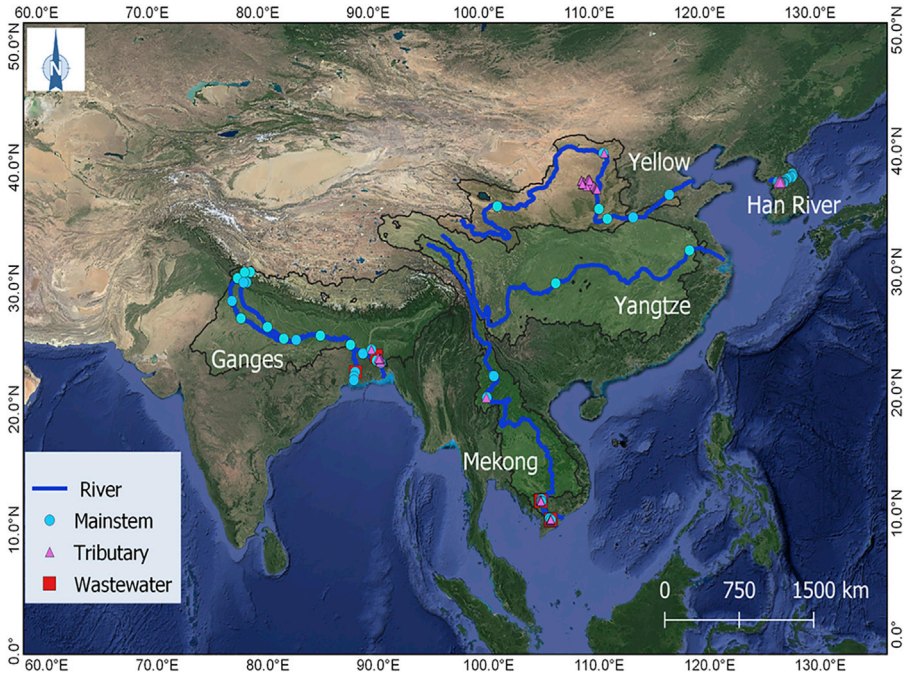

FIGURE 1 | Study map showing the sampling sites across the mainstems, tributaries, and polluted urban tributaries or wastewater effluents of four large rivers (the Ganges, Mekong, Yangtze, and Yellow River) and a smaller, urbanized river system in Korea (the Han River).

emissions can be overestimated if values of pCO_2 are calculated from low-pH and low-alkaline river systems without proper corrections. Specifically, we tested the hypothesis that increasing inputs of soil-derived organic acids during monsoonal floods can decrease pH and dilute TA in the river water, causing potential pCO_2 overestimation. In contrast, increasing discharge of untreated or poorly treated wastewater may not only alter the composition of the riverine organic matter (OM) but also increase the pH and TA during dry periods due to lack of dilution in river water.

2 METHODS

2.1 Study Sites

We compared pCO_2 measurements with values of pCO_2 calculated from the concomitant water quality measurements in five Asian rivers—the Ganges, Mekong, Yangtze, Yellow, and Han River (**Figure 1**). The Ganges, Mekong, Yangtze, and Yellow River all originate from the Himalayan-Tibetan Plateau, draining some of the largest watersheds in the world (Milliman and Farnsworth, 2011). These river systems share certain common hydrological and demographic characteristics, such as intense monsoon-driven seasonality of flow and high population density along their banks (Park et al., 2018). The Ganges River is 2,515 km long, flowing from the Himalayas through India, Nepal, and Bangladesh to the Bay of Bengal, with a drainage area of $1,050 \times 10^3$ km^2 (Meybeck and Ragu, 2012). The Mekong River is 4,800 km long, flowing from the Tibetan Plateau through six countries to the South China Sea, with a drainage area of 800×10^3 km^2 (Milliman and Farnsworth, 2011). The 5,500 km long Yellow River flows from the Tibetan Plateau through nine provinces in Northern China to the Bohai Sea, with a drainage area of 750×10^3 km^2 (Milliman and Farnsworth, 2011). The Yangtze River traverses 6,380 km eastward from the Tibetan Plateau to the East China Sea, draining a total area of 1810×10^3 km^2 and, covering the Sichuan Basin and Middle-Lower Reach Plains (Ran et al., 2017a). The 494 km long Han River, consisting of the North Han and South Han branches and the lower Han River, drains an area of 34×10^3 km^2 in the middle of the Korean Peninsula and flows westward into the Yellow Sea (Kim et al., 2021). A large population living in this region is affected by heavy monsoon rainfalls and associated sediment transport to the floodplains. For agricultural irrigation, and domestic, or industrial purposes, people depend on river water *via* many dams and reservoirs being constructed on the rivers over the last few decades (Lehner et al., 2011).

Four large rivers excluding the Han River were sampled in the mainstem, tributary, and wastewater drain sites from March 2015 to July 2019 to explore spatial and seasonal variations in pCO_2 and other water quality parameters (**Figure 1**; **Supplementary Table S1**). Four main branches of the Ganges traversing were considered as the mainstem, including the Yamuna and Ganga traversing the northern India and two bifurcated distributaries, namely the Hooghly in India and the Padma in Bangladesh flowing towards the Bay of Bengal. The Mekong River mainstem comprises the upper Mekong (Lancang) and the lower Mekong River. The Yangtze and Yellow River consist of a single mainstem. Sampling was conducted along the mainstems, urban tributaries, and wastewater drains within or downstream of

major metropolitan areas (e.g., Kolkata and Dhaka). Measurements include water temperature, pH, TA, pCO_2, and DOC. This study focused on the analysis of CO_2 as well as DOC for the five river basins across Asia. Monsoonal samples were collected from 65 locations, including 22 in the Ganges, 19 in the Mekong, 2 in the Yangtze, and 22 in the Yellow River, while dry-season samples were collected from 65 locations, including 22 in the Ganges, 23 in the Mekong, and 20 in the Yellow River.

In the Han River, field surveys were repeated at various intervals from July 2014 to May 2020 to explore the spatial and seasonal variations as well as localized pollution impacts that vary longitudinally along the river. The mainstem was divided into three reaches: the upper (U), middle (M), and lower (L) reaches. Different sites along urban tributaries and effluents from a wastewater treatment plant were also sampled together with mainstem sites. Water temperature, pH, TA, pCO_2, and DOC were measured at 31 locations, including 4 in the upper reaches, 7 in the middle reaches, 5 in the lower reaches, 14 in tributaries, and one discharge of a wastewater treatment plant during the monsoon (from June to September) and dry season (from October to May). It should be noted that sporadic rainfalls have been recorded during the dry season.

The data of pCO_2 measured in the Ganges, Mekong, and Yellow River have been reported by Begum et al. (2021). pCO_2 data measured in the Wuding River, a Yellow River tributary, have been reported by Ran et al. (2017b), while measurements in the Yangtze River in 2018 have not yet been published. While pCO_2 data measured in the Han River from 2014 to 2017 have been reported by Jin et al. (2018), more recent measurements from 2018 to 2020 have not yet been published. Field surveys in the Ganges, Mekong, and Yellow River from 2016 to 2019 included concomitant measurements of water temperature, pH, TA, pCO_2, and DOC (Begum et al., 2021), while field measurements in the Yangtze, Wuding, and Han River from 2014 to 2020 included simultaneous measurements of water temperature, pH, TA, pCO_2, and DOC.

2.2 Sampling and *In Situ* Measurements

Water samples were collected at 10–20 cm below the surface. In the Ganges, Mekong, Yangtze, and Yellow rivers, water samples were directly collected using acid-washed polycarbonate bottles and immediately frozen before being transported in an icebox to the lab in Korea within a week of collection. In the Han River, water samples were collected through a peristaltic pump (Masterflex E/S, Cole-Parmer, IL, USA) into acid-washed amber glass bottles. A portable multiparameter meter (Orion 5-Star Portable, Thermo Scientific, USA) was used to measure *in situ* water quality parameters, such as water temperature, pH, dissolved oxygen (DO), and electrical conductivity (EC). The barometric pressure and air temperature were measured *in situ* using a portable sensor (Watchdog 1,650 Micro Station, Spectrum Technologies, IL, USA) or collected from the Internet (https://www.timeanddate.com/weather/).

The manual headspace equilibration method was performed on site with water samples collected from the same water depth as water samples (Yoon et al., 2016). For the headspace equilibration, a polypropylene syringe (60 ml; HSW Norm-Ject Luer Lock Tip; Henke-Sass Wolf GmbH, Germany) was used to collect a 30 ml water sample and then a 30 ml ambient air sample. At the same time, a 30 ml ambient air sample was collected in another syringe to measure the CO_2 mixing ratio in ambient air separately. After vigorously shaking water and air samples in the syringe for 2 min (Yoon et al., 2016), approximately 20 ml of the equilibrated air sample was transferred to a pre-evacuated 12 ml Exetainer vial for gas analysis in the laboratory. The stored gas sample was greater than the vial volume to generate overpressure and hence minimize concentration changes associated with potential gas leakage. Vials had been flushed with high-purity N_2 gas before the vial was evacuated using a pump. "Blanks" (without samples) were analyzed together with the samples to correct the effect of any remaining CO_2 gases after evacuation. The gas analysis was generally completed within a month after sampling.

Continuous underway measurements of riverine pCO_2 during the dry season were conducted in the lower Ganges and a tributary near Dhaka in February 2018, and in the Mekong and connected Tonle Sap around Phnom Penh in January 2017. Continuous measurements of pCO_2 were conducted using a spray-type equilibrator connected to an infrared gas analyzer (IRGA; LI820, Li-Cor, USA), as described by Yoon et al. (2016) (**Table 1**).

2.3 Laboratory Analyses

CO_2 concentrations in equilibrated and ambient air samples were measured using gas chromatography (GC; 7890A, Agilent, USA) (Jin et al., 2018). Measured gas concentrations in equilibrated and ambient air samples were used together with the barometric pressure and water temperature to calculate pCO_2 and dissolved CO_2 concentrations based on Henry's law (Hudson, 2004).

Water samples were filtered using pre-combusted (450°C) glass fiber filters (GF/F, Whatman; nominal pore size 0.7 μm) in the laboratory, and filtered water samples were then analyzed for DOC and TA. The concentration of DOC was measured by a total organic carbon (TOC) analyzer using high-temperature combustion of OM followed by thermal detection of CO_2 (TOC-V_{CPH}, Shimadzu, Japan). TA was measured with 40–80 ml filtered samples using an automated electric titrator (EasyPlus Titrator Easy pH, Metrohm, Switzerland) based on the Gran titration method. To determine the equivalence point at pH between 3 and 4, a strong acid (0.1 N HCl) was used for the titration (Gran, 1952). As part of quality assurance, duplicate analyses of DOC and pCO_2 were performed for approximately 10% of all analyzed samples, while triplicate analyses of TA were conducted for the same samples. Standards with known concentrations and ultrapure water were analyzed for each batch of ten samples to determine instrumental stability and accuracy. The relative standard deviation for replicate measurements of DOC and TA was ≤5%.

2.4 pCO_2 Calculation From pH and TA

pCO_2 was calculated using the CO2SYS program (Lewis and Wallace, 1998; Pierrot et al., 2006), which has been widely used to calculate riverine pCO_2 from temperature, pH, and TA. We calculated values of pCO_2 from temperature, pH, and TA, using the carbonic acid dissociation constants of Millero (1979) for freshwater systems and the CO_2 solubility constant

TABLE 1 | Summary of the partial pressure of CO_2 (pCO_2) methods used in this study, including manual headspace equilibration, automated equilibration, and CO2SYS (carbonate equilibria-based model).

System	Principle	Measurement/calculation method	Equilibration time (min)	References
Manual headspace equilibration	Direct measurement	Gas equilibration by manual shaking in the headspace above the water sample collected in a syringe or bottle	<2	Kling et al. (1992), Hope et al. (1995), Yoon et al. (2016)
Spray-type equilibrator	Direct measurement	Gas equilibration by spraying gas-containing water droplets	1–12	Feely et al. (1998), Webb et al. (2016), Yoon et al. (2016)
CO2SYS	Carbonate equilibria-based calculation	Carbonate equilibria-based model using TA, pH, and temperature as input parameters to calculate pCO_2		Lewis and Wallace (1998), Pierrot et al. (2006)

from Weiss (1974). The difference in the calculated pCO_2 using this method is 2% lower than that of the PHREEQC program reported by Hunt et al. (2011). Abril et al. (2015) suggested that large discrepancies between the calculated and measured pCO_2 values may not be related to differences in software or dissociation constants (Abril et al., 2015).

2.5 Statistical Analyses

The relationships between calculated pCO_2 and other measured parameters, including pH, TA, and DOC were analyzed using best-fit regressions in SigmaPlot (Systat Software Inc.). Regression analysis determined the agreement between the calculated and measured pCO_2 in the mainstem, tributary, and wastewater sites across the four large Asian rivers and Han River. All statistical analyses were performed after applying the Shapiro-Wilk test to examine the normal distribution of the data using SigmaPlot or R. Given the nonnormal distributions of data sets, we conducted a nonparametric t-test (Mann Whitney *U* test) to explore seasonal differences in pCO_2, pH, TA, DOC, and water temperature for the mainstems, tributaries, wastewater drains or urban streams for each of the five Asian rivers. Statistical significance was set at $p < 0.05$, unless otherwise stated.

3 RESULTS

3.1 Comparison of Measured and Calculated pCO_2 in Five River Systems

Measured values of pCO_2 revealed large spatial variations among mainstems, tributaries, and wastewater drains across the five river basins (**Table 2**). In the four large Asian rivers excluding the Han River, pCO_2 varied between 224 and 34,151 μatm, with the lowest pCO_2 value observed along the upper reaches of the Ganges (**Table 2**). The highest pCO_2 of 34,151 μatm was observed in wastewater drains of the Mekong basin during the dry season. In the Han River basin, pCO_2 varied between 43 μatm and 13,094 μatm, with the mean pCO_2 increasing downstream along the mainstem as affected by higher pCO_2 levels in tributaries and wastewater effluents along the lower reach (**Table 2**). The highest pCO_2 level in the Han River was measured in the wastewater effluents during a dry period.

DOC concentrations varied between 0.2 mg L^{-1} and 26.3 mg L^{-1}, with the lowest DOC observed in a headwater stream of the Ganges during the monsoon season (**Table 2**). The highest DOC concentration was found in the middle reach of the Yamuna that drains the Delhi metropolitan area during a dry period. The pH value varied between 3.0 and 9.3, with the lowest pH observed in the upper reach of the mainstem Han River (**Table 2**). The highest level of pH was found in a tributary of the Yellow River during a dry season. TA varied between 27 and 11,000 μeq L^{-1}, the lowest TA was observed in a tributary of the Han River during a monsoon season (**Table 2**). The highest level of TA was observed in a tributary of the Yellow River during a monsoon season.

The comparison between calculated and measured pCO_2 values in the five river basins exhibited stronger positive deviations when the pH was lower than 7 (**Figure 2**). Mean pCO_2 deviations were higher at the sites with lower pH (<7) and TA (<500 μeq L^{-1}) during both monsoon and dry seasons (**Table 3**). In the four large rivers, calculated pCO_2 reached 46,476 μatm (measured pCO_2: 1,670 μatm) at a pH of 6.34 at a wastewater site on the Ganges River during the monsoon season, and deviations between the calculated and measured pCO_2 values ranged from −5,911 to +44,806 μatm. In the Han River basin, during the monsoon season calculated pCO_2 reached 6,773,9120 μatm (measured pCO_2: 1782 μatm) at a headwater stream at a low pH of 3.0; deviations between the calculated and measured pCO_2 values ranged from −1,683 to +67,737,338 μatm (**Figure 2B**). In contrast, potential underestimations of pCO_2 compared to measured pCO_2 were observed in the samples with pH > 9.2 (**Figure 2B**). The comparison between the calculated and measured pCO_2 values in the four large rivers exhibited negative deviations at wastewater sites during dry periods (**Figure 3A**). In contrast, the comparison between calculated and measured pCO_2 values exhibited large positive deviations in the mainstems, tributaries, and wastewater sites during the monsoon season (**Figure 3B**). Across the Han River, the comparison between the calculated and measured pCO_2 values exhibited relatively large positive deviations for the mainstem and tributary sites during dry periods (**Figure 3C**). For the mainstem, tributaries, and wastewater sites of the Han River, stronger positive deviations were observed during the monsoon season than during the dry season (**Figures 3C,D**).

3.2 Relationships Between pCO_2 and Other Environmental Variables

The calculated pCO_2 subtracted from the measured pCO_2 were negatively correlated with pH for the mainstem, tributaries, and wastewater sites of the five river basins during both monsoon and dry seasons ($p < 0.05$; **Figures 4**, **6**). Large deviations of the calculated pCO_2 from the measured pCO_2 were found for the samples with relatively low concentrations of DOC and TA

TABLE 2 | Comparison of water temperature (Temp), pH, total alkalinity (TA), dissolved organic carbon (DOC), and partial pressure of CO_2 (pCO_2) measured in five river systems in Asia between monsoon (wet) and dry season. Values are means followed by ranges in parentheses. N represents the number of the study sites.

Rivers	N		Temp (°C)		pH		TA (μeq L^{-1})		DOC (mg L^{-1})		pCO_2 (μatm)	
	Dry	Wet	Dry	Wet	Dry	Wet	Dry	Wet	Dry	Wet	Dry	Wet
Ganges	22	22	21.2 (13.8–27.1)	26.5** (4.0–31.6)	7.7 (6.9–8.5)	7.5 (6.1–8.3)	2,439 (593–6,898)	1,093 (84–1923)	5.6 (0.5–26.3)	2.1 (0.2–5.9)	5,678 (335–20,580)	1807 (224–5,659)
Mainstem	11	15	19.2 (13.8–23.4)	25.9** (4.0–31.6)	7.9 (6.9–8.4)	7.8 (6.1–8.3)	1787 (593–6,898)	1,172 (84–1923)	3.32 (0.5–26.3)	1.9 (0.2–5.0)	2,647 (335–20,580)	1732 (224–5,660)
Tributary	7	4	22.3 (21.7–22.9)	28.1** (25.5–30.0)	7.3 (6.9–8.5)	7.1 (6.3–8.2)	2,462 (598–5,102)	732 (365–994)	4.12 (0.5–8.1)	2.0 (0.94–3.18)	7,340* (664–15,010)	1936 (746–3,905)
Wastewater	4	3	24.9 (23.2–27.1)	27.3 (26.0–29.0)	7.4 (7.2–7.7)	6.8 (6.3–7.2)	4,198 (3,754–4,893)	1,178** (962–1,450)	14.3 (7.7–19.2)	3.2** (1.7–5.9)	11,109 (3,685–18,623)	2024 (1,670–2,287)
Mekong	23	19	28.7 (25.0–31.3)	28.3 (26.8–31.2)	7.3 (6.8–7.6)	7.0 (6.4–8.2)	1821 (455–4,483)	881** (660–2016)	3.8 (1.6–10.1)	2.9 (1.7–8.9)	7,833 (1,347–34,151)	3,387 (1,101–7,086)
Mainstem	10	9	26.2 (21.4–29.2)	27.3 (23.8–29.5)	7.5 (6.4–8.4)	7.3 (6.7–7.5)	1,083 (573–1,478)	1,020 (387–2,335)	1.7 (1.0–3.6)	1.8 (1.4–2.0)	2,333 (433–3,729)	2,345 (1846–2,948)
Tributary	7	6	28.2 (25.0–31.3)	28.3 (26.7–30.4)	7.2 (6.8–7.6)	7.0 (6.4–7.5)	1,511 (455–3,583)	716 (660–774)	2.9 (1.6–4.4)	2.1 (1.7–3.0)	4,079 (1,347–6,229)	3,775 (1860–7,753)
Wastewater	6	4	29.2 (28.8–29.9)	28.0 (26.8–31.2)	7.3 (7.0–7.5)	6.9 (6.4–8.2)	2,183 (1,065–4,483)	1,101 (718–2016)	4.8 (1.9–10.1)	4.1 (2.0–8.9)	12,213 (1766–34,151)	3,896 (1,101–7,086)
Yellow	20	22	13.5 (7.1–22.6)	25.4** (15.1–30.5)	8.5 (7.9–9.3)	8.6 (7.9–9.2)	5,563 (3,090–9,950)	5,328 (264–11,000)	4.7 (1.4–9.5)	5.5 (2.3–11.4)	1,063 (500–4,429)	1,009 (470–2,708)
Mainstem	3	3	19.0 (16.0–22.6)	27.3* (24.0–29.3)	8.1 (8.1–8.2)	8.1 (7.9–8.1)	3,240 (3,090–3,345)	1,112 (709–1,386)	2.2 (2.2–2.3)	5.0 (2.3–10.4)	1,403 (1,253–1,513)	2088 (1,314–2,708)
Tributary	17	19	12.5 (7.1–18.7)	25.1** (15.1–30.2)	8.6 (7.9–9.3)	8.7 (8.4–9.2)	5,973 (3,650–9,950)	5,993 (224–11,000)	5.1 (1.4–9.5)	5.5 (2.9–11.4)	1,003 (500–4,429)	839 (470–2,647)
Yangtze		2		26.5 (24.0–28.6)		7.7 (7.6–7.7)		1,505 (1,424–1,585)		2.1 (1.9–2.2)		1866 (1819–1914)
Mainstem												
Han River	31	30	12.7 (0.1–29.6)	24.0** (9.2–34.2)	7.4 (5.3–9.0)	7.2** (5.7–9.3)	1,132 (37–2,746)	851** (27–2,409)	2.5 (0.5–18.9)	2.5 (0.6–5.5)	2,194 (43–13,094)	2,621 (48–10,186)
Mainstem (U)	4	4	9.3 (0.1–19.5)	21.7** (11.7–31.0)	7.4 (5.3–8.5)	7.1** (6.0–8.1)	713 (37–1,357)	507 (60–1,068)	1.4 (0.5–2.3)	1.8* (0.6–3.0)	779 (43–1,575)	1,330** (159–2,690)
Mainstem (M)	7	7	12.1 (1.3–20.2)	25.5** (22.1–30.8)	7.5 (6.3–9.0)	7.8 (6.5–9.3)	981 (342–1,379)	802 (343–1,287)	2.1 (1.2–2.6)	2.0 (1.2–3.4)	961 (128–2038)	1,021 (51–2,714)
Mainstem (L)	5	5	13.4 (0.7–22.7)	26.0** (20.6–34.2)	7.4 (6.3–8.6)	7.4 (6.4–8.8)	1,008 (449–1,483)	892* (449–1,244)	2.4 (1.4–3.6)	2.3 (1.6–3.2)	1,490 (86–3,944)	2,411 (59–5,633)
Tributary	14	13	14.8 (3.6–29.6)	22.5** (9.2–30.1)	7.5 (6.3–8.7)	6.9** (5.7–8.6)	1,626 (53–2,746)	1,075** (27–2,409)	3.3 (0.9–18.9)	3.2 (1.8–4.1)	3,651 (44–9,865)	4,272 (48–9,638)
Wastewater	1	1	16.7 (11.9–22.9)	27.6 (24.4–30.8)	6.6 (6.4–6.8)	6.6 (6.3–6.8)	1,337 (804–1,676)	1,240 (804–1,676)	4.9 (4.2–5.7)	4.7 (3.9–5.5)	10,326 (8,958–13,094)	8,886 (7,568–10,186)

Yangtze River included data only for the mainstem sites; U: upper reach; M: middle reach; L: lower reach; Significant differences between monsoon and dry season for different locations of the river and each river basin at $p < 0.05$ *and* $p < 0.01$ *are indicated by * and **, respectively.*

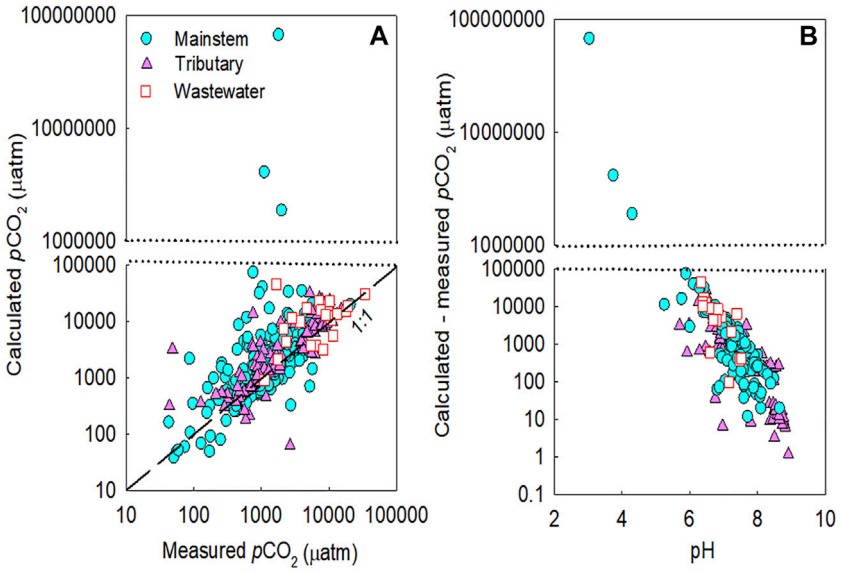

FIGURE 2 | Comparison of the measured and calculated partial pressure of CO_2 (pCO_2) **(A)** and the difference between calculated and measured pCO_2 as a function of pH **(B)** in the mainstems (M), tributaries (T), and polluted urban tributaries or wastewater effluents (W) of the five studied river basins across Asia. The studied rivers include the Ganges, Mekong, Yangtze, Yellow, and Han River. The dashed black line represents the 1:1 line.

TABLE 3 | Seasonal variations in the mean partial pressure of CO_2 (pCO_2) deviations (calculated minus measured values and their proportions in measured values), pH, total alkalinity (TA), and dissolved organic carbon (DOC) in the five Asian Rivers during the dry and monsoon (wet) seasons.

	Sample number (N)		pCO_2 deviation (µatm)		Relative pCO_2 deviation (% of measured pCO_2)		pH		TA (µeq L^{-1})		DOC (mg L^{-1})	
	Dry	Monsoon	Dry	Monsoon	Dry	Monsoon	Dry	Monsoon	Dry	Monsoon	Dry	Monsoon
Ranked by calculated- measured pCO_2 as % of measured pCO_2												
>−10%	35	29	−1,083	−908	−40%	−39%	7.8	7.9	1,463	1,003	2	3
<−10%	18	16	−307	−65	−5%	−5%	7.9	7.9	3,743	2,820	4	2
<+10%	23	20	167	59	4%	3%	7.8	8.2	3,196	4,331	5	5
<+50%	50	18	1,050	580	29%	25%	7.4	7.4	1,496	809	4	2
>+50%	27	11	1,329	1781	74%	72%	7.4	7.3	1,119	931	2	2
>+100%	45	51	5,153	8,123	491%	529%	7.2	6.9	1,182	874	2	3
Ranked by pH												
pH > 8	50	42	8	−305	25%	−1%	8.4	8.5	3,199	3,358	3	4
pH 7–8	108	54	437	590	85%	190%	7.5	7.5	1,434	966	3	2
pH < 7	38	46	5,411	8,523	278%	349%	6.7	6.7	927	802	3	3
pH < 6	2	3	13,755	2,341	1,558%	271%	5.5	5.9	117	41	1	2
Ranked by TA (µeq L^{-1})												
TA>2000	48	23	7	130	28%	−0.4%	8.1	8.5	4,200	5,435	6	5
TA 1000–2000	90	41	2,238	3,634	130%	142%	7.4	7.5	1,252	1,319	3	3
TA<1,000	39	58	971	3,811	142%	175%	7.5	7.3	768	779	2	2
TA<500	18	16	1,628	2,204	203%	204%	7.0	7.0	328	346	1	3
TA<100	3	7	3,931	1,407	640%	175%	6.2	6.3	58	57	1	2
Ranked by DOC (mg L^{-1})												
DOC>20	1		−311		−2%		7.3		6,898		26	
DOC 10–20	5	2	−1,625	−2,479	−7%	−93%	7.4	8.3	4,011	487	16	11
DOC<10	18	12	1,123	4,046	22%	255%	7.7	8.2	3,818	4,629	7	7
DOC<5	174	131	1,545	2,859	137%	187%	7.5	7.4	1,463	1,326	2	2
All samples	198	145	1,418	2,884	122%	187%	7.5	7.5	1769	1,588	3	3

For Han River, we included monthly data from 2014 to 2020 (31 sites). Excluded samples with low pH (pH < 5) values.

(DOC<2.5; TA<500 µeq L^{-1}) across various sites of the four large rivers (**Figure 4**). In contrast, the discrepancy between measured and calculated pCO_2 is negligible for the sites with higher DOC and TA, and no trend was discernable for the calculated minus measured pCO_2 with these two variables (**Figure 4**). Although it was weak, a significant positive correlation was found between

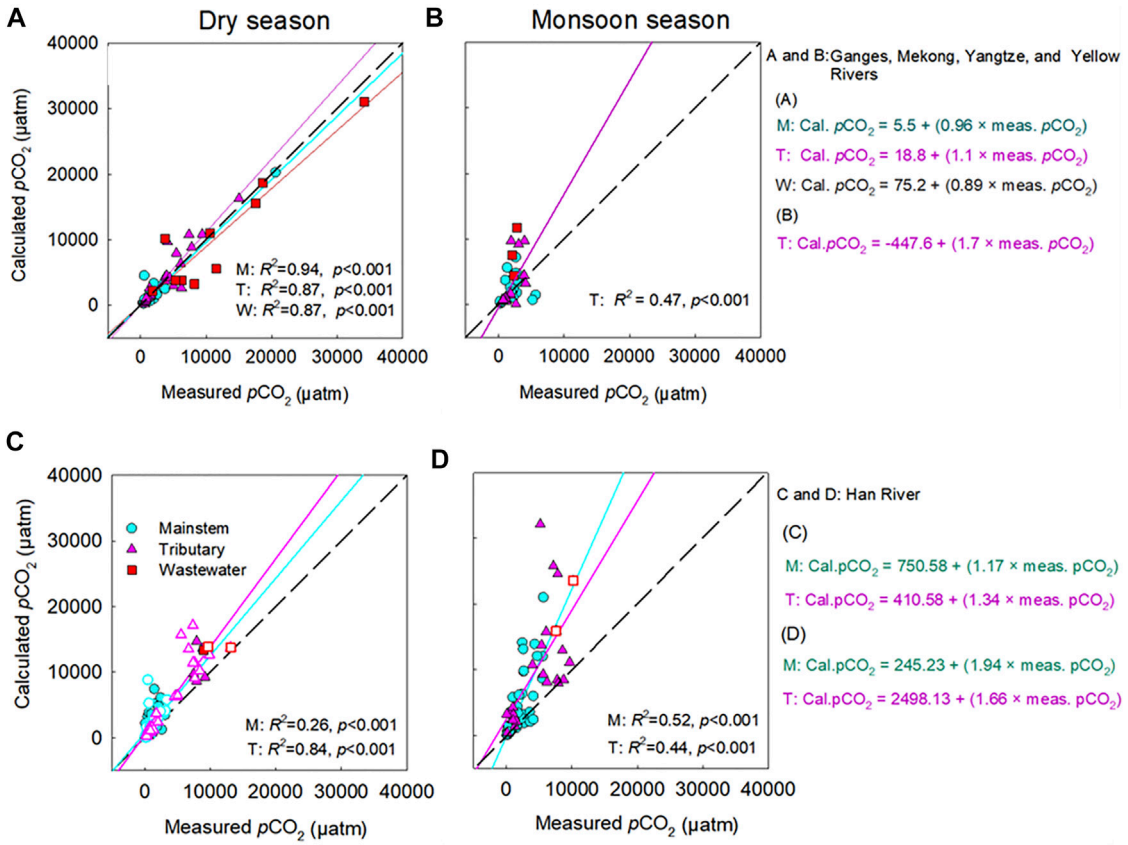

FIGURE 3 | Comparison of the measured and calculated partial pressure of CO_2 (pCO_2) in the mainstems (M), tributaries (T), and polluted urban tributaries or wastewater effluents (W) of the four large Asian rivers [**(A,B)**: the Ganges, Mekong, Yangtze, and Yellow River] and Han River **(C,D)** between the dry season **(A, C)** and monsoon season **(B, D)**. For the four large rivers, 122 data points are presented from **Figure 2** (excluding 8 samples with the large discrepancies between the calculated and measured values obtained at pH < 6.5 and pH < 6.3 during the monsoon and dry periods, respectively), including the mainstem (M) (n: 27 for monsoon season; 23 for dry season), tributaries (T) (n: 27 for monsoon season; 31 for dry season) and wastewater (W) (n: 4 for monsoon season; 10 for dry season) from 2015 to 2019. For the Han River, 209 data points are presented from **Figure 2** (excluding 9 samples with the large discrepancies between the calculated and measured values obtained at pH < 6.4 during the dry periods), including the mainstem (M) (n: 53 for monsoon season; 81 for dry season), tributaries (T) (n: 25 for monsoon season; 44 for dry season) and wastewater (W) (n: 2 for monsoon season; 4 for dry season) from 2014 to 2020. For the Han River, dry seasonal samples are indicated by filled symbols for the months without "rainfall," while void symbols represent the months with "sporadic rainfall." The significant relationship ($p < 0.05$) is indicated by the regression line, while the dashed black line represents the 1:1 line.

pH and DOC ($p < 0.05$; **Figure 5D**) for the tributary sites during the monsoon season. For the mainstem sites of the Han River, the deviations of the calculated pCO_2 from the measured pCO_2 were positively correlated with a relatively short range of DOC concentrations from 0.64 mg L^{-1}–3.35 mg L^{-1} ($p < 0.001$; **Figure 6E**), while DOC concentrations had a negative correlation with the large span of pH from 6.0 to 9.3 during the monsoon season ($p < 0.05$; **Figure 7D**).

A comparison between the calculated and two different measurements of pCO_2 (i.e., headspace equilibration and spray-type equilibrator) was made in addition to the point samplings during the continuous underway measurement of pCO_2 along the Mekong-Tonle Sap around Phnom Penh, Cambodia (in January 2017) and the Buriganga-Meghna-Ganges near Dhaka, Bangladesh (in February 2018) and exhibited very consistent results; the deviation from the 1:1 line was always less than 10% (**Figure 8**). Strong agreement was observed between the calculated and measured pCO_2 values, obtained from the two different measurement techniques (i.e., headspace equilibration and spray-type equilibrator) during the underway measurements across the Ganges and Mekong. Both measurements exhibited strong linear relationships with the calculated values ($R^2 > 0.90$; $p < 0.001$; **Figure 8**).

4 DISCUSSION

4.1 Sources of Error in Calculating pCO_2

Across the five river basins, large discrepancies between the measured and calculated values of pCO_2 were associated with low pH (<7), particularly during the monsoon seasons (**Figures 4**, **6**). The significant decrease in pH across the five rivers during the monsoon season may result from acid rain (pH: 3.5–5; Kim et al., 2007), which is caused by anthropogenic S and N emissions to the atmosphere (Guo et al., 2010; Bisht et al., 2015). In the Han River

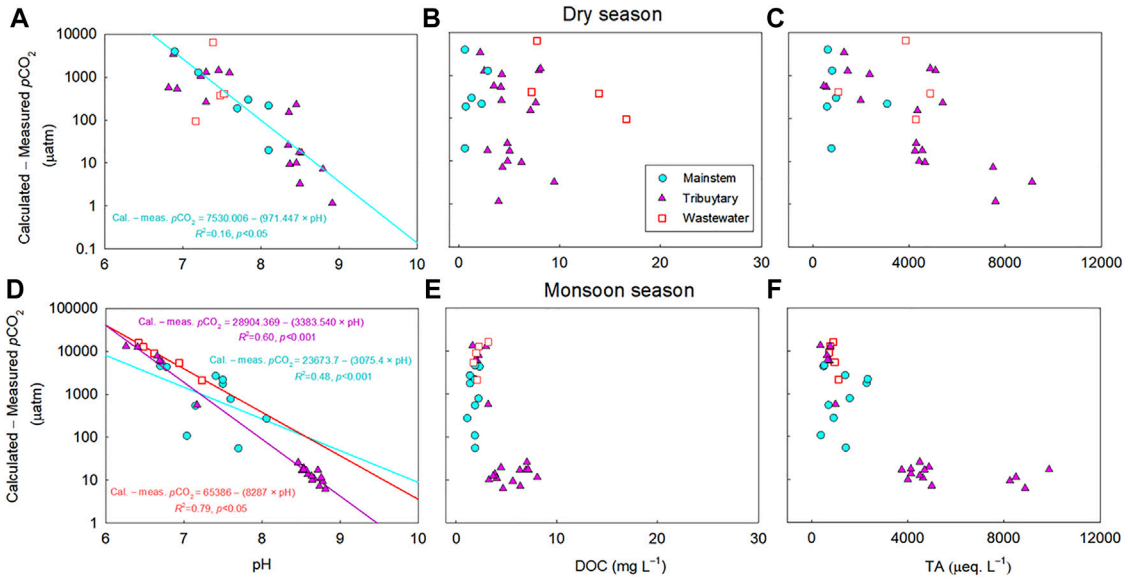

FIGURE 4 | Relationships between the calculated minus measured partial pressure of CO_2 (pCO_2) and pH **(A, D)**, dissolved organic carbon (DOC) **(B, E)**, or total alkalinity (TA) **(C, F)** in the mainstems (M), tributaries (T), and polluted urban tributaries or wastewater effluents (W) of the four large rivers during the monsoon and dry seasons. For the four large rivers, 128 data points are presented from **Figure 2** (excluding 2 extreme values exceeding 25,000 µatm during the monsoon season), including the mainstem (M) (n: 29 for monsoon season; 24 for dry season), tributaries (T) (n: 29 for monsoon season; 30 for dry season), and wastewater (W) (n: 6 for monsoon season; 10 for dry season) from 2015 to 2019. The significant relationship (p < 0.05) is indicated by a regression line through the plot. The difference between calculated pCO_2 and measured pCO_2 against pH was plotted in y-axis in log-scale.

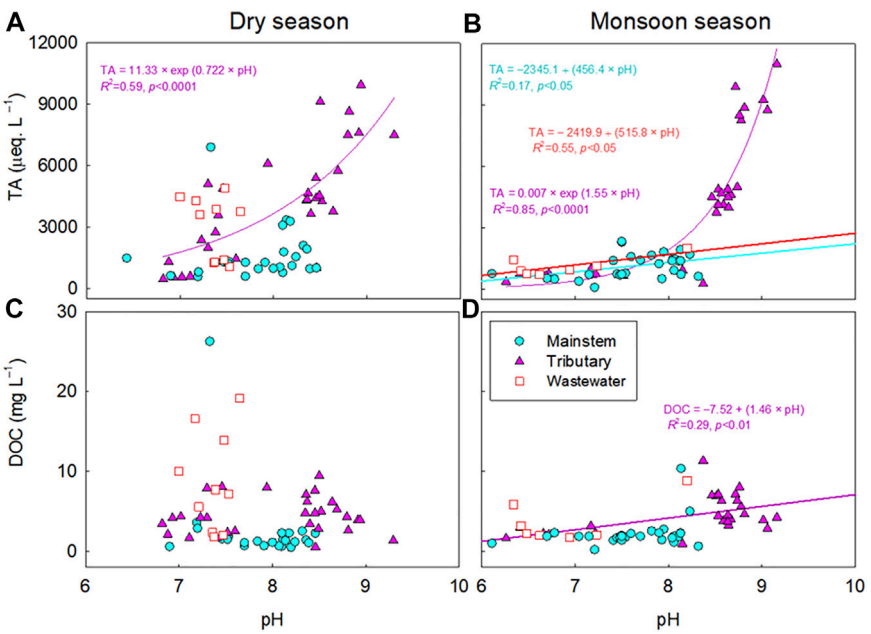

FIGURE 5 | Relationships between pH and total alkalinity (TA) **(A,B)** or dissolved organic carbon (DOC) **(C,D)** in the mainstems (M), tributaries (T), and polluted urban tributaries or wastewater effluents (W) of the Ganges, Mekong, Yangtze, and Yellow River. The significant relationship (p < 0.05) for each water type during the monsoon or dry season is indicated by a regression line through the plot.

basin, the significant correlation between DOC and pH (**Figure 7**) implies that soil-derived organic acids flushed from monsoonal floods, combined with low buffering capacity, may be responsible for the overestimation of pCO_2 at sites with low pH and alkalinity (Jin et al., 2018). The observed overestimation of pCO_2 at low pH is consistent with the previous findings of overestimated pCO_2 in

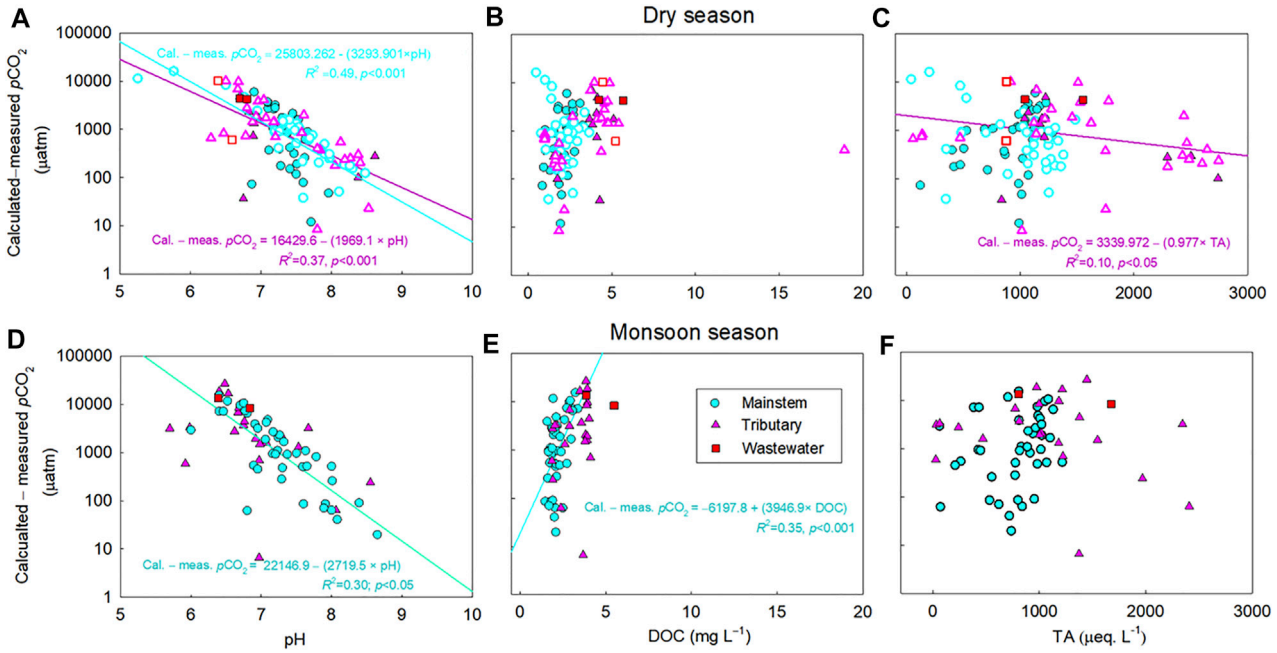

FIGURE 6 | Relationships between the calculated minus measured partial pressure of CO_2 (pCO_2) and pH **(A, D)**, dissolved organic carbon (DOC) **(B, E)**, and total alkalinity (TA) **(C, F)** in the mainstems (M), tributaries (T), and wastewater effluents (W) of the Han River during the monsoon and dry seasons. For the Han River, 212 data points are presented from **Figure 2** (excluding 6 extreme values exceeding 35,000 and 25,000 µatm during the monsoon and dry periods, respectively), including the mainstem (M) (n: 55 for monsoon season; 83 for dry season), tributaries (T) (n: 25 for monsoon season; 43 for dry season), and wastewater (W) (n: 2 for monsoon season; 4 for dry season) from 2014 to 2020. For the dry season, samples are indicated by filled symbols for the months without "rainfall," while void symbols represent the months with "sporadic rainfall." The significant relationship (p < 0.05) is indicated by a regression line through the plot. The difference between calculated pCO_2 and measured pCO_2 against pH was plotted in y-axis in log-scale.

organic-rich, acid freshwater systems (Abril et al., 2005; Abril et al., 2015; Liu et al., 2020). When pCO_2 is calculated from pH and TA, the freshwater TA is often assumed to be dominated by bicarbonate and carbonate (Millero, 1995). Despite this assumption, organic acids and inorganic ions such as PO_4^{3-} and NH_4^+ can contribute significant non-carbonate alkalinity, leading to overestimated calculations of pCO_2 (**Supplementary Table S2**; Hunt et al., 2011; Abril et al., 2015). In particular, large biases in estimating pCO_2 can occur in systems with low alkalinity values (e.g., TA< 500 µeq L^{-1}; Abril et al., 2015; Hunt et al., 2011), while pCO_2 calculations from carbonate equilibria have been successfully applied to rivers and estuaries with moderate to high alkalinity (Raymond et al., 1997; Frankignoulle and Borges 2001).

In the four large river basins, lowered carbonate alkalinity during the monsoon season, combined with relatively low concentrations of DOC, implies an increased sensitivity of pCO_2 calculation to the lowered carbonate alkalinity at low pH, rather than that of organic alkalinity (Hunt et al., 2011; Abril et al., 2015). A large increase in monsoonal rainfall has been shown to considerably dilute TA (Manaka et al., 2015). This rainfall-induced dilution of carbonate alkalinity can become a primary factor for the overestimation of pCO_2 at sites with low pH and alkalinity (Li et al., 2013; Manaka et al., 2015). In contrast, the increasing proportion of wastewater in the receiving river reaches during dry periods can increase the river water alkalinity due to the lack of dilution by rainwater (Hassan et al., 2017), resulting in relatively lower discrepancies between the calculated and measured pCO_2 values in the four large Asian rivers during dry periods compared to wet periods (**Figure 4A**). Small discrepancies between the calculated and measured values of pCO_2 during the cruise expedition along the Ganges and Mekong (**Figure 8**) also suggest that carbonate equilibria-based calculations can be reliably applied to large rivers to calculate pCO_2 from the usual ranges of pH and alkalinity under low-flow conditions. In the case of the Han River, inputs of soil-derived organic acids during sporadic rainfall events may decrease pH even during the dry season (Jin et al., 2018), which appears to be responsible for the observed discrepancies between the measured and calculated pCO_2.

As some sites of the four large Asian rivers, such as wastewater sites of the Ganges and Mekong (i.e., W1, W5–W7, W9, and W10), some dry-seasonal negative discrepancies between the calculated and measured pCO_2 (**Figure 3A**) were observed at pH 7–8 (**Figure 4**). Wastewater discharges of organic and inorganic alkalinity under conditions of low flows without rain-induced dilution, not only altered the composition of riverine OM but also increased pH and TA, resulting in negative deviations of the calculated pCO_2 from well-buffered samples (**Figures 4C**, **5A**; **Supplementary Figure S1C**). The dry seasonal negative discrepancies between the calculated and measured pCO_2 observed at the various sites of the Han River (**Figure 3C**) indicate the potential role of enhanced

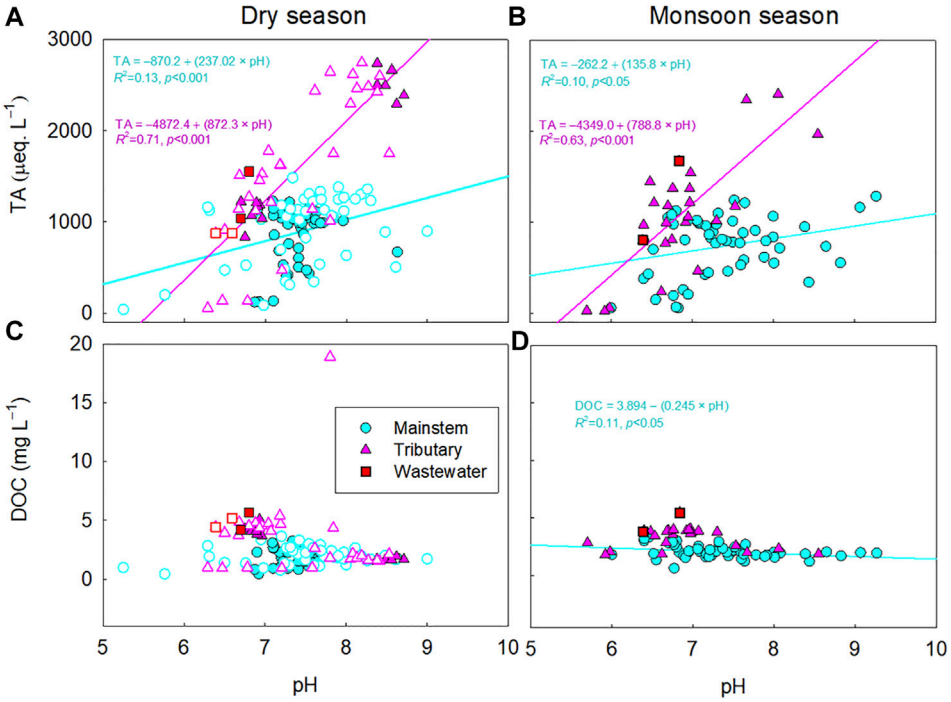

FIGURE 7 | Relationships between pH and total alkalinity (TA) **(A,B)** or dissolved organic carbon (DOC) **(C,D)** in the mainstems (M), tributaries (T), and wastewater effluents (W) of the Han River during the monsoon and dry seasons. For the dry season, samples are indicated by filled symbols for the months without "rainfall," while void symbols represent the months with "sporadic rainfall." The significant relationship ($p < 0.05$) is indicated by a regression line through the plot.

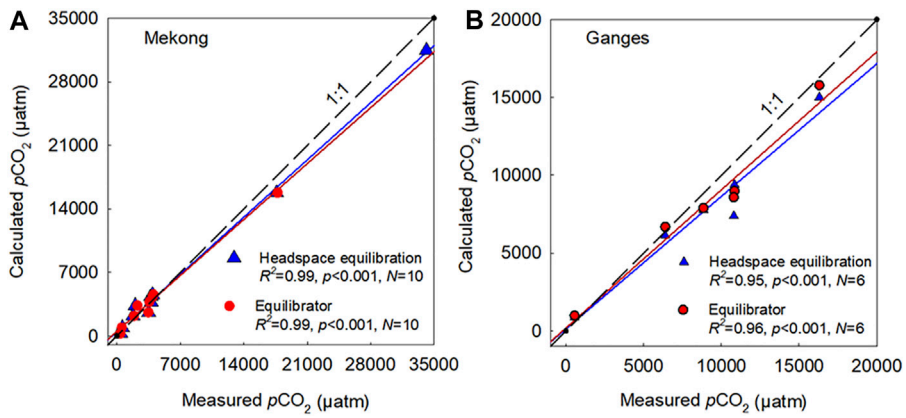

FIGURE 8 | Comparison of the calculated (CO2SYS) and measured partial pressure of CO_2 (pCO_2) using manual headspace equilibration and spray-type equilibrator along the Mekong **(A)** and the Ganges **(B)**. Manual measurements were obtained during a cruise expedition in February 2018 from 6 sampling locations along the mainstems and tributaries of the Lower Ganges near Dhaka, Bangladesh and during a cruise expedition in January 2017 from 10 sampling sites along the Mekong-Tonle Sap and urban tributaries around Phnom Penh, Cambodia.

phytoplanktonic uptake of CO_2 in the low DOC and neutral to basic pH systems (**Figures 6A**, **7B**; **Supplementary Figure S3A**; Jin et al., 2018). Calculated values of pCO_2 below the 1:1 line during the dry season were found at low-pCO_2 sites along the mainstem and impounded sites (i.e., H1–H3, H7, H11, H13–H14) of the Han River (**Figure 3C**). We observed potential underestimations of the calculated pCO_2 at highly basic pH (**Figure 2B**; pH: 9.3–10), such as in the Yellow River, which was consistent with observations of previous research on the Zambezi River in Africa (Abril et al., 2015). Abril et al. (2015) provided no clear explanation for the potential underestimation of the calculated pCO_2 at the high pH range.

TABLE 4 | Summary of the significant linear regressions between the calculated and measured partial pressure of CO_2 (pCO_2) presented in **Figure 3** with adjusted R^2, number of observation (*N*), and *p* values for the regression model.

Season	River	Site	Equations	R^2	*P*	*N*
Dry						
	Ganges, Mekong, Yangtze, Yellow	Mainstem	Cal. pCO_2 = 5.5 + (0.96 × meas. pCO_2)	0.94	<0.001	23
		Tributary	Cal. pCO_2 = 18.8 + (1.1 × meas. pCO_2)	0.87	<0.001	31
		Wastewater	Cal. pCO_2 = 75.2 + (0.89 × meas. pCO_2)	0.87	<0.001	10
	Han	Mainstem	Cal. pCO_2 = 750.58 + (1.17 × meas. pCO_2)	0.26	<0.001	81
		Tributary	Cal. pCO_2 = 410.58 + (1.34 × meas. pCO_2)	0.84	<0.001	44
Monsoon (Wet)						
	Ganges, Mekong, Yangtze, Yellow	Tributary	Cal. pCO_2 = −447.6 + (1.7 × meas. pCO_2)	0.47	<0.001	27
	Han	Mainstem	Cal. pCO_2 = 245.23 + (1.94 × meas. pCO_2)	0.52	<0.001	53
		Tributary	Cal. pCO_2 = 2,498.1 + (1.66 × meas. pCO_2)	0.44	<0.001	25

4.2 Implications of pCO_2 Overestimations for Estimating Riverine CO_2 Emissions

These results point to potential overestimations of previous regional to global-scale riverine CO_2 emissions that were mostly based on carbonate equilibria (pH-TA or pH-DIC). Raymond et al. (2013) excluded pCO_2 values calculated from pH < 5.4 to avoid any potential overestimations. However, our results (**Figure 2B**; **Table 3**) reveal that overestimations of calculated pCO_2 can occur at pH much higher than 5.4, which is consistent with previous findings from a wide range of river systems (Abril et al., 2015; Ran et al., 2021). When we discarded samples with low pH values (pH < 6.5 for the monsoon and <6.3 for the dry season) reasonably good agreements were established between the calculated and measured pCO_2 in the mainstem, tributary, and wastewater sites of the four large rivers (**Figures 3A,B**; **Table 4**). Ran et al. (2021) also excluded the pCO_2 values calculated from samples with low pH values (pH < 6.5) to avoid potential biases in the calculated pCO_2. A more conservative approach by Lauerwald et al. (2015) excluded all polluted sites of rivers across Europe and America to avoid potential overestimations. Our analysis revealed that anthropogenic acids from wastewater effluents and/or soil-flushed CO_2 and organic acids could decrease both pH and TA, causing overestimation of the calculated pCO_2 in the polluted urban rivers during both monsoon and dry seasons (Wang et al., 2017).

Across the five Asian rivers, relatively low average overestimation of pCO_2 was found for dry seasonal samplings than for monsoonal samplings (dry: 122%, monsoon: 187%; **Table 3**). Abril et al. (2015) reported a range of overestimation of pCO_2 (50–300%), while our average overestimations of pCO_2 for seasonal samplings were lower than their highest value (300%). The dry seasonal overestimation of pCO_2 for the mainstem sites of the Han River was higher than that of the four larger rivers (**Supplementary Figures S2, S4**). This implies that inputs of organic acids and inorganic anions such as PO_4^{3-} from wastewater effluents and/or soils can increase non-carbonate alkalinity while the buffering capacity of the carbonate systems can decrease at low pH, resulting in potential overestimation of pCO_2 (Hunt et al., 2011; Abril et al., 2015; Jin et al., 2018).

4.3 Recommendations for Improving Estimation Accuracy

The observed overestimations of pCO_2 during the monsoon and dry seasons suggest that corrective measures be taken when employing a carbonate equilibria model to calculate pCO_2 in rivers with wide ranges of acidity and organic loads under varying weather conditions, particularly during high flow periods. We recommend the constrained use of pCO_2 calculations depending on sites and seasonal conditions. To avoid large overestimations of calculated pCO_2 using pH and TA, we recommend presenting pCO_2 values calculated from low pH values (pH < 6.5 for monsoon and pH < 6.3 for dry season) together with the original pH values to warn the potential overestimation of pCO_2 from low pH values. Although potential overestimations of pCO_2 from low pH values have been reported in previous studies (Abril et al., 2005; Hunt et al., 2011; Abril et al., 2015; Liu et al., 2020), these have often been from acidic, organic-rich waters. Our study provides evidence that intense rainfalls and increasing loads of wastewater can also amplify discrepancies between the calculated and measured pCO_2 from low pH values during both monsoon and dry seasons (**Figures 4**, **6**).

Preestablished regressions between measured pCO_2 and environmental variables can be used to correct overestimated pCO_2 values, particularly during wet periods when major deviations in pH and other conditions are expected. Corrective measures such as adjusting pH to reduce the bias associated with low pH values can reduce uncertainty levels of pH-based pCO_2 calculations. However, this approach would require more empirical relationships to be established to be applied to specific sites. Given the growing interest in evaluating the contribution of riverine CO_2 emissions to the global C budget, it is urgent to obtain more field measurements of pCO_2 across previously understudied river systems where monsoon floods induce various effects on riverine loads of organic acids and TA, thereby affecting pH and carbonate buffering. The lack of direct measurements of pCO_2, however, necessitates the use of carbonate equilibria-based calculations of pCO_2 for many river systems in the near future. In the long-term, direct measurements of pCO_2 using manual headspace equilibration or sensor-based instrumental measurements will provide increasingly more reliable field-based data.

DATA AVAILABILITY STATEMENT

Data are available and can be requested from the corresponding author (jhp@ewha.ac.kr).

AUTHOR CONTRIBUTIONS

OKN and JHP designed the study and wrote the manuscript. MSB and LR obtained and analyzed data for the research. All authors contributed to the discussion of research results and manuscript revision. Funding for this research was arranged by JHP.

FUNDING

This work was supported by the Asia-Pacific Network for Global Change Research (CRRP2016-01MY-Park) and the National Research Foundation of Korea funded by the Korean Government (2017R1D1AB06035179; 2021M3I6A1091270).

ACKNOWLEDGMENTS

We thank Yewon Chun, Dohee Kim, Ju-Hee Lim, and Sung-Hee Choi for their help with fieldwork and sample analyses in the Han River. It is also gratefully acknowledged that the collaborators of the APN-funded project, including Eliyan Chae, Sanjeev Kumar, Xixi Lu, V. V. S. S. Sarma, Shafi Tareq, Do Thi Xuan, and Ruihong Yu, provided invaluable assistance for fieldwork, sample analyses, or data work in the Ganges, Mekong, Yangtze, and Yellow River.

SUPPLEMENTARY MATERIAL

The Supplementary Material for this article can be found online at: https://www.frontiersin.org/articles/10.3389/feart.2021.778215/full#supplementary-material

REFERENCES

Abril, G., Bouillon, S., Darchambeau, F., Teodoru, C. R., Marwick, T. R., Tamooh, F., et al. (2015). Technical Note: Large Overestimation of pCO_2 Calculated from pH and Alkalinity in Acidic, Organic-Rich Freshwaters. *Biogeosciences* 12, 67–78. doi:10.5194/bg-12-67-2015

Abril, G., Guérin, F., Richard, S., Delmas, R., Galy-Lacaux, C., Gosse, P., et al. (2005). Carbon Dioxide and Methane Emissions and the Carbon Budget of a 10-year Old Tropical Reservoir (Petit Saut, French Guiana). *Glob. Biogeochem. Cycles* 19. doi:10.1029/2005GB002457

Abril, G., Richard, S., and Guérin, F. (2006). *In Situ* measurements of Dissolved Gases (CO_2 and CH_4) in a Wide Range of Concentrations in a Tropical Reservoir Using an Equilibrator. *Sci. Total Environ.* 354, 246–251. doi:10.1016/j.scitotenv.2004.12.051

Begum, M. S., Bogard, M. J., Butman, D. E., Chea, E., Kumar, S., Lu, X., et al. (2021). Localized Pollution Impacts on Greenhouse Gas Dynamics in Three Anthropogenically Modified Asian River Systems. *J. Geophys. Res. Biogeosci.* 126, e2020JG006124. doi:10.1029/2020JG006124

Bisht, D. S., Tiwari, S., Srivastava, A. K., Singh, J. V., Singh, B. P., and Srivastava, M. K. (2015). High Concentration of Acidic Species in Rainwater at Varanasi in the Indo-Gangetic Plains, India. *Nat. Hazards* 75, 2985–3003. doi:10.1007/s11069-014-1473-0

Borges, A. V., Darchambeau, F., Teodoru, C. R., Marwick, T. R., Tamooh, F., Geeraert, N., et al. (2015). Globally Significant Greenhouse-Gas Emissions from African Inland Waters. *Nat. Geosci.* 8, 637–642. doi:10.1038/ngeo2486

Butman, D., and Raymond, P. A. (2011). Significant Efflux of Carbon Dioxide from Streams and Rivers in the United States. *Nat. Geosci.* 4, 839–842. doi:10.1038/ngeo1294

Cole, J. J., Prairie, Y. T., Caraco, N. F., McDowell, W. H., Tranvik, L. J., Striegl, R. G., et al. (2007). Plumbing the Global Carbon Cycle: Integrating Inland Waters into the Terrestrial Carbon Budget. *Ecosystems* 10, 172–185. doi:10.1007/s10021-006-9013-8

Feely, R. A., Wanninkhof, R., Milburn, H. B., Cosca, C. E., Stapp, M., and P. Murphy, P. (1998). A New Automated Underway System for Making High Precision pCO_2 Measurements Onboard Research Ships. *Analytica Chim. Acta* 377, 185–191. doi:10.1016/S0003-2670(98)00388-2

Frankignoulle, M., and Borges, A. V. (2001). Direct and Indirect pCO_2 Measurements in a Wide Range of pCO_2 and Salinity Values. *Aquat. Geochem.* 7, 267–273. doi:10.1023/a:1015251010481

Golub, M., Desai, A. R., Mckinley, G. A., Remucal, C. K., and Stanley, E. H. (2017). Large Uncertainty in Estimating PCO_2 from Carbonate Equilibria in Lakes. *J. Geophys. Res. Biogeosci.* 122, 2909–2924. doi:10.1002/2017jg003794

Gran, G. (1952). Determination of Equivalence point in Potentiometric Titrations of Seawater with Hydrochloric Acid. *Oceanol. Acta* 5, 209–218.

Guo, J. H., Liu, X. J., Zhang, Y., Shen, J. L., Han, W. X., Zhang, W. F., et al. (2010). Significant Acidification in Major Chinese Croplands. *Science* 327, 1008–1010. doi:10.1126/science.1182570

Hassan, T., Parveen, S., Bhat, B. N., and Ahmad, U. (2017). Seasonal Variations in Water Quality Parameters of River Yamuna, India. *Int. J. Curr. Microbiol. App. Sci.* 6, 694–712. doi:10.20546/ijcmas.2017.605.079

Hope, D., Dawson, J. J. C., Cresser, M. S., and Billett, M. F. (1995). A Method for Measuring Free CO_2 in upland Streamwater Using Headspace Analysis. *J. Hydrol.* 166, 1–14. doi:10.1016/0022-1694(94)02628-O

Hudson, F. (2004). *Sample Preparation and Calculations for Dissolved Gas Analysis in Water Samples Using GC Headspace Equilibration Technique*. RSKSOP-175, Revision No. 2. USA: U.S. Environmental Protection Agency.

Hunt, C. W., Salisbury, J. E., and Vandemark, D. (2011). Contribution of Non-carbonate Anions to Total Alkalinity and Overestimation of pCO_2 in New England and New Brunswick Rivers. *Biogeosciences* 8, 3069–3076. doi:10.5194/bg-8-3069-2011

Jin, H., Yoon, T. K., Begum, M. S., Lee, E.-J., Oh, N.-H., Kang, N., et al. (2018). Longitudinal Discontinuities in Riverine Greenhouse Gas Dynamics Generated by Dams and Urban Wastewater. *Biogeosciences* 15, 6349–6369. doi:10.5194/bg-15-6349-2018

Kim, M. G., Kim, O. J., and Lee, H. Y. (2007). A Case Study on Acid Rain over Jeju Island, Korea. *J. Clim. Res.* 2, 33–49. http://db.koreascholar.com/article.aspx?code=43648.

Kim, D., Lim, J.-H., Chun, Y., Nayna, O. K., Begum, M. S., and Park, J.-H. (2021). Phytoplankton Nutrient Use and CO_2 Dynamics Responding to Long-Term Changes in Riverine N and P Availability. *Water Res.*, 203. doi:10.1016/j.watres.2021.117510

Kling, G. W., Kipphut, G. W., and Miller, M. C. (1992). The Flux of CO_2 and CH_4 from Lakes and Rivers in Arctic Alaska. *Hydrobiologia* 240, 23–36. doi:10.1007/BF00013449

Lauerwald, R., Laruelle, G. G., Hartmann, J., Ciais, P., and Regnier, P. A. G. (2015). Spatial Patterns in CO_2 evasion from the Global River Network. *Glob. Biogeochem. Cycles* 29, 534–554. doi:10.1002/2014GB004941

Lehner, B., Liermann, C. R., Revenga, C., Vörösmarty, C., Fekete, B., Crouzet, P., et al. (2011). High-resolution Mapping of the World's Reservoirs and Dams for Sustainable River-flow Management. *Front. Ecol. Environ.* 9, 494–502. doi:10.1890/100125

Lewis, E., Wallace, D., and Allison, L. J. (1998). *Program Developed for CO_2 System Calculations*. United States Oak Ridge, Tennessee: Carbon dioxide Information Analysis Center, Oak Ridge National Laboratory, U.S. Department of Energy. doi:10.2172/639712

Li, S. Y., Lu, X. X., and Bush, R. T. (2013). CO_2 Partial Pressure and CO_2 Emission in the Lower Mekong River. *J. Hydrol.* 504, 40–56. doi:10.1016/j.jhydrol.2013.09.024

Liu, S., Butman, D. E., and Raymond, P. A. (2020). Evaluating CO_2 Calculation Error from Organic Alkalinity and pH Measurement Error in Low Ionic Strength Freshwaters. *Limnol. Oceanogr. Methods* 18, 606–622. doi:10.1002/lom3.10388

Liu, S., Lu, X. X., Xia, X., Zhang, S., Ran, L., Yang, X., et al. (2016). Dynamic Biogeochemical Controls on River pCO_2 and Recent Changes under Aggravating River Impoundment: An Example of the Subtropical Yangtze River. *Glob. Biogeochem. Cycles* 30, 880–897. doi:10.1002/2016gb005388

Manaka, T., Ushie, H., Araoka, D., Otani, S., Inamura, A., Suzuki, A., et al. (2015). Spatial and Seasonal Variation in Surface Water pCO_2 in the Ganges, Brahmaputra, and Meghna Rivers on the Indian Subcontinent. *Aquat. Geochem.* 21, 437–458. doi:10.1007/s10498-015-9262-2

Meybeck, M., and Ragu, A. (2012). *GEMS-GLORI World River Discharge Database. Laboratoire de Géologie Appliquée, Université Pierre et Marie Curie*. Paris, France: PANGAEA. doi:10.1594/PANGAEA.804574

Millero, F. J. (1979). The Thermodynamics of the Carbonate System in Seawater. *Geochim. Cosmochim. Acta* 43, 1651–1661. doi:10.1016/0016-7037(79)90184-4

Millero, F. J. (1995). Thermodynamics of the Carbon Dioxide System in the Oceans. *Geochim. Cosmochim. Acta* 59, 661–677. doi:10.1016/0016-7037(94)00354-o

Milliman, J. D., and Farnsworth, K. L. (2011). *River Discharge to the Coastal Ocean: A Global Synthesis*. Cambridge, UK: Cambridge University Press, 13–69.

Park, J.-H., Nayna, O. K., Begum, M. S., Chea, E., Hartmann, J., Keil, R. G., et al. (2018). Reviews and Syntheses: Anthropogenic Perturbations to Carbon Fluxes in Asian River Systems - Concepts, Emerging Trends, and Research Challenges. *Biogeosciences* 15, 3049–3069. doi:10.5194/bg-15-3049-2018

Park, P. K. (1969). Oceanic Co_2 System: an Evaluation of Ten Methods of Investigation1. *Limnol. Oceanogr.* 14, 179–186. doi:10.4319/lo.1969.14.2.0179

Pierrot, D., Lewis, E., and Wallace, D. W. R. (2006). *MS Excel Program Developed for CO_2 System Calculations, ORNL/CDIAC-105a*, 3. Oak Ridge, Tennessee: Carbon dioxide Information Analysis Center, Oak Ridge National Laboratory, U.S. Department of Energy.

Ran, L., Butman, D. E., Battin, T. J., Yang, X., Tian, M., Duvert, C., et al. (2021). Substantial Decrease in CO_2 Emissions from Chinese Inland Waters Due to Global Change. *Nat. Commun.* 12, 1730. doi:10.1038/s41467-021-21926-6

Ran, L., Li, L., Tian, M., Yang, X., Yu, R., Zhao, J., et al. (2017b). Riverine CO_2 emissions in the Wuding River Catchment on the Loess Plateau: Environmental Controls and Dam Impoundment Impact. *J. Geophys. Res. Biogeosci.* 122, 1439–1455. doi:10.1002/2016JG003713

Ran, L., Lu, X. X., and Liu, S. (2017a). Dynamics of Riverine CO_2 in the Yangtze River Fluvial Network and Their Implications for Carbon Evasion. *Biogeosciences* 14, 2183–2198. doi:10.5194/bg-14-2183-2017

Ran, L., Lu, X. X., Richey, J. E., Sun, H., Han, J., Yu, R., et al. (2015). Long-term Spatial and Temporal Variation of CO_2 Partial Pressure in the Yellow River, China. *Biogeosciences* 12, 921–932. doi:10.5194/bg-12-921-2015

Raymond, P. A., Caraco, N. F., and Cole, J. J. (1997). Carbon Dioxide Concentration and Atmospheric Flux in the Hudson River. *Estuaries* 20, 381–390.

Raymond, P. A., Hartmann, J., Lauerwald, R., Sobek, S., McDonald, C., Hoover, M., et al. (2013). Global Carbon Dioxide Emissions from Inland Waters. *Nature* 503, 355–359. doi:10.1038/nature12760

Smethie, W. M., Takahashi, T., Chipman, D. W., and Ledwell, J. R. (1985). Gas Exchange and CO_2 flux in the Tropical Atlantic Ocean Determined from ^{222}Rn and pCO_2 measurements. *J. Geophys. Res.* 90, 7005–7022. doi:10.1029/jc090ic04p07005

Wang, X., He, Y., Yuan, X., Chen, H., Peng, C., Zhu, Q., et al. (2017). pCO_2 and CO_2 fluxes of the Metropolitan River Network in Relation to the Urbanization of Chongqing, China. *J. Geophys. Res. Biogeosci.* 122, 470–486. doi:10.1002/2016jg003494

Wang, Z. A., Bienvenu, D. J., Mann, P. J., Hoering, K. A., Poulsen, J. R., Spencer, R. G. M., et al. (2013). Inorganic Carbon Speciation and Fluxes in the Congo River. *Geophys. Res. Lett.* 40, 511–516. doi:10.1002/grl.50160

Webb, J. R., Maher, D. T., and Santos, I. R. (2016). Automated, *In Situ* Measurements of Dissolved CO_2 , CH_4 , and δ^{13} C Values Using Cavity Enhanced Laser Absorption Spectrometry: Comparing Response Times of Air-Water Equilibrators. *Limnol. Oceanogr. Methods* 14, 323–337. doi:10.1002/lom3.10092

Weiss, R. F. (1974). Carbon Dioxide in Water and Seawater: The Solubility of a Non-ideal Gas. *Mar. Chem.* 2, 203–215. doi:10.1016/0304-4203(74)90015-2

Yoon, T. K., Jin, H., Oh, N.-H., and Park, J.-H. (2016). Technical Note: Assessing Gas Equilibration Systems for Continuous pCO_2 Measurements in Inland Waters. *Biogeosciences* 13, 3915–3930. doi:10.5194/bg-13-3915-2016

Conflict of Interest: The authors declare that the research was conducted in the absence of any commercial or financial relationships that could be construed as a potential conflict of interest.

The handling Editor declared a past co-authorship with the authors ON, SB, LR, and JP.

Publisher's Note: All claims expressed in this article are solely those of the authors and do not necessarily represent those of their affiliated organizations, or those of the publisher, the editors and the reviewers. Any product that may be evaluated in this article, or claim that may be made by its manufacturer, is not guaranteed or endorsed by the publisher.

frontiers in Earth Science

ORIGINAL RESEARCH
published: 18 February 2022
doi: 10.3389/feart.2022.806897

Distribution and Dynamics of Radiatively Active Gas (RAG) Emissions From Major Estuaries of the Sundarbans Mangrove, India

*Avanti Acharya[1], Prasun Sanyal[1], Madhusudan Paul[1], Vandana Kumari Gupta[1], Sneha Bakshi[1] and Sandip Kumar Mukhopadhyay[1,2]**

[1]Department of Marine Science, University of Calcutta, Kolkata, India, [2]Ministry of Earth Sciences, Government of India, New Delhi, India

OPEN ACCESS

Edited by:
Mashura Shammi, Jahangirnagar University, Bangladesh

Reviewed by:
Anirban Akhand, Port and Airport Research Institute (PARI), Japan
Abhijit Chatterjee, Bose Institute, India

***Correspondence:**
Sandip Kumar Mukhopadhyay
skm.caluniv@gmail.com

Specialty section:
This article was submitted to Biogeoscience, a section of the journal Frontiers in Earth Science

Received: *01 November 2021*
Accepted: *05 January 2022*
Published: *18 February 2022*

Citation:
Acharya A, Sanyal P, Paul M, Gupta VK, Bakshi S and Mukhopadhyay SK (2022) Distribution and Dynamics of Radiatively Active Gas (RAG) Emissions From Major Estuaries of the Sundarbans Mangrove, India. Front. Earth Sci. 10:806897. doi: 10.3389/feart.2022.806897

The world's largest mangroves ecosystem, the Sundarbans, being highly productive and a place for extensive organic matter cycling, is considered to be the hotspot for biogeochemical studies in the tropical estuarine environment. Hence, the spatial and temporal dynamics of the biogenic gases (CO_2, CH_4, and N_2O), also known as radiatively active gases, were measured in mangrove-dominated estuaries of the system. In addition to spatial and seasonal observation, three full tidal cycles were observed at one site. Results showed that the air/water gas saturations were widely distributed and highly variable along the stretch. The gas saturations showed varying responses to salinity and tidal fluctuations. This indicated that localized biogeochemical processes may be more influential than simple mixing and dilution processes in controlling the variability of these gases. The surface waters were always supersaturated with CH_4 (Up to 13,133%) relative to the atmosphere. However, N_2O ranged from 8 to 1,286% and CO_2 from 30 to 2075%. N_2O fluxes were ~4.8 times higher in the pre-monsoon than the post-monsoon. CH_4 fluxes were ~3.6 times higher in the pre-monsoon than both the monsoon and the post-monsoon. CO_2 fluxes were ~10 times higher in the monsoon than both the pre-monsoon and the post-monsoon. The seasonality in the gas saturation could be linked more to the availability of substrates than physicochemical parameters. Overall, air/water CH_4 fluxes varied maximally (0.4–18.4 $\mu mol\, m^{-2}\ d^{-1}$), followed by CO_2 fluxes (–0.6–10.9 $mmol\, m^{-2}\ d^{-1}$), and N_2O fluxes varied the least of all (–0.6–5.4 $\mu mol\, m^{-2}\ d^{-1}$). Interestingly, CH_4 and N_2O fluxes were positively correlated to each other ($p < 0.05$), suggesting organic matter decomposition as the key factor in the production of these two gases. Finally, these water–air CO_2, CH_4, and N_2O flux estimates show that the estuaries are a modest source of CH_4 but fluctuate between sources and sinks for CO_2 and N_2O gases.

Keywords: carbon dioxide, distribution of RAGs, Indian sundarban, methane, nitrous oxide, air/water fluxes

INTRODUCTION

Rapid changes in the global climate being of primary concern have recently led to investigations regarding the recent developments in the phenomenon of radiative forcing. Currently, the global mole fractions of the gases are at an all-time high (IPCC, 2014). According to IPCC 2014, particularly, the concentrations of the major greenhouse gases like carbon dioxide (CO_2), methane (CH_4), and nitrous oxide (N_2O) have been major contributors in radiative forcing, more than solar radiation. The radiative equilibrium of the Earth can be influenced by CO_2, CH_4, and N_2O, causing a net gain of solar energy by the atmosphere, particularly infrared radiation (IR), which eventually causes warming. These greenhouse gases can, therefore, be termed alternatively as radiatively active gases or RAGs.

Detailed accounts of each of these gases have since been obtained from studies first carried out in the oceans and seas (Bange, 2008; Forster et al., 2009). It is imperative to quantify CO_2, CH_4, and N_2O because the global greenhouse gas flux budget needs accurate information on the contribution of these gases (Khalil et al., 2002; Wuebbles and Hayhoe, 2002).

Natural sources of N_2O and CH_4 account for an estimated 44%–54% of N_2O emissions (9.6–10.8 Tg y^{-1} N_2O) and 30%–40% of CH_4 emissions (150–237 Tg y^{-1} CH_4) (IPCC, 2014). In the global list, tropical soils and wetlands make for significant natural sources, contributing approximately 22%–27% (N_2O) and 24% (CH_4), respectively, toward this list (Griggs and Noguer, 2002; Whalen, 2005). Spatial emission studies in tropical and subtropical estuarine systems suggest that these areas serve as strong sources of atmospheric CH_4, N_2O, and CO_2 (Guo et al., 2009; Musenze et al., 2014). On the other hand, reports of relatively pristine river-dominated Tay Estuary, United Kingdom (Harley et al., 2015) revealed lower annual emission of RAGs, contradictory to that usually estimated for European estuaries. Again, flux estimation in the Tubul-Raqui estuary, central Chile (36°S) (Daniel et al., 2013) showed that the estuary acts as a sink for N_2O but a source for CH_4 and CO_2. These estimates are teeming with uncertainties when considering distinct environmental features of each estuarine system, such as the extent of stratification, anthropogenic influence, nitrogen budget, and tidal influence (Barnes and Upstill-Goddard, 2011; Alberto V; Borges, 2011; Ivens et al., 2011; Crosswell et al., 2012; Laruelle et al., 2013). Although these areas have notably contributed to the global estimate for RAGs, the values may have been overestimated in most cases, since nutrient-impacted estuaries and macrotidal estuaries have been more in focus for global estimation than their pristine counterparts (Frankignoulle et al., 1998).

In mangrove-dominated estuaries, a significant amount of organic matter, both in dissolved and particulate forms as well as dissolved nutrients, is added to the estuarine water column, resulting in a very complex and dynamic environment for the nutrients. This is because mangroves reportedly store 937 t C ha^{-1} organic matter in soil with a mean global burial rate of 174 g C m^{-1} y^{-1} (Alongi, 2012). These estuaries also have high concentrations of suspended particulate matter (SPM) relative to adjacent coastal waters. The interaction of nutrients and other dissolved species with these particles is an important biogeochemical process in these waters. This SPM is derived from river inputs or resuspension or imported from adjacent coastal waters with a minor contribution from atmospheric inputs.

Microbial processes in the mangrove sediments and water column regenerate organic matter and release dissolved nutrients back to the water column by consuming these suspended particles and organic-rich aggregates. This organic matter regeneration process utilizes dissolved oxygen. This leads to hypoxic, or sometimes anoxic, conditions favoring anaerobic microbial processes like methanogenesis and denitrification. These processes release trace gases like CH_4 and N_2O, respectively. The presence of a constant tidal activity helps accumulate large amounts of organic matter in the sediment. This, in turn, prompts redox conditions in the sediment, intensifying the anaerobic processes. Methanogenesis is one of the terminal processes of the anaerobic degradation of carbon. Environments with a high input of organic carbon and less competition from oxidants such as O_2, NO_3^-, Mn^{4+}, Fe^{3+}, and SO_4^{2-} particularly favor methanogenesis. Estuaries are known to be low in SO_4^{2-} concentrations and are hence favorable for methanogenesis (Middelburg et al., 2000). N_2O production *via* denitrification may be reduced if O_2 and NO_3^- are absent; N_2O is consumed by denitrifying bacteria as the terminal electron acceptor. The combined effect causes the sediment porewater to be enriched with CH_4 and N_2O, which, finally through advective transport, enriches the level of those gases in the estuarine water column. Denitrification can also occur in the water column alongside nitrification, where NH_4^+ is oxidized to NO_2^-, releasing N_2O as a byproduct (Bange, 2008). Both the processes rely heavily on the available dissolved oxygen content (Brase et al., 2017). CH_4 and N_2O are important biogenic trace gases and together account for ~20% enhanced greenhouse forcing (Forster et al., 2009). Current best estimates are that marine waters provide <5% of tropospheric CH_4 and 29%–55% of tropospheric N_2O; the highest contributions are from estuaries and shallow coastal shelves (Seitzinger and Kroeze, 1998).

For our study, we have stressed 1) the distribution of CO_2, CH_4, and N_2O, the three major radiatively active gases (also called greenhouse gases) in water, and 2) their flux dynamics in the Indian Sundarban, comprising the Saptamukhi-Thakuran-Matla estuarine region concerning spatial, diel, and seasonal variability. The chosen area is a comparatively pristine buffer zone with no previous reports based on wide spatial coverage of the three RAGs together. Hypothesizing the fact that these estuaries are a source of CO_2, CH_4, and N_2O, the dissolved concentrations were used to calculate the air/water fluxes for each station. The findings from our study can be contributory to further research on the biogeochemical processes related to the production of CO_2, CH_4, and N_2O in the Indian part of Sundarban.

MATERIAL AND METHODS

Study Site

The Indian Sundarban estuaries, about 40% of the total Sundarban shared between India and Bangladesh, are situated

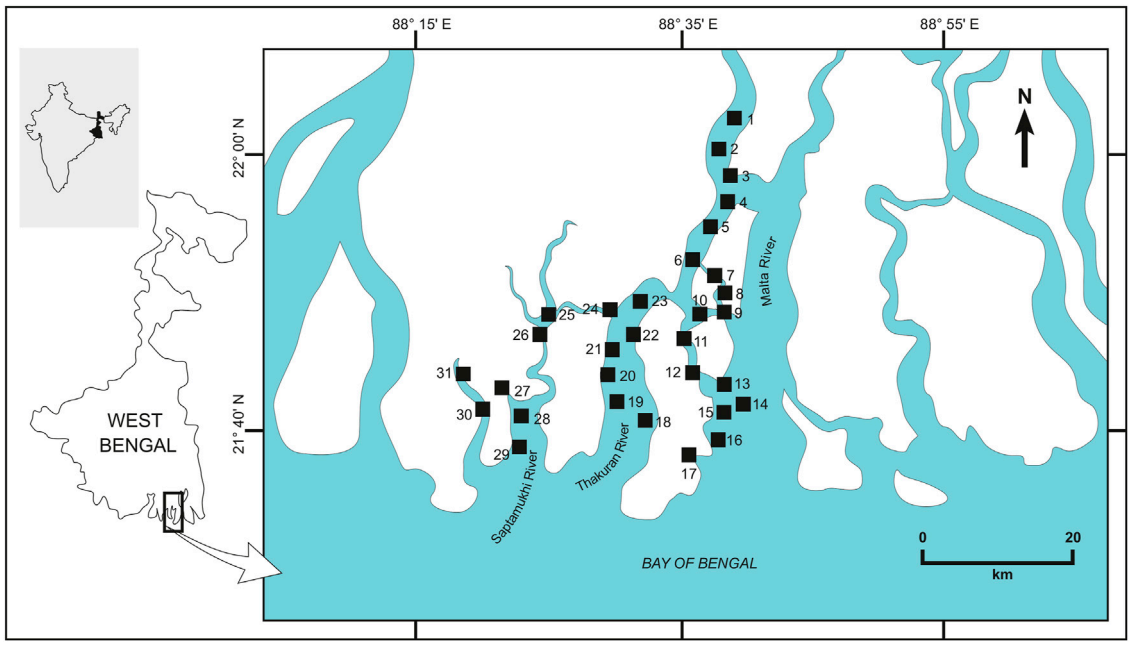

FIGURE 1 | Map of the study area showing points off observation in the Indian Sundarban region.

on the northeast coast of India and drain into the Bay of Bengal. The estuary has an area of 1,800 km^2 (Dutta et al., 2019) with a tidal range of 4.32 and 5.58 m (Chatterjee et al., 2013). The intertidal area is 45% of 4,260 km^2 (Dutta et al., 2017). Overall, the estuaries have a mean depth of ~6 m (Dutta et al., 2019) with a semidiurnal tide pattern and limited freshwater supply, making the estuaries marine dominated (Dutta et al., 2015). The estuaries receive partial anthropogenic inputs in the monsoon. The mean annual rainfall is 1,973 mm, most of which is received by the area between the months of June and September (Ray et al., 2013).

The Indian part of Sundarban stretches for approximately 50–70 km from the north to the southern margin of the Bay of Bengal and 140 km from east to west. For the study, the estuaries Saptamukhi, Thakuran, and Matla were chosen as they have several interconnected channels exhibiting the semi-diurnal tidal nature and forming a major part of the Indian Sundarban estuaries (Sanyal et al., 2020).

The Saptamukhi estuary, located at 21.604°N and 88.352°E, shows a tidal range of 1.8–5.2 m (Mukhopadhyay et al., 2006). It is about 41 km long and 10 km wide. It receives a considerable amount of inputs from agricultural lands and other anthropogenic sources *via* run-off but has no perennial source of freshwater. Several mangrove-dominated islands, some of which also have human settlements, flank the waters. Its eastern part is stronger and widens in its last 10 km to the Bay of Bengal.

With similar tide conditions and mangrove-dominated islands, the Thakuran estuary is located at 21.658 °N and 88.492°E. About 62 km long and 10 km wide, this estuary is situated close to the Bay of Bengal. The mouth of the Thakuran estuary is vulnerable to bank erosion. The mid-channel bars show varying sediment compositions ranging from mud to sand (Das, 2016).

Of the two estuaries, the Matla estuary (21.603°N, 88.655°E), runs the longest distance from Canning to the Bay of Bengal. At its head, human settlement and agriculture are now common activity. Currently subject to heavy sedimentation, its depth has shortened considerably to about 2–6 m (Akhand et al., 2021). The mouth of the estuary is about 26 km wide, which allows substantial amounts of marine waters of the Bay of Bengal to flow in at high tide. The present conditions of the Matla suggest that both human intervention and forces have led to a considerable reduction in its freshwater supply.

Water Sampling and Analysis

Water samples from the estuaries were collected for the measurement of physicochemical parameters and RAG concentrations from a hired mechanized boat from 31 stations from April 2016 to August 2019 (**Figure 1**). On sampling occasions of July 2017, June 2019, and August 2019, the sampling was conducted over a 24 h period, with samples collected every 2 h, at one site (site 27), Lothian island, located at the confluence of the Saptamukhi estuary and the Bay of Bengal (Biswas et al., 2007), to assess the temporal variation over three full tidal cycles and compare them. Water samples were collected using 5 L Niskin bottles (OceanTest Equipment, Fort Lauderdale, FL, USA). Subsamples for dissolved oxygen (DO), nutrients (nitrate and ammonium), chlorophyll-*a,* and total alkalinity were collected in triplicate Niskin sampling at all stations.

Water temperature and salinity were recorded using a conductivity–temperature–depth profiler (SBE 19 plus; Sea-

Bird Electronics, Bellevue, WA, USA) (±0.005 standard deviation) and deployed bi-hourly for diurnal observations. DO was sampled in 125 ml glass DO bottles and estimated by Winkler's titrimetric method with ±3.6 μM standard deviation between duplicates. Nutrients were filtered in GF/F 0.45 μm filter papers and filtrates analyzed as per standard protocols (Wangersky, 1978) at ±0.02 μM standard deviation. Chlorophyll-a (chl-*a*) subsamples were collected in 500 ml HDPE dark bottles and filtered using 47 mm GF/F filter papers (pre-combusted at 350°C for 4 h), which were later stored in Cryochill™ vials and transported back to the laboratory in a liquid nitrogen can. Subsequently, chl-*a* was measured using the spectrophotometric method (Parsons et al., 1984) with an analytical precision of ±2.5%. pH (NBS scale) and water temperature were measured onboard immediately after sampling using Ross combination electrode pH meter (Orion Star A211) fitted with an additional water temperature sensor. Total alkalinity (TA) was measured after bringing the samples back to the laboratory preserved in 60 ml polypropylene bottles with 30 μl saturated mercuric chloride ($HgCl_2$), using the potentiometric titration method in an open cell at 25°C at 0.78% uncertainty (Steven Bouillon et al., 2003; Chou et al., 2013) when tested against Dickson Standard (CRM131-0,215). Unfiltered DIC samples were determined using a coulometer (Model Coulometer CM5017; UIC Inc., Joliet, IL, USA). The mean relative uncertainty of DIC was found to be 4.6% when tested against the same Dickson Standard. Wind speed was logged continuously using Weather Station (Davis Vantage Pro2, USA) fitted on the roof of the boat at 10 m above.

Measurement of Dissolved CO_2, CH_4, and N_2O

Gas concentrations were determined using the headspace method in surface water sampled in triplicate at ~0.5 cm from the surface waters from each study point. The water samples were collected in 60 ml borosilicate vials right after the collection of DO samples. Samples were preserved immediately from microbial activity using 30 μl saturated mercuric chloride ($HgCl_2$) and sealed using a rubber septum and aluminum cap. CH_4 and N_2O were analyzed on a Trace 1,110 gas chromatograph (M/s. Thermo) with a built-in flame ionization detector and an electron capture detector for [N_2O] was used for the determination of dissolved gas concentrations. Concentrations were determined from the peak areas of a set of two standard gas mixtures (CH_4/N_2O: 183/0.517; 414/1.0 ppm) with an accuracy of ±5%. The dissolved concentrations were expressed as nmol L^{-1} for CH_4 and N_2O (Bange et al., 2019). The standard runs were included before and after the analysis. The concentrations of dissolved (and expected saturation percent concerning atmospheric concentration) CH_4 and N_2O were calculated from the concentrations measured from the headspace using solubility coefficients as a function of temperature and salinity given by (Wiesenburg and Guinasso Jr, 1979; Weiss and Price, 1980). Saturation percents for the gases were determined as the ratio of the concentration of the dissolved gas and the expected atmospheric equilibrium water concentrations.

The partial pressure of dissolved CO_2 was expressed as μatm and obtained from CO2SYS software (Excel version 2.3) using the TA-DIC couple, dissociation constants of salinity range 0–40 (Cai and Wang, 1998), and $KHSO_4$ constant (Dickson, 1990). The propagated uncertainty of the calculated pCO_2 was found to be 2.1% (Hoppe et al., 2010; Orr et al., 2018).

Calculating CO_2, CH_4, and N_2O Air/Water Fluxes From the Estuaries

The air/water gas fluxes (WA-F_{Gas}) were calculated using

$$WA - F_{Gas} = k_i\left([Gas]_w - [Gas]_{eq} \right) \quad (1)$$

where k_i (cm h^{-1}) is the gas transfer velocity, $[Gas]_w$ (nmol L^{-1}) is the dissolved gas concentration, and $[Gas]_{eq}$ (nmol L^{-1}) is the dissolved concentration at equilibrium with the appropriate atmospheric concentration. As k was not measured in our study, gas fluxes were estimated, applying four parameterizations of k based on their widespread use in the literature (Clark et al., 1995; Raymond and Cole, 2001; Ho et al., 2011; Wanninkhof, 2014).

C95: Clark et al. (1995):

$$k_{600} = 2.0 + 0.24\,(u_{10}) \quad (2)$$

RC01: Raymond and Cole (2001):

$$k_{600} = 1.91 \times e^{0.35u}10 \quad (3)$$

H11: Ho et al. (2011):

$$k_{600} = a + 0.266\,(u_{10})^2 \quad (4)$$

W14: Wanninkhof (2014):

$$k_{600} = 0.25 \times u10^2 \quad (5)$$

where k_{600} is the gas transfer velocity of CO_2 normalized to 20°C (cm h^{-1}) and u_{10} is the mean wind speed (m s^{-1}) of each month of the sampling campaign, calculated from the continuous wind speed measured daily using a Davis Vantage Pro2 portable weather station (United States). The "a" in H11 equation was considered 0 based on the depth and the dimension of the estuary studied (Akhand et al., 2021). The water temperature and salinity influence the gas transfer velocity, which again differs among gases. From the obtained values of k_{600}, k_i was calculated at the observed temperature and salinity in the field measurements following the method of Ferrón et al. (2007a):

$$k_i = k_{600}\,(Sc_i/Sc_{600})^{-0.5} \quad (6)$$

Sc_i is the Schmidt number, the ratio of the kinematic viscosity of water to the diffusivity of the gas, and is calculated using the method of Wanninkhof (2014), assuming that Sc_i varies linearly with salinity and k_i is directly proportional to $Sc^{-0.5}$ (Ferrón et al., 2007b; Harley et al., 2015). The fluxes were expressed in mmol m^{-2} h^{-1} for CO_2 and in μmol m^{-2} h^{-1} for CH_4 and N_2O.

The calculated k values were then used to obtain the gas flux density using **Eq. 1** and extrapolated to the total estuarine area of 1,800 km^2 (Dutta et al., 2019) by multiplying the total estuary area

to the mean flux density (n = 244) and expressed as yearly emission. The fluxes were also expressed as CO_2 equivalents by multiplying emissions by their global warming potentials (GWPs); 1 for CO_2, 28 for CH_4, and 265 for N_2O.

Analysis of Sediment/Air and Sediment/Water RAG Fluxes From Intertidal Sediments

The fluxes (CO_2, CH_4, and N_2O) from the intertidal sediments of the mangrove systems were done by collecting the gas samples by using the 'manual closed chamber method' (Bhattacharyya et al., 2013a, 2016) at site 27 close to the Saptamukhi estuary. Chamber deployment was not allowed in other sites due to government restrictions. In this method, the gas samples for RAG fluxes (CO_2, CH_4, and N_2O) were collected from the Perspex chamber (53 × 37 × 51 cm^3) set at the lower, middle, and upper littoral zones respectively at each study site. A battery-operated air circulation pump with an air displacement of 1.5 L min^{-1} was connected to a polyethylene tubing to mix the air inside the chamber and draw the air samples into a plastic syringe (Bhattacharyya et al., 2013b) at 0,15, and 30-min intervals. For this system, gas samples were collected in presence of the pneumatophores in sediments. The gas samples were collected at 20 locations within the site with three replicates. The RAG concentrations were then analyzed by using gas chromatography (Model no: Trace 1,110 Gas Chromatograph; M/s Thermo).

The sediment/air RAG flux was calculated following the method of (Collier et al., 2014; Kahmark and Millar, 2020). The slope of T_0, T_{15}, and T_{30} concentrations over time was determined, in ppmv min^{-1}, equivalent to μl l^{-1} min^{-1}. The slope was designated as α_v. This slope was converted to the unit of mass designated as α_m, in μg l^{-1} min^{-1} and corrected for field temperature applying the ideal gas law:

$$\alpha_m = (\alpha_v \times M \times P)/(R \times T) \quad (7)$$

where: α_m is μg RAG l^{-1} min^{-1}; M = molar weight of RAG (44 μg μmol^{-1} CO_2 or N_2O or 16 μg μmol^{-1} CH_4); p = 1 atm (standard atmospheric pressure); R = universal gas constant = 0.0821 μl atm μmol^{-1} K^{-1}; T = field temperature, in K = °C + 273.

The flux (SA-F_{Gas}) of RAG was then calculated as μg RAG m^{-2} h^{-1} using the following equation:

$$SA - F_{Gas} = (\alpha_m \times V \times 60)/A \quad (8)$$

where: α_m is μg RAG l^{-1} min^{-1}; V is the volume of the gas in the chamber in l; and A = sediment surface areas covered by the chamber in m^2. The fluxes were finally expressed in terms of moles to ease the comparison with the air/water RAG fluxes.

To verify the influence of intertidal areas on the RAG fluxes in the estuary, porewater samples were collected from 1 m deep pit holes made into 14 locations using a steel corer in the intertidal zones around sites 17, 19, and 27 on the sampling occasions of April 2019, June 2019, and August 2019. The porewater samples were collected into 500 ml PVC bottles using a manually operated suction pump. Porewater salinity was also measured using the Mohr–Knudsen method. RAG concentrations were measured using the same gas chromatograph from the porewater samples to calculate the advective transport of the gases from sediment porewater to adjacent estuarine water on sampling occasions. The advective transport was then calculated using the formula:

$$F_{ISW} = d \times [Gas]_{ISW} \quad (9)$$

where d = specific discharge and $[Gas]_{ISW}$ = porewater RAG concentration in the sediment (interstitial water). The mean specific discharge of 0.006 cm min^{-1} (Dutta et al., 2015) was used to calculate the F_{ISW}. The fluxes were expressed in terms of moles.

Statistical Analyses

Statistical analysis was performed using Minitab version 18. A seasonality index was produced by splitting the data into two groups: late monsoon/post-monsoon (December 2018, November 2016, December 2018, January 2019, and January 2020) and pre-monsoon/early monsoon (April 2016, May 2017, June 2017, July 2017, October 2017, March 2018, September 2018, April 2019, June 2019, and August 2019). Given its six-month-long duration, the monsoon period was subcategorized into early and late monsoon to address differences in gas saturations within the period. The pre-monsoon/early monsoon means were divided by the late-monsoon/post-monsoon means to derive the seasonality index for the estuary and each sampling site. Index values close to 1 would indicate little seasonal difference, while values above 1 would mean higher gas saturations in pre-monsoon/early monsoon than late monsoon/post-monsoon (Harley et al., 2015). Significant differences between the two pairs of saturation were tested with two-sample t-tests. A two-way analysis of variance was also applied on the gas saturations, air/water, and sediment/water fluxes based on estuary and season as factors to assess the spatial and seasonal variability, while light and tide were factors (high tide or low tide) chosen to assess the tidal variability. Spearman rho correlation coefficients were then calculated to examine relationships between the measured gas saturations and other physicochemical parameters. In addition, the stepwise regression of gas saturation with other physicochemical parameters was performed to discern the key factors controlling the variability of the gas saturation.

RESULTS AND DISCUSSION

Spatial Pattern

All the gases and the associated physicochemical parameters of the estuaries showed random distributions against distance from the mouth of the estuary (**Figure 2**). This meant that no distinct increasing or decreasing pattern was found in the gases and the parameters that suggest little hydrological differences between the three estuaries, owing to their well-mixed nature (Dutta et al., 2015).

N_2O saturations ranged from 8 to 1,286% (**Figure 2**). However, the majority of the saturation values lay within 400%. The distribution was random throughout the extent of the study area, corroborating the studies on N_2O that identify the

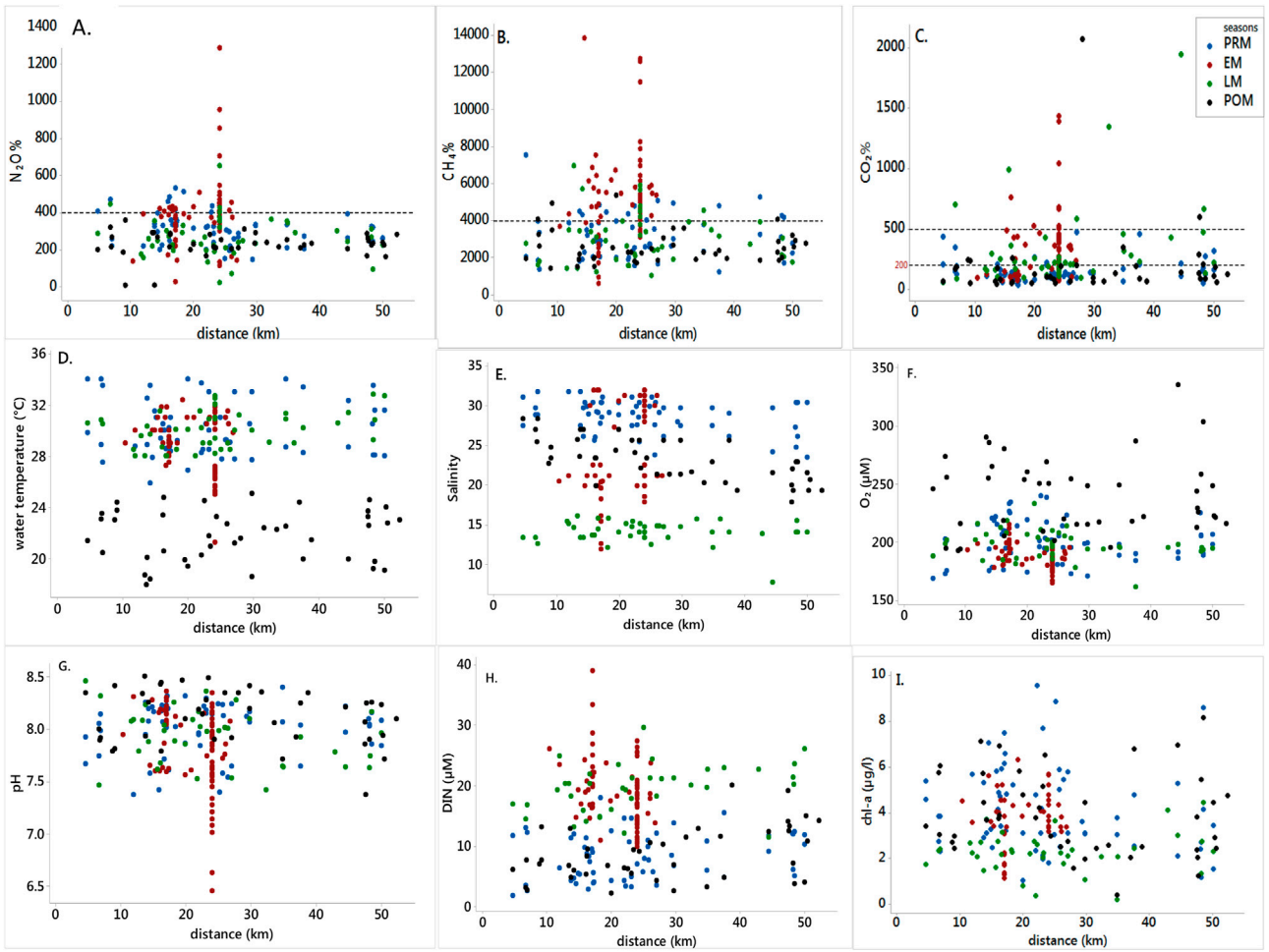

FIGURE 2 | Scatter plots showing CO_2, CH_4, and N_2O saturation and estuarine physicochemical parameters measured from the head to the mouth of the Indian Sundarban estuary between April 2016 and January 2020. The *x*-axis represents the distance from the mouth of the estuary. Blue dots represent observations from pre-monsoon (PRM), red dots represent early monsoon (EM), green for late monsoon (LM), and black dots are for post-monsoon (POM).

gas as spatially heterogeneous (Murray et al., 2015). According to sampling campaigns, maximum saturation could be observed in June 2019 (mean of 473%), while the minimum mean saturation of 180% was recorded in November 2016. Being an organic material-rich system, which receives a huge mangrove litterfall and marine algae as significant ways of nutrient input *via* tidal pumping (Sanyal et al., 2020), the overall mean N_2O saturation percent of 317 ± 134% in the Indian Sundarban was higher than those of the Arabian Sea (mean of 186 ± 37%) (Naqvi and Noronha, 1991) and the Bay of Bengal (81 ± 6%) (Rao et al., 2013a). The means of N_2O% saturation of the three estuaries showed significant differences ($F = 4.25$; $p = 0.015$). The saturation was higher in the Saptamukhi (mean of 352 ± 176%) than in the other two (Thakuran: 284 ± 119% and Matla: 302 ± 112%) estuaries. This could be due to the anthropogenic input in the form of run-off from the agricultural lands close to the Saptamukhi estuary (Dutta et al., 2015), which brings in nitrogenous fertilizer waste, adding to the inorganic nitrogen substrate in the estuary (Ray et al., 2014). Furthermore, a portion of the anthropogenic-influenced Hooghly estuary flows into the Saptamukhi estuary (Sanyal et al., 2020) bringing in more inorganic nitrogen material. Coupled together, these two inputs may have enhanced N_2O production in the Saptamukhi estuary, thereby increasing its N_2O % compared to the other two estuaries.

Indian Sundarban estuaries showed higher average N_2O% than other Indian estuaries, which showed an average N_2O% ranging between 108 ± 53% and 292 ± 150% (Rao and Sarma, 2013b). Unlike other Indian estuaries that experience high flushing time during discharge along with adequate freshwater supply to wash away most of the fertilizer waste accumulated in the waters, the Sundarban estuaries receive a limited freshwater discharge that causes the materials to linger in the system, thus facilitating N_2O production. Similar to the pattern of N_2O in other Indian estuaries (Rao and Sarma, 2013b), the overall significant positive correlation between N_2O% and NH_4^+ along with water temperature, salinity, and chl-*a* concentrations and negative correlation with O_2 concentration in the Indian

TABLE 1 | Spearman's correlation coefficient for pooled data (n = 225) and by seasons (n = 57) (values marked in bold are significant ($p < 0.05$).

	All data	PRM	EM	LM	POM
	CO_2%	CO_2%	CO_2%	CO_2%	CO_2%
CH_4%	**0.34**	**0.34**	**0.32**	0.08	0.16
N_2O%	**0.20**	–0.07	**0.29**	0.18	0.02
Water temp. (°C)	**0.35**	**0.56**	**0.38**	–0.02	0.25
Salinity	0.03	0.16	**0.46**	0.12	–0.06
[O_2]	**–0.41**	**–0.54**	**–0.33**	0.10	–0.28
pH	**–0.76**	**–0.40**	**–0.86**	**–0.97**	**–0.83**
[NO_3^-]	**0.31**	**0.53**	–0.22	–0.13	–0.05
[NH_4^+]	–0.02	–0.12	**–0.34**	0.10	0.06
CHL–a	**–0.17**	**–0.30**	0.19	0.05	–0.25
[DIN]	**0.25**	**0.48**	**–0.43**	–0.09	0.06
	All data	PRM	EM	LM	POM
	CH_4%	**CH_4%**	**CH_4%**	**CH_4%**	**CH_4%**
CH_4%					
N_2O%	**0.54**	**0.26**	**0.24**	**0.56**	0.25
WT (°C)	**0.32**	**0.65**	0.02	0.17	0.13
Salinity	**0.17**	**0.55**	0.14	–0.28	0.08
[O_2]	**–0.48**	**–0.30**	–0.17	–0.21	–0.22
pH	**–0.37**	**–0.36**	**–0.27**	–0.26	–0.19
[NO_3^-]	**0.19**	**0.67**	**–0.34**	–0.12	–0.14
[NH_4^+]	**0.31**	**0.46**	**–0.33**	0.32	–0.19
CHL-a	**0.16**	–0.18	**0.48**	0.02	–0.17
[DIN]	**0.26**	**0.76**	**–0.45**	–0.01	–0.12
	All data	PRM	EM	LM	POM
	N_2O%	**N_2O%**	**N_2O%**	**N_2O%**	**N_2O%**
CH_4%					
N_2O%					
WT (°C)	**0.35**	0.05	**0.44**	**0.35**	–0.03
Salinity	**0.29**	0.08	**0.53**	–0.29	0.01
[O_2]	**–0.43**	0.04	**–0.56**	**–0.44**	0.03
pH	**–0.24**	0.09	**–0.35**	**–0.44**	0.16
[NO_3^-]	0.09	0.10	–0.19	**–0.49**	0.04
[NH_4^+]	**0.23**	0.09	–0.17	0.22	–0.24
CHL-a	**0.23**	0.11	**0.35**	–0.18	0.11
[DIN]	0.09	0.09	**–0.31**	**–0.41**	–0.08

Sundarban estuaries suggest that estuarine nitrification is a possible pathway for N_2O production. A stepwise regression between N_2O% and the key physicochemical parameters as independent variables resulted in salinity, O_2 concentration, and pH being significant factors ($p < 0.05$) on N_2O% (N_2O% = 1,310 + 5.77 S—0.886 [O_2]—120.8 pH; R^2 = 29.9%). However, these parameters could explain only about 30% of the variability in N_2O%, implying the contribution of other external factors that influence N_2O in the Sundarban estuaries.

CH_4 dynamics have been studied in great detail in previous studies on the Indian Sundarban estuaries (Biswas et al., 2007; Dutta et al., 2013, 2015; Dutta and Mukhopadhyay, 2016). CH_4 concentration in the Indian Sundarbans has been suggested to be exogenous (Biswas et al., 2007; Dutta et al., 2015); in other words, advective and diffusive transport of CH_4 from the sediment to the estuary dominates the CH_4 concentration in the estuary waters. The mean (3,280%) measured in our study is within the range of mean values reported from another study in the Saptamukhi (2,483.02 ± 50.18 to 3,525.45 ± 1,053.72) (Dutta et al., 2015). The range (1,020%–13,844%) is narrower than the values reported for other Indian estuaries (180%–22,340% (Rao and Sarma, 2016)). Similar to N_2O, there was no spatial pattern in CH_4 saturation as well (**Figure 2**). The saturation values were highly random throughout the study area. The saturation range was dispersed over the entire study area, with no specific increasing or decreasing pattern from the head to the mouth of the estuary. The lack of a steady pattern in the distribution of CH_4 saturation indicated that the degradation of organic matter loads varied among study points along with varying advective transport rates from the adjacent intertidal sediments. The advective signal coupled with well-mixed nature finally rendered the CH_4 distribution as random.

CH_4 saturation, in general, was significantly correlated with all physicochemical parameters for our study period (**Table 1**) suggesting that estuarine physicochemical water parameters played a significant role in controlling CH_4 dynamics in addition to the advective transport of CH_4 from the intertidal sediments. Contrary to previous studies, CH_4 saturation and salinity, in general, were found to be positively correlated in our study for a salinity range from 11.9 to 31.9. This could be due to highly saline porewater from the intertidal areas entering the estuary waters (range: 19.8–54.2 for our study period). This positive correlation between CH_4 saturation and salinity for our system is in contrast to other Indian estuaries where freshwater acts as a significant source for CH_4 (Rao and Sarma, 2016). A further stepwise regression on CH_4% pinpointed water temperature, salinity, pH, NO_3^-, and DIC to be significant factors ($p < 0.05$) in controlling its dynamics (CH_4% = 6,911 + 79.2 WT (°C) + 101.3 salinity—848 pH + 71.4 NO_3 + 55.9 NH_4 - 1.417 DIC; R^2 = 30.7%) although only about 30% of the variability could be attributed to these parameters.

CO_2 dynamics have also been studied exhaustively in the Indian Sundarbans in recent years. Throughout the study period, CO_2 saturation ranged from 30 to 2,075% (n = 229). A few of the measurements indicated undersaturation ranging from 30 to 98% (n = 54), while the majority of the estuary waters was predominantly supersaturated with CO_2, with supersaturation ranging from 101 to 2,075% (n = 175). The highest CO_2 saturations were in June 2019 (mean of 471%) and the lowest in January 2020 (mean of 48%). Our range of CO_2 saturation is much larger than those reported in the earlier studies [76%–156%, Thakuran estuary, and 81%–289% Matla estuary (Akhand et al., 2021; Akhand et al., 2021b)]. The difference could be due to larger spatial coverage than the previous studies. The distribution of CO_2 saturation per cent in the Indian Sundarban estuary did not vary among the estuaries (**Figure 2**). The CO_2 saturation at most data points was within 200% throughout the stretch of the study area (**Figure 2**), with few points going beyond 500%. The moderate level of supersaturation is also due to a lack of adequate supply of CO_2-rich freshwater from rivers as observed in a recent study in the Matla estuary (Akhand et al., 2021b). However, 1,000%–1,500% of CO_2 saturation values were recorded at site 27 between 20 and 30 km (**Figure 2**) in the early monsoon month. Such high values could be a result of CO_2-rich freshwater draining into the system in addition to the advective

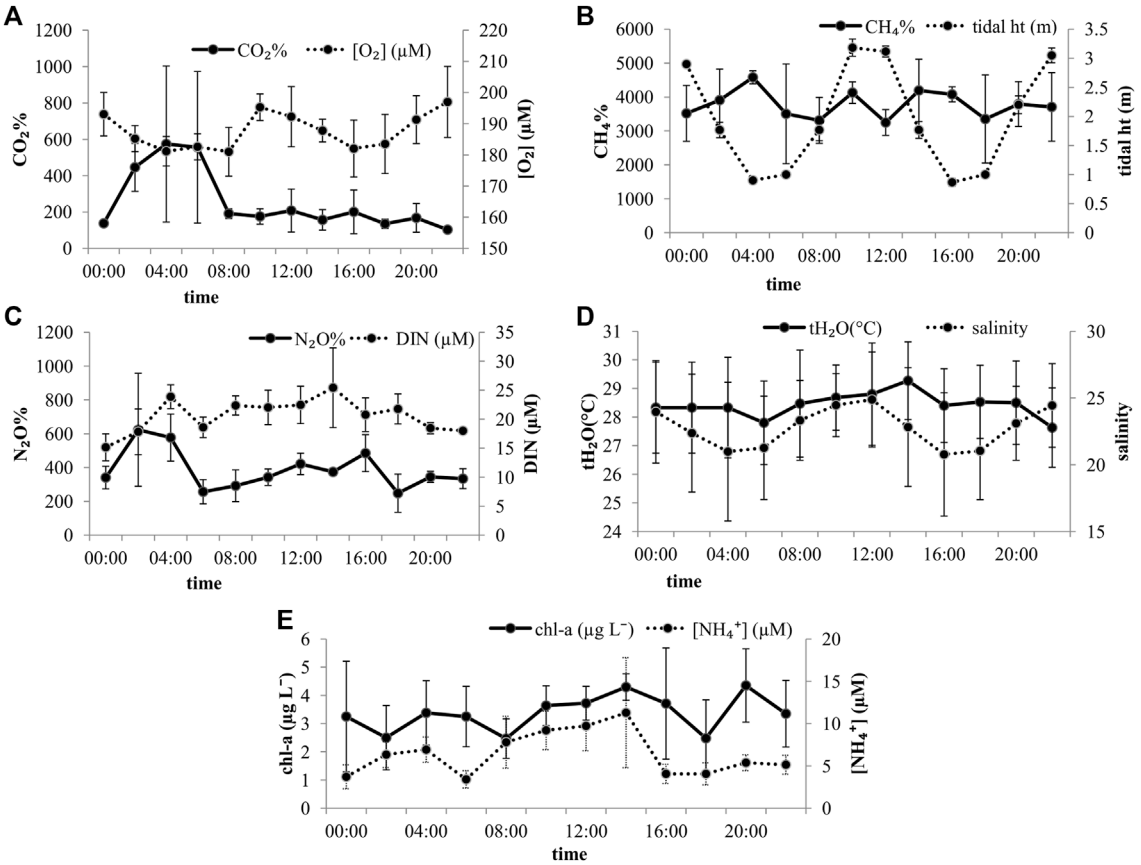

FIGURE 3 | Mean gas saturations and water chemistry across an average of three full tidal cycles at site 27, near Lothian Island in the Indian Sundarban estuary. Error bars equal the standard error of the mean (n = 3).

transport of CO_2 from the intertidal areas into the adjacent estuary waters.

On the spatial scale, CO_2% showed a positive correlation with water temperature, salinity, NO_3^-, and DIC concentrations. CO_2%-pH negative correlation is typical of the carbonate system where the CO_2 saturation regulates the pH of the system. The CO_2%-O_2 and CO_2%-chl-*a* correlations are mainly the results of increased turbidity in the estuary waters in the monsoon on receiving adequate organic material from the adjacent intertidal zone to perform microbial degradation. With increased transparency in the estuarine water in the post-monsoon along with the rise in the phytoplankton bio-volume (Biswas et al., 2004), CO_2 is consumed during photosynthesis, which explains the low levels of CO_2 saturation in the waters in January 2020. The stepwise regression of CO_2% with the physicochemical parameters narrowed the influencing factors to salinity, pH, and chl-*a* of the estuary waters, which explained 35% of the CO_2% variability (CO_2% = 4,431—6.17 salinity—499.2 pH—19.6 chl-*a*; R^2 = 35.3%).

CH_4 and CO_2 have been observed to show a positive relationship in well-mixed estuaries, meaning the increase in allochthonous carbon inputs could raise the rates of organic matter decomposition, thus increasing the production of the two gases (Borges and Abril, 2012). A positive correlation between N_2O% and CO_2% in the estuaries implies that the factors that influence the production of these two gases could be common ((Harley et al., 2015). In our study, both N_2O% and CH_4% were positively correlated to CO_2%, suggesting that both the gases were produced *via* the decomposition of the organic material obtained from advective transport from the intertidal areas adjacent to the estuaries (Sierra et al., 2020). The correlation between N_2O% and CO_2% suggests that denitrification occurring in the intertidal sediments may also be of interest in discussing the dynamics of N_2O for this system (Harley et al., 2015).

Tidal Pattern

Only one site in the Saptamukhi, the Lothian Island, was chosen to carry out three tidal observations to assess the tidal pattern of the gases. Several studies have been conducted on this site (Dutta et al., 2019; Ray et al., 2013), considering its position at the confluence of the estuary and the Bay of Bengal and its stable condition that provides a better tidal observation. Comparing the three tidal cycles (**Figure 3**), it was observed that the approximate tide heights were similar, thus confirming stable tidal variation at the site. The salinity did not show a significant difference between high tide (mean of 23.6 ± 5.5) and low tide (mean of 22.0 ± 6.1).

The mean N_2O% varied between 248 and 623% during the tidal cycles. Considering the average of the three tidal cycles, no clear pattern was observed between the N_2O saturation values and the salinity of the tidal variation. The values did not vary among tidal cycles as well. Neither light nor tide conditions showed any significant influence on the N_2O saturation, suggesting that intertidal sediments were not the only contributor to N_2O%. The average tidal variation of estuarine DIN was well aligned with the average N_2O tidal variation (**Figure 3C**), further providing an evidence of nitrification. An evidence of microbe-mediated nitrification has been observed in the water column (Mukherjee et al., 2020). Taken together, this means that the *in situ* N_2O production occurs within a short time frame and the well-mixed nature of the estuary homogenizes the N_2O% in the waters.

Since the observations were carried out only in the early monsoon months, it is not clear what the response of N_2O might be to tidal variation in the pre-monsoon or post-monsoon months.

In contrast, across the full tidal cycles, high CH_4 saturation corresponded to low tide conditions. This indicates that tidal pumping brings in CH_4 produced in the sediments to the water column. Similar findings can be cited where, despite no freshwater inputs, the system showed high CH_4 concentrations at low tide (Bouillon et al., 2008). Although there was not much statistically significant difference in mean salinity between the high tide salinity and low tide, **Figure 3** shows that higher CH_4 saturation corresponded with lower salinity at low tide, opposite to what was observed at the spatial scale. The mean CH_4% varied between 3,249 and 4,582% considering all three tidal cycles.

CO_2% too showed a clear tidal variability ($F = 4.72$; $p = 0.037$) (**Figure 3**). The tidal pattern of CO_2% varied even with each tidal cycle ($F = 7.49$; $p = 0.002$) with higher saturations at low tide. The mean CO_2% varied between 103 and 574%. However, light conditions did not affect its variability. This suggests that the variability of CO_2 cannot be detected at the spatial scale but is more prominent at the temporal scale, thus corroborating with the diurnal studies on CO_2 dynamics in the Indian Sundarban (Dutta et al., 2019; Akhand et al., 2021). For all three cycles, the increase in CO_2 saturation at low tide can be attributed to the advective transport of porewater CO_2 in the waters mixing with the estuarine waters. The association of O_2 and chl-*a* with CO_2 saturation observed on the spatial scale was not found on the temporal scale. This ambiguity in the CO_2–physicochemical parameter relationship further implies that assessing CO_2 variability at the temporal scale may prove effective to study its dynamics and biogeochemistry.

Seasonality

The distribution of the key water parameters, water temperature, salinity, and O_2 concentration showed a prominent seasonality (**Figure 2**). In response to this seasonality, the seasonality index scores of the gas saturations are depicted in **Figure 4**.

The seasonality index of N_2O% was, however, found close to 1 (range: 0.8–1.7). This indicates that the N_2O dynamics in the Indian Sundarban are not entirely influenced by the seasonality of the environmental variables. Rao and Sarma (2013b) showed that the east coast estuaries have higher N_2O concentration in the dry

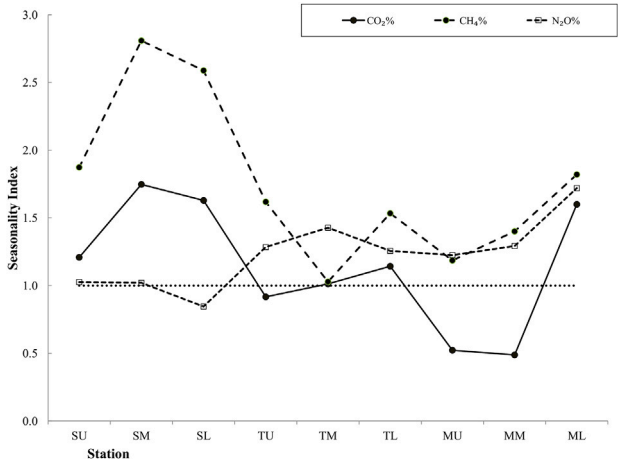

FIGURE 4 | Seasonality index (mean pre-monsoon/early monsoon gas saturation divided by mean late-monsoon/post-monsoon saturations) along the estuary. Study points have been clustered into upper, mid-, and lower regions of the Saptamukhi (SU, SM, SL); Thakuran (TU, TM, TL); and the Matla (MU, MM, ML) for an overview of the seasonality index. Values above a seasonality index of 1 indicate higher pre-monsoon/early monsoon saturations.

period, owing to higher temperatures that enhance the bacterial production of N_2O, while the west coast estuaries did not show any seasonality. Considering most of the significant correlation of N_2O% with several physicochemical parameters that occurred in the early monsoon and the late monsoon (**Table 1**), it can be said that the monsoon season influenced N_2O saturation in the Indian Sundarban. N_2O% was the highest in the early monsoon (mean of 386 ± 174%). However, it decreased gradually in the late monsoon (mean of 269 ± 104%) to post-monsoon (231 ± 66%), possibly with receding freshwater discharge. In the pre-monsoon, N_2O% rose to 311 ± 87%. The increase in saturation in the early monsoon may have been due to advective transport brought in by monsoonal discharge that augmented the water column nitrification. The cause of least mean N_2O% in the post-monsoon may be attributed to the negative overall correlation of O_2 concentration with N_2O. The rise in O_2 concentration to a maximum in the post-monsoon (mean of 240 μM) may have limited N_2O production in the waters by facilitating its transformation to NO_3^- instead of nitrification.

For CH_4, the seasonality index score was always above 1, indicating visibly higher pre-monsoon/early monsoon CH_4 saturation than its late-monsoon/post-monsoon counterpart for our study. The index score was the highest in the mid-Saptamukhi region, suggesting significant sources of CH_4-rich water from the adjacent mangrove swamps (Biswas et al., 2007) within this region that are most active in the pre-monsoon/early monsoon period. However, previous studies, which also pinpointed the high seasonality of CH_4 in the estuaries of the Sundarban mangroves, had observed peak CH_4 concentration in the post-monsoon period (Biswas et al., 2007). Those studies attributed this high concentration to methane production from phytoplankton bloom (Biswas et al., 2007). For our study, the

TABLE 2 | A. Annual emission estimation of air/water RAG emission with global warming potential and B. Seasonal emission estimate of air/water RAG emission integrated from the flux estimates calculated from four different parameterizations of gas transfer rate.

		Gg CO_2 y^{-1}	GWP	Gg CH_4 y^{-1}	GWP	Gg N_2O y^{-1}	GWP
A	**C95**	368.2	368.2	0.7	18.5	0.3	88.6
	RC01	573.8	573.8	1.6	45.2	0.9	230.4
	H11	419.2	419.2	0.8	22.5	0.5	120.0
	W14	394.0	394.0	1.1	29.5	0.4	112.8
B	**PRM**	131		0.682		0.478	
	EM	721		1.74		0.878	
	LM	512		0.473		0.213	
	POM	171		0.29		0.150	

reversal in seasonality can be attributed to the high mean CH_4 saturations in June 2019 and August 2019 than other sampling months (**Table 1**). The reversal could also be due to the positive correlation between chl-*a* (an indicator of primary productivity) and CH_4% in the early monsoon season (**Table 2**). Such a correlation suggests that the conditions were favorable for the phytoplankton to produce CH_4 (Biswas et al., 2007). The seasonal dynamics in CH_4% in the entire estuary can also be justified by the seasonal changes in temperature and O_2 concentrations affecting the microbial methanogenesis process in the intertidal sediments since CH_4% was significantly positively correlated with water temperature and negatively correlated with O_2 (**Table 1**). Similar observations have been found in the Tay Estuary, United Kingdom (Harley et al., 2015).

Although CO_2 saturation showed significant seasonality ($F = 6.56$, $p = 0.00$), considering the site clusters of the upper, middle, and lower regions in each of the Saptamukhi, Thakuran, and the Matla estuaries, there was no significant difference between the pre-monsoon/early monsoon and the late-monsoon/post-monsoon saturations as per the *t*-test. This pattern was also observed for the relationships of CO_2 saturation with physicochemical parameters (**Table 1**). In general, CO_2 saturation was significantly correlated with several physicochemical parameters like water temperature, oxygen concentration, pH, NO_3^-, DIN, and chlorophyll-*a* (**Table 1**). However, the correlations varied between seasons, and most of the correlations became nonexistent beyond early monsoon (**Table 1**). For instance, the CO_2%–water temperature positive relationship was present in general, but there was no significant relationship in the late-monsoon and post-monsoon season. Similarly, the CO_2%–O_2 negative relationship was significant in general (**Table 1**) and from the pre-monsoon to the early monsoon. Late monsoon onwards, the relationship lost its significance.

Seasonal Variation of the Advective Transport and Emission of the RAGs From the Intertidal Sediment

Several studies have already established that the Indian Sundarban estuaries receive organic materials from the adjacent intertidal areas. In this regard, the seasonal variation is regarded as one of the prominent factors influencing RAG emissions from the mangrove swamps (Padhy et al., 2020). In our study, we attempted to estimate the emission of the RAGs from the intertidal areas of the mangrove swamps to relate to the influence of porewater RAGs on the estuary-dissolved RAGs. The advective transport of the porewater-dissolved RAGs from the intertidal sediment to the adjacent waters of the estuaries was estimated to assess their impact on the gas saturation. **Figures 5A–C** compare the means of the advective transport of the gases for pre-monsoon and monsoon, and **Figures 5C–E** compare the means of the gas emission from the mangrove sediment for site 27. Only seasonal comparison has been made using the transport rates from all the three estuaries since the transport rates did not vary by estuaries but showed significant seasonal variation.

The advective transport of N_2O from the intertidal sediment to the estuary water ranged from 0.02 to 0.19 μmol m^{-2} h^{-1}. The transport increased from pre-monsoon to monsoon (**Figure 5A**). This is obvious because the monsoon is characterized by substantial inputs of C- and N-material to the sediments *via* run-off. This suggests that the porewater N_2O is an important contributor to the rise in water N_2O% in the early monsoon. The emission of N_2O from the mangrove sediments ranged from −5.02 to19.2 μmol m^{-2} h^{-1}, with wider variation than that recorded for other Indian mangroves ;0.38–0.76 μmol m^{-2} h^{-1} in the Muthupet mangroves (Krithika et al., 2008); 0.2–4.3 μmol m^{-2} h^{-1} in the Bhitarkanika mangroves (Chauhan et al., 2015)]. Such high variation is probably a direct result of the larger spatial area (~1,800 km^2; Dutta et al., 2015) of the Indian Sundarban mangroves than the compared mangroves (68 km^2, Muthupet mangroves, Krithika et al., 2008; 670 km^2, Bhitarkanika mangroves, Chauhan et al., 2015). Added to the large spatial cover is the entry of substantial amounts of allochthonous inorganic nitrogen from the agricultural fields *via* rainfall run-off (Ray et al., 2014).

In contrast, the advective transport of CH_4 varied by a wide range with no visible influence of seasons. For CH_4, the transport rate ranged from 0.27 to 41.48 μmol m^{-2} h^{-1}. Similarly, the variation in sediment CH_4 emissions (−51.95–64.14 μmol m^{-2} h^{-1}) was too high to pinpoint seasonality (**Figure 5E**). Since all measurements using the static chamber were conducted at low tide, the effect of tidal fluctuation cannot be discussed here. This aberrant pattern of CH_4 emission hints at a complex interaction between the porewater salinity, microbial activity, and advective transport of porewater-dissolved CH_4 rather than seasons.

The advective transport of CO_2 varied between 0.17 and 2.03 mmol m^{-2} h^{-1}. The advective transport of CO_2 was found to increase in the monsoon, albeit with a large variation about the mean, whose effects can be seen on the increase in estuary CO_2% in the monsoon. The CO_2-rich porewater seeps out more into the estuary waters in the monsoon and adds to the rainfall run-off. This ultimately increases the mean CO_2% in the waters. The sediment/air emission of CO_2, however, did not show any prominent seasonality for the study period.

RAG Fluxes and Annual Emission Estimates

The gas transfer rates computed by each parameterization varied considerably, with the mean k_{600} for each parameterization

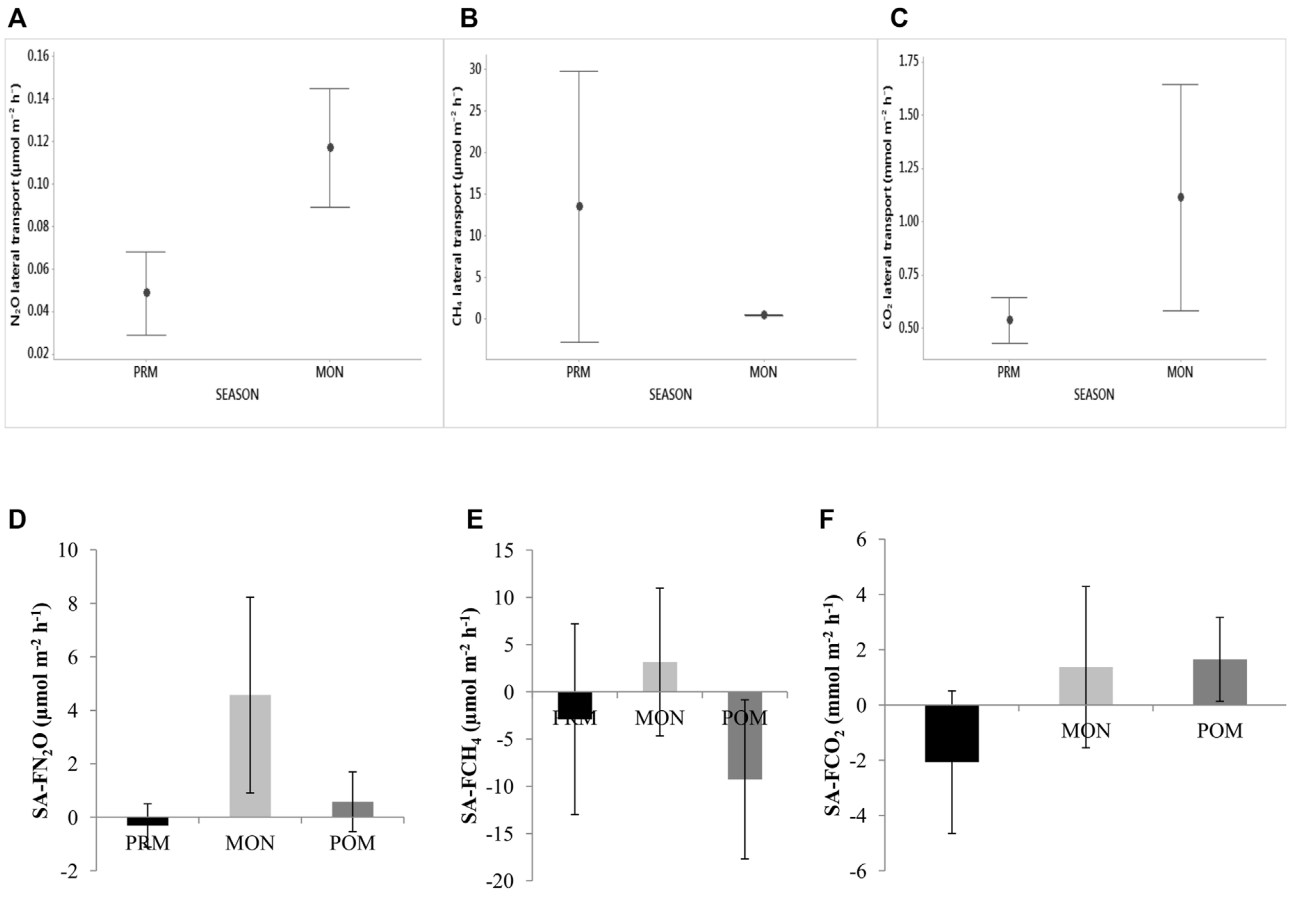

FIGURE 5 | Comparison between intertidal sediment/water transport of RAGs and sediment/air RAG emission by seasons. Error bars indicate standard deviation.

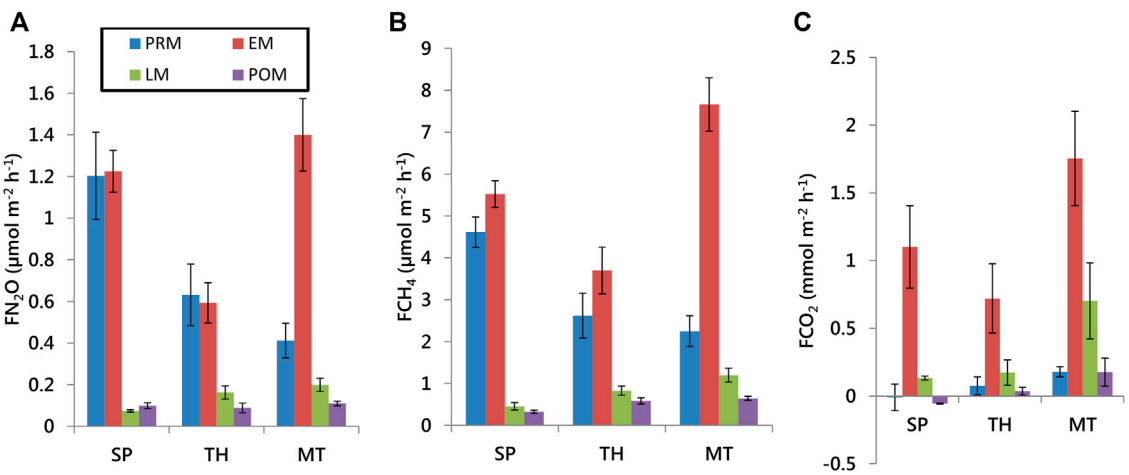

FIGURE 6 | Air/water flux densities in the three estuaries of the Indian Sundarbans (SP–Saptamukhi, TH- Thakuran, and MT- Matla in the pre-monsoon, early monsoon, late monsoon, and the post-monsoon).

TABLE 3 | Comparative of RAG fluxes of this study with reports from other estuaries.

Study area	FCO_2 (mmol m^{-2} d^{-1})	FCH_4 (μmol m^{-2} d^{-1})	FN_2O (μmol m^{-2} d^{-1})	References
Indian Sundarban estuaries (this study)	−0.6–10.9	0.4–18.4	-0.6–5.4	
Hooghly-Matla Est	—	1.97–134.6	—	Biswas et al. (2007)
Saptamukhi Est	—	6.36–12.36	—	(M K Dutta et al., 2013)
Matla	−0.6–89.2	—	—	Akhand et al. (2021)
26 Indian estuaries	—	0.01–298	1.07–1.65	(G D Rao and Sarma, 2016; Rao and Sarma, 2013b)
Hooghly R. Est	−2.78–84.4	—	—	Mukhopadhyay et al. (2002)
Brisbane R. Est	—	0.02–1.74	0.002–0.077	Musenze et al. (2014)
Tubul-Raqui Est	−319–714	330–2,500	−59–28	Daniel et al. (2013)
Guadalete R. Est	—	20.3–3,645	92.8	Burgos et al. (2015)
Pearl R. Est	—	—	37 ± 15	Lin et al. (2016)
Rio San Pedro	73–177	34–150	24–62	Ferrón et al. (2007a)

ranging from 2.76 to 5.00 cm h^{-1}, implying the uncertainty involved in using k-wind parameterizations. The uncertainty, is, however, outlined by reporting a range of values (minimum: C95 equation and maximum: RC01 equation).

From **Figure 6**, it is clear that the air/water flux densities of all the gases were highly variable among the estuaries. The fluxes of the gases in the Thakuran estuary, in general, were less than the other two estuaries. This could be attributed to greater tidal influence and proximity to the marine waters of the Bay of Bengal that dilute the gas concentrations (Chauhan et al., 2015). Seasonally, the flux densities were also the highest in the early monsoon. This could be a response to the enhanced advective transport of the porewater rich in these gases into the water column that may have augmented the estuarine production of the gases.

For N_2O, the fluxes in the late monsoon and post-monsoon dipped considerably. Although the advective transport increased for N_2O in the monsoon, the oxygenated environment of the waters may have immediately led to its oxidation to NO_3^- by the blooming phytoplankton for consumption by late monsoon, thus suppressing the water/air fluxes in the subsequent seasons. The minimum flux reached a negative value perhaps due to local consumption of N_2O *via* nitrification (**Table 3**).

A clear seasonality of CH_4 fluxes reinforces the dependence of CH_4 concentration on water parameters which are, in turn, influenced by seasons (**Figure 6B**). Our reported range is larger than the previous reports covering only the Saptamukhi and Matla estuaries of the Indian Sundarban (**Table 3**). All positive flux densities reiterate the previous studies that this estuary is a considerable source of CH_4.

The air/water emissions of CO_2 fluctuated between negative and positive, similar to N_2O (**Figure 6C**). The average pre-monsoon and post-monsoon CO_2 fluxes in the Saptamukhi were negative. Since heterotrophy is known to be the lowest in the Indian Sundarban estuaries in the post-monsoon due to bloom conditions (Biswas et al., 2004), this could explain the low flux rates of CO_2 in the Saptamukhi estuary. Our study suggests that heterotrophy is suppressed even in the pre-monsoon despite the advective input of organic matter from the intertidal areas. Combined with the lack of freshwater supply and suppressed heterotrophy in two seasons, inadequate production of CO_2 leads to rather low emission rates relative to the amount of organic matter input received by the Sundarban estuary waters (Dutta et al., 2019).

Considering the average of air/water flux densities estimated from the four chosen gas transfer velocity equations, the air/water flux values obtained for our study were extrapolated to the total estuarine area of 1,800 km^2 to estimate the annual air/water emission of the gases (**Table 2**). The estimated annual N_2O emission ranges from 0.3 to 0.9 Gg N_2O y^{-1} corresponding to a GWP of 88.6–230.4. CH_4 emission ranges from 0.7 to 1.6 Gg CH_4 y^{-1} corresponding to a GWP of 18.5–45.2, in contrast to CO_2 emission that ranges from 368.2 to 573 Gg CO_2 y^{-1} (**Table 2**). We have not estimated the annual sediment-to-air emission of the RAGs for the whole mangrove intertidal sediment area as estimation using measurements from only one site could lead to gross uncertainty in the estimated emission. With more information on other estuaries available in the future, annual sediment/air emission can become relevant.

Table 3 summarizes a comparative between the RAG air/water fluxes in other estuaries. Compared to other estuaries, the CO_2 fluxes in our study were found to vary over a narrower range; CH_4 fluxes were within the range of 26 Indian estuaries (Rao and Sarma, 2016), and the N_2O flux range included the flux values of all other Indian estuaries.

CONCLUSION

In summary, the distribution of the fluxes of CO_2, CH_4, and N_2O in the Indian Sundarban estuaries had more pronounced seasonal influence, particularly during the early monsoon. While N_2O may be a product of combined pelagic metabolism and advective transport of porewater, CH_4 and CO_2 are of sedimentary origin, supplied to the estuary *via* advective transport. These production and utilization processes that govern the dynamics of their concentration and fluxes require further insight. For water–air fluxes, different estuarine regimes, and their physicochemical and meteorological patterns combined, play a key role. Finally, these water–air CO_2, CH_4, and N_2O flux

estimates show that the estuaries are a modest source of CH_4 but fluctuate between sources and sinks for CO_2 and N_2O gases. The estimates can be used to add to the basic inventories for the database on RAGs of Indian Sundarban. In addition, the revised database will be helpful for the future modeling of CO_2, CH_4, and N_2O budgets for these estuaries.

DATA AVAILABILITY STATEMENT

The original contributions presented in the study are included in the article, further inquiries can be directed to the corresponding author.

AUTHOR CONTRIBUTIONS

AA collected the gas samples, carried out the analysis and wrote the manuscript. PS, MP, and SB helped with the measurements of water parameters like salinity, nutrients, VKG helped with the field measurements and datasheet preparation. SKM supervised the entire process from data collection to writing the manuscript.

FUNDING

West Bengal State Council of Science and Technology Award number: 130/WBSCST/F/0443/13 (Pt-I) dt February 29, 2016 Awarded the Meghnad Saha Research Fellowship in River Science and Research to carry out this research for 4 years.

ACKNOWLEDGMENTS

The authors are immensely grateful to the Divisional Forest Office, South 24 Parganas for providing permission for field visits to Indian Sundarban. The author AA acknowledges the West Bengal State Council of Science and Technology for providing Meghnad Saha Research Fellowship in River Science and Research to carry out this research and Dr. Pratap Bhattacharyya, NRRI, Cuttack for instrument facilities.

REFERENCES

Akhand, A., Chanda, A., Watanabe, K., Das, S., Tokoro, T., Chakraborty, K., et al. (2021). Low CO2 Evasion Rate from the Mangrove-Surrounding Waters of the Sundarbans. *Biogeochemistry* 153 (1), 95–114. doi:10.1007/s10533-021-00769-9

Akhand, A., Chanda, A., Watanabe, K., Das, S., Tokoro, T., Hazra, S., et al. (2021). Reduction in Riverine Freshwater Supply Changes Inorganic and Organic Carbon Dynamics and Air-Water CO 2 Fluxes in a Tropical Mangrove Dominated Estuary. *J. Geophys. Res. Biogeosci* 126, 1–22. doi:10.1029/2020jg006144

Alongi, D. M. (2012). Carbon Sequestration in Mangrove Forests. *Carbon Manag.* 3 (3), 313–322. doi:10.4155/cmt.12.20

Bange, H. W. (2008, Gaseous Nitrogen Compounds (NO, N2O, N2, NH3) in the Ocean). *Chapter 2 - Gaseous Nitrogen Compounds (NO, N2O, N2, NH3) in the Ocean* (D. G. Capone, D. A. Bronk, and M. R. Mulholland, & E. J. B. T.-N. in the M. E.(Second E. Carpenter (eds.); pp. 51–94). Academic Press. doi:10.1016/B978-0-12-372522-6.00002-5

Bange, H. W., Sim, C. H., Bastian, D., Kallert, J., Kock, A., Mujahid, A., et al. (2019). Nitrous Oxide (N2O) and Methane (CH4) in Rivers and Estuaries of Northwestern Borneo. *Biogeosciences* 16, 4321–4335. doi:10.5194/bg-16-4321-2019

Barnes, J., and Upstill-Goddard, R. C. (2011). N2O Seasonal Distributions and Air-Sea Exchange in UK Estuaries: Implications for the Tropospheric N2O Source from European Coastal Waters. *J. Geophys. Res.* 116 (1). doi:10.1029/2009JG001156

Bhattacharyya, P., Nayak, A. K., Mohanty, S., Tripathi, R., Shahid, M., Kumar, A., et al. (2013a). Greenhouse Gas Emission in Relation to Labile Soil C, N Pools and Functional Microbial Diversity as Influenced by 39 Years Long-Term Fertilizer Management in Tropical rice. *Soil Tillage Res.* 129, 93–105. doi:10.1016/j.still.2013.01.014

Bhattacharyya, P., Nayak, A. K., Mohanty, S., Tripathi, R., Shahid, M., Kumar, A., et al. (2013b). Greenhouse Gas Emission in Relation to Labile Soil C, N Pools and Functional Microbial Diversity as Influenced by 39 Years Long-Term Fertilizer Management in Tropical rice. *Soil Tillage Res.* 129, 93–105. doi:10.1016/j.still.2013.01.014

Bhattacharyya, P., Roy, K. S., Das, M., Ray, S., Balachandar, D., Karthikeyan, S., et al. (2016). Elucidation of rice Rhizosphere Metagenome in Relation to Methane and Nitrogen Metabolism under Elevated Carbon Dioxide and Temperature Using Whole Genome Metagenomic Approach. *Sci. Total Environ.* 542, 886–898. doi:10.1016/j.scitotenv.2015.10.154

Biswas, H., Mukhopadhyay, S. K., De, T. K., Sen, S., and Jana, T. K. (2004). Biogenic Controls on the Air-Water Carbon Dioxide Exchange in the Sundarban Mangrove Environment, Northeast Coast of Bay of Bengal, India. *Limnol. Oceanogr.* 49 (1), 95–101. doi:10.4319/lo.2004.49.1.0095

Biswas, H., Mukhopadhyay, S. K., Sen, S., and Jana, T. K. (2007). Spatial and Temporal Patterns of Methane Dynamics in the Tropical Mangrove Dominated Estuary, NE Coast of Bay of Bengal, India. *J. Mar. Syst.* 68 (1–2), 55–64. doi:10.1016/j.jmarsys.2006.11.001

Borges, Alberto. V. (2011). *Oceans and the Atmospheric Carbon Content*. doi:10.1007/978-90-481-9821-4

Borges, A. V., and Abril, G. (2011). "Carbon Dioxide and Methane Dynamics in Estuaries," in *Treatise on Estuarine and Coastal Science*, 119–161. doi:10.1016/B978-0-12-374711-2.00504-0

Bouillon, S., Connolly, R. M., and Lee, S. Y. (2008). Organic Matter Exchange and Cycling in Mangrove Ecosystems: Recent Insights from Stable Isotope Studies. *J. Sea Res.*, 59(1), 44–58. doi:10.1016/j.seares.2007.05.001

Bouillon, S., Frankignoulle, M., Dehairs, F., Velimirov, B., Eiler, A., Abril, G., et al. (2003). Inorganic and Organic Carbon Biogeochemistry in the Gautami Godavari Estuary (Andhra Pradesh, India) during Pre-monsoon: The Local Impact of Extensive Mangrove Forests. *Glob. Biogeochem. Cycles* 17 (4), a–n. doi:10.1029/2002GB002026

Brase, L., Bange, H. W., Lendt, R., Sanders, T., and Dähnke, K. (2017). High Resolution Measurements of Nitrous Oxide (N2O) in the Elbe Estuary. *Front. Mar. Sci.* 4 (May). doi:10.3389/fmars.2017.00162

Burgos, M., Sierra, A., Ortega, T., and Forja, J. M. (2015). Anthropogenic Effects on Greenhouse Gas (CH4 and N2O) Emissions in the Guadalete River Estuary (SW Spain). *Sci. Total Environ.* 503-504, 179–189. doi:10.1016/j.scitotenv.2014.06.038

Cai, W.-J., and Wang, Y. (1998). The Chemistry, Fluxes, and Sources of Carbon Dioxide in the Estuarine Waters of the Satilla and Altamaha Rivers, Georgia. *Limnol. Oceanogr.* 43 (4), 657–668. doi:10.4319/lo.1998.43.4.0657

Chatterjee, M., Shankar, D., Sen, G. K., Sanyal, P., Sundar, D., Michael, G. S., et al. (2013). Tidal Variations in the Sundarbans Estuarine System, India. *J. Earth Syst. Sci.* 122 (4), 899–933. doi:10.1007/s12040-013-0314-y

Chauhan, R., Datta, A., Ramanathan, A., and Adhya, T. K. (2015). Factors Influencing Spatio-Temporal Variation of Methane and Nitrous Oxide Emission from a Tropical Mangrove of Eastern Coast of India. *Atmos. Environ.* 107, 95–106. doi:10.1016/j.atmosenv.2015.02.006

Chou, W.-C., Gong, G.-C., Hung, C.-C., and Wu, Y.-H. (2013). Carbonate mineral Saturation States in the East China Sea: Present Conditions and Future

Scenario. *Biogeosciences Discuss.* 10 (3), 5555–5590. doi:10.5194/bgd-10-5555-2013

Clark, J. F., Schlosser, P., Simpson, H. J., Stute, M., Wanninkhof, R., and Ho, D. T. (1995). Relationship between Gas Transfer Velocities and Wind Speeds in the Tidal Hudson River Determined by Dual Tracer Technique. *Air-Water Gas Transfer*, 785–800. Available at: http://hci.iwr.uni-heidelberg.de/publications/dip/1995/AWGT1995/CHAPTERS/6_11.PDF.

Collier, S. M., Ruark, M. D., Oates, L. G., Jokela, W. E., and Dell, C. J. (2014). Measurement of Greenhouse Gas Flux from Agricultural Soils Using Static chambers. *J. Vis. Exp.* 90, e52110. doi:10.3791/52110

Crosswell, J. R., Wetz, M. S., Hales, B., and Paerl, H. W. (2012). Air-water CO2fluxes in the Microtidal Neuse River Estuary, North Carolina. *J. Geophys. Res.* 117 (8), a–n. doi:10.1029/2012JC007925

Daniel, I., DeGrandpre, M., and Farías, L. (2013). Greenhouse Gas Emissions from the Tubul-Raqui Estuary (central Chile 36°S). *Estuarine, Coastal Shelf Sci.* 134 (3), 31–44. doi:10.1016/j.ecss.2013.09.019

Das, G. K. (2016). Geomorphic Environments of the Thakuran River of the Sunderbans, India. *Earth Sci. India* 9 (3). doi:10.31870/esi.09.3.2016.9

Dickson, A. G. (1990). Thermodynamics of the Dissociation of Boric Acid in Synthetic Seawater from 273.15 to 318.15 K. *Deep Sea Research Part A. Oceanographic Research Papers*, 37 (5), 755–756. doi:10.1016/0198-0149(90)90004-F

Dutta, M. K., Bianchi, T. S., and Mukhopadhyay, S. K. (2017). Mangrove Methane Biogeochemistry in the Indian Sundarbans: A Proposed Budget. *Front. Mar. Sci.* 4 (JUN). doi:10.3389/fmars.2017.00187

Dutta, M. K., Chowdhury, C., Jana, T. K., and Mukhopadhyay, S. K. (2013). Dynamics and Exchange Fluxes of Methane in the Estuarine Mangrove Environment of the Sundarbans, NE Coast of India. *Atmos. Environ.* 77, 631–639. doi:10.1016/j.atmosenv.2013.05.050

Dutta, M. K., Kumar, S., Mukherjee, R., Sharma, N., Acharya, A., Sanyal, P., et al. (2019). Diurnal Carbon Dynamics in a Mangrove-Dominated Tropical Estuary (Sundarbans, India). *Estuarine, Coastal Shelf Sci.*, 229(May), 106426. doi:10.1016/j.ecss.2019.106426

Dutta, M. K., Mukherjee, R., Jana, T. K., and Mukhopadhyay, S. K. (2015). Biogeochemical Dynamics of Exogenous Methane in an Estuary Associated to a Mangrove Biosphere; the Sundarbans, NE Coast of India. *Mar. Chem.* 170, 1–10. doi:10.1016/j.marchem.2014.12.006

Dutta, M. K., and Mukhopadhyay, S. K. (20162016). Reviews and Syntheses: Methane Biogeochemistry in Sundarbans Mangrove Ecosystem, NE Coast of India; a Box Modeling Approach. *Biogeosciences Discuss.* (February), 1–61. doi:10.5194/bg-2016-58

Ferrón, S., Ortega, T., Gómez-Parra, A., and Forja, J. M. (2007a). Seasonal Study of Dissolved CH4, CO2 and N2O in a Shallow Tidal System of the bay of Cádiz (SW Spain). *J. Mar. Syst.* 66 (1–4), 244–257. doi:10.1016/j.jmarsys.2006.03.021

Ferrón, S., Ortega, T., and Gómez-Parra, A. (2007b). Seasonal Study of Dissolved CH4, CO2, and N2O in a Shallow Tidal System of the bay of Cádiz (SW Spain). undefined. (n.d.). Elsevier. Available at: https://www.sciencedirect.com/science/article/pii/S0924796306001886 (Retrieved May 26, 2021).

Forster, G., Upstill-Goddard, R. C., Gist, N., Robinson, C., Uher, G., and Woodward, E. M. S. (2009). Nitrous Oxide and Methane in the Atlantic Ocean between 50°N and 52°S: Latitudinal Distribution and Sea-To-Air Flux. *Deep Sea Res. Part Topical Stud. Oceanography* 56 (15), 964–976. doi:10.1016/j.dsr2.2008.12.002

Frankignoulle, M., Abril, G., Borges, A., Bourge, I., Canon, C., Delille, B., et al. (1998). Carbon Dioxide Emission from European Estuaries. *Science* 282 (October), 434–436. doi:10.1126/science.282.5388.434

Griggs, D. J., and Noguer, M. (2002). Climate Change 2001: The Scientific Basis. Contribution of Working Group I to the Third Assessment Report of the Intergovernmental Panel on Climate Change. *wea* 57 (8), 267–269. doi:10.1256/004316502320517344

Guo, X., Dai, M., Zhai, W., Cai, W.-J., and Chen, B. (2009). CO2flux and Seasonal Variability in a Large Subtropical Estuarine System, the Pearl River Estuary, China. *J. Geophys. Res.* 114 (December 2008). doi:10.1029/2008JG000905

Harley, J. F., Carvalho, L., Dudley, B., Heal, K. V., Rees, R. M., and Skiba, U. (2015). Spatial and Seasonal Fluxes of the Greenhouse Gases N2O, CO2 and CH4 in a UK Macrotidal Estuary. *Estuarine, Coastal Shelf Sci.* 153, 62–73. doi:10.1016/j.ecss.2014.12.004

Ho, D. T., Wanninkhof, R., Schlosser, P., Ullman, D. S., Hebert, D., and Sullivan, K. F. (2011). Toward a Universal Relationship between Wind Speed and Gas Exchange: Gas Transfer Velocities Measured with3He/SF6during the Southern Ocean Gas Exchange Experiment. *J. Geophys. Res.* 116 (7). doi:10.1029/2010JC006854

Hoppe, C. J. M., Langer, G., Rokitta, S. D., Wolf-Gladrow, D. A., and Rost, B. (2010). On CO2 Pertubation Experiments: Over-determination of Carbonate Chemistry Reveals Inconsistencies. *On CO_2 Perturbation Experiments: Over-Determination Carbonate Chem. Reveals Inconsistencies* 7 (2), 1707–1726. doi:10.5194/bgd-7-1707-2010

IPCC (2014). "Summary for Policymakers," in *Climate Change 2014: Synthesis Report*. doi:10.1017/CBO9781107415324*Contribution of Working Groups I, II, and III to the Fifth Assessment Report of the Intergovernmental Panel on Climate Change*

Ivens, W. P., Tysmans, D. J., Kroeze, C., Löhr, A. J., and van Wijnen, J. (2011). Modeling Global N2O Emissions from Aquatic Systems. *Curr. Opin. Environ. Sustainability* 3 (5), 350–358. doi:10.1016/j.cosust.2011.07.007

Kahmark, K., and Millar, N. (2020). *Static Chamber Method for Measuring Soil Greenhouse Gas Fluxes*. Hickory Corners, MI: KBS LTER Special Publication. doi:10.5281/zenodo.3629774

Khalil, M. A. K., Rasmussen, R. A., and Shearer, M. J. (2002). Atmospheric Nitrous Oxide: Patterns of Global Change during Recent Decades and Centuries. *Chemosphere*, 47(8), 807–821. doi:10.1016/S0045-6535(01)00297-1

Krithika, K., Purvaja, R., and Ramesh, R. (2008). Fluxes of Methane and Nitrous Oxide from an Indian Mangrove. *Curr. Sci.* 94 (2), 218–224.

Laruelle, G. G., Dürr, H. H., Lauerwald, R., Hartmann, J., Slomp, C. P., Goossens, N., et al. (2013). Global Multi-Scale Segmentation of continental and Coastal Waters from the Watersheds to the continental Margins. *Hydrol. Earth Syst. Sci.* 17 (5), 2029–2051. doi:10.5194/hess-17-2029-2013

Lin, H., Dai, M., Kao, S.-J., Wang, L., Roberts, E., Yang, J.-Y. T., et al. (2016). Spatiotemporal Variability of Nitrous Oxide in a Large Eutrophic Estuarine System: The Pearl River Estuary, China. *Mar. Chem.* 182, 14–24. doi:10.1016/j.marchem.2016.03.005

Middelburg, J. J., Klaver, G., Nieuwenhuize, J., and Vlug, T. (2000). Carbon and Nitrogen Cycling in Intertidal Sediments Near Doel. *Scheldt Estuary* 311, 57–69. doi:10.1007/bf00008571

Mukherjee, R., Acharya, A., Gupta, V. K., Bakshi, S., Paul, M., Sanyal, P., et al. (2020). Diurnal Variation of Abundance of Bacterioplankton and High and Low Nucleic Acid Cells in a Mangrove Dominated Estuary of Indian Sundarbans. *Continental Shelf Res.* 210, 104256. doi:10.1016/j.csr.2020.104256

Mukhopadhyay, S. K., Biswas, H., De, T. K., and Jana, T. K. (2006). Fluxes of Nutrients from the Tropical River Hooghly at the Land-Ocean Boundary of Sundarbans, NE Coast of Bay of Bengal, India. *J. Mar. Syst.* 62 (1–2), 9–21. doi:10.1016/j.jmarsys.2006.03.004

Mukhopadhyay, S. K., Biswas, H., De, T. K., Sen, S., and Jana, T. K. (2002). Seasonal Effects on the Air-Water Carbon Dioxide Exchange in the Hooghly Estuary, NE Coast of Bay of Bengal, India. *J. Environ. Monit.* 4 (4), 549–552. doi:10.1039/B201614A

Murray, R. H., Erler, D. V., and Eyre, B. D. (2015). Nitrous Oxide Fluxes in Estuarine Environments: Response to Global Change. *Glob. Change Biol.* 21, 3219–3245. doi:10.1111/gcb.12923

Musenze, R. S., Werner, U., Grinham, A., Udy, J., and Yuan, Z. (2014). Methane and Nitrous Oxide Emissions from a Subtropical Estuary (The Brisbane River Estuary, Australia). *Sci. Total Environ.* 472, 719–729. doi:10.1016/j.scitotenv.2013.11.085

Naqvi, S. W. A., and Noronha, R. J. (1991). Nitrous oxide in the Arabian Sea. *Deep Sea Research Part A. Oceanographic Research Papers*, 38 (7), 871–890. doi:10.1016/0198-0149(91)90023-9

Noronha, R. J. (1991). *Nitrous Oxide in the Arabian Sea December 1988*. in *Water Samples Were Collected Usually Covering the Entire Water Column*, 38.7

Orr, J. C., Epitalon, J.-M., Dickson, A. G., and Gattuso, J.-P. (2018). Routine Uncertainty Propagation for the marine Carbon Dioxide System. *Mar. Chem.* 207, 84–107. doi:10.1016/j.marchem.2018.10.006

Padhy, S. R., Bhattacharyya, P., Dash, P. K., Reddy, C. S., Chakraborty, A., and Pathak, H. (1991). Seasonal Fluctuation in Three Mode of Greenhouse Gases Emission in Relation to Soil Labile Carbon Pools in Degraded Mangrove, Sundarban, India. *Science of the Total Environment* 705, 135909. doi:10.1016/j.scitotenv.2019.135909

Parsons, T. R., Maita, Y., and Lalli, C. M. (1984). *A Manual of Chemical and Biological Methods for Seawater Analysis*. Pergamon Press.

Rao, G. D., and Sarma, V. V. S. S. (2016). Variability in Concentrations and Fluxes of Methane in the Indian Estuaries. 39 (6), 1–23.doi:10.1007/s12237-016-0112-2

Rao, G. D., Rao, V. D., and Sarma, V. V. S. S. (2013a). Distribution and Air-Sea Exchange of Nitrous Oxide in the Coastal Bay of Bengal during Peak Discharge Period (Southwest Monsoon). *Mar. Chem.* 155, 1–9. doi:10.1016/j.marchem.2013.04.014

Rao, G. D., and Sarma, V. V. S. S. (2013b). Contribution of N2O Emissions to the Atmosphere from Indian Monsoonal Estuaries. *Tellus B: Chem. Phys. Meteorology* 65 (1), 1–9. doi:10.3402/tellusb.v65i0.19660

Ray, R., Chowdhury, C., Majumder, N., Dutta, M. K., Mukhopadhyay, S. K., and Jana, T. K. (2013). Improved Model Calculation of Atmospheric CO2 Increment in Affecting Carbon Stock of Tropical Mangrove forest. *Tellus B: Chem. Phys. Meteorology* 65 (1), 18981–19011. doi:10.3402/tellusb.v65i0.18981

Ray, R., Majumder, N., Das, S., Chowdhury, C., and Jana, T. K. (2014). Biogeochemical Cycle of Nitrogen in a Tropical Mangrove Ecosystem, East Coast of India. *Mar. Chem.* 167, 33–43. doi:10.1016/j.marchem.2014.04.007

Raymond, P. A., and Cole, J. J. (2001). Gas Exchange in Rivers and Estuaries: Choosing a Gas Transfer Velocity. *Estuaries* 24, 312. Gas Exchange in Rivers and Estuaries : Choosing a Gas Transfer. April. doi:10.2307/1352954

Sanyal, P., Ray, R., Paul, M., Gupta, V. K., Acharya, A., Bakshi, S., et al. (2020). Assessing the Dynamics of Dissolved Organic Matter (DOM) in the Coastal Environments Dominated by Mangroves, Indian Sundarbans. *Front. Earth Sci.* 8 (July), 1–21. doi:10.3389/feart.2020.00218

Seitzinger, S. P., and Kroeze, C. (1998). Global Distribution of Nitrous Oxide Production and N Inputs in Freshwater and Coastal marine Ecosystems. *Glob. Biogeochem. Cycles* 12 (1), 93–113. doi:10.1029/97GB03657

Sierra, A., Jiménez-López, D., Ortega, T., Gómez-Parra, A., and Forja, J. (2020). Factors Controlling the Variability and Emissions of Greenhouse Gases (CO2, CH4 and N2O) in Three Estuaries of the Southern Iberian Atlantic Basin during July 2017. *Mar. Chem.* 226 (July), 103867. doi:10.1016/j.marchem.2020.103867

Simon, J. L. (1997). Resampling: The New Statistics. *Cardiovasc. Res.* 80 (October), 321–323. Available at: http://www.resample.com/content/text/index.shtml.

Wangersky, P. J. (1978). Methods of Seawater Analysis, Issue 1, *Marine Chemistry*, 7. doi:10.1016/0304-4203(78)90045-2

Wanninkhof, R. (2014). Relationship between Wind Speed and Gas Exchange over the Ocean Revisited. *Limnol. Oceanogr. Methods* 12 (JUN), 351–362. doi:10.4319/lom.2014.12.351

Weiss, R. F., and Price, B. A. (1980). Nitrous Oxide Solubility in Water and Seawater. *Mar. Chem.* 8 (4), 347–359. doi:10.1016/0304-4203(80)90024-9

Whalen, S. C. (2005). Biogeochemistry of Methane Exchange between Natural Wetlands and the Atmosphere. *Environ. Eng. Sci.* 22 (Issue 1), 73–94. doi:10.1089/ees.2005.22.73

Wiesenburg, D. A., and Guinasso, N. L., Jr (1979). Equilibrium Solubilities of Methane, Carbon Monoxide, and Hydrogen in Water and Sea Water. *J. Chem. Eng. Data* 24 (4), 356–360. doi:10.1021/je60083a006

Wuebbles, D. J., and Hayhoe, K. (2002). Atmospheric Methane and Global Change. *Earth-Science Rev.*, 57(3), 177–210. doi:10.1016/S0012-8252(01)00062-9

Conflict of Interest: The authors declare that the research was conducted in the absence of any commercial or financial relationships that could be construed as a potential conflict of interest.

Publisher's Note: All claims expressed in this article are solely those of the authors and do not necessarily represent those of their affiliated organizations, or those of the publisher, the editors and the reviewers. Any product that may be evaluated in this article, or claim that may be made by its manufacturer, is not guaranteed or endorsed by the publisher.

frontiers in Earth Science

ORIGINAL RESEARCH
published: 04 March 2022
doi: 10.3389/feart.2022.826907

Factors Controlling the Spatial Distribution of Dissolved Organic Matter With Changes in the C/N Ratio From the Upper to Lower Reaches of the Ishikari River, Japan

Yuji Takaki[1]*, *Keisuke Hattori*[1] and *Youhei Yamashita*[1,2]

[1]Graduate School of Environmental Science, Hokkaido University, Sapporo, Japan, [2]Faculty of Environmental Earth Science, Hokkaido University, Sapporo, Japan

Dissolved organic matter (DOM), particularly dissolved organic nitrogen (DON), is an important source of energy and/or organic nutrients for heterotrophic microorganisms in rivers. Although various factors controlling the quantity and quality of stream and riverine DOM have been extensively studied, DON has been under-researched compared to dissolved organic carbon (DOC). The spatial distribution of DOC and DON concentrations with respect to the C/N ratio and DOM optical properties was investigated in the Ishikari River and its tributaries in Hokkaido, northern Japan. Here, the upper reaches are forested and the middle and lower reaches are encompassed by agricultural land, in particular paddy fields. Furthermore, dark incubation experiments were conducted using filtered riverine water (<0.7 μm) to determine the bioavailability of DOC and DON (particularly due to small microorganisms) considered as a factor controlling the spatial distribution. In the mainstream, DOC and DON concentrations increased with river flow in the upper and middle reaches and remained unchanged in the lower reaches. The C/N ratio of bulk DOM decreased continuously from the upper reaches to lower reaches. The optical properties exhibited changes in the DOM characteristics in terms of higher molecular weight and higher aromaticity from the upper to middle reaches, suggesting that flooded paddy fields largely altered the riverine DOM concentration and composition. In the lower reaches, the C/N ratio of the bulk DOM decreased with the river flow. However, according to principal component analysis, no changes were observed in the optical properties with river flow, suggesting that the C/N ratio of bulk DOM changed owing to *in situ* biological activity in the river. DOC biodegradation was observed at four sites in the upper and middle reaches but not at the two sites in the lower reaches. However, the DON concentration during the dark incubation experiments at all sites did not differ significantly, which implies that microbial degradation, particularly by small microorganisms, is a factor that decreased the C/N ratio of bulk DOM in the upper and middle reaches. In contrast, large microorganisms possibly degraded C-rich DOM to decrease the C/N ratio of bulk DOM in the lower reaches of the Ishikari River.

Keywords: riverine dissolved organic matter, carbon/nitrogen (C/N) ratio, optical properties, land use land cover, bioavailability, Ishikari River

OPEN ACCESS

Edited by:
Shafi Mohammad Tareq, Jahangirnagar University, Bangladesh

Reviewed by:
Kaijun Lu, University of Texas at Austin, United States
Ding He, Zhejiang University, China

***Correspondence:**
Yuji Takaki
yujitakaki@ees.hokudai.ac.jp

Specialty section:
This article was submitted to Biogeoscience, a section of the journal Frontiers in Earth Science

Received: *01 December 2021*
Accepted: *14 February 2022*
Published: *04 March 2022*

Citation:
Takaki Y, Hattori K and Yamashita Y (2022) Factors Controlling the Spatial Distribution of Dissolved Organic Matter With Changes in the C/N Ratio From the Upper to Lower Reaches of the Ishikari River, Japan. Front. Earth Sci. 10:826907. doi: 10.3389/feart.2022.826907

INTRODUCTION

Dissolved organic matter (DOM) in rivers is an essential component of biogeochemical cycles (Findlay and Sinsabaugh, 2003), and three major sources of DOM in rivers include 1) soils, 2) riparian zones, and 3) biological production *in situ* in rivers (Bertilsson and Jones, 2003; Willett et al., 2004; Yamashita et al., 2010; Bianchi, 2011; Yamashita et al., 2011; Drake et al., 2018). The chemical characteristics of DOM may vary depending on its origin. DOM is the source of energy and carbon in riverine ecosystems, particularly for heterotrophic microorganisms (Wetzel, 1992; Battin et al., 2016), and its bioavailability depends on its composition and structure (Amon and Benner, 1996; Amon et al., 2001). Therefore, the environmental dynamics of DOM in rivers must be determined by considering their origin and bioavailability for an improved understanding of riverine ecosystems.

In addition to providing energy, dissolved organic nitrogen (DON) plays an important role as an organic nutrient in riverine ecosystems (Wymore et al., 2015). The ratio of dissolved organic carbon (DOC) to DON (i.e., the C/N ratio of DOM) of bio-labile DOM is generally lower than that of bio-refractory DOM in marine environments (Hopkinson and Valino, 2005; Lønborg and Álvarez-Salgado, 2012), implying that nitrogen-containing DOM is relatively easily consumed by heterotrophic microbes in the ocean. The C/N ratio of riverine DOM is generally higher than that of marine DOM because of the inputs from soil-derived DOM, which has a higher C/N ratio (Lara et al., 1998; Lee et al., 2020). In contrast, DOM produced by algae in rivers and derived from wastewater and agricultural land have lower C/N values than soil-derived DOM (Westerhoff and Mash, 2002; Voss et al., 2021). Furthermore, Wiegner et al. (2006) conducted a degradation experiment in rivers on the east coast of the United States at 25°C under dark conditions for 6 days and observed that DON had a higher degradation rate and higher bioavailability than DOC. Similar results have been observed in different rivers (Hendrickson et al., 2007; Petrone et al., 2009; Wiegner et al., 2009; Islam et al., 2019). The contribution of protein-like fluorophores to total fluorophores has been related to the bioavailability of bulk DOM (Balcarczyk et al., 2009; Fellman et al., 2009; Petrone et al., 2011), implying that at least fractions of the DON, such as peptides and proteins, are actively involved in the metabolism of lower trophic levels in riverine ecosystems.

Previous studies have also suggested that DON bioavailability is controlled by dissolved inorganic nitrogen (DIN) concentration. Heterotrophic microorganisms, such as bacteria, can use DIN for nitrogen assimilation and DON as a carbon and energy source (Lutz et al., 2011; Wymore et al., 2015). DON concentration may increase with increasing DIN concentration under the condition that DON has the role of nutrient source for microorganisms (Wymore et al., 2015). On the other hand, Kaushal and Lewis (2005) and Pisani et al. (2017) proposed a model for the relationship between DIN concentration and DON bioavailability. In the model, DON bioavailability was reduced in DIN-rich environments.

The evaluation of factors controlling DOC concentration in rivers often involves comparison with the DOC quality determined by optical means along with its comparison with land use and land cover (Aitkenhead and McDowell, 2000; Mulholland, 2003; Yamashita et al., 2011; Lu et al., 2014; Mann et al., 2016; Williams et al., 2016; Connolly et al., 2018). However, compared with the factors controlling DOC concentration, those controlling the DON concentration and C/N ratio of bulk DOM in rivers have been evaluated in a relatively small number of studies. For example, Willet et al. (2004) observed that DON concentrations remained stable across a wide range of hydrologically and ecologically diverse catchments with highly varying DIN concentrations. Jacobs et al. (2017) compared DOC and DON concentrations in rivers with different land use patterns, namely forest, field, and plantation agriculture, and observed that both DOC and DON concentrations were not affected by land use land cover in the catchment. DOM in forest areas generally have higher C/N ratios than those in urban/suburban and agricultural areas (Seitzinger et al., 2002; Graeber et al., 2015; Heinz et al., 2015; Yates et al., 2019; Voss et al., 2021). Yates et al. (2019) also reported that the C/N ratio of DOM in the blanket peatland area was higher than that in the coniferous woodland area. In contrast, Bhattacharya and Osburn (2020) reported that the C/N ratio of stream DOM in the Neuse River Basin, the largest watershed in the state of North Carolina, United States, exhibited slightly higher values in wetland and agricultural areas than in urban and forested areas. Thus, the factors controlling DON concentrations and the C/N ratio of bulk DOM in rivers have not been well documented (Heinz et al., 2015).

In this study, we determined the spatial distribution of DOC and DON concentrations and the optical properties of DOM in the Ishikari River Basin in Hokkaido, northern Japan. The biodegradability of DOC and DON was also determined by 40-days dark incubation experiments. The aim of this study was to estimate the factors controlling the DOC and DON concentrations and C/N ratio of bulk DOM in the Ishikari River to improve our understanding of the influence of C/N ratio on the environmental dynamics of riverine DOM.

MATERIALS AND METHODS

Study Sites and Sampling

Study Sites

The study area was located in the catchment of the Ishikari River, Hokkaido, Japan (**Figure 1**). This stream originates from Mt. Ishikari (1967 m) and is the longest river in Hokkaido, with a basin area of 14,330 km^2 and a river length of 268 km. The stream has many tributaries, from large to small, and transports freshwater to the Sea of Japan. The Ishikari River generally has a maximum annual flow in April because of snowmelt in the spring (Duan et al., 2013). In addition, the river flow is relatively high in August and September because of heavy precipitation from typhoons and fronts.

The topography of the watershed is 60% mountains and 40% plains. Most of the upper reaches of the watershed are mountainous. The watershed of the upper reaches of the Ishikari River Basin comprises the Taisetsu Mountains, which

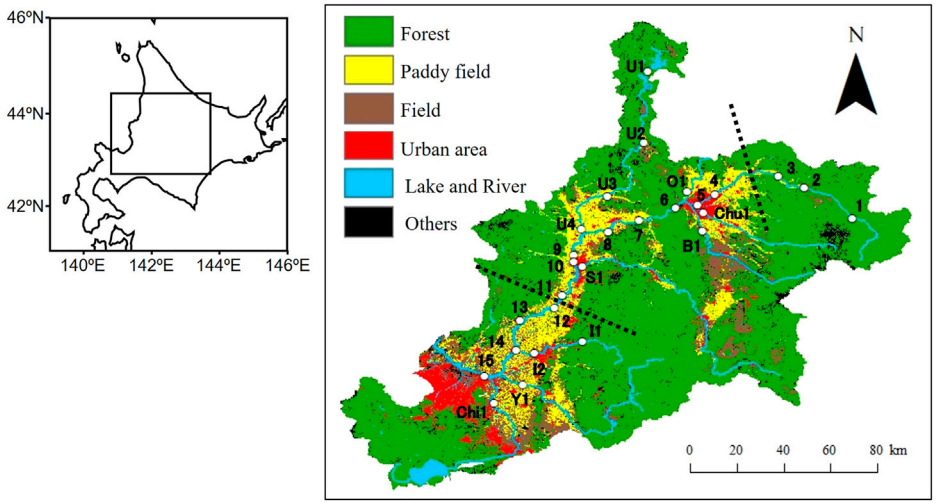

FIGURE 1 | Map of the study area. White plots indicate the sampling sites and the number next to the plot denotes the site number. The black dotted lines divide upper, middle and lower reaches. This map was created by processing "Digital National Land Information (Data of Land use in 2016)" (Ministry of Land, Infrastructure, Transport and Tourism) (https://nlftp.mlit.go.jp/ksj/index.html).

TABLE 1 | Information on the study area during observations.

Site No	Latitude	Longitude	River name	Distance from river mouth (km) (Mainstream only)	Sampling date	Water temperature (°C)	EC (mS cm^{-1})
1	43°43′37″N	142°57′02″E	Ishikari	221	2020/7/23	15.2	0.072
2	43°50′30″N	142°46′01″E	Ishikari	200	2020/7/23	18.5	0.082
3	43°53′20″N	142°40′05″E	Ishikari	188	2020/7/23	17.1	0.07
4	43°49′07″N	142°25′34″E	Ishikari	164	2020/7/23	19.7	0.084
5	43°46′44″N	142°21′36″E	Ishikari	157	2020/7/23	20.3	0.085
6	43°45′56″N	142°16′33″E	Ishikari	149	2020/7/24	19.6	0.111
7	43°43′01″N	142°08′05″E	Ishikari	130	2020/7/24	19.6	0.111
8	43°40′22″N	142°01′05″E	Ishikari	114	2020/7/24	21.1	0.135
9	43°35′12″N	141°52′58″E	Ishikari	105	2020/7/24	22.4	0.126
10	43°33′38″N	141°53′02″E	Ishikari	94	2020/7/24	22.5	0.125
11	43°25′49″N	141°50′21″E	Ishikari	77	2020/7/24	23.3	0.132
12	43°23′06″N	141°48′43″E	Ishikari	71	2020/7/24	22.8	0.131
13	43°20′15″N	141°40′36″E	Ishikari	58	2020/7/27	22.3	0.138
14	43°13′22″N	141°39′44″E	Ishikari	45	2020/7/27	22.2	0.141
15	43°07′24″N	141°32′34″E	Ishikari	27	2020/7/27	20.3	0.161
U1	44°17′21″ N	142°10′08″E	Uryu		2020/7/23	12.9	0.068
U2	44°00′53″ N	142°09′07″E	Uryu		2020/7/23	19.3	0.085
U3	43°48′33″N	142°00′49″E	Uryu		2020/7/23	21.7	0.095
U4	43°41′01″N	141°54′55″E	Uryu		2020/7/23	22.4	0.113
Chu1	43°44′53″N	142°22′46″E	Chubetsu		2020/7/24	17.8	0.122
B1	43°40′46″N	142°22′40″E	Biei		2020/7/24	16.6	0.212
O1	43°49′50″N	142°19′12″E	Osarappe		2020/7/24	19.7	0.077
S1	43°32′36″N	141°55′09″E	Sorachi		2020/7/24	23.7	0.132
I1	43°15′20″N	141°55′06″E	Ikushunbetsu		2020/7/27	14.7	0.117
I2	43°12′35″N	141°43′60″E	Ikushunbetsu		2020/7/27	18	0.141
Y1	43°05′20″N	141°41′27″E	Yubari		2020/7/27	17.8	0.128
Chi1	43°01′06″N	141°34′45″E	Chitose		2020/7/27	19.6	0.178

are a group of volcanoes reaching heights of up to 2,000 m. In contrast, the lower reaches of the watersheds are plain, represented by the Ishikari Plain, and wetlands have also developed.

The land use land cover of watersheds is largely dominated by forests (Kunii and Saito, 2009; Duan et al., 2015). Alpine vegetation was evident in the headwaters of the watersheds. In other mountainous areas, deciduous broad-leaved forests are

developed, with partial distribution of planted coniferous forests. Paddy fields are widely developed, in both basins and the plains. In addition, the land is utilized for other agricultural purposes such as cultivation of vegetables and beans. The cropping period for paddy fields and other agricultural land is approximately from April to October, with variations depending on the crop. Moreover, urban areas, such as Sapporo and Asahikawa, exist in the watershed.

Sampling

In this study, stream water samples were collected from the Ishikari River and its eight major tributaries (**Table 1**; **Figure 1**). Thus, 27 sampling sites were selected mostly from bridges near gauging stations operated by the Hokkaido Development Bureau of the Ministry of Land, Infrastructure, Transport and Tourism. Fifteen sites were selected from the Ishikari River (mainstream) (1–15), four sites from the Uryu River (U1 to U4), two sites from Ikushunbetsu River (I1 and I2), and one site each from the Chubetsu, Biei, Osarappe, Sorachi, Yubari, and Chitose rivers (Chu1, B1, O1, S1, Y1, and Chi1, respectively) (**Figure 1**).

Observations were conducted at Sites 1–5 and U1–U4 on 23 July 2020; Sites 6–12, Chu1, B1, O1, and S1 on 24 July 2020; and Sites 13–15, I1–I2, Y1, and Chi1 on 27 July 2020. The weather on the observation days was sunny and cloudy, with no precipitation. Surface water samples were collected from the bridge using a stainless-steel bucket with a rope and poured into 500 ml acid-washed (soaked in 1 M hydrochloric acid overnight and washed with Milli-Q water) polycarbonate bottles. Both buckets and bottles utilized for water sampling were rinsed thrice with river water. The water temperature and electrical conductivity (EC) of the river water were measured using an electrical conductivity meter (LAQUAact ES-71, Horiba Scientific).

Samples were filtered on site through a pre-combusted (450°C, 3 h) glass fiber filter (Whatman GF/F filter, pore size: approximately 0.7 μm) under reduced pressure. The filtrate was dispensed into two acid-washed 10 ml acrylic tubes and two 40 ml glass vials and subsequently stored in a cooler. All tubes and glass vials were rinsed thrice with filtered sample water. Immediately after returning to the laboratory at the Faculty of Environmental Earth Science, Hokkaido University, the acrylic tubes were kept frozen in the dark for inorganic nutrient and total dissolved nitrogen (TDN) analyses. In addition, glass vials for DOM analyses were kept refrigerated in the dark.

Chemical Analysis

Concentrations of DOC, TDN, and Inorganic Nutrients

The concentration of DOC (μMC) was measured by the combustion catalytic oxidation method using a total organic carbon analyzer (TOC-L CSH, Shimadzu). The DOC concentration was calculated from the standard curve using a potassium hydrogen phthalate solution and was determined daily.

DIN (NH_4^+, NO_2^-, and NO_3^-) and phosphate (PO_4^-) concentrations (μMN and μMP, respectively) were measured by colorimetric analysis using a continuous flow analyzer (QuAAtro, BRAN + LUEBBE GmbH). The TDN concentration (μMN) was determined by measuring the NO_3^- concentration after oxidative decomposition by the wet oxidation method using potassium peroxydisulfate (Yamashita et al., 2021). The detection limit was calculated as the sum of the mean of the blank concentration and thrice the standard deviation. The detection limits were 0.26 μMN for NH_4^+, 0.06 μMN for NO_2^-, 0.59 μMN for NO_3^- + NO_2^-, 0.02 μMP for PO_4^-, and 0.48 μMN for TDN. The DON concentration (μMN) was estimated by subtracting the DIN concentration from the TDN concentration. The C/N ratio of DOM was calculated as the molar ratio of the DOC concentration to the DON concentration.

Optical Properties of DOM

UV-Vis absorption spectra were measured using a spectrophotometer (UV-1900i, Shimadzu) to measure the UV-Vis absorbance of DOM. These absorption spectra were acquired with a 5 cm quartz-windowed cell at wavelengths between 200 and 800 nm at 0.5 nm intervals. The absorbance spectrum of the sample was baseline-corrected by subtracting average values ranging from 683 to 687 nm from the entire spectrum, according to Babin et al. (2003).

The spectral slope ratio (S_R) was determined as the ratio of the spectral slope of the shorter wavelength region (275–295 nm) to that of the longer wavelength region (350–400 nm) (Helms et al., 2008). S_R is known to be related to the molecular weight of DOM, with a high value representing low molecular weight organic matter and vice versa. The specific UV absorbance at 254 nm ($SUVA_{254}$), an index representing the relative contribution of aromatic compounds of DOC, was calculated by dividing the decadic absorption coefficient at 254 nm [A_{254} (m^{-1})] by the DOC concentration (mg L^{-1}) (Weishaar et al., 2003).

The fluorescence properties of DOM were measured using a spectrofluorometer (Fluoromax-4, Horiba Scientific). Excitation-emission matrix (EEM) spectra were acquired in a 1 cm quartz cell at excitation wavelengths between 250 and 450 nm at 5 nm intervals according to Tanaka et al. (2014), with few modifications. The emission wavelengths were acquired from 290 to 550 nm at 2 nm intervals. The integration time was set to 0.1 s. All fluorescence spectra were determined after inner filter correction with absorbance spectrum (McKnight et al., 2001), instrumental bias correction (Cory et al., 2010), and subtraction of the EEM of Milli-Q water. The fluorescence unit was converted to a Raman unit with a water Raman peak analyzed daily at 350 nm excitation of Milli-Q water (Lawaetz and Stedmon, 2009).

Three typical peaks were determined from the EEM patterns of samples from the Ishikari River and its major tributaries. The peaks were categorized as B peak (Ex/Em = 275/310, protein-like), A peak (Ex/Em = 250/450, humic-like), and C peak (Ex/Em = 320/440, humic-like) according to (Coble 1996; Coble et al., 1998). Ratios of fluorescence intensity of protein-like peak B to that of humic-like peaks A or C (B/C or B/A) were determined as qualitative parameters of fluorescent DOM. The fluorescence index (FI) was determined as the ratio of the fluorescence intensity at emission wavelengths of 470 and 520 nm with that at an excitation wavelength of 370 nm (McKnight et al., 2001; Cory and McKnight, 2005). The FI is an indicator of the origin of humic-like fluorescent DOM; lower and higher values of FI indicate allochthonous sources and

autochthonous sources, respectively (McKnight et al., 2001). The humification index (HIX) indicates the degree of humification of DOM and was determined as the ratio of the peak area at 435–480 and 300–345 nm with that at 255 nm excitation (Zsolnay, 2003). The higher the value of HIX, the more highly conjugated the humic-like substances, and vice versa (Zsolnay, 2003).

Bioassay

To evaluate the bioavailability of DOC and DON in stream water, biodegradation experiments were conducted at six sites (Sites 1, 6, 10, 11, 14, and 15) from the mainstream of the Ishikari River according to Hasegawa et al. (2010) and Yamashita et al. (2013), with few modifications.

The sample water was filtered through a Whatman GF/F filter (pore size: approximately 0.7 μm), dispensed into three 40 ml glass vials for each site, and incubated for 40 days in a cool incubator (CN-40A, Mitsubishi Electric) under dark conditions at 20°C, similar to the river water temperature at the time of observation. After 40 days of incubation, the DOC concentration was measured immediately, without further filtration. The sample water was dispensed into acid-washed 10 ml acrylic tubes and kept frozen until DIN concentration measurement. Although this bioassay method is simpler and expected to have lower possibility of contamination than the method of adding inoculum, large microbes might be removed from the incubations by filtration with the GF/F filter (Hasegawa et al., 2010).

The average of the triplicate incubation results was implemented as the concentration after the bioassay. In addition, standard deviation was used to determine the error associated with the bioassay. The amount of decomposed DOC was calculated by subtracting the DOC concentration after the bioassay from that before. The amount of DON decomposition was calculated by subtracting the DIN concentration before the bioassay from that after, considering that DIN is not converted to organic matter or lost during the decomposition experiment; instead, DIN is produced by the decomposition of DON. The rate of change (in %) was calculated by dividing the amount of decomposed DOC (DON) by the DOC (DON) concentration before the bioassay and multiplying it by 100.

Statistical Analysis

Linear regression analysis was performed to examine the relationship between DON and DOC concentrations. The Pearson's correlation coefficient was determined for each parameter. Principal component analysis (PCA) was performed on the data pertaining to the C/N ratio of DOM, FI, HIX, B/C, B/A, A/C, $SUVA_{254}$, and S_R to comprehensively evaluate the chemical properties of DOM at each site. All statistical analyses were performed using R 4.1.1 (R Core Team, 2021).

RESULTS

Water Temperature and Electrical Conductivity

The water temperature and EC values are presented in **Table 1**. The water temperature ranged from 12.9 to 23.7°C with an overall average of 18.9°C. In the upper reaches, the water temperature was lower than that in the lower reaches of the mainstream (Ishikari River), and in the major tributaries, it was similar to or lower than that in the mainstream.

The EC ranged from 0.070 to 0.161 mS cm^{-1} in the mainstream and from 0.068 to 0.212 mS cm^{-1} in the major tributaries. Regardless of the mainstream or tributaries, the EC in the upper reaches was lower than that in the lower reaches.

Concentrations of DOC, DON, and Inorganic Nutrients

DOC concentrations, DON concentrations, and the C/N ratio of DOM are summarized in **Table 2**, and their spatial variations are shown in **Figure 2**. In the mainstream, the DOC concentration ranged from 34 μMC (Site 1) to 197 μMC (Site 10). The DOC concentration in the mainstream increased with the river flow in the upper and middle reaches and remained unchanged in the lower reaches. The DOC concentration in each major tributary was generally lower than that at each confluence with the mainstream, except for the Uryu River. The highest DOC concentration (310 μMC) was observed in the middle reaches of the Uryu River (Site U2).

The DON concentration in the mainstream ranged from 1.8 μMN (Site 1) to 14.0 μMN (Site 15) and increased with the river flow in the upper and middle reaches, remaining unchanged in the lower reaches. As with the DOC concentrations, each major tributary demonstrated lower DON concentrations than the concentration at each confluence with the mainstream, with the exception of the Uryu River. The highest DON concentration (15.4 μMN) was observed in the lower reaches of the Uryu River (Site U4).

A positive linear relationship existed between DOC and DON concentrations in the Ishikari River and the tributaries (**Figure 3**).

The C/N ratio exhibited spatial variation in the Ishikari River Basin (**Table 2**; **Figure 2**). In the mainstream, the C/N ratio ranged from 12.1 (Site 15) to 22.0 (Site 3) and continuously decreased with the river flow from the upper to the lower reaches. The C/N ratio of the major tributaries (12.3–23.6) was similar to that of the mainstream.

The DIN and PO_4^- concentrations are listed in **Table 2**. The DIN concentration ranged from 7.4 to 76.8 μMN in the Ishikari River and the major tributaries. DIN concentrations in the upper reaches were lower than those in the middle and lower reaches. The DIN concentrations in the major tributaries were heterogeneous. Overall, the DIN concentrations were approximately three times higher than the DON concentrations at most sites.

The PO_4^- concentration was less than 1 μMP at all sites (ranging from 0.08 to 0.99 μMP). The PO_4^- concentrations in the upper reaches were lower than those in the middle and lower reaches of the mainstream. In the major tributaries, the PO_4^- concentrations were distributed heterogeneously. The N/P ratio of inorganic nutrients ranged from 25 to 293, with an average ± standard deviation of 95 ± 52.

Optical Properties of DOM

The optical properties of DOM, such as S_R, $SUVA_{254}$, B/C, B/A, A/C, FI, and HIX, at each site are summarized in **Table 2**.

TABLE 2 | Stream water chemistry for all the sites.

Site No	DOC (μMC)	DON (μMN)	DIN (μMN)	PO_4^- (μMP)	C/N	S_R	SUVA (L mg^{-1} m^{-1})	B peak (RU)	A peak (RU)	C peak (RU)	B/C	B/A	A/C	FI	HIX
1	34	1.8	7.4	0.16	19.2	1.06	2.47	0.01	0.05	0.02	0.52	0.27	1.95	1.61	7.99
2	63	3.4	16.1	0.21	18.6	0.97	3.25	0.02	0.10	0.06	0.40	0.22	1.82	1.49	6.74
3	68	3.1	12.7	0.22	22.0	0.91	3.75	0.03	0.12	0.06	0.40	0.22	1.80	1.51	5.58
4	125	7.4	22.9	0.25	16.9	0.79	4.06	0.06	0.28	0.14	0.41	0.21	1.95	1.53	4.91
5	125	8.8	34.3	0.30	14.1	0.81	4.07	0.06	0.26	0.14	0.43	0.23	1.90	1.52	4.95
6	165	10.1	22.7	0.30	16.5	0.83	3.73	0.11	0.36	0.20	0.55	0.30	1.85	1.52	4.04
7	161	10.5	59.0	0.39	15.3	0.86	3.50	0.10	0.35	0.20	0.52	0.30	1.74	1.58	3.97
8	161	13.0	55.9	0.47	12.4	0.83	3.75	0.10	0.37	0.21	0.49	0.27	1.80	1.57	4.22
9	190	13.5	34.5	0.35	14.1	0.77	4.41	0.11	0.48	0.26	0.43	0.23	1.85	1.56	4.68
10	197	11.3	33.8	0.31	17.4	0.78	4.28	0.10	0.51	0.27	0.36	0.19	1.89	1.56	5.01
11	182	13.2	31.3	0.37	13.7	0.80	4.19	0.11	0.45	0.24	0.46	0.25	1.88	1.55	4.80
12	185	11.9	32.2	0.41	15.5	0.79	4.09	0.09	0.45	0.24	0.38	0.20	1.88	1.53	4.89
13	163	11.9	28.3	0.32	13.7	0.80	3.98	0.09	0.44	0.23	0.38	0.20	1.90	1.54	5.24
14	156	12.3	26.3	0.28	12.6	0.80	4.32	0.09	0.46	0.24	0.40	0.21	1.94	1.52	5.10
15	170	14.0	42.8	0.49	12.1	0.75	4.86	0.10	0.58	0.30	0.33	0.17	1.95	1.56	5.34
U1	137	5.8	16.9	0.12	23.6	0.80	4.36	0.06	0.30	0.16	0.35	0.19	1.86	1.46	6.60
U2	310	13.8	18.7	0.31	22.4	0.78	4.59	0.14	0.63	0.33	0.41	0.22	1.89	1.47	4.80
U3	193	10.4	12.3	0.33	18.5	0.82	4.42	0.09	0.43	0.22	0.40	0.20	2.00	1.51	5.03
U4	287	15.4	14.2	0.56	18.7	0.76	5.10	0.17	0.79	0.39	0.43	0.21	2.01	1.51	4.95
Chu1	72	5.7	41.0	0.25	12.5	0.90	3.05	0.03	0.14	0.07	0.44	0.23	1.94	1.60	4.67
B1	74	5.1	49.8	0.17	14.5	0.92	3.07	0.02	0.14	0.08	0.29	0.16	1.76	1.59	6.57
O1	159	8.5	12.7	0.37	18.8	0.76	4.61	0.10	0.42	0.22	0.45	0.24	1.89	1.54	4.75
S1	132	10.2	30.5	0.31	12.9	0.98	3.02	0.05	0.26	0.13	0.40	0.21	1.94	1.53	5.19
I1	118	5.9	9.6	0.08	20.0	0.97	4.40	0.08	0.25	0.12	0.62	0.31	2.01	1.48	3.69
I2	133	7.3	11.1	0.16	18.2	0.98	4.75	0.10	0.33	0.15	0.66	0.31	2.12	1.51	3.51
Y1	128	10.4	9.3	0.14	12.3	0.89	3.96	0.07	0.31	0.15	0.43	0.21	2.02	1.56	5.16
Chi1	135	10.0	76.8	0.99	13.6	0.65	5.34	0.12	0.45	0.23	0.54	0.27	1.97	1.59	3.94

S_R in the Ishikari River Basin ranged from 0.65 at the Chitose River (Site Chi1) to 1.06 at the upper reaches of the mainstream (Site 1) with average ± standard deviation of 0.84 ± 0.09. S_R in the mainstream decreased with the river flow in the upper reaches and remained unchanged in the middle and lower reaches. The S_R values of the major tributaries were heterogeneously distributed.

The overall average ± standard deviation of $SUVA_{254}$ is 4.05 ± 0.68 (2.47 at Site 1 to 5.34 at Site Chi1). In the mainstream, $SUVA_{254}$ increased with the river flow in the upper and lower reaches, while the $SUVA_{254}$ values in the middle reaches and in major tributaries were heterogeneously distributed.

In the mainstream, the ratio of protein-like fluorophores to humic-like fluorophores, B/C and B/A, was higher in the middle reaches (in particular Sites 6 to 8 and 11) than in the upper and lower reaches, even though the ratios in the most upstream site (Site 1) had high values. The ratios in the major tributaries (Sites I2, Y1, and Chi1) whose confluence was located at the lower reaches were higher than those in the major tributaries with confluence in the upper and middle reaches.

The ratio of humic-like fluorophores, A/C, in the Ishikari River and the major tributaries did not change considerably (from 1.74 at Site 7 to 2.12 at Site I2, average ± standard deviation = 1.91 ± 0.09).

The FI exhibited a narrow range from 1.61 at the most upper reaches of the mainstream (Site 1) to 1.41 at the upper reaches of the Uryu River (Site U1), with an average ± standard deviation of 1.54 ± 0.04. The value in the mainstream increased with the river flow from Sites 2 to 7 and then decreased toward Site 14. The values of the major tributaries exhibited a heterogeneous distribution.

The HIX ranged from 3.51 at the Ikushunbetsu River (Site I2) to 7.99 at the most upper reaches of the mainstream (Site 1), and its average ± standard deviation was 5.05 ± 0.09. The HIX value in the mainstream was the highest in the uppermost site (Site 1), decreased with river flow up to Site 7, and then increased slightly toward Site 10, even though the values in the lower reaches did not change significantly. The HIX in the major tributaries was distributed heterogeneously.

Principal Component Analysis

The PCA results are shown in **Figure 4**. PC1 accounted for a variance of 33%, with a large positive coefficient of HIX and negative coefficients of B/A and B/C. In addition, PC2 accounted for a variance of 26%, with a large positive coefficient of $SUVA_{254}$ and a large negative coefficient of S_R. In particular, the positive score of PC1 indicated high humification, and the negative score indicated a high abundance of protein-like fluorophores. Furthermore, PC2 demonstrated a high molecular weight and aromaticity with a positive score and a low molecular weight with a negative score. On one hand, in the mainstream, a large positive PC1 score was observed in the upper reaches (Sites 1, 2, and 3) and

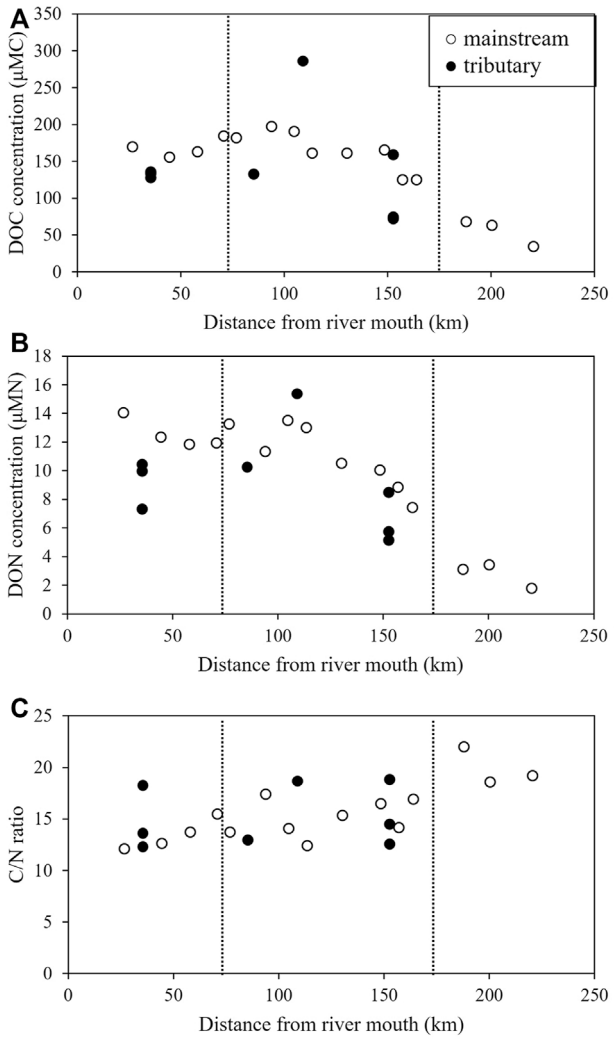

FIGURE 2 | The spatial distribution of the **(A)** Dissolved organic carbon (DOC) concentration, **(B)** Dissolved organic nitrogen (DON) concentration, and **(C)** Carbon/nitrogen (C/N) ratio in the Ishikari River Basin. White plots represent mainstream and black plots represent major tributaries. Plots of major tributaries are inserted at the confluence with the mainstream. The lowermost reaches of each tributary are plotted in the figures. The black dotted lines divide upper, middle and lower reaches.

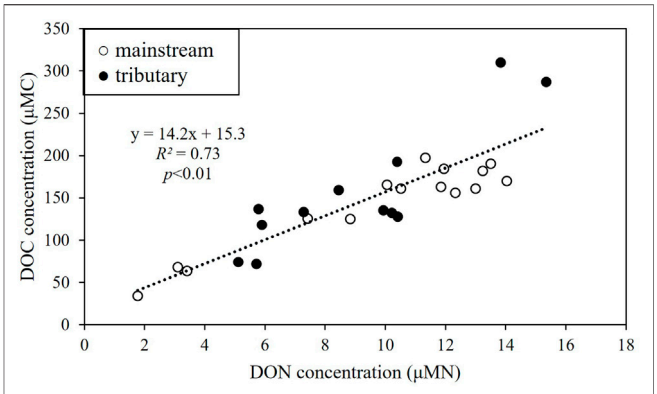

FIGURE 3 | Relationship between dissolved organic nitrogen (DON) and dissolved organic carbon (DOC) concentrations. White plots represent the mainstream, and black plots represent the major tributaries. The black dotted line is a linear regression line for all samples.

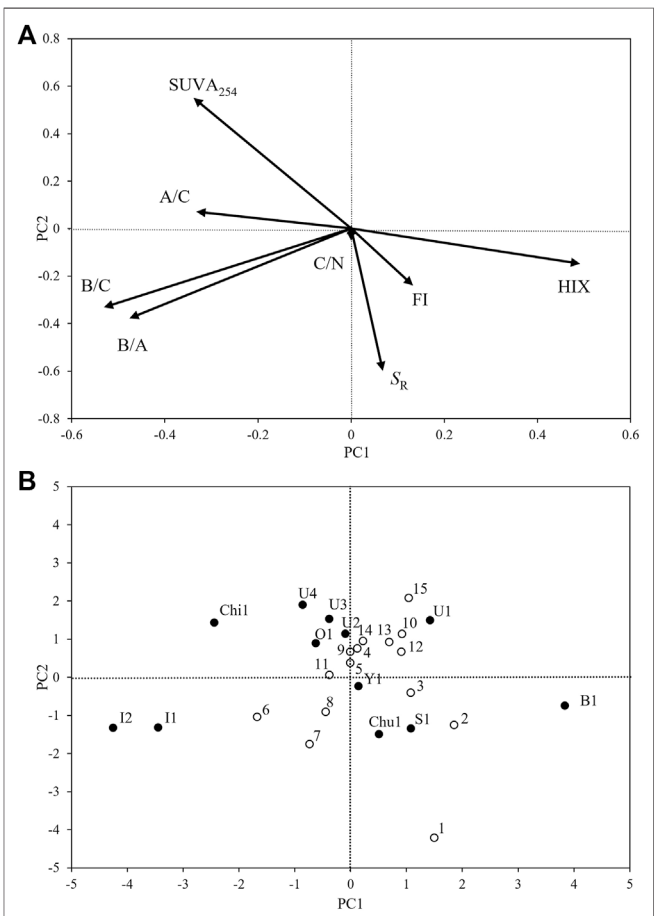

FIGURE 4 | Results of principal component analysis (PCA) **(A)** coefficients, and **(B)** scores using qualitative indicators of dissolved organic matter (DOM) at each site. White and black plots in (b) represent the mainstream and major tributaries, respectively. The number next to the plot is the site number.

some of the middle and lower reaches (Sites 10, 12, 13, and 15). On the other hand, a large negative PC1 was evident in the middle reaches (Sites 6, 7, and 8). For PC2, sites in the upper and middle reaches (Sites 1, 2, 3, 6, 7, and 8) exhibited negative scores, while other sites in the middle reaches (Sites 4, 5, and 9–11) and those in the lower reaches exhibited positive scores. The PC scores of the tributaries were generally more dispersed than those of the mainstream.

Bioassay

The changes in DOC and DON concentrations in the 40-days dark incubation experiments are shown in **Figure 5**. The reproducibility of the triplicate incubations was good, and

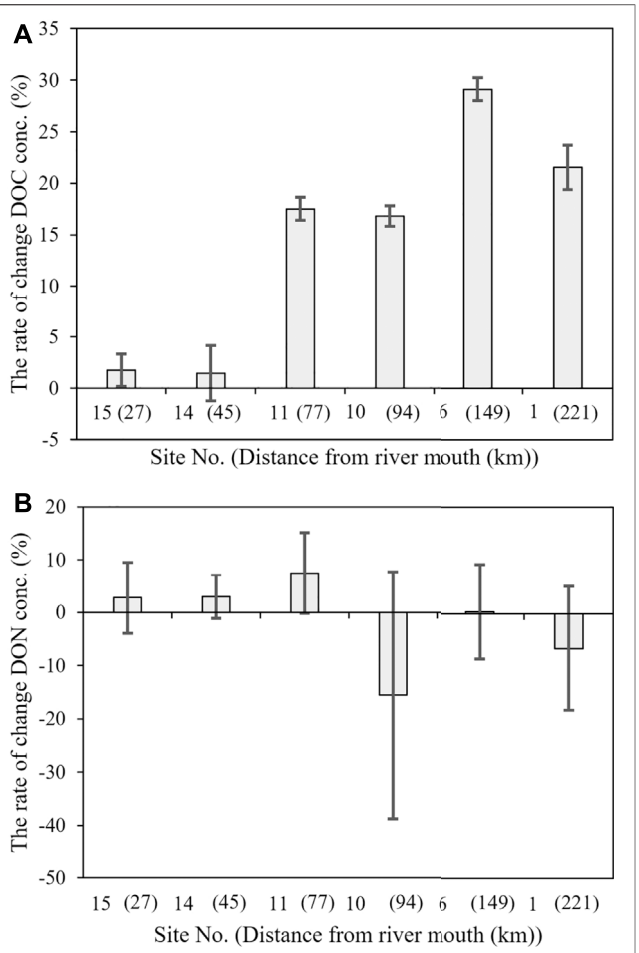

FIGURE 5 | Changes in the **(A)** dissolved organic carbon (DOC) concentrations and **(B)** dissolved organic nitrogen (DON) concentrations associated with the 40-days bioassay. Error bars represent the standard deviation from triplicate incubation.

17–29% of the initial DOC decreased (in 40 days) at four sites in the upper and middle reaches. In contrast, the DOC concentrations did not change significantly at the two sites in the lower reaches.

The DON concentrations at any of the six sites did not significantly differ before and after incubation, because variations in DON concentration by incubation were smaller than the standard deviation of the triplicate incubations.

DISCUSSIONS

Factors Controlling the DOM Concentration in the Ishikari River

The DOC and DON concentrations in the mainstream increased with the river flow in the upper and middle reaches and remained unchanged in the lower reaches (**Figure 2**). A positive linear relationship was observed between DOC and DON concentrations in the Ishikari River and the major tributaries (**Figure 3**). The spatial distribution of DOC and DON concentrations and their linear relationship indicate that allochthonous DOM inputs mostly dominated DOM in the Ishikari River Basin, as suggested by Bernal et al. (2018). DOC and DON concentrations were negatively and positively correlated with S_R and $SUVA_{254}$, respectively (**Figure 6**), implying that allochthonous DOM might be characterized by high molecular weight and high aromaticity. Interestingly, the DOC and DON concentrations in each major tributary were generally lower than those at each confluence with the mainstream (**Figure 2**), suggesting that major tributaries were not the major factors controlling the DOM concentration and composition in the mainstream.

A decrease in the C/N ratio of bulk DOM with the river flow from the upper reaches to the lower reaches of the Ishikari River (**Figure 2**) suggests: 1) changes in the C/N ratio of allochthonous DOM from minor tributaries, including the agricultural channel (which were not observed in this study), from the upper to the lower reaches, 2) substantial contribution of DOM from riverine riparian zone and biological production, or 3) preferential removal of C-rich DOM than N-rich DOM.

The DOC and DON concentrations increased slightly in the upper reaches of the Ishikari River (Sites 1–3) and nearly doubled between the upper (Site 3) and the middle (Site 4) reaches. The C/N ratio of bulk DOM decreased substantially from Sites 3 to 4 (**Figure 2**). The physical and chemical properties of watershed soils are strongly related to land use land cover (Smith, 2008), which might induce a relationship between land use land cover and DOM concentration (Yates et al., 2019). In this study, the upper reaches (Sites 1–3) were located in a canyon in the mountains, and most of the land use land cover in the watershed was forest. However, Site 4 was located in the basin, with paddy fields and urban areas distributed around the site (**Figure 1**). Connolly et al. (2018) stated that a small slope in the watershed increases the residence time of water in the soil, which enhances the leaching of DOM from the soil and, thus, increases the DOM concentration in the stream. The contribution of wetlands in the watershed is a well-known and major factor controlling riverine DOC concentrations (Mulholland, 2003; Laudon et al., 2004; Yamashita et al., 2010). Paddy field outflow has also been suggested as a source of DOM in riverine water (Ruark et al., 2010; Krupa et al., 2012; Suzuki et al., 2015). The quality of DOM at Site 1, evaluated using PCA, could be characterized as having a low molecular weight and low aromaticity. The quality changed to high molecular weight and high aromaticity at Site 4 (**Figure 4**). Reportedly, DOM originating from forests has low molecular weight (Inamdar et al., 2012; Bhattacharya and Osburn, 2020). However, DOM from agriculture and wetlands have high molecular weights and are rich in humic (Royer and David, 2005; Fellman et al., 2010; Bhattacharya and Osburn, 2020). Allochthonous DOM with humic characteristics was reported to load from flooded paddy fields to tributaries during the cropping period, which strongly influenced the DOM quality in tributaries (Abe et al., 2011). These results imply that the increase in DOM concentration accompanying the change in the quality from the upper to the middle reaches is probably due to the contribution of the paddy field outflow to the mainstream.

	DOC	DON	DIN	PO_4^-	C/N	S_R	SUVA	B peak	A peak	C peak	B/C	B/A	A/C	FI	HIX
DOC	1														
DON	**0.85****	1													
DIN	N.S.	N.S.	1												
PO_4^-	N.S.	**0.52***	**0.67****	1											
C/N	N.S.	**-0.41***	**-0.6****	N.S.	1										
S_R	**-0.63****	**-0.68****	**-0.42***	**-0.7****	N.S.	1									
SUVA	**0.64****	**0.56****	N.S.	**0.5****	N.S.	**-0.72****	1								
B peak	**0.89****	**0.85****	N.S.	**0.58****	N.S.	**-0.67****	**0.76****	1							
A peak	**0.93****	**0.9****	N.S.	**0.54****	N.S.	**-0.75****	**0.77****	**0.93****	1						
C peak	**0.94****	**0.91****	N.S.	**0.54****	N.S.	**-0.76****	**0.74****	**0.93****	**1****	1					
B/C	N.S.	N.S.	N.S.	N.S.	N.S.	N.S.	N.S.	N.S.	N.S.	N.S.	1				
B/A	N.S.	N.S.	N.S.	N.S.	N.S.	N.S.	N.S.	N.S.	N.S.	N.S.	**0.96****	1			
A/C	N.S.	N.S.	**-0.41***	N.S.	N.S.	N.S.	N.S.	N.S.	N.S.	N.S.	**0.4***	N.S.	1		
FI	N.S.	N.S.	**0.6****	N.S.	**-0.62****	N.S.	N.S.	N.S.	N.S.	N.S.	N.S.	N.S.	N.S.	1	
HIX	**-0.42***	**-0.48****	N.S.	N.S.	N.S.	N.S.	N.S.	**-0.64****	**-0.42***	**-0.42***	**-0.55****	**-0.54****	N.S.	N.S.	1

FIGURE 6 | Matrix of Pearson's correlation coefficients among each parameter. The significance is indicated by * ($p < 0.05$), ** ($p < 0.01$) and N.S. (non-significant). The sample number for analysis was 27.

The DOC and DON concentrations increased with decreasing C/N ratio in the middle reaches of the Ishikari River (Sites 4–11) (**Figure 2**). Moreover, the changes in these concentrations could not always be explained by the contribution of high levels of DOC and DON from major tributaries (**Figure 2**). This implies that the contribution of high levels of DOM with low C/N ratios from minor tributaries, riparian zones, and/or biological production is a probable reason for the increase in DOC and DON concentrations. The DOM composition in downstream of major tributaries is affected by various land use land cover in the wide area of the watershed of the major tributaries, while that in minor tributaries (including agricultural channels) may be affected by simple land use land cover because the watershed area of the minor tributaries is relatively small. Therefore, similar to the change in DOM quantity from the upper to the middle reaches, the increase in DOM concentrations might be due to the contribution of flooded paddy field-derived DOM from minor tributaries that were not sampled in this study. Furthermore, the PCA results showed that the DOM was rich in protein-like fluorophores in the middle reaches, particularly at Sites 6–8 and 11. Protein-like fluorophore-rich DOM might have originated from microbial sources and recent biological activity in both stream water and riparian zones (Bernal et al., 2018). Moreover, the autochthonous DOM, such as proteins, is known to increase in the middle reaches owing to the open canopy of riparian forests and shallow water depths that facilitate biological production, such as algal growth. The production of protein-rich materials by algae decreases the C/N ratio of bulk riverine DOM (Westerhoff and Mash, 2002). In addition, a negative correlation was evident between the C/N ratio of the bulk DOM and FI ($R = 0.62$, $p < 0.01$; **Figure 6**). These results imply that the C/N ratio in the middle reaches was affected by the contribution of autochthonous DOM, including protein-like and autochthonous humic-like fluorophores. Furthermore, the influx of groundwater-derived DOM from the riparian zone in the middle reaches might have reduced the C/N ratio. This is because low molecular weight and protein-like DOM is abundant in the groundwater, as high molecular weight and aromatic DOM is adsorbed by the soil (Inamdar et al., 2012).

In the lower reaches of the Ishikari River (Sites 12–15), DOC and DON concentrations were variable, but the C/N ratio tended to decrease with the river flow. The major tributaries did not affect the DOM concentration substantially in the mainstream of the Ishikari River (**Figure 2**). PCA loadings in the downstream sites were plotted within a narrow region with positive PC1 and PC2 (**Figure 4**), implying that the composition of allochthonous DOM from minor tributaries, including the agricultural channels (which were not observed in this study), was similar to that of the mainstream at the lower reaches of the Ishikari River. These results imply that the contribution of allochthonous DOM from minor tributaries, including agricultural channels flowing directly into the mainstream, might be an important factor controlling the DOC and DON concentrations in the lower reaches of the Ishikari River. DOM in the lower reaches had higher molecular weights and higher aromaticity than those in the upper reaches (**Figure 4**). Thus, similar to the changes in the quantity and quality of DOM in the upper to middle reaches, paddy field-derived DOM was the probable source for the minor tributaries, including the agricultural channels. Although the DOM quality, mainly determined by its optical properties, was similar in the lower reaches, the C/N ratio (which was not largely influenced in the PCA) of bulk DOM decreased with the river flow in the lower reaches, suggesting that the C/N ratio of paddy field-derived DOM might be changed *in situ* in the mainstream.

The preferential removal of C-rich or N-rich DOM may result in negligible changes in the DOM concentrations but is evident as a change in the C/N ratio (Wymore et al., 2015). Photochemical and microbial degradation is the major degradation process for riverine DOM (Wiegner and Seitzinger, 2001; Cory and Kling, 2018). The

humic-like substances and lignin phenols, which are components of aromatic allochthonous DOM, are preferentially degraded by sunlight (Opsahl and Benner, 1998; Moran et al., 2000; Benner and Kaiser, 2011) and might contribute to the decrease in the C/N ratio of DOM along with river flow. However, $SUVA_{254}$, which is an index of the relative contribution of aromatic compounds of DOC, increased with the river flow in the upper and lower reaches. The S_R values have been reported to increase with the photodegradation of DOM (Helms et al., 2008), while they do not change with the photodegradation of oceanic DOM (Yamashita et al., 2013). The S_R values decreased in the upper reaches and remained unchanged in the middle and lower reaches, implying that variations in S_R in the Ishikari River cannot be explained solely by photodegradation. Furthermore, peak A-type fluorescence components have been reported to be photodegradation products or photorefractory components (Chen et al., 2010; Yamashita et al., 2010). The ratio of humic-like fluorophores (A/C) in the Ishikari River did not change significantly with the river flow. These distribution patterns of the optical proxies imply that photodegradation is not a major process controlling the optical properties of DOM and the C/N ratio of DOM in the Ishikari River.

Some studies have reported the preferential removal of amino acids and neutral sugars by riverine and marine microbes (Yamashita and Tanoue, 2003; Davis and Benner, 2007; Davis et al., 2009; Benner and Kaiser, 2011). The C/N ratio of labile DOM is generally lower than that of refractory DOM in marine environments (Hopkinson and Vallino, 2005). The preferential removal of N-rich DOM over C-rich DOM has also been documented for riverine DOM (Wiegner et al., 2006; Hendrickson et al., 2007; Wiegner et al., 2009; Islam et al., 2019). However, in this study, DOC concentration decreased while DON concentration did not change after 40 days of dark incubation in samples obtained from the upper and middle reaches (**Figure 5**). The results of the degradation experiments suggested that DOC decomposed, while DON remained unchanged, causing a decrease in the C/N ratio with the river flow in the upper and middle reaches of the Ishikari River. The possible factors contributing to the different degradations of DOC and DON are discussed in the following subsection. In contrast, both DOC and DON did not decompose during the 40 days of dark incubation in samples obtained from the lower reaches (**Figure 5**). These results suggest that the decrease in the C/N ratio of DOM with river flow in the lower reaches might be the result of biodegradation of C-rich DOM by large microorganisms (>0.7 μm) that were not present in the bioassay of the study.

Bioavailability of DON and DOC in the River

Bioassay experiments were conducted to evaluate the bioavailability of DOM in riverine water. The initial DOC concentration was degraded by 17–29% in 40 days at four sites in the upper and middle reaches, but the DOC concentrations did not change significantly at the two downstream sites. This result suggests that the labile DOC in the river is utilized by microorganisms in the upper and middle reaches, whereas the bio-refractory DOC accounts for a large proportion of DOM in the lower reaches. However, the results of this study might underestimate the actual loss of DOC, because large sized microorganisms (>0.7 μm) were removed from the bioassay experiments through filtration. As discussed in the previous subsection, the decrease in the C/N ratio of DOM with river flow in the lower reaches implies that large microorganisms preferentially remove C-rich DOM over N-rich DOM.

The degradation rate of DOC (%) was not significantly correlated with PO_4^{-} or DIN concentrations at the six sites (R = -0.49, p = 0.33, and n = 6 for PO_4^{-}; and R = -0.55, p = 0.26, and n = 6 for DIN), suggesting that differences in the concentration of inorganic nutrients did not affect the biodegradation of riverine DOC, particularly by small microorganisms (<0.7 μm), in this study.

Microbial degradation of DOC has been observed in previous studies (Wikner et al., 1999; Royer and David, 2005; Wiegner et al., 2009). The bio-degraded DOM at four sites in the upper and middle reaches was probably derived from forest or paddy fields, while bio-refractory DOM at the two sites in the lower reaches might be derived from paddy fields. Although the direct relationship between microbial reactivity and land use land cover has not been extensively studied, Asmala et al. (2013) reported that DOM originating from a catchment dominated by natural forests and peatlands was less biodegradable than that from agricultural areas.

DOM in the lower reaches (Sites 14 and 15) can be characterized as possessing high molecular weight and high aromaticity (**Figure 4**), which is generally considered to be typical characteristics of bio-refractory materials (Bhattacharya and Osburn, 2020). The biodegradability of DOM has been related to the contribution of protein-like fluorophores to the total fluorophores (Balcarczyk et al., 2009; Fellman et al., 2009; Petrone et al., 2011). Relationships between biodegradability and B/A and B/C, which correspond to the contribution of protein-like fluorophores in total fluorophores, were observed in this study (R = 0.83, p = 0.04, and n = 6 for B/A; and R = 0.82, p = 0.05, and n = 6 for B/C). These results imply that the abundance of protein-like substances may affect the biodegradability of riverine DOC, particularly by small microorganisms, in the Ishikari River.

Notably, no significant change occurred in the DON concentration during the biodegradation experiments at any of the six sites. DON generally degrades during incubation in the dark (Seitzinger and Sanders, 1997; Stepanauskas et al., 2000; Wiegner et al., 2009), and N-rich DOM is generally considered to be more biodegradable than C-rich DOM (Wiegner et al., 2006; Hendrickson et al., 2007; Petrone et al., 2009; Wiegner et al., 2009; Islam et al., 2019). In contrast, no change or increase in DON concentration was observed in several dark incubation experiments conducted previously (Kaushal and Lewis, 2005; Wiegner et al., 2006; Pisani et al., 2017), which was similar to the results of our dark incubation experiments (**Figure 5**).

The fact that DON concentration did not change but the DOC concentration decreased can be considered to be a case where riverine microorganisms degrade non-N-containing organic compounds but do not decompose N-containing organic compounds. However, this mechanism did not seem to be the case for riverine DOM in this study, because DOC degradability was related to the relative abundance of protein-like fluorophores (peak B), and DON concentration was positively correlated with the abundance of protein-like

fluorophores ($R = 0.85$; **Figure 6**). These results imply that protein-like fluorophores, which are N-containing organic compounds, were selectively degraded during the dark incubation period.

Another possible explanation for the different behaviors of DOC and DON during the biodegradation experiments is that the decomposition and production of N-containing organic compounds occur at the same extent. Hence, the microorganisms take up N-containing organic compounds with higher C/N ratios and release N-containing organic compounds with lower C/N ratios. This mechanism is consistent with the findings of Pisani et al. (2017), who reported the production of many new N-containing organic compounds during dark microbial incubation of riverine DOM.

CONCLUSIONS AND IMPLICATIONS

This study investigated the spatial distribution of DOC and DON concentrations and the C/N ratio with DOM optical properties in the Ishikari River Basin, and dark incubation experiments were conducted to determine the bioavailability of DOC and DON as a factor controlling their spatial distribution. A major factor influencing the DOC and DON concentrations as well as the optical properties of DOM in the mainstream might be the input of high levels of DOM with high molecular weight and high aromaticity from flooded paddy fields. In addition to the allochthonous input, the input of autochthonous DOM with a low C/N ratio and selective removal of C-rich DOM were suggested to be important factors in decreasing the C/N ratio of DOM with the river flow in the mainstream.

This study discussed the factors determining riverine DOM characteristics based on changes in the DOM concentration and optical properties. However, using optical properties of DOM alone may not be sufficient to identify the origin and dynamics of riverine DOM. The addition of other parameters to optical properties of DOM may lead to improved identification of the origin and dynamics of riverine DOM. For example, the stable carbon isotope ($\delta^{13}C$) of DOC can be used to determine the origin of DOM in rivers (Bhattacharya and Osburn, 2020).

The results of the dark incubation experiments and changes in the C/N ratio of DOM with river flow in the mainstream suggest different roles of small and large microorganisms in the degradation of riverine DOM. The dark incubations of riverine DOM with different sizes of inoculum (Grunert et al., 2010) may clarify the relationships between the degradability of various DOM components and the size of microorganisms. In addition, the role of biofilms at the riverbed in the degradation of riverine DOM should be explored (Battin et al., 2016). The relationship between degradable DOM components involved in the C/N ratio and the type of microorganisms may improve our understanding of riverine DOM as a source of energy and/or organic nutrients in river ecosystems.

DATA AVAILABILITY STATEMENT

The original contributions presented in the study are included in the article/Supplementary Material, further inquiries can be directed to the corresponding author.

AUTHOR CONTRIBUTIONS

Conceptualization: YT, YY, Data curation: YT, KH, and YY, Formal analysis: YT, KH, Funding acquisition: YY, Investigation: YT, KH, and YY, Methodology: YT, KH, and YY, Project administration: YY, Resources: YY, Supervision: YY, Validation: YY, Visualization: YT, Writingoriginal draft: YT, YY, Writingreview and editing: YT, YY.

FUNDING

This research was partly supported by the Japan Society for the Promotion of Science grant KAKENHI JP19H04249 to Y.Y.

ACKNOWLEDGMENTS

We wish to acknowledge the help of Yuka Sazuka, Soushi Abe, and Kota Ishizaka for their assistance with observations and DOM analysis. We would also like to acknowledge I. Kudo and his lab members for their help with inorganic nutrient analysis. We would like to thank Editage (www.editage.com) for English language editing.

REFERENCES

Abe, Y., Maie, N., and Shima, E. (2011). Influence of Irrigated Paddy fields on the Fluorescence Properties of Fluvial Dissolved Organic Matter. *J. Environ. Qual.* 40 (4), 1266–1272. doi:10.2134/jeq2010.0374

Aitkenhead, J. A., and McDowell, W. H. (2000). Soil C:N Ratio as a Predictor of Annual Riverine DOC Flux at Local and Global Scales. *Glob. Biogeochem. Cycles* 14 (1), 127–138. doi:10.1029/1999GB900083

Amon, R. M. W., and Benner, R. (1996). Bacterial Utilization of Different Size Classes of Dissolved Organic Matter. *Limnol. Oceanogr.* 41 (1), 41–51. doi:10.4319/lo.1996.41.1.0041

Amon, R. M. W., Fitznar, H.-P., and Benner, R. (2001). Linkages Among the Bioreactivity, Chemical Composition, and Diagenetic State of marine Dissolved Organic Matter. *Limnol. Oceanogr.* 46 (2), 287–297. doi:10.4319/lo.2001.46.2.0287

Asmala, E., Autio, R., Kaartokallio, H., Pitkänen, L., Stedmon, C. A., and Thomas, D. N. (2013). Bioavailability of Riverine Dissolved Organic Matter in Three Baltic Sea Estuaries and the Effect of Catchment Land Use. *Biogeosciences* 10, 6969–6986. doi:10.5194/bg-10-6969-2013

Babin, M., Stramski, D., Ferrari, G. M., Claustre, H., Bricaud, A., Obolensky, G., et al. (2003). Variations in the Light Absorption Coefficients of Phytoplankton, Nonalgal Particles, and Dissolved Organic Matter in Coastal Waters Around Europe. *J. Geophys. Res.* 108 (C7), 3211. doi:10.1029/2001JC000882

Balcarczyk, K. L., Jones, J. B., Jaffé, R., and Maie, N. (2009). Stream Dissolved Organic Matter Bioavailability and Composition in Watersheds Underlain with Discontinuous Permafrost. *Biogeochemistry* 94, 255–270. doi:10.1007/s10533-009-9324-x

Battin, T. J., Besemer, K., Bengtsson, M. M., Romani, A. M., and Packmann, A. I. (2016). The Ecology and Biogeochemistry of Stream Biofilms. *Nat. Rev. Microbiol.* 14, 251–263. doi:10.1038/nrmicro.2016.15

Benner, R., and Kaiser, K. (2011). Biological and Photochemical Transformations of Amino Acids and Lignin Phenols in Riverine Dissolved Organic Matter. *Biogeochemistry* 102, 209–222. doi:10.1007/s10533-010-9435-4

Bernal, S., Lupon, A., Catalán, N., Castelar, S., and Martí, E. (2018). Decoupling of Dissolved Organic Matter Patterns between Stream and Riparian Groundwater in a Headwater Forested Catchment. *Hydrol. Earth Syst. Sci.* 22, 1897–1910. doi:10.5194/hess-22-1897-2018

Bertilsson, S., and Jones, J. B. (2003). "Supply of Dissolved Organic Matter to Aquatic Ecosystems," in *Aquatic Ecosystems: Interactivity of Dissolved Organic Matter* (San Diego: Academic Press), 3–24. doi:10.1016/b978-012256371-3/50002-0

Bhattacharya, R., and Osburn, C. L. (2020). Spatial Patterns in Dissolved Organic Matter Composition Controlled by Watershed Characteristics in a Coastal River Network: The Neuse River Basin, USA. *Water Res.* 169, 115248. doi:10.1016/j.watres.2019.115248

Bianchi, T. S. (2011). The Role of Terrestrially Derived Organic Carbon in the Coastal Ocean: A Changing Paradigm and the Priming Effect. *Proc. Natl. Acad. Sci.* 108 (49), 19473–19481. doi:10.1073/pnas.1017982108

Chen, M., Price, R. M., Yamashita, Y., and Jaffé, R. (2010). Comparative Study of Dissolved Organic Matter from Groundwater and Surface Water in the Florida Coastal Everglades Using Multi-Dimensional Spectrofluorometry Combined with Multivariate Statistics. *Appl. Geochem.* 25 (6), 872–880. doi:10.1016/j.apgeochem.2010.03.005

Coble, P. G. (1996). Characterization of marine and Terrestrial DOM in Seawater Using Excitation-Emission Matrix Spectroscopy. *Mar. Chem.* 51 (4), 325–346. doi:10.1016/0304-4203(95)00062-3

Coble, P. G., Del Castillo, C. E., and Avril, B. (1998). Distribution and Optical Properties of CDOM in the Arabian Sea during the 1995 Southwest Monsoon. Deep-Sea Res. Part II-Top. Stud. *Oceanogr* 45, 10–11. doi:10.1016/S0967-0645(98)00068-X

Connolly, C. T., Khosh, M. S., Burkart, G. A., Douglas, T. A., Holmes, R. M., Jacobson, A. D., et al. (2018). Watershed Slope as a Predictor of Fluvial Dissolved Organic Matter and Nitrate Concentrations across Geographical Space and Catchment Size in the Arctic. *Environ. Res. Lett.* 13, 104015. doi:10.1088/1748-9326/aae35d

Cory, R. M., and Kling, G. W. (2018). Interactions between Sunlight and Microorganisms Influence Dissolved Organic Matter Degradation along the Aquatic Continuum. *Limnol Oceanogr Lett.* 3, 102–116. doi:10.1002/lol2.10060

Cory, R. M., and McKnight, D. M. (2005). Fluorescence Spectroscopy Reveals Ubiquitous Presence of Oxidized and Reduced Quinones in Dissolved Organic Matter. *Environ. Sci. Technol.* 39 (21), 8142–8149. doi:10.1021/es0506962

Cory, R. M., Miller, M. P., McKnight, D. M., Guerard, J. J., and Miller, P. L. (2010). Effect of Instrument-specific Response on the Analysis of Fulvic Acid Fluorescence Spectra. *Limnol. Oceanogr. Methods* 8, 67–78. doi:10.4319/lom.2010.8.67

Davis, J., and Benner, R. (2007). Quantitative Estimates of Labile and Semi-labile Dissolved Organic Carbon in the Western Arctic Ocean: A Molecular Approach. *Limnol. Oceanogr.* 52, 2434–2444. doi:10.4319/lo.2007.52.6.2434

Davis, J., Kaiser, K., and Benner, R. (2009). Amino Acid and Amino Sugar Yields and Compositions as Indicators of Dissolved Organic Matter Diagenesis. *Org. Geochem.* 40 (3), 343–352. doi:10.1016/j.orggeochem.2008.12.003

Drake, T. W., Raymond, P. A., and Spencer, R. G. M. (2018). Terrestrial Carbon Inputs to Inland Waters: A Current Synthesis of Estimates and Uncertainty. *Limnol Oceanogr Lett.* 3, 132–142. doi:10.1002/lol2.10055

Duan, W. L., He, B., Takara, K., Luo, P. P., Nover, D., and Hu, M. C. (2015). Modeling Suspended Sediment Sources and Transport in the Ishikari River basin, Japan, Using SPARROW. *Hydrol. Earth Syst. Sci.* 19, 1293–1306. doi:10.5194/hess-19-1293-2015

Duan, W., Takara, K., He, B., Luo, P., Nover, D., and Yamashiki, Y. (2013). Spatial and Temporal Trends in Estimates of Nutrient and Suspended Sediment Loads in the Ishikari River, Japan, 1985 to 2010. *Sci. Total Environ.* 461-462, 499–508. doi:10.1016/j.scitotenv.2013.05.022

Fellman, J. B., Hood, E., Edwards, R. T., and Jones, J. B. (2009). Uptake of Allochthonous Dissolved Organic Matter from Soil and Salmon in Coastal Temperate Rainforest Streams. *Ecosystems* 12, 747–759. doi:10.1007/s10021-009-9254-4

Fellman, J. B., Hood, E., and Spencer, R. G. M. (2010). Fluorescence Spectroscopy Opens New Windows into Dissolved Organic Matter Dynamics in Freshwater Ecosystems: A Review. *Limnol. Oceanogr* 55, 2452. doi:10.4319/lo.2010.55.6.2452

Findlay, S., and Sinsabaugh, R. (2003). Aquatic Ecosystems: Interactivity of Dissolved Organic Matter. *J. North Am. Benthological Soc.* 23. doi:10.1899/0887-3593(2004)023<0662:AEIODO>2.0.CO;2

Graeber, D., Boëchat, I. G., Encina-Montoya, F., Esse, C., Gelbrecht, J., Goyenola, G., et al. (2015). Global Effects of Agriculture on Fluvial Dissolved Organic Matter. *Sci. Rep.* 5, 16328. doi:10.1038/srep16328

Grunert, B. K., Tzortziou, M., Neale, P., Menendez, A., and Hernes, P. (2010). DOM Degradation by Light and Microbes along the Yukon River-Coastal Ocean Continuum. *Sci. Rep.* 11, 10236. doi:10.1038/s41598-021-89327-9

Hasegawa, T., Kasai, H., Ono, T., Tsuda, A., and Ogawa, H. (2010). Dynamics of Dissolved and Particulate Organic Matter during the spring Bloom in the Oyashio Region of the Western Subarctic Pacific Ocean. *Aquat. Microb. Ecol.* 60, 127–138. doi:10.3354/ame01418

Heinz, M., Graeber, D., Zak, D., Zwirnmann, E., Gelbrecht, J., and Pusch, M. T. (2015). Comparison of Organic Matter Composition in Agricultural versus Forest Affected Headwaters with Special Emphasis on Organic Nitrogen. *Environ. Sci. Technol.* 49 (4), 2081–2090. doi:10.1021/es505146h

Helms, J. R., Stubbins, A., Ritchie, J. D., Minor, E. C., Kieber, D. J., and Mopper, K. (2008). Absorption Spectral Slopes and Slope Ratios as Indicators of Molecular Weight, Source, and Photobleaching of Chromophoric Dissolved Organic Matter. *Limnol. Oceanogr.* 53 (3), 955–969. doi:10.4319/lo.2008.53.3.0955

Hendrickson, J., Trahan, N., Gordon, E., and Ouyang, Y. (2007). Estimating Relevance of Organic Carbon, Nitrogen, and Phosphorus Loads to a Blackwater River Estuary1. *J. Am. Water Resour. Assoc.* 43 (1), 264–279. doi:10.1111/j.1752-1688.2007.00021.x

Hopkinson, C. S., and Vallino, J. J. (2005). Efficient export of Carbon to the Deep Ocean through Dissolved Organic Matter. *Nature* 433, 142–145. doi:10.1038/nature03191

Inamdar, S., Finger, N., Singh, S., Mitchell, M., Levia, D., Bais, H., et al. (2012). Dissolved Organic Matter (DOM) Concentration and Quality in a Forested Mid-Atlantic Watershed, USA. *Biogeochemistry* 108, 55–76. doi:10.1007/s10533-011-9572-4

Islam, M. J., Jang, C., Eum, J., Jung, S.-m., Shin, M.-S., Lee, Y., et al. (2019). C:N:P Stoichiometry of Particulate and Dissolved Organic Matter in River Waters and Changes during Decomposition. *J Ecology Environ.* 43, 4. doi:10.1186/s41610-018-0101-4

Jacobs, S. R., Breuer, L., Butterbach-Bahl, K., Pelster, D. E., and Rufino, M. C. (2017). Land Use Affects Total Dissolved Nitrogen and Nitrate Concentrations in Tropical Montane Streams in Kenya. *Sci. Total Environ.* 603-604, 519–532. doi:10.1016/j.scitotenv.2017.06.100

Kaushal, S. S., and Lewis, W. M. (2005). Fate and Transport of Organic Nitrogen in Minimally Disturbed Montane Streams of Colorado, USA. *Biogeochemistry* 74, 303–321. doi:10.1007/s10533-004-4723-5

Krupa, M., Spencer, R. G. M., Tate, K. W., Six, J., van Kessel, C., and Linquist, B. A. (2012). Controls on Dissolved Organic Carbon Composition and export from rice-dominated Systems. *Biogeochemistry* 108, 447–466. doi:10.1007/s10533-011-9610-2

Kunii, D., and Saito, G. (2009). Relationships between Land Use and River Nutrient in the River Basins of Kitakami River and Ishikari River Using Remote Sensing and GIS. *J. Integrat Field Sci.* 6, 59–70.

Lara, R. J., Rachold, V., Kattner, G., Hubberten, H. W., Guggenberger, G., Skoog, A., et al. (1998). Dissolved Organic Matter and Nutrients in the Lena River, Siberian Arctic: Characteristics and Distribution. *Mar. Chem.* 59, 3–4. doi:10.1016/S0304-4203(97)00076-5

Laudon, H., Kohler, S., and Buffam, I. (2004). Seasonal TOC export from Seven Boreal Catchments in Northern Sweden. *Aquat. Sci. - Res. Across Boundaries* 66, 223–230. doi:10.1007/s00027-004-0700-2

Lawaetz, A. J., and Stedmon, C. A. (2009). Fluorescence Intensity Calibration Using the Raman Scatter Peak of Water. *Appl. Spectrosc.* 63 (8), 936–940. doi:10.1366/000370209788964548

Lee, S.-A., Kim, T.-H., and Kim, G. (2020). Tracing Terrestrial versus marine Sources of Dissolved Organic Carbon in a Coastal bay Using Stable Carbon Isotopes. *Biogeosciences* 17, 135–144. doi:10.5194/bg-17-135-2020

Lønborg, C., and Álvarez-Salgado, X. A. (2012). Recycling versus export of Bioavailable Dissolved Organic Matter in the Coastal Ocean and Efficiency of the continental Shelf Pump. *Glob. Biogeochem. Cycles* 26, GB3018. doi:10.1029/2012GB004353

Lu, Y. H., Bauer, J. E., Canuel, E. A., Chambers, R. M., Yamashita, Y., Jaffé, R., et al. (2014). Effects of Land Use on Sources and Ages of Inorganic and Organic Carbon in Temperate Headwater Streams. *Biogeochemistry* 119, 275–292. doi:10.1007/s10533-014-9965-2

Lutz, B. D., Bernhardt, E. S., Roberts, B. J., and Mulholland, P. J. (2011). Examining the Coupling of Carbon and Nitrogen Cycles in Appalachian Streams: the Role of Dissolved Organic Nitrogen. *Ecology* 92, 720–732. doi:10.1890/10-0899.1

Mann, P. J., Spencer, R. G. M., Hernes, P. J., Six, J., Aiken, G. R., Tank, S. E., et al. (2016). Pan-Arctic Trends in Terrestrial Dissolved Organic Matter from Optical Measurements. *Front. Earth Sci.* 4, 25. doi:10.3389/feart.2016.00025

McKnight, D. M., Boyer, E. W., Westerhoff, P. K., Doran, P. T., Kulbe, T., and Andersen, D. T. (2001). Spectrofluorometric Characterization of Dissolved Organic Matter for Indication of Precursor Organic Material and Aromaticity. *Limnol. Oceanogr.* 46 (1), 38–48. doi:10.4319/lo.2001.46.1.0038

Moran, M. A., Sheldon, W. M., and Zepp, R. G. (2000). Carbon Loss and Optical Property Changes during Long-Term Photochemical and Biological Degradation of Estuarine Dissolved Organic Matter. *Limnol. Oceanogr.* 45, 1254–1264. doi:10.4319/lo.2000.45.6.1254

Mulholland, P. J. (2003). "Large-scale Patterns in Dissolved Organic Carbon Concentration, Flux, and Sources," in *Aquatic Ecosystems: Interactivity of Dissolved Organic Matter* (San Diego: Academic Press), 139–159. doi:10.1016/b978-012256371-3/50007-x

Opsahl, S., and Benner, R. (1998). Photochemical Reactivity of Dissolved Lignin in River and Ocean Waters. *Limnol. Oceanogr* 43, 1297. doi:10.4319/lo.1998.43.6.1297

Petrone, K. C., Fellman, J. B., Hood, E., Donn, M. J., and Grierson, P. F. (2011). The Origin and Function of Dissolved Organic Matter in Agro-Urban Coastal Streams. *J. Geophys. Res.* 116. doi:10.1029/2010JG001537

Petrone, K. C., Richards, J. S., and Grierson, P. F. (2009). Bioavailability and Composition of Dissolved Organic Carbon and Nitrogen in a Near Coastal Catchment of South-Western Australia. *Biogeochemistry* 92, 27–40. doi:10.1007/s10533-008-9238-z

Pisani, O., Boyer, J. N., Podgorski, D. C., Thomas, C. R., Coley, T., and Jaffé, R. (2017). Molecular Composition and Bioavailability of Dissolved Organic Nitrogen in a lake Flow-Influenced River in South Florida, USA. *Aquat. Sci.* 79, 891–908. doi:10.1007/s00027-017-0540-5

R Core Team (2021). *R: A Language and Environment for Statistical Computing R Foundation for Statistical Computing*. Vienna, Austria. Available at: : https://www.R-project.org/.

Royer, T. V., and David, M. B. (2005). Export of Dissolved Organic Carbon from Agricultural Streams in Illinois, USA. *Aquat. Sci.* 67, 465–471. doi:10.1007/s00027-005-0781-6

Ruark, M. D., Linquist, B. A., Six, J., van Kessel, C., Greer, C. A., Mutters, R. G., et al. (2010). Seasonal Losses of Dissolved Organic Carbon and Total Dissolved Solids from Rice Production Systems in Northern California. *J. Environ. Qual.* 39, 304–313. doi:10.2134/jeq2009.0066

Seitzinger, S. P., Sanders, R. W., and Styles, R. (2002). Bioavailability of DON from Natural and Anthropogenic Sources to Estuarine Plankton. *Limnol. Oceanogr.* 47 (2), 353–366. doi:10.4319/lo.2002.47.2.0353

Seitzinger, S., and Sanders, R. (1997). Contribution of Dissolved Organic Nitrogen from Rivers to Estuarine Eutrophication. *Mar. Ecol. Prog. Ser.* 159, 1–12. doi:10.3354/meps159001

Smith, P. (2008). Land Use Change and Soil Organic Carbon Dynamics. *Nutr. Cycl Agroecosyst* 81, 169–178. doi:10.1007/s10705-007-9138-y

Stepanauskas, R., Laudon, H., and Jørgensen, N. O. G. (2000). High DON Bioavailability in Boreal Streams during a spring Flood. *Limnol. Oceanogr.* 45, 1298–1307. doi:10.4319/lo.2000.45.6.1298

Suzuki, T., Nagao, S., Horiuchi, M., Maie, N., Yamamoto, M., and Nakamura, K. (2015). Characteristics and Behavior of Dissolved Organic Matter in the Kumaki River, Noto Peninsula, Japan. *Limnology* 16, 55–68. doi:10.1007/s10201-014-0441-4

Tanaka, K., Kuma, K., Hamasaki, K., and Yamashita, Y. (2014). Accumulation of Humic-like Fluorescent Dissolved Organic Matter in the Japan Sea. *Sci. Rep.* 4, 5292. doi:10.1038/srep05292

Voss, M., Asmala, E., Bartl, I., Carstensen, J., Conley, D. J., Dippner, J. W., et al. (2021). Origin and Fate of Dissolved Organic Matter in Four Shallow Baltic Sea Estuaries. *Biogeochemistry* 154, 385–403. doi:10.1007/s10533-020-00703-5

Weishaar, J. L., Aiken, G. R., Bergamaschi, B. A., Fram, M. S., Fujii, R., and Mopper, K. (2003). Evaluation of Specific Ultraviolet Absorbance as an Indicator of the Chemical Composition and Reactivity of Dissolved Organic Carbon. *Environ. Sci. Technol.* 37 (20), 4702–4708. doi:10.1021/es030360x

Westerhoff, P., and Mash, H. (2002). Dissolved Organic Nitrogen in Drinking Water Supplies: a Review. *J. Water Supply Res. Technol.-Aqua* 51 (8), 415–448. doi:10.2166/aqua.2002.0038

Wetzel, R. G. (1992). Gradient-dominated Ecosystems: Sources and Regulatory Functions of Dissolved Organic Matter in Freshwater Ecosystems. *Hydrobiologia* 229, 181–198. doi:10.1007/BF00007000

Wiegner, T. N., Tubal, R. L., and MacKenzie, R. A. (2009). Bioavailability and export of Dissolved Organic Matter from a Tropical River during Base- and Stormflow Conditions. *Limnol. Oceanogr.* 54 (4), 1233–1242. doi:10.4319/lo.2009.54.4.1233

Wiegner, T., Seitzinger, S., Glibert, P., and Bronk, D. (2006). Bioavailability of Dissolved Organic Nitrogen and Carbon from Nine Rivers in the Eastern United States. *Aquat. Microb. Ecol.* 43, 277–287. doi:10.3354/ame043277

Wiegner, T., and Seitzinger, S. (2001). Photochemical and Microbial Degradation of External Dissolved Organic Matter Inputs to Rivers. *Aquat. Microb. Ecol.* 24 (1), 27–40. doi:10.3354/ame024027

Wikner, J., Cuadros, R., and Jansson, M. (1999). Differences in Consumption of Allochthonous DOC under Limnic and Estuarine Conditions in a Watershed. *Aquat. Microb. Ecol.* 17, 289–299. doi:10.3354/ame017289

Willett, V. B., Reynolds, B. A., Stevens, P. A., Ormerod, S. J., and Jones, D. L. (2004). Dissolved Organic Nitrogen Regulation in Freshwaters. *J. Environ. Qual.* 33, 201–209. doi:10.2134/jeq2004.2010

Williams, C. J., Frost, P. C., Morales-Williams, A. M., Larson, J. H., Richardson, W. B., Chiandet, A. S., et al. (2016). Human Activities Cause Distinct Dissolved Organic Matter Composition across Freshwater Ecosystems. *Glob. Change Biol.* 22, 613–626. doi:10.1111/gcb.13094

Wymore, A. S., Rodríguez-Cardona, B., and McDowell, W. H. (2015). Direct Response of Dissolved Organic Nitrogen to Nitrate Availability in Headwater Streams. *Biogeochemistry* 126, 1–10. doi:10.1007/s10533-015-0153-9

Yamashita, Y., Kloeppel, B. D., Knoepp, J., Zausen, G. L., and Jaffé, R. (2011). Effects of Watershed History on Dissolved Organic Matter Characteristics in Headwater Streams. *Ecosystems* 14, 1110–1122. doi:10.1007/s10021-011-9469-z

Yamashita, Y., Kojima, D., Yoshida, N., and Shibata, H. (2021). Relationships between Dissolved Black Carbon and Dissolved Organic Matter in Streams. *Chemosphere* 271, 129824. doi:10.1016/j.chemosphere.2021.129824

Yamashita, Y., Nosaka, Y., Suzuki, K., Ogawa, H., Takahashi, K., and Saito, H. (2013). Photobleaching as a Factor Controlling Spectral Characteristics of Chromophoric Dissolved Organic Matter in Open Ocean. *Biogeosciences* 10 (11), 7207–7217. doi:10.5194/bg-10-7207-2013

Yamashita, Y., Scinto, L. J., Maie, N., and Jaffé, R. (2010). Dissolved Organic Matter Characteristics across a Subtropical Wetland's Landscape: Application of Optical Properties in the Assessment of Environmental Dynamics. *Ecosystems* 13, 1006–1019. doi:10.1007/s10021-010-9370-1

Yamashita, Y., and Tanoue, E. (2003). Distribution and Alteration of Amino Acids in Bulk DOM along a Transect from bay to Oceanic Waters. *Mar. Chem.* 82, 3–4. doi:10.1016/S0304-4203(03)00049-5

Yates, C. A., Johnes, P. J., Owen, A. T., Brailsford, F. L., Glanville, H. C., Evans, C. D., et al. (2019). Variation in Dissolved Organic Matter (DOM) Stoichiometry in U.K. Freshwaters: Assessing the Influence of Land Cover and Soil C:N Ratio on DOM Composition. *Limnol. Oceanogr* 64, 2328–2340. doi:10.1002/lno.11186

Zsolnay, Á. (2003). Dissolved Organic Matter: Artefacts, Definitions, and Functions. *Geoderma* 113, 3–4. doi:10.1016/S0016-7061(02)00361-0

Conflict of Interest: The authors declare that the research was conducted in the absence of any commercial or financial relationships that could be construed as a potential conflict of interest.

Publisher's Note: All claims expressed in this article are solely those of the authors and do not necessarily represent those of their affiliated organizations, or those of the publisher, the editors, and the reviewers. Any product that may be evaluated in this article, or claim that may be made by its manufacturer, is not guaranteed or endorsed by the publisher.

frontiers | Frontiers in Earth Science

ORIGINAL RESEARCH
published: 20 June 2022
doi: 10.3389/feart.2022.821050

Investigating Dissolved Organic Matter Dynamics in the Downstream Reaches of the Ganges and Brahmaputra Rivers Using Fluorescence Spectroscopy

Nahin Mostofa Niloy[1], *Mashura Shammi*[1†*], *Md. Morshedul Haque*[1,2] *and Shafi M. Tareq*[1†*]

[1]Hydrobiogeochemistry and Pollution Control Laboratory, Department of Environmental Sciences, Jahangirnagar University, Dhaka, Bangladesh, [2]Department of Environmental Science and Engineering, Bangladesh University of Textile, Dhaka, Bangladesh

The Ganges and the Brahmaputra, two major rivers in Bangladesh, contribute major loads of dissolved organic matter (DOM) into the Bay of Bengal. The composition, sources, availability, and seasonal heterogeneity of DOM in these two rivers are thus very important to know about the biogeochemical cycles, fate, and ecological and environmental aspects before discharge into the Bay of Bengal. In this study, DOM was characterized in the downstream reaches of the Ganges and Brahmaputra rivers before their confluence with each other. The concentration of dissolved oxygen decreased in the pre-monsoon and monsoon in both rivers due to the increased decomposition and oxidation of rainfall-washed substances and thus made the water unsuitable for drinking. The amount of total coliform also made the water of both rivers unsuitable for drinking, recreational, and irrigation purposes. In total, four DOM components (one humic, one detergent-, and two protein-like) in the Ganges River and five DOM components (three humic- and two protein-like) in the Brahmaputra River were identified at their downstream reaches using fluorescence spectroscopy, three-dimensional excitation emission matrix (EEM) measurement, and parallel factor analysis (PARAFAC). The abundances of DOM components were higher in the pre-monsoon and monsoon seasons than in the post-monsoon season. Protein-like components contributed the most in two rivers. DOM was obtained mostly from terrestrial sources and was matured and less aromatic. This study also identifies that sewage water is the largest contributor to DOM in surface water, next to natural sources, and indicates the excessive anthropogenic activities in the river basins of Bangladesh.

Keywords: Dissolved organic matter, fluorescence spectroscopy, excitation-emission matrix, parallel factor analysis, anthropogenic activities

OPEN ACCESS

Edited by:
Francien Peterse,
Utrecht University, Netherlands

Reviewed by:
Bernhard Wehrli,
ETH Zürich, Switzerland
Tomonori Isada,
Hokkaido University, Japan

***Correspondence:**
Mashura Shammi
mashura926@juniv.edu
Shafi M. Tareq
smtareq@juniv.edu

***ORCID:**
Mashura Shammi
orcid.org/0000-0001-5449-4761
Shafi M. Tareq
orcid.org/0000-0002-6417-3846

Specialty section:
This article was submitted to Biogeoscience, a section of the journal Frontiers in Earth Science

Received: *23 November 2021*
Accepted: *04 May 2022*
Published: *20 June 2022*

Citation:
Niloy NM, Shammi M, Haque MM and Tareq SM (2022) Investigating Dissolved Organic Matter Dynamics in the Downstream Reaches of the Ganges and Brahmaputra Rivers Using Fluorescence Spectroscopy. Front. Earth Sci. 10:821050. doi: 10.3389/feart.2022.821050

1 INTRODUCTION

Dissolved organic matter (DOM) is a complex pool of compounds critical in the global carbon cycle (Wünsch and Murphy, 2021) and plays a vital role in aquatic ecosystems (Chaves et al., 2020; He et al., 2021). Identifying the molecular composition of riverine DOM is essential for knowing the source, mobility, and fate across landscapes. Geomorphological characteristics of the watershed, land use, and sediment load can change DOM's quality, quantity, and reactivity over time (Wagner et al., 2015). Globally, large rivers are significant sources of DOM to the oceans and connect the terrestrial and marine biogeochemical cycle (Wagner et al., 2015; Riedel et al., 2016; Pang et al., 2020). The Ganges–Brahmaputra–Meghna (GBM) river basin is the third-largest hydrological system globally in terms of freshwater flow to the ocean. It is also one of the most populated deltas (Sharma et al., 2021). These transboundary river basins confront intensified stress on water resources (Munia et al., 2020). Moreover, the structure and composition of DOM remain poorly understood in rivers flowing through different climates and landforms (Liu et al., 2021). Therefore, a more detailed study is needed on DOM quality, quantity, and reactivity on their global drivers, such as changes in local natural runoff and inflows from upstream parts of a basin and local and upstream water consumption.

Himalayan rivers play a pivotal role in regional water and food supply, global sediments, and carbon budgets (Chen et al., 2020). Land use and anthropogenic activities directly affect downstream DOM quality and carbon (C) fluxes in the Asian rivers (Wagner et al., 2015; Park et al., 2018). Considering the physicochemical parameters, the water quality was found to be in the maximum deteriorated state during the monsoon and in the minimum state in the pre-monsoon in the Ganges and Brahmaputra rivers in Bangladesh (Tareq et al., 2013). Heavy metals were found exceeding the standard limits during the monsoon in the Brahmaputra River in Bangladesh (Rahman et al., 2017; Bhuyan et al., 2019). The water quality in the upstream Ganges River in Bangladesh was found to be unsuitable for drinking purpose and household consumption (Haque et al., 2020). The fluorescent DOM properties in the upstream Ganges of fulvic acid (M-type), fulvic acid (C-type), and protein-like were higher in the pre-monsoon (March–June) and monsoon (July–October) periods than in the post-monsoon (November–February). The components were fresh, autochthonous, and had less aromatic characteristics from natural and anthropogenic sources. The DOM components were abundant from the late pre-monsoon to the monsoon period in the upstream Ganges River in Bangladesh (Niloy et al., 2021a; Niloy et al., 2021c). However, there is no insight into the downstream evolution of DOM composition in the Ganges and Brahmaputra rivers in Bangladesh.

Fluorescence spectroscopy is a powerful, sensitive, and broadly used method to characterize DOM in fresh and marine water (Hudson et al., 2007; Mostofa et al., 2010; Nelson and Gauglitz, 2016). Fluorescence measurements require no pre-concentration of samples to generate three-dimensional excitation emission matrix (EEM) landscapes of conjugated DOM components. The particular wavelength position in an EEM landscape can reveal the DOM components, sources, and compositional states. Further analyzing EEM landscapes using a parallel factor multivariate analysis (PARAFAC) can separate the conjugated DOM components from the EEM (Stedmon and Markager, 2005a; Stedmon and Markager, 2005b; Stedmon and Bro, 2008). PARAFAC could separate the conjugated DOM components from the EEM. The simple sample preparation technique and facile duo function of EEM-PARAFAC in fluorescence spectroscopy were worth using in this study.

The degradation potential index (DPI) is used to observe differences in the degradability of DOM among sources. It is defined as the ratio of availability of the labile to recalcitrant organic components (Liao et al., 2021). The DPI is nowadays tagged with an end-member mixing (EMM) model to identify the contribution of various DOM sources to surface water (Yang et al., 2015; Liao et al., 2021). The Ganges and Brahmaputra rivers carry huge loads of natural and anthropogenic organic matters from their origin to downstream before the confluence (Steckler et al., 2022). The fluorescence intensity of DOM and microbial contamination was higher in the Brahmaputra River than that in the Ganges at the upstream position of these two rivers (Niloy et al., 2021a; Niloy et al., 2022).

On the contrary, the Ganges River contained more aromatic, high molecular size and weight DOM, and anthropogenically derived pollutants than the Brahmaputra River at the upstream location of these rivers in Bangladesh. Both terrestrial and aquatic-originated DOM were present, fluctuations in DOM intensity were related to rainfall, and other climatic effects, photodegradation, and microbial activity affected the DOM composition in both rivers (Niloy et al., 2021a; Niloy et al., 2022). The selection of the downstream position was thus very significant to know about the types and concentration of DOM, their originations, and factors influencing their availability in both rivers. Considering these needs, this study aimed to characterize DOM components and identify their sources and fate downstream of the Ganges and Brahmaputra rivers of Bangladesh. This study also targeted determining the degradation level of DOM of various origins and their contribution to the river water.

2 MATERIALS AND METHODS

2.1 Study Area

The Ganges and Brahmaputra rivers are major transboundary rivers and originate from the Gangotri and Chemayungdung glaciers of the Himalayas. After flowing through the Indian regions, the Ganges and Brahmaputra River enter Bangladesh through northwestern and northern districts named Chapainawabganj and Nilphamary. The Ganges–Brahmaputra system discharges around 30,770 m^3/s of water monthly. It carries about 1.84 billion tons of sediment/year, securing the third greatest water discharge and maximum sediment loads among world rivers (Papa et al., 2012; Steckler et al., 2022). Both river basins are greatly affected by the tropical climate. The average monthly rainfall data in the corresponding sampling location

FIGURE 1 | Map of the study areas and monitoring stations at the Ganges and Brahmaputra rivers. The map was created using ArcGIS 10.3.1 and the topographic image modified from ArcGIS/ESRI online.

were collected using a rain gage during the study period to identify its roles in DOM intensity fluctuations (**Supplementary Table S1**). About 400 million and 83 million people live in the Ganges and Brahmaputra river basins, and in Bangladesh, the population density is around 390 person/km^2 and 828 person/km^2 (Mahanta et al., 2014; The Himalayan Climate and Water Atlas, 2015). The Ganges–Brahmaputra basin is used for agricultural production, fisheries, recreation, irrigation, and navigation, making it an economic hub. However, the basins of the two rivers are affected by biophysical, socioeconomic challenges, climatic stress, and substantial anthropogenically derived pollutants (Anwar, 2006; Rahman et al., 2020).

2.2 Sampling and Field Monitoring

The downstream water samples of the Ganges and Brahmaputra rivers were collected from the river stretch in the Rajbari district (23° 46' 52.2" N, 89° 38' 36.9" E) and the Nogorbari port in the Manikganj district (23° 6' 48.6" N, 89° 39' 5.8" E) of Bangladesh from April 2018 to March 2019 (**Figure 1**). The sampling locations were significantly far away from the bank of the two rivers. Water samples were collected in polypropylene bottles. The sample bottles were washed with 10% HCl, followed by distilled water and drying. The water samples were filtered using a pre-combusted (at 450°C for 4 h in a Muffle furnace) Whatman GF/F glass fiber filter (0.7 μm) immediately by a hand pump in the field. The filtered water samples were then preserved in the cooler box at 4°C, while transported to the hydrobiogeochemistry and pollution control laboratory at the Department of Environmental Sciences, Jahangirnagar University. All the instrumental measurements and chemical analyses of samples were completed immediately after reaching the department laboratory after sampling. The water quality parameters such as pH, dissolved oxygen (DO), electrical conductivity (EC), turbidity, and total dissolved solids (TDSs) were measured *in situ* using an YSI multiparameter. The other water quality parameters, such as biological oxygen demand (BOD), chemical oxygen demand (COD), and total coliform, were also measured.

2.3 DOC and DOM Measurement

DOC was determined using a catalytic oxidation method (Shimadzu TOC analyzer LCPH/CPN) at high temperature through a non-dispersive infrared (NDIR) detector. The samples were tested for fluorescence characterization in Hitachi F-4600. The samples were measured keeping excitation (Ex) wavelength 225–400 nm and emission (Em) wavelength 250–550 nm with 5- and 1-nm intervals, respectively. The excitation and emission slits were set to 5 nm of band-pass at 1200 nm min^{-1} scan speed. Before analysis, all the quartz cuvettes were rinsed with a 5% (w/w) nitric acid solution. The Milli-Q water blank EEM spectra were taken before the sample spectra. EEM data were further rectified for inner filter effects (Panigrahi and Mishra, 2019). The ultrapure Milli-Q water was used as a blank reference sample and was also used to convert arbitrary units of data into Raman units. The filtered samples were also measured using an UV spectrophotometer (SPECORD 210 Plus, Analytikjena) concurrently in the wavelength ranges between 190–1100 nm, keeping scanning speed at 60 nm/min.

2.4 Parallel Factor Analysis of Dissolved Organic Matter Components

The parallel factor analysis (PARAFAC) model was used to separate individual DOM components from the EEM using the DOMFluor toolbox (v1.7) in MATLAB software (v.2016a) (Stedmon and Bro, 2008). Blank Milli-Q water data were subtracted from the original sample data to remove Raman and Rayleigh scattering (Goletz et al., 2011; Stedmon and Bro, 2008). Sample data were validated properly using the split-half technique to identify the exact number of DOM components. The identified intensity (i.e., F_{max}) values were read at Raman Unit (RU).

2.5 Degradation Potential Index Calculation and its Coupling with the End-Member Mixing Model

The degradation potential index (DPI) was calculated from the labile/recalcitrant ratio of the DOM components (Liao et al., 2021). The humic (C)-like DOM component shows fluorophores at a longer wavelength (UV–Visible), while the humic (M)-like component shows fluorophores at the midrange wavelengths (UV-A) (**Table 2**; **Supplementary Table S5**). Tryptophan-, tyrosine-, and detergent-like components show fluorophores at shorter wavelengths (UV-B and UV-C) (**Table 2**; **Supplementary Table S5**). The fluorophores in longer wavelengths might be significantly affected by photodegradation and lose their availability significantly, while fluorophores of shorter wavelengths are more susceptible to microbial degradation (Mostofa et al., 2010; Mann et al., 2012; Zhou et al., 2019; Yang et al., 2020). The tyrosine-like component could be removed entirely by biodegradation (Cory and Kaplan, 2012). However, tryptophan-like components exist as a persistent DOM in water as microbes cannot ingest and metabolize them properly (Cory and Kaplan, 2012). The differentiation of lability and recalcitrant nature of DOM was defined considering both photo- and microbial degradation in this study. The synergistic effects of photo- and microbial degradation widely reduce humic (C)-, tyrosine-, and detergent-like components. However, due to mid-wavelength position and microbial inability in mineralization, the photo- and microbial degradation effects could remove humic (M)- and tryptophan-like components in small amounts from river water (Mostofa et al., 2010; Cory and Kaplan, 2012; Mann et al., 2012; Zhou et al., 2019; Yang et al., 2020). Considering the degradation effects on the DOM, humic (C)-, tyrosine-, and detergent-like components were susceptible to being labile and humic (M), and tryptophan-like substances might be persistent DOMs in this study.

Algae, groundwater, industrial effluents, soil, terrestrial plants, and sewerage water were considered the main DOM contributors to surface water. The percentage contribution of DOM in a specific source was used to quantify its DPI value. The DPI of a distinct source was calculated from the equation:

$$\mathrm{DPI} = \frac{\text{Sum of the percentage contribution of refractory/recalcitrant components}}{\text{Sum of the percentage contribution of labile components}}. \quad (1)$$

The DPI was further coupled with the DOM end-member mixing model (Liao et al., 2021). The dual model was run in MATLAB software (v. 2016a) (Liao et al., 2021). The percentage contribution of DOM components from each natural/anthropogenic source into rivers was calculated (Liao et al., 2021) as follows:

$$\mathrm{DPI_R} = (\mathrm{DPI_A} \times f_A) + (\mathrm{DPI_{GW}} \times f_{GW}) + (\mathrm{DPI_{IE}} \times f_{IE}) + (\mathrm{DPI_S} \times f_S) + (\mathrm{DPI_{TP}} \times f_{TP}) + (\mathrm{DPI_{SW}} \times f_{SW}), \quad (2)$$

where $\mathrm{DPI_R}$ is the DPI of river water. $(\mathrm{DPI_A} \times f_A)$, $(\mathrm{DPI_{GW}} \times f_{GW})$, $(\mathrm{DPI_{IE}} \times f_{IE})$, $(\mathrm{DPI_S} \times f_S)$, $(\mathrm{DPI_{TP}} \times f_{TP})$, and $(\mathrm{DPI_{SW}} \times f_{SW})$ describe the multiplication of DPI and percentage DOM contribution of algae, groundwater, industrial effluents, soil, terrestrial plants, and sewerage water, respectively.

$$\text{Here, } f_A + f_{GW} + f_{IE} + f_S + f_{TP} + f_{SW} = 1. \quad (3)$$

2.6 Quality Control and Quality Assurance and Data Analysis

Quality control and quality assurance (QA/QC) were maintained in all analyses in this study. All samples were measured three times. Data entry was performed using Microsoft Excel, and the standard deviation was calculated. Pearson's correlation of DOM components in the downstream reaches of the Ganges and Brahmaputra rivers was computed using SPSS. All graphs were prepared using Sigmaplot, Originpro, and MATLAB. The map was prepared using ArcGIS.

3 RESULTS AND DISCUSSION

3.1 Comparative Analysis of Water Quality Parameters

The temperatures in both river basins had higher values in the pre-monsoon and monsoon than in post-monsoon and showed a similar pattern of seasonal variation ($r = 0.992$, $p < 0.01$) (**Table 1**). Turbidity was higher in the monsoon than in pre-monsoon and post-monsoon, and this might be due to the significant organic matter inputs by rain in both the Ganges and Brahmaputra rivers. The water was alkaline in both rivers (**Table 1**). It exceeded the permissible limits set by the Department of Environment (DoE) in Bangladesh (BECR, 1997) for drinking, irrigation, and fishery purposes most of the time of the year in the two rivers. DO was comparatively low in the monsoon in both rivers, indicating the additional oxygen consumption to decompose and oxidize increased organic matters (**Table 1**). However, DO was within the accessible limit according to the standards set by the DoE (BECR, 1997) to use water for drinking, fisheries, and irrigation. EC was comparatively lower in the monsoon (**Table 1**). According to the World Health Organization WHO, (2004), EC was within the permissible limit. TDS was relatively lower in the pre-monsoon and monsoon than in post-monsoon (**Table 1**). TDS was within the acceptable limits according to WHO, (2004). BOD was comparatively high and

TABLE 1 | Physicochemical parameters in the downstream of Ganges (G) and Brahmaputra (B) rivers.

Parameters	River	Mar 2019	Apr 2018	May 2018	June 2018	July 2018	Aug 2018	Sep 2018	Oct 2018	Nov 2018	Dec 2018	Jan 2019	Feb 2019
Temperature (°C)	G	28.5	33.9	31.8	32.2	30.9	32	30.8	32.5	25.7	20.7	21	22.9
	B	26.7	33.3	30.7	30.9	29.7	31.1	30.5	29.7	24.3	18.7	18.2	21.2
pH	G	8.8	9	9.4	8.4	8.9	8.3	8.8	8.4	8.5	8.4	8.3	8.7
	B	8.4	9.2	8.7	8.4	9.2	8.2	8.8	8.3	7.5	8.4	8.2	8.6
DO (mg/L)	G	8.7	7.2	7.3	7.9	7.7	8.1	7.6	7.4	7.8	9.2	11.3	10.3
	B	8.2	7.4	7.4	7.7	7.5	7.4	7.6	7.6	7.8	9.5	10.8	9.6
EC (μS/cm)	G	244.2	189.2	204.6	154	157.3	195.8	134.2	146.3	158.4	182.6	232.1	237.6
	B	245.3	200.2	184.8	160.6	156.2	161.7	132	149.6	169.4	172.7	260.7	243.1
TDS (mg/L)	G	116.6	83.6	181.5	143	67.1	112.2	148.5	156.2	225.5	231	240.9	254.1
	B	117.7	90.2	162.8	152.9	68.2	84.7	147.4	158.4	215.6	239.8	269.5	256.3
Turbidity (FTU)	G	9.2	19.5	43.5	141.2	167.6	133.9	149.4	145.2	75.1	21.5	20.8	16.7
	B	11.9	15.9	37.2	108.2	149.2	95	123.3	185.8	22.7	11.4	15.7	18.8
BOD (mg/L)	G	2.6	3.9	7	4.7	4.3	2.8	2.2	2	2.6	2.7	3.9	4.5
	B	2.5	2.8	6.1	5.1	3.7	2.6	1.5	2	2.6	3.3	4.2	4.4
COD (mg/L)	G	27.5	45.1	82.5	61.6	53.9	51.7	44	42.9	42.9	37.4	29.7	25.3
	B	20.9	47.3	72.6	50.6	47.3	48.4	42.9	40.7	34.1	31.9	19.8	17.6
Total coliform (CFU)*10^3	G	1.53	1.78	2.02	2.07	0.23	0.44	1.16	0.85	0.94	1.05	1.19	0.83
	B	1.49	1.64	1.8	1.89	0.47	0.29	1.87	0.91	1.11	1.18	1.01	0.64

exceeded the permissible limit set by the DoE (BECR, 1997) at the end of the pre-monsoon (**Table 1**). COD was also higher from pre-monsoon to the entire monsoon in both the rivers (**Table 1**). COD values exceeded the permissible limit set by the DoE (BECR, 1997) for drinking purposes throughout the year. Total coliform was in a minimum amount in the early monsoon in both rivers (**Table 1**). This could be due to the large deposition of organic matter and resistance to the growth of coliform bacteria by intense chlorophyll a production in eutrophication (Seo et al., 2019). However, the total coliform exceeded the limits set by the DoE (BECR, 1997) and confirmed that the water was unsuitable for drinking, recreational, and irrigation purposes in both rivers.

3.2 Excitation Emission Matrix, Parallel Factor Analysis, and DOC Concentration

The EEM measurement identified five fluorophores in the Ganges River: Peak A (Ex/Em = 245/414 nm), Peak M (310/398 nm), Peak W (340/428 nm), Peak T (275/334 nm), and Peak Tuv (230/346 nm) and seven fluorophores in the Brahmaputra River: Peak A (Ex/Em = 245/418 nm), Peak C (365/442 nm), Peak M (295/404 nm), Peak T (275/312 nm), Peak Tuv (230/304 nm), Peak T (275/358 nm), and Peak Tuv (230/348 nm) (**Figure 2**, **Supplementary Figure S1**). Peaks A, C, and M represent humic-like component (Coble, 1996), while Peak W represents detergent-like anthropogenic substance (Mostofa et al., 2010; Niloy et al., 2021c). Peak T and Peak Tuv describe the tyrosine- and tryptophan-like component at the low and high emission wavelengths, respectively (Coble et al., 1990). The identified fluorophores thus indicated the natural and anthropogenically derived DOM components in the two rivers. PARAFAC analysis identified DOM components in the Ganges and Brahmaputra rivers, considering monthly water samples of each year. The PARAFAC analysis found four DOM components in the Ganges River: C1-G (Ex/Em = 230/406 nm, 310/406 nm), C2-G (265/462 nm, 340/462 nm), C3-G (225/334, 270/338), and C4-G (285/354) (**Supplementary Figure S2**). C1-G could be characterized as humic (M)-like, C2-G as detergent-like, and C3-G and C4-G as protein-like components (**Table 2**). C1-G in such wavelength could be labile and originated from terrestrial sources (Goldman and Sullivan, 2017). FI, HIX, and $SUVA_{254}$ values also indicated the composition and source of C1-G as labile, less aromatic, and terrestrially derived (**Supplementary Table S2**). Anthropogenically derived component C2-G is widely used as a fluorescent whitening agent (FWA) in maximum commercial and household detergents in Bangladesh at a concentration higher than the usage standard (Niloy et al., 2021c). This component was also identified upstream of the Ganges River in Bangladesh (Niloy et al., 2021a), in the rainwater of Bangladesh (Niloy et al., 2021b), and even in the sewerage drainage water in China (Mostofa et al., 2010). C3-G and C4-G are two tryptophan-like components (Mostofa et al., 2010; Baghoth et al., 2011; Wu et al., 2011). Anthropogenically derived C3-G component is available in sewerage water and municipal leachate, while C4-G is autochthonous and could be found in water treatment plants (**Table 2**). Tryptophan-like component is a dominant organic compound found in microbially derived precursor materials, and a small portion of this component is labile or semi-labile. The encapsulation of tryptophan-like component in the humic matrix helps it behave as a recalcitrant molecule in the environment (Cory and Kaplan, 2012). This persistent nature of the tryptophan-like component has well-resembled with the C3-G in this study in terms of similar wavelength ranges (**Table 2**). C4-G had a bathochromic shift (red shift) in emission wavelength, and it could be due to its increased solvent polarity and bonding with metal ions (Kowalczuk et al., 2009).

The PARAFAC analysis also identified five DOM components: C1-B (Ex/Em = 260/462 nm, 365/462 nm), C2-B (235/418 nm), C3-B (230/342 nm, 275/342 nm), C4-B (230/302 nm, 265/298 nm), and C5-B (250/386 nm, 295/386 nm) in the Brahmaputra River (**Supplementary Figure S2**). Among the

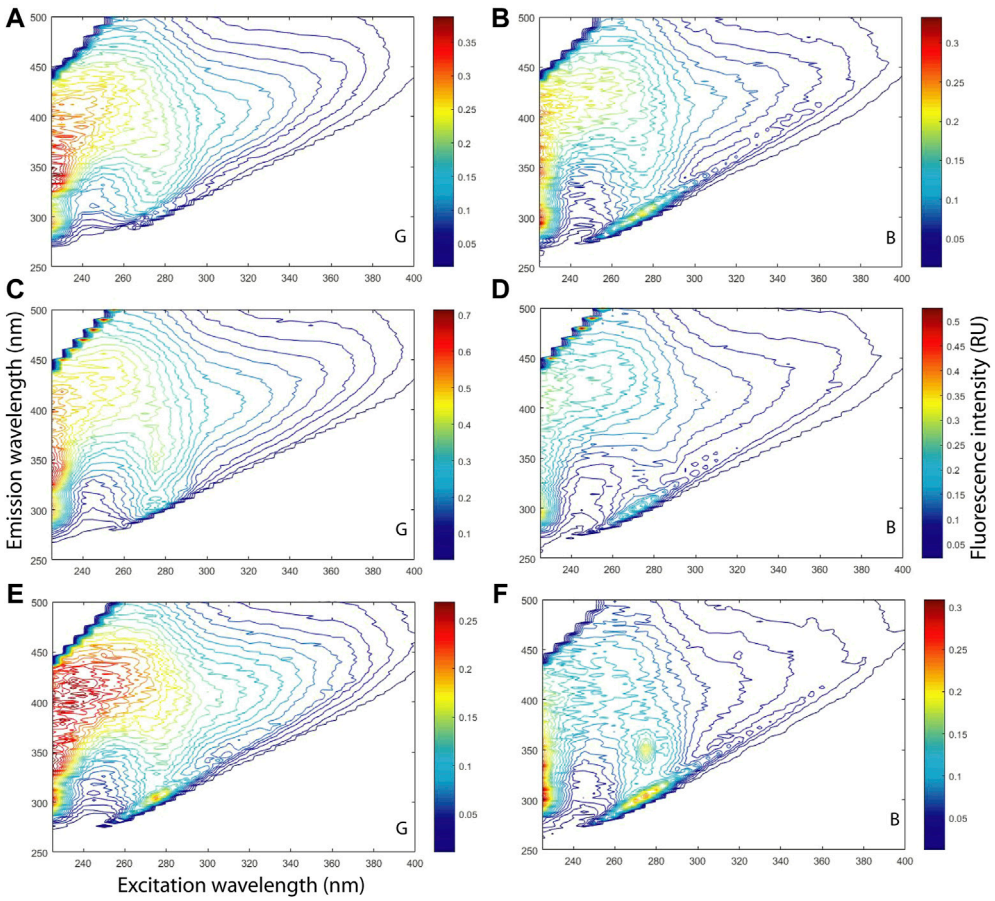

FIGURE 2 | Three-dimensional EEM measurement of DOM using monthly fluorescence data in the pre-monsoon (April): **(A)**-G and **(B)**-B; monsoon (August): **(C)**-G and **(D)**-B; and post-monsoon (December): **(E)**-G and **(F)**-B in the Ganges **(G)** and Brahmaputra rivers. **(B)**. Identified fluorophores in the Ganges River: Peak A (Ex/Em = 245/414 nm), Peak M (310/398 nm), Peak W (340/428 nm), Peak T (275/334 nm), and Peak Tuv (230/346 nm) and in the Brahmaputra River: Peak A (Ex/Em = 245/418 nm), Peak C (365/442 nm), Peak M (295/404 nm), Peak T (75/312 nm), Peak Tuv (230/304 nm), Peak T (275/358 nm), and Peak Tuv (230/348 nm).

TABLE 2 | Characteristics of identified DOM components in the PARAFAC analysis in Ganges and Brahmaputra rivers.

Component in this study	Wavelength (nm)	Characteristics of components	References
C1-G (Ganges River)	230/406 (Peak A), 310/406 (Peak M)	Humic-like, labile, possibly altered by microbial processing, and correlate to DOC	Goldman and Sullivan, (2017)
C2-G (Ganges River)	265/462 (Peak A), 340/462 (Peak W)	Detergent-like and anthropogenically derived	Mostofa et al. (2010), Niloy et al. (2021c)
C3-G & C3-B (Ganges and Brahmaputra River)	225–230/334–342 (Peak Tuv), 270–275/338–342 (Peak T)	Tryptophan-like, anthropogenic originated, availably present in sewerage drainage samples, washing samples collected from washing clothes, and municipal leachate	Coble, (1996), Mostofa et al. (2010), Wu et al. (2011)
C4-G (Ganges River)	Peak T (285/354)	Autochthonous protein-like component and can also be found in drinking water treatment plants	Kowalczuk et al. (2009), Baghoth et al. (2011)
C1-B (Brahmaputra River)	260/462 (Peak A), 365/462 (Peak C)	Terrestrial-derived humic substances, ubiquitous, semi-labile, less aromatic, high molecular weight, photochemically degradable, and correlated to DOC	Murphy et al. (2011), Cory and Kaplan, (2012)
C2-B (Brahmaputra River)	235/418 (Peak A)	Widespread UV (C) humic-like fluorophore, terrestrial-derived, availably found in forest streams and wetlands with highest concentration, but absent in wastewater	Stedmon et al. (2003)
C4-B (Brahmaputra River)	230/302 (Peak Tuv), 265/298 (Peak T)	Tyrosine-like, autochthonous-derived, and phenols (phenol and p-cresol) are microbial metabolites produced from tyrosine	Coble, (1996), Goldman and Sullivan, (2017)
C5-B (Brahmaputra River)	250/386 (Peak A), 295/386 (Peak M)	UV humic-like, terrestrial-derived, less aromatic, exported from natural catchments, and abundant in wastewater	Salve et al. (2012), Gao et al. (2016)

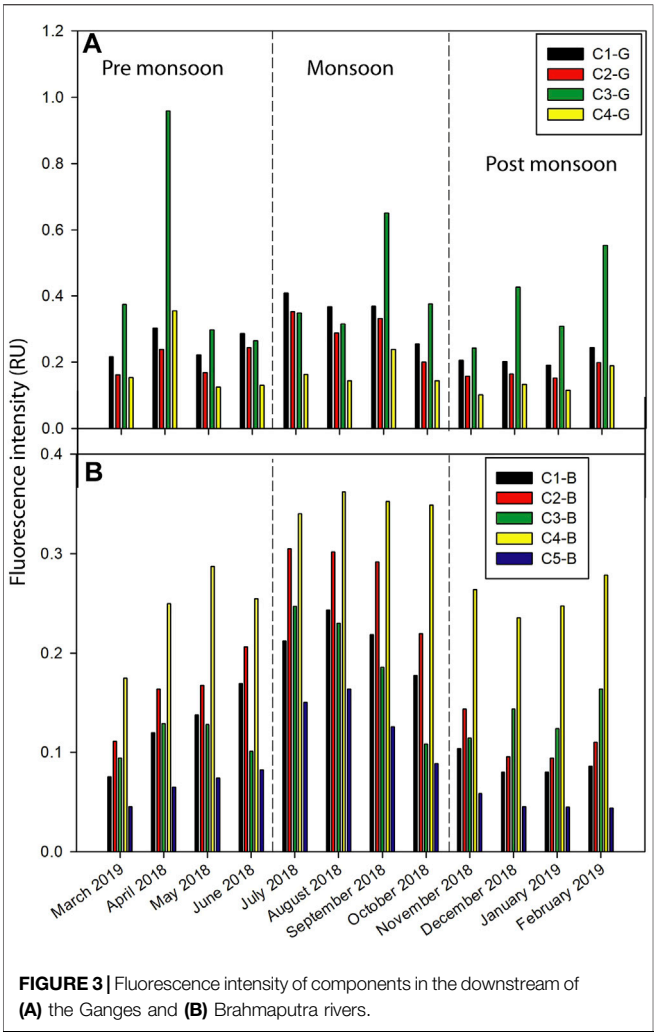

FIGURE 3 | Fluorescence intensity of components in the downstream of **(A)** the Ganges and **(B)** Brahmaputra rivers.

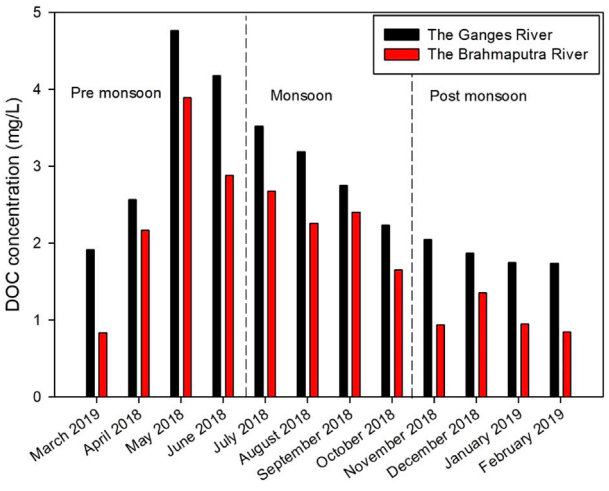

FIGURE 4 | DOC concentration in the downstream of the Ganges and Brahmaputra rivers.

identified DOM components in the Brahmaputra River, C1-B could be characterized as humic-like, C2-B as UV (C) humic-like, C3-B as tryptophan-like, C4-B as tyrosine-like, and C5-B as UV humic-like substances (**Table 2**). C1-B could originate from terrestrial sources and be found in the wastewater-impacted environments (Murphy et al., 2011; Cory and Kaplan, 2012). C2-B was a forest- and wetland-derived compound (Stedmon et al., 2003). The tryptophan-like component in the Brahmaputra River C3-B had similar characteristics to C3-G of the Ganges River (**Table 2**).

DOM components showed seasonal variability at both the rivers. The intensity of fluorophores in the two rivers is depicted in **Supplementary Figure S1**. Humic- (C1-G) and detergent-like (C2-G) components showed maximum intensity in the monsoon. On the contrary, two protein-like components, C3-G and C4-G, had higher intensity in the pre-monsoon than in other seasons in the Ganges River (**Figure 3A**). The intensities of all DOM components were minimum in the post-monsoon season (**Figure 3A**). The maximum intensity contribution of component C3-G at all seasons and detergent-like component C2-G indicated the probability of dense human settlement and continuous anthropogenic activities around the river basin. Humic- and detergent-like components C1-G and C2-G were significantly dependent on rainfall-runoff ($r = 0.8$, $p < 0.01$) to enter the Ganges River from the terrestrial environment (**Supplementary Table S3**). However, rainfall had an insignificant negative correlation with tryptophan-like components from anthropogenically derived C3-G ($r = -0.2$, $p > 0.05$) and autochthonous-originate d C4-G ($r = -0.01$, $p > 0.05$) (**Supplementary Table S3**). Poor correlation between C3-G and rain indicated that this DOM component did not depend on rain to enter the river. Instead, C3-G might be mixed with the Ganges River water through pipelines from sewerage, washing, and leachate sources or disposal by anthropogenic sources directly. This direct input of C3-G into the Ganges River water described the possibility of dense household and industrial settlements in the river basin. High intensity of C3-G was also marked as a possibility for microbial activities on a large scale throughout the year in the Ganges River, according to the method described by Nowicki et al. (2019).

The fluorescence intensities of DOM components also showed seasonal heterogeneity in the Brahmaputra River. All DOM components in this river showed maximum intensity in the monsoon (**Figure 3B**). After the monsoon, humic-like components (C1-B, C2-B, and C5-B) showed high intensities in the pre-monsoon, while the protein-like components (C3-B and C4-B) showed their second higher intensities in the post-monsoon (**Figure 3B**). All humic-like ($r = 0.9$, $p < 0.01$) and protein-like ($r = 0.6$, $p < 0.05$) components in the Brahmaputra River had a significant positive correlation with rain (**Supplementary Table S4**). The significant correlation described the dependence of DOM components in the Brahmaputra River on rainfall-runoff to enter the river. DOM characterization in the Brahmaputra River by PARAFAC analysis (**Table 2**) described that components could enter from forest streams, natural catchments, and various wastewater sources. The dependency of DOM components on rain indicated that the

components from wastewater sources do not enter the Brahmaputra River water through closed sewerage pipelines or direct disposal by humans like in the Ganges River. The Brahmaputra River basin is supposed to contain more natural forests and wetlands covered in its surroundings as natural humic-like components were dominant in this river (4.9 RU) compared to the Ganges River (3.3 RU) (**Figure 3**). On the contrary, the higher intensity of anthropogenically derived protein-like components and the presence of detergents indicated a more significant amount of anthropogenic activities in the Ganges River basin than in the Brahmaputra River (**Figure 3**).

DOC concentration varied between 1.74 and 4.76 mg/L (2.71 ± 1.01) and 0.84 and 3.89 mg/L (1.90 ± 0.97) downstream of the Ganges and Brahmaputra River, respectively (**Figure 4**). Annual average DOC concentration in some major Asian rivers, such as the Yellow River, Yangtze River, and Pearl River, was found at 2.70 mg/L, 2.24 mg/L, and 1.51 mg/L, respectively (Shi et al., 2016). DOC concentration in the downstream reaches of the Ganges and the Brahmaputra rivers was comparable to that mentioned above for the major Asian rivers (**Figure 4**). The seasonal DOC concentration followed the order pre-monsoon > monsoon > post-monsoon in both rivers (**Figure 4**). However, the fluorescent intensities of DOM components were higher in monsoon than in pre-monsoon at both rivers (**Figure 3**). The different seasonal fluctuation of DOC and DOM components in pre-monsoon and monsoon might be due to the additional presence of nitrogenous, phosphoric, and other organic compounds. Protein-like components were found in maximum intensity during the monsoon in the Brahmaputra River (**Figure 3B**). The comparison of protein-like components with DOC concentration indicated that the Brahmaputra River might contain additional nitrogenous compounds during the monsoon than in the other two seasons. On the contrary, the protein-like component showed the second-highest intensity in the monsoon in the Ganges River (**Figure 3A**). The comparison of protein-like components with DOC concentration suggested that the Ganges River might contain phosphoric and other organic compounds in addition to carbonaceous and nitrogenous substances.

3.2.1 Statistical Correlation of Dissolved Organic Matter Components in the Downstream Reaches of the Ganges and Brahmaputra River

The microbially degradable component C1-G could contribute to the DOC in the aquatic system (Goldman and Sullivan, 2017). However, in this study, C1-G had an insignificant correlation with DOC concentration ($r = 0.41$, $p > 0.05$), indicating that this carbon-dominated component might be incorporated with nitrogenous, phosphorous, and other organic compounds (**Supplementary Table S3**). Moreover, bonding with metal ions and low pH could also quench the fluorescence intensity of the DOM (Kowalczuk et al., 2009). pH values were higher in the Ganges River (**Table 1**). The insignificant correlation between DOC and C1-G thus described a possibility of intensity quench of this component due to its attachment with metal ions. The humic-like component in the Ganges River C1-G degraded due to the temperature effect ($r = 0.6$, $p < 0.05$) (**Supplementary Table S3**). C1-G and C4-G also had a significant positive correlation ($r = 0.6–0.7$, $p < 0.05$) with $E_{250/365}$, indicating that the intensity of these two DOM components increased with the decrease of their molecular size (**Supplementary Table S3**).

C1-B contributed significantly to the DOC concentration ($r = 0.6$, $p < 0.05$), unlike C1-G. Both C1-B ($r = 0.7$, $p < 0.01$) and C2-B ($r = 0.7$, $p < 0.05$) had a strong correlation with HIX, suggesting their major contributions to the aromaticity in the Brahmaputra River, though the total aromaticity was low in the river water (**Supplementary Table S4**). The temperature could quench fluorescent intensity due to molecular collision effects (Henderson et al., 2009). However, the inverse function of this parameter could also be seen to be playing an important role in photodegradation, thermal decomposition, and mineralization and thus increasing the intensity of components (Gruenheid et al., 2008; Porcal et al., 2015). The role of temperature in the degradation and mineralization of humic-like components C1-B, C2-B, and C5-B and thus loss of their relative molecular size increasing intensity could be described from the strong positive correlation ($r = 0.6–0.7$, $p < 0.05$, 0.01) of these three DOM components with temperature and relative molecular size values ($E_{250/365}$) in this study (**Supplementary Table S4**). C5-B could also contribute significantly to the autochthonous DOM production through microbial degradation unlike C1-B and C2-B, which could be described from its strong positive correlation with BIX and the Freshness index ($r = 0.6$, $p < 0.05$) in the Brahmaputra River (**Supplementary Table S4**). The increase of humic-like components C1-B, C2-B, and C5-B significantly reduced the DO concentration ($r = −0.6–0.7$, $p < 0.05$), causing deleterious effects on aquatic species due to their presence (**Supplementary Table S4**). On the contrary, protein-like components in the Brahmaputra River and humic-, protein-, and detergent-like components in the Ganges River hardly reduce DO concentration ($r = −0.2–0.4$, $p > 0.05$) (**Supplementary Table S4**).

3.3 Degradation Potential Index and Source Apportion of Dissolved Organic Matter Into Surface Water

The EEM and PARAFAC analyses identified fluorophores and DOM components of various natural and anthropogenic sources in surface water. EEM analysis, detail characterization, and intensities of identified DOM components are depicted in **Figure 5** and **Supplementary Tables S5, S6**, respectively. The EEM and PARAFAC identified two humic- and two protein-like components in algae, three humic-like components in groundwater, two humic- and one protein-like component in industrial effluents, four humic-like components in soil, three humic-like components in terrestrial plants, and two humic-, one protein-, and one detergent-like component in sewerage water samples (**Supplementary Table S5**). The DOM degradation varied among sources: sewerage water > terrestrial plants >

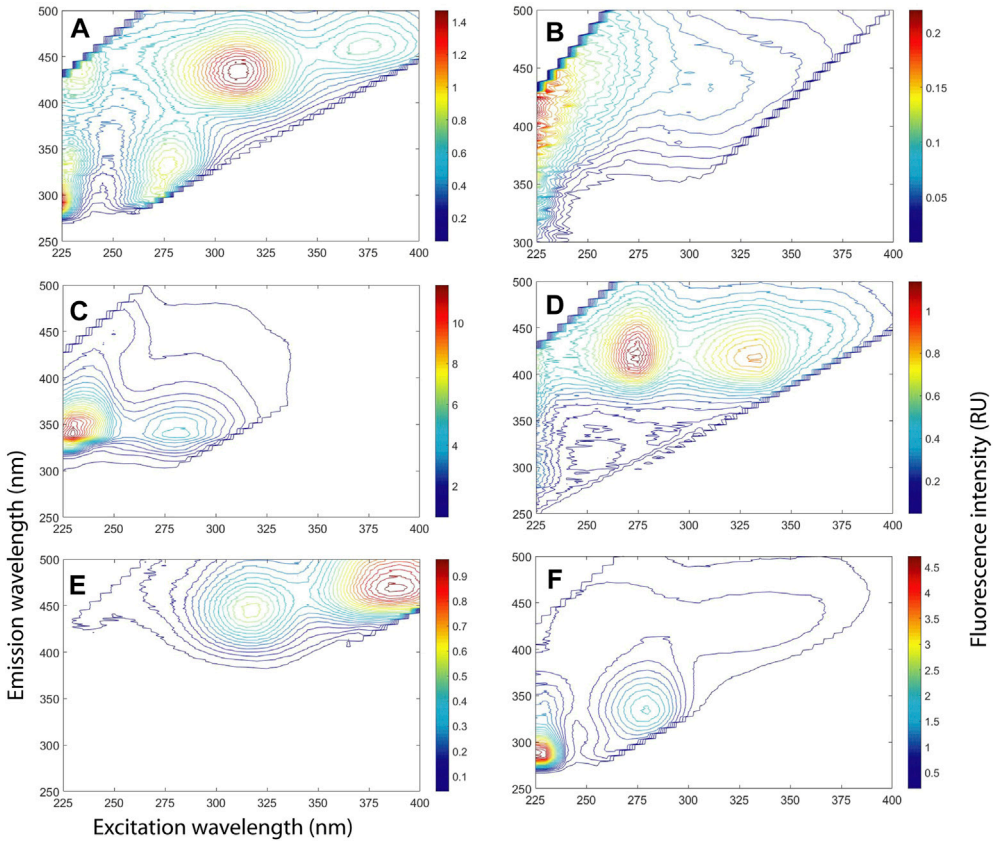

FIGURE 5 | EEM spectra of common natural and anthropogenic DOM sources during the late monsoon at the Ganges and Brahmaputra rivers basins: **(A)** algae, **(B)** groundwater, **(C)** industrial effluents, **(D)** soil, **(E)** terrestrial plants, and **(F)** sewerage water. These samples were collected separately from their sources and measured using a fluorescence spectrophotometer.

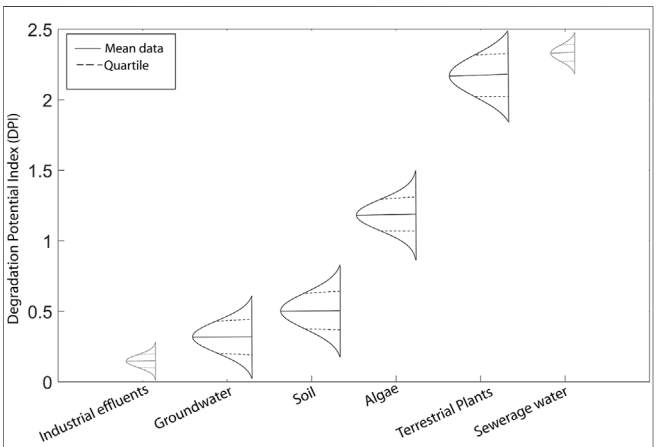

FIGURE 6 | Degradation potential index (DPI) of common natural and anthropogenic DOM sources in the environment. The DPI of sources was calculated using equation (i).

algae > soil > groundwater > industrial effluents (**Figure 6**). The minimum DPI value indicated the presence of persistent organic molecules in industrial effluents.

The DOM contributions from sources were calculated by coupling the DPI values of sources with the contributing DOM components in surface water. Algae, groundwater, industrial effluents, soil, terrestrial plants, and sewerage water contributed around 13.3–19.2%, 2.8–4.2%, 0.8–1.2%, 5.5–7.1%, 19.8–25.2%, and 44.7–56.7% DOM throughout the year, respectively (**Figure 7**). The contribution from similar sources could change insignificantly with spatiotemporal variability Liao et al. (2021). The production of DOM from algae depends on its decay influenced by photo-irradiation and microbial activity (Hansen et al., 2016). The produced DOM from algae was both labile and recalcitrant, ensuring its long-term stability in water. The contribution of algal DOM was comparable to that of terrestrial DOM contributed by plants (**Figure 7**). Groundwater also contributed a minimal amount of DOM to surface water (**Figure 7**). Due to heavy rainfall, the infiltration and percolation of terrestrial-derived DOM in large amounts into groundwater might increase its contribution to surface water in the monsoon ($r = 0.7$, $p < 0.05$) (**Figure 7**). The minimum contribution of DOM from groundwater indicated water table sink due to insufficient rain ($r = 0.8$, $p < 0.05$). The contribution from the industrial effluents into surface water was minimum among all sources (**Figure 7**). However, rivers in Bangladesh are highly

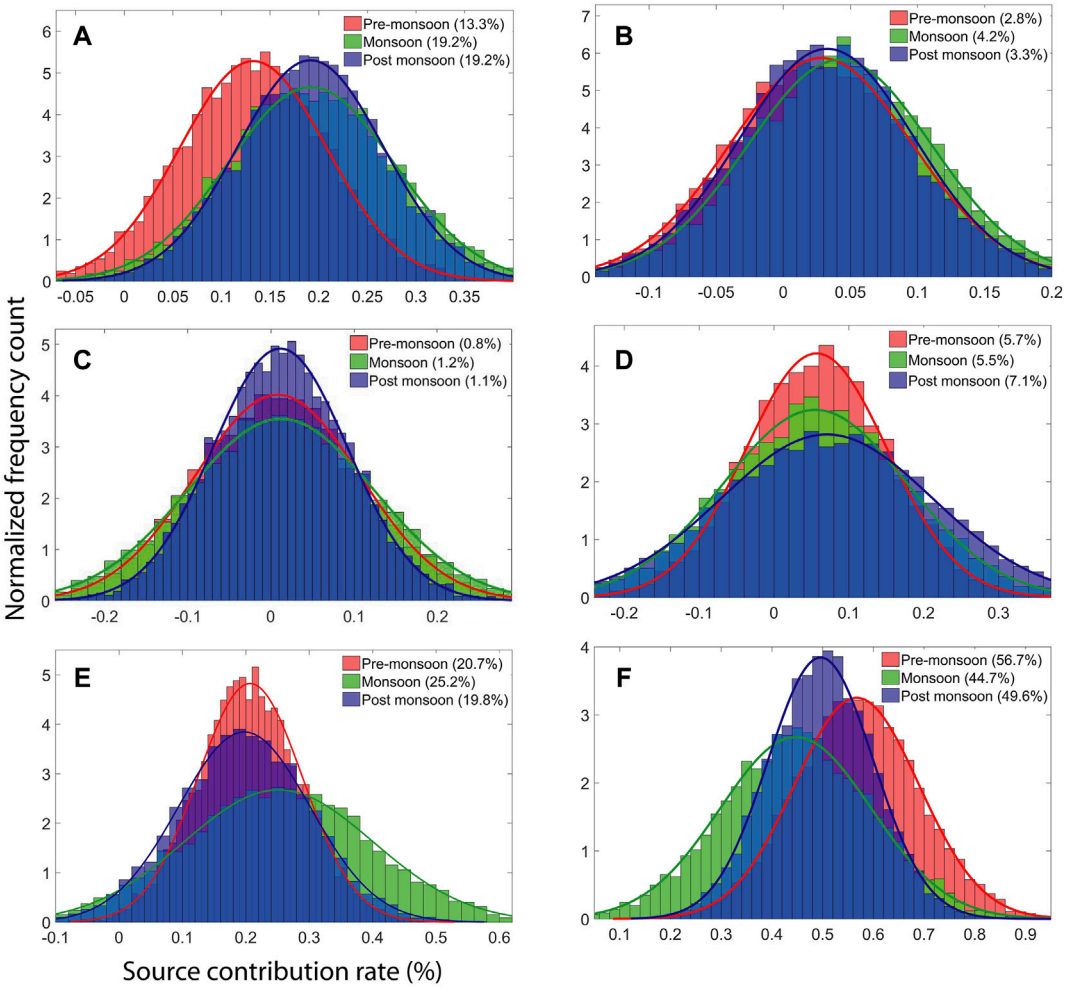

FIGURE 7 | Seasonal variation (pre-monsoon, monsoon, and post-monsoon) in the DOM contribution (in percentage, %) from various natural and anthropogenic sources in the environment to the downstream of the Ganges and Brahmaputra rivers in the pre-monsoon (March–June), monsoon (July–October), and post-monsoon (November–February). The considered natural and anthropogenic DOM sources here are **(A)** algae, **(B)** groundwater, **(C)** industrial effluents, **(D)** soil, **(E)** terrestrial plants, and **(F)** sewerage water.

contaminated by untreated inputs of industrial effluents and solid wastes (Aktar and Moonajilin, 2017; Uddin and Jeong, 2021).

Nevertheless, lower DOM contribution might be due to the abundant presence of hydrophobic, non-polar, and dispersing chemicals and dyes in industrial effluents. The two terrestrial-derived natural sources, soil and terrestrial plants, responded inversely to rainfall (**Figure 7**). DOM from the soil contributed least in monsoon and most in the dry post-monsoon (**Figure 7**). However, due to heavy rain in the monsoon, dilution effects could hardly affect DOM exudation from terrestrial plant sources ($r = -0.7$, $p < 0.05$). Instead, significant rain washed DOM in high amounts from terrestrial plants into surface water, thus contributing to the maximum in the monsoon ($r = 0.8$, $p < 0.01$) (**Figure 7**). Terrestrial plants contributed minimum in the post-monsoon into surface water. The entirely anthropogenically originated sewerage water contributed the most among all sources (**Figure 7**). The slight rainfall rapidly washed long deposited sewerage wastes ($r = 0.8$, $p < 0.01$) in large amounts into the surface water and thus increased DOM contribution in the pre-monsoon. However, DOM contribution from sewerage sources was minimum during the monsoon, which might be due to the dilution effects ($r = -0.5$, $p > 0.05$) (**Figure 7**). The high DOM contribution from the sewerage water confirmed the enormous waste disposals unethically and a wide range of anthropogenic activity.

3.4 Fate of Dissolved Organic Matter in the Ganges and Brahmaputra Rivers

The concentration and sources of DOM changed dynamically from upstream to downstream in both the Ganges and Brahmaputra Rivers in Bangladesh. The factors such as local climate, hydrology, physical and chemical interaction among DOM, source variation, surrounding forest cover, human settlement, and state of the industrialization played a pivotal role in DOM dynamicity in the two rivers.

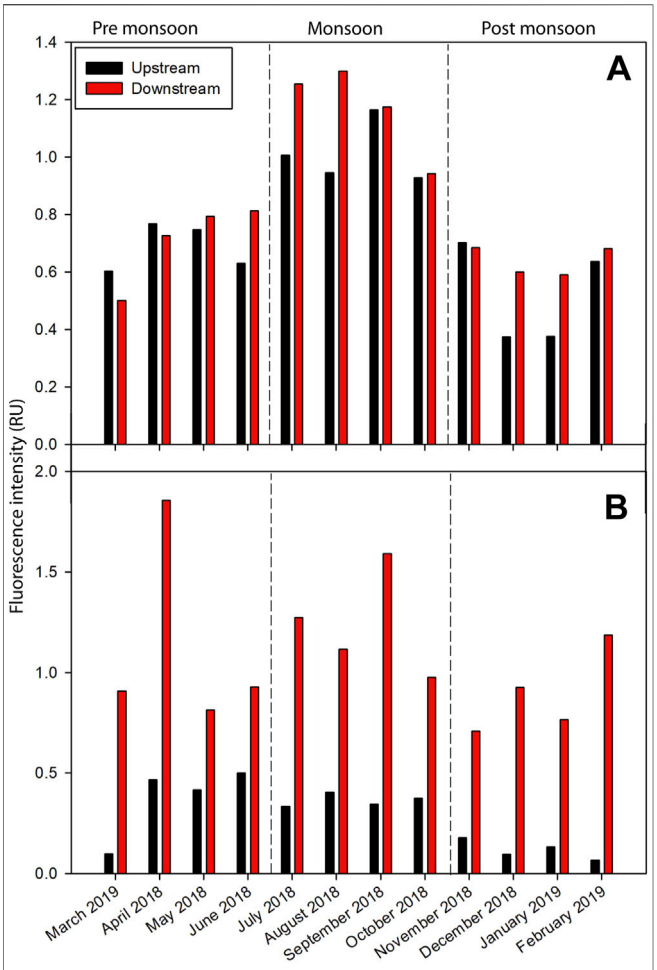

FIGURE 8 | Comparison of DOM intensities between upstream and downstream of **(A)** Brahmaputra and **(B)** Ganges rivers. The fluorescence intensities in the upstream of Ganges and Brahmaputra rivers of Bangladesh were derived from Niloy et al. (2021a) and Niloy et al. (2022).

The upstream of the Ganges River, four DOM components, including detergent-like, protein-like, and two humic-like, were identified in the PARAFAC analysis (Niloy et al., 2021a). Detergent- and protein-like components came from anthropogenic sources, whereas two humic-like substances originated from natural terrestrial sources and microbial processing. DOM components were primarily fresh, immediately humified, and aromatic (Niloy et al., 2021a). The relative molecular weight was maximum from the late monsoon to the entire post-monsoon (**Supplementary Table S7**). Autochthonous DOM production was also high. Total intensities of DOM components were higher in the pre-monsoon and monsoon than post-monsoon. Rainfall played a significant role ($r = 0.741$, $p < 0.01$) in the fluctuation of DOM intensities (Niloy et al., 2021a). The Ganges River water was in the intermediate-risk category due to the microbial contamination throughout the entire monsoon (Niloy et al., 2021a).

PARAFAC also identified four DOM components downstream of the Ganges River (**Supplementary Figure S2**). However, the specified DOM components: a humic-like, a detergent-like, and two protein-like components, indicated the loss of natural humic components and increased anthropogenic protein-like substances compared to the upstream (**Supplementary Figure S2**, **Table 2**). The total fluorescent intensity in the downstream was 1.8–17.7 times higher than that in the upstream of the river (**Figure 8**). The intensities of humic-like components increased by 0.7–8.0 times, protein-like components by 4.2–135.0 times, and detergent-like components by 1.1–5.6 times downstream than the upstream of the river (**Figure 3**; **Supplementary Figure S4**). The increase of anthropogenically derived protein- and detergent-like components and their intensities indicated higher population density and industrialization at the downstream of the river basin than the upstream. Unlike significant seasonal heterogeneity ($r = 0.387$, $p > 0.05$), DOM showed descending order of intensity: pre-monsoon > monsoon > post-monsoon and monsoon > pre-monsoon > post-monsoon in the upstream and downstream of the river (**Figure 3**; **Supplementary Figure S4**). The only identified humic-like component in this study originated through microbial processing resembling the upstream (**Table 2**). However, higher intensity of humic (M)-like and tryptophan-like substances indicated more microbial activity downstream than upstream in this river (**Figure 3**). Inputs of protein-like components in downstream hardly depended on rain ($p > 0.05$), though their intensity decreased to some extent might be due to dilution effects ($r = -0.177$, $p > 0.05$) for precipitation. DOM components were less humified and aromatic and matured in downstream compared to the upstream (**Supplementary Tables S2, S7**). The molecular size and weight of DOM were also less in downstream than upstream of this river (**Supplementary Tables S2, S7**). Photo-irradiation and microbial activity might function intensely to decrease DOM molecular size and weight in the downstream.

PARAFAC identified four DOM components (two humic- and two protein-like) in the upstream of the Brahmaputra River (Niloy et al., 2022). Total intensities of DOM were maximum in the monsoon and minimum in the post-monsoon (**Figure 8A**). The intensities of protein-like components were 0.8–3.3 times higher than those of the humic-like components (**Supplementary Figure S5**). DOM components came from both allochthonous and autochthonous sources, were matured, poorly humified, and less aromatic (Niloy et al., 2022). The relative molecular weight of DOM was maximum in the monsoon and minimum during post-monsoon (Niloy et al., 2022). However, the relative molecular size of DOM in the Brahmaputra river was slightly low in the pre-monsoon and monsoon, indicating that DOM components might be attached to other high weight and low size containing substances, debris, or metals during these times (Niloy et al., 2022). The concentration of anthropogenically derived tryptophan-like components was high and indicated water quality deterioration at intermediate/high levels due to intense microbial activity (Niloy et al., 2022). However, rainfall played a significant positive role in fluctuating humic-like moieties ($r = 0.845$, $p < 0.01$), and it had a weak negative influence on seasonal variation of protein-like components ($r = -0.306$, $p > 0.05$) (Niloy et al., 2022).

Downstream of Brahmaputra River, the PARAFAC analysis identified five components: three humic-like and two protein-like (**Supplementary Figure S2**). A terrestrial-derived and

wastewater abundant humic-like component was added with the previously identified four DOM components in the downstream (**Table 2**). The Brahmaputra is a classic example of a braided river, and continuous river erosion and riverine island formation diverted the channel and anabranches in the pathways (Ullah et al., 2010; Islam et al., 2020). Local people cultivate crops and dwell with unhealthy sanitation, mostly in the grown-up large sandbars and islands of the Brahmaputra River (Ullah et al., 2010; Salam et al., 2019). The more agricultural cultivation or grasslands than the upstream could be the possible reason for adding another humic (C)-like natural DOM component downstream of the Brahmaputra River. The humic (C)-like component increased its intensity about 2–3 times downstream than the upstream (**Figure 3B**; **Supplementary Figure S5**). On the contrary, microbial-derived humic (M)-like, anthropogenically originated tryptophan- and tyrosine-like components had lower intensity in the downstream reaches of the Brahmaputra River than the upstream reaches (**Figure 3B**; **Supplementary Figure S5**). Such results indicated that natural agricultural and forest cover dominate and lower microbial and anthropogenic activities exist in the downstream of the Brahmaputra River than upstream. Total intensities of DOM were 0.8–1.6 times higher in the downstream than upstream (**Figure 8A**). Humic- and protein-like moieties were 0.9–1.7 and 0.6–1.9 times higher in the downstream than upstream, respectively (**Figure 3B**; **Supplementary Figure S5**). Rainfall played a strong role in fluctuating humic-like components ($r = 0.922$, $p < 0.01$) in the downstream similar to upstream (**Supplementary Table S4**). Conversely, unlike the upstream, a significant correlation between rainfall and protein fractions ($r = 0.682$, $p < 0.05$) indicated that protein-like components mostly came from the terrestrial washout by rain in the Brahmaputra River rather than from other sources such as household sewage and industrial discharge (**Supplementary Table S4**). Humic-like components also showed similar seasonal heterogeneity ($r = 0.911$, $p < 0.01$) in both streams, whereas protein-like components described unlike seasonal heterogeneity ($r = 0.514$, $p > 0.05$), showing intensities in descending order monsoon > pre-monsoon > post-monsoon and monsoon > post-monsoon > pre-monsoon in the upstream and downstream of the river (**Figure 3**; **Supplementary Table S1**; **Supplementary Figures S4, S5**). The decrease of protein-like components in the pre-monsoon might be due to dilution effects caused by rainfall, and this could be explained by the strong relation ($r = 0.682$, $p < 0.05$) between rainfall and the availability of protein moieties (**Supplementary Table S4**). Like the upstream, humic-like DOM components originated from allochthonous sources and were matured, poorly humified, and non-aromatic (**Supplementary Tables S2, S7**). The relative molecular weight was higher in downstream than upstream in the Brahmaputra River (**Supplementary Tables S2, S7**). However, like the upstream, the relative molecular weight of DOM was higher in the monsoon and pre-monsoon, while inversely, the relative molecular size of DOM was higher in the post-monsoon than in other seasons (**Supplementary Tables S2, S7**). Water quality was in the high-risk category due to the presence of tryptophan-like components throughout the year in both streams of the river, according to the method by Nowicki et al. (2019).

4 CONCLUSION

This study provided a precise figure about the insights of the DOM components in the downstream of the Ganges and the Brahmaputra rivers. Both natural and anthropogenically derived DOM prevailed in both rivers. The fluorescent intensity of DOM components was higher in the pre-monsoon and monsoon than in post-monsoon seasons in both rivers. DOM components were mostly from terrestrial sources in both rivers. The significant presence of detergent- and tryptophan-like DOM in the Ganges River indicated intense anthropogenic activities nearby its basin. On the contrary, the Brahmaputra River basin was mainly covered by forest and vegetation due to the dominant presence of humic-like components. The DPI and EMM identified sewerage water as the maximum DOM contributing source, followed by terrestrial plants > algae > soil > groundwater > industrial effluents. DOM components were matured and less aromatic. DOM molecules contained lower energy from the late pre-monsoon to the entire monsoon than the rest of the year. The downstream Ganges and the Brahmaputra River had more DOM than the upstream portion in Bangladesh. The deteriorated condition in the downstream warned about the severe health effects on living species and suggested taking prompt actions to control and treat anthropogenic sources of DOM before discharging into surface water.

DATA AVAILABILITY STATEMENT

The original contributions presented in the study are included in the article/**Supplementary Material**; further inquiries can be directed to the corresponding author.

AUTHOR CONTRIBUTIONS

ST and MS planned and designed the study. NN and MH collected data and analyzed samples. All authors wrote and reviewed the manuscript.

ACKNOWLEDGMENTS

The authors would like to acknowledge the Organization for Women in Science for the Developing World (OWSD), a UNESCO program, hosted by The World Academy of Sciences (TWAS). The grant was provided to Dr. MS (Award Agreement No.: 4500384865) under the Early career fellowship program 2018. This project was further supported by the University Grants Commission (UGC), Bangladesh, and Jahangirnagar University Faculty of Mathematical & Physical Sciences Research Grant for FY

(2020–2021) and provided to Dr. MS. Furthermore, this work was carried out with the aid of a grant from the UNESCO and the International Development Research Center (IDRC), Ottawa, Canada. The views expressed herein do not necessarily represent those of UNESCO, IDRC or its Board of Governors.

SUPPLEMENTARY MATERIAL

The Supplementary Material for this article can be found online at: https://www.frontiersin.org/articles/10.3389/feart.2022.821050/full#supplementary-material

REFERENCES

Aktar, P., and Moonajilin, M. S. (2017). Assessment of Water Quality Status of Turag River Due to Industrial Effluent. *Int. J. Eng. Inf. Syst.* 1 (6), 105–118.

Anwar, J. (2006). Pollution in the Ganges Brahmaputra Delta Plain. Available at: http://www.sos-arsenic.net/english/environment/ganges.html (Accessed November 1, 2021).

Baghoth, S. A., Sharma, S. K., and Amy, G. L. (2011). Tracking Natural Organic Matter (NOM) in a Drinking Water Treatment Plant Using Fluorescence Excitation-Emission Matrices and PARAFAC. *Water Res.* 45, 797–809. doi:10.1016/j.watres.2010.09.005

BECR (1997). Industrial Effluents Quality Standard for Bangladesh. *Bangladesh Gaz. Addit.*, 179–227.

Bhuyan, M. S., Bakar, M. A., Rashed-Un-Nabi, M., Senapathi, V., Chung, S. Y., and Islam, M. S. (2019). Monitoring and Assessment of Heavy Metal Contamination in Surface Water and Sediment of the Old Brahmaputra River, Bangladesh. *Appl. Water Sci.* 9, 1–13. doi:10.1007/s13201-019-1004-y

Chaves, R. C., Figueredo, C. C., Boëchat, I. G., de Oliveira, J. T. M., and Gücker, B. (2020). Fluorescence Indices of Dissolved Organic Matter as Early Warning Signals of Fish Farming Impacts in a Large Tropical Reservoir. *Ecol. Indic.* 115, 106389. doi:10.1016/j.ecolind.2020.106389

Chen, M., Zeng, C., Zhang, F., Kang, S., and Li, C. (2020). Characteristics of Dissolved Organic Matter from a Transboundary Himalayan Watershed: Relationships with Land Use, Elevation, and Hydrology. *ACS Earth Space Chem.* 4, 449–456. doi:10.1021/acsearthspacechem.9b00329

Coble, P. G. (1996). Characterization of Marine and Terrestrial DOM in Seawater Using Excitation-Emission Matrix Spectroscopy. *Mar. Chem.* 51, 325–346. doi:10.1016/0304-4203(95)00062-3

Coble, P. G., Green, S. A., Blough, N. V., and Gagosian, R. B. (1990). Characterization of Dissolved Organic Matter in the Black Sea by Fluorescence Spectroscopy. *Nature* 348, 432–435. doi:10.1038/348432a0

Cory, R. M., and Kaplan, L. A. (2012). Biological Lability of Streamwater Fluorescent Dissolved Organic Matter. *Limnol. Oceanogr.* 57, 1347–1360. doi:10.4319/lo.2012.57.5.1347

Gao, S.-J., Zhao, C., Shi, Z.-H., Zhong, J., Liu, J.-G., and Li, J.-Q. (2016). Spectroscopic Characteristics of Dissolved Organic Matter in Afforestation Forest Soil of Miyun District, Beijing. *J. Anal. Methods Chem.* 2016, 1–10. doi:10.1155/2016/1480857

Goldman, J. H., and Sullivan, A. B. (2017). Characteristics of Dissolved Organic Matter in the Upper Klamath River , Lost River , and Klamath Straits Drain , Oregon and California. *U.S. Geol. Surv. Open File Rep.* 21, 2017–1160. doi:10.3133/ofr20171160

Goletz, C., Wagner, M., Grübel, A., Schmidt, W., Korf, N., and Werner, P. (2011). Standardization of Fluorescence Excitation – Emission-Matrices in Aquatic Milieu. *Talanta* 85, 650–656. doi:10.1016/j.talanta.2011.04.045

Gruenheid, S., Huebner, U., and Jekel, M. (2008). Impact of Temperature on Biodegradation of Bulk and Trace Organics During Soil Passage in an Indirect Reuse System. *Water Sci. Technol.* 57, 987–994. doi:10.2166/wst.2008.207

Hansen, A. M., Kraus, T. E. C., Pellerin, B. A., Fleck, J. A., Downing, B. D., and Bergamaschi, B. A. (2016). Optical Properties of Dissolved Organic Matter (DOM): Effects of Biological and Photolytic Degradation. *Limnol. Oceanogr.* 61, 1015–1032. doi:10.1002/lno.10270

Haque, M. M., Niloy, N. M., Nayna, O. K., Fatema, K. J., Quraishi, S. B., Park, J.-H., et al. (2020). Variability of Water Quality and Metal Pollution Index in the Ganges River, Bangladesh. *Environ. Sci. Pollut. Res.* 27, 42582–42599. doi:10.1007/s11356-020-10060-3

He, Q., Gao, L., Wang, Z., Tang, Y., Pan, B., and Li, M. (2021). Fluorescence Characteristics of Dissolved Organic Matter in Several Independent Water Bodies: Possible Sources and Land-Use Effects. *Environ. Sci. Pollut. Res.* 28, 33241–33253. doi:10.1007/s11356-021-12972-0

Henderson, R. K., Baker, A., Murphy, K. R., Hambly, A., Stuetz, R. M., and Khan, S. J. (2009). Fluorescence as a Potential Monitoring Tool for Recycled Water Systems: A Review. *Water Res.* 43, 863–881. doi:10.1016/j.watres.2008.11.027

Hudson, N., Baker, A., and Reynolds, D. (2007). Fluorescence Analysis of Dissolved Organic Matter in Natural, Waste and Polluted Waters-A Review. *River Res. applic.* 23, 631–649. doi:10.1002/rra.1005

Islam, M. M., Islam, F., Akter, M. S., Kundu, G. K., Barman, A., and Khan, M. I. (2020). Transformative Adaptations to Climate Change: Cases from the Jamuna River Fishing Communities of Bangladesh. *J. Fish. Environ.* 44 (3), 1–18.

Kowalczuk, P., Durako, M. J., Young, H., Kahn, A. E., Cooper, W. J., and Gonsior, M. (2009). Characterization of Dissolved Organic Matter Fluorescence in the South Atlantic Bight with Use of PARAFAC Model: Interannual Variability. *Mar. Chem.* 113, 182–196. doi:10.1016/j.marchem.2009.01.015

Liao, Z.-l., Zhao, Z.-c., Chen, H., and Wu, J. (2021). Quantitative Source Apportionment of Dissolved Organic Matters in Wet Weather Overflows of Storm Drainage Systems Based on Degradation Potential Index and End Member Mixing Model. *Sci. Total Environ.* 792, 148493. doi:10.1016/j.scitotenv.2021.148493

Liu, T., Wang, X., Zhu, E., Liu, Z., Zhang, X., Guo, J., et al. (2021). Evolution of the Dissolved Organic Matter Composition along the Upper Mekong (Lancang) River. *ACS Earth Space Chem.* 5, 319–330. doi:10.1021/acsearthspacechem.0c00292

Mahanta, C., Zaman, A. M., Newaz, S. M. S., Rahman, S. M. M., Rahman, S. M. M., Choudhury, R., et al. (2014). *Physical Assessment of the Brahmaputra River*. Dhaka, Bangladesh: IUCN, International Union for Conservation of Nature.

Mann, P. J., Davydova, A., Zimov, N., Spencer, R. G. M., Davydov, S., Bulygina, E., et al. (2012). Controls on the Composition and Lability of Dissolved Organic Matter in Siberia's Kolyma River Basin. *J. Geophys. Res.* 117, 1–15. doi:10.1029/2011jg001798

Mostofa, K. M. G., Wu, F., Liu, C.-Q., Fang, W. L., Yuan, J., Ying, W. L., et al. (2010). Characterization of Nanming River (Southwestern China) Sewerage-Impacted Pollution Using an Excitation-Emission Matrix and PARAFAC. *Limnology* 11, 217–231. doi:10.1007/s10201-009-0306-4

Munia, H. A., Guillaume, J. H. A., Wada, Y., Veldkamp, T., Virkki, V., and Kummu, M. (2020). Future Transboundary Water Stress and its Drivers under Climate Change: A Global Study. *Earth's Future* 8, 0–3. doi:10.1029/2019EF001321

Murphy, K. R., Hambly, A., Singh, S., Henderson, R. K., Baker, A., Stuetz, R., et al. (2011). Organic Matter Fluorescence in Municipal Water Recycling Schemes: Toward a Unified PARAFAC Model. *Environ. Sci. Technol.* 45, 2909–2916. doi:10.1021/es103015e

Nelson, N. B., and Gauglitz, J. M. (2016). Optical Signatures of Dissolved Organic Matter Transformation in the Global Ocean. *Front. Mar. Sci.* 2, 1–15. doi:10.3389/fmars.2015.00118

Niloy, N. M., Haque, M. M., and Tareq, S. M. (2021a). Characteristics, Sources, and Seasonal Variability of Dissolved Organic Matter (DOM) in the Ganges River, Bangladesh. *Environ. Process.* 8, 593–613. doi:10.1007/s40710-021-00499-y

Niloy, N. M., Haque, M. M., and Tareq, S. M. (2021b). Characterization of Dissolved Organic Matter at Urban and Industrial Rainwater of Bangladesh by Fluorescence Spectroscopy and EEM-PARAFAC Modeling. *Environ. Challenges* 5, 100250. doi:10.1016/j.envc.2021.100250

Niloy, N. M., Haque, M. M., and Tareq, S. M. (2021c). Fluorescent Whitening Agents in Commercial Detergent: A Potential Marker of Emerging Anthropogenic Pollution in Freshwater of Bangladesh. *Environ. Nanotechnol. Monit. Manag.* 15, 100419. doi:10.1016/j.enmm.2020.100419

Niloy, N. M., Haque, M. M., and Tareq, S. M. (2022). Temporal Changes in Hydrochemistry and DOM Characteristics of the Brahmaputra River:

Implication to the Seasonality of Water Quality. *Environ. Sci. Pollut. Res.* 29, 35165–35178 doi:10.1007/s11356-022-18618-z

Nowicki, S., Lapworth, D. J., Ward, J. S. T., Thomson, P., and Charles, K. (2019). Tryptophan-Like Fluorescence as a Measure of Microbial Contamination Risk in Groundwater. *Sci. Total Environ.* 646, 782–791. doi:10.1016/j.scitotenv.2018.07.274

Panigrahi, S. K., and Mishra, A. K. (2019). Inner Filter Effect in Fluorescence Spectroscopy: As a Problem and as a Solution. *J. Photochem. Photobiol. C Photochem. Rev.* 41, 100318. doi:10.1016/j.jphotochemrev.2019.100318

Pang, Y., Wang, K., Sun, Y., Zhou, Y., Yang, S., Li, Y., et al. (2021). Linking the Unique Molecular Complexity of Dissolved Organic Matter to Flood Period in the Yangtze River Mainstream. *Sci. Total Environ.* 764, 142803. doi:10.1016/j.scitotenv.2020.142803

Papa, F., Bala, S. K., Pandey, R. K., Durand, F., Gopalakrishna, V. V., Rahman, A., et al. (2012). Ganga-Brahmaputra River Discharge from Jason-2 Radar Altimetry: An Update to the Long-Term Satellite-Derived Estimates of Continental Freshwater Forcing Flux into the Bay of Bengal. *J. Geophys. Res.* 117, a–n. doi:10.1029/2012JC008158

Park, J.-H., Nayna, O. K., Begum, M. S., Chea, E., Hartmann, J., Keil, R. G., et al. (2018). Reviews and Syntheses: Anthropogenic Perturbations to Carbon Fluxes in Asian River Systems - Concepts, Emerging Trends, and Research Challenges. *Biogeosciences* 15, 3049–3069. doi:10.5194/bg-15-3049-2018

Porcal, P., Dillon, P. J., and Molot, L. A. (2015). Temperature Dependence of Photodegradation of Dissolved Organic Matter to Dissolved Inorganic Carbon and Particulate Organic Carbon. *Plos One* 10, e0128884. doi:10.1371/journal.pone.0128884

Rahman, M., Islam, M., and Khan, M. (2017). Status of Heavy Metal Pollution of Water and Fishes in Balu and Brahmaputra Rivers. *Prog. Agric.* 27, 444–452. doi:10.3329/pa.v27i4.32129

Rahman, M. M., Ghosh, T., Salehin, M., Ghosh, A., Haque, A., Hossain, M. A., et al. (2020). "Ganges-Brahmaputra-Meghna Delta, Bangladesh and India: A Transnational Mega-Delta," in *Deltas in the Anthropocene*. Editors R. J. Nicholls, N. Adger, C. W. Hutton, and S. E. Hanson (Springer Nature Switzerland AG), 23–51. doi:10.1007/978-3-030-23517-8_2

Riedel, T., Zark, M., Vähätalo, A. V., Niggemann, J., Spencer, R. G. M., Hernes, P. J., et al. (2016). Molecular Signatures of Biogeochemical Transformations in Dissolved Organic Matter from Ten World Rivers. *Front. Earth Sci.* 4, 1–16. doi:10.3389/feart.2016.00085

Salam, M. A., Khan, M. S., and Sarker, M. A. H. (2019). Impacts and Coping Techniques to Flood : the Case Study of Two Char Lands of Jamuna River in Sirajgonj District, Bangladesh. *Int. Res. J. Environ. Sci.* 8 (3), 53–61.

Salve, P. R., Lohkare, H., Gobre, T., Bodhe, G., Krupadam, R. J., Ramteke, D. S., et al. (2012). Characterization of Chromophoric Dissolved Organic Matter (CDOM) in Rainwater Using Fluorescence Spectrophotometry. *Bull. Environ. Contam. Toxicol.* 88, 215–218. doi:10.1007/s00128-011-0424-7

Seo, M., Lee, H., and Kim, Y. (2019). Relationship between Coliform Bacteria and Water Quality Factors at Weir Stations in the Nakdong River, South Korea. *water* 11, 1171. doi:10.3390/w11061171

Sharma, C., Shukla, A. K., and Zhang, Y. (2021). Climate Change Detection and Attribution in the Ganga-Brahmaputra-Meghna River Basins. *Geosci. Front.* 12, 101186. doi:10.1016/j.gsf.2021.101186

Shi, G., Peng, C., Wang, M., Shi, S., Yang, Y., Chu, J., et al. (2016). The Spatial and Temporal Distribution of Dissolved Organic Carbon Exported from Three Chinese Rivers to the China Sea. *PLoS ONE* 11, e0165039. doi:10.1371/journal.pone.0165039

Steckler, M. S., Oryan, B., Wilson, C. A., Grall, C., Nooner, S. L., Mondal, D. R., et al. (2022). Synthesis of the Distribution of Subsidence of the Lower Ganges-Brahmaputra Delta, Bangladesh. *Earth-Science Rev.* 224, 103887. doi:10.1016/j.earscirev.2021.103887

Stedmon, C. A., and Bro, R. (2008). Characterizing Dissolved Organic Matter Fluorescence with Parallel Factor Analysis: A Tutorial. *Limnol. Oceanogr. Methods* 6, 572–579. doi:10.4319/lom.2008.6.57210.4319/lom.2008.6.572b

Stedmon, C. A., Markager, S., and Bro, R. (2003). Tracing Dissolved Organic Matter in Aquatic Environments Using a New Approach to Fluorescence Spectroscopy. *Mar. Chem.* 82, 239–254. doi:10.1016/S0304-4203(03)00072-0

Stedmon, C. A., and Markager, S. (2005a). Resolving the Variability in Dissolved Organic Matter Fluorescence in a Temperate Estuary and its Catchment Using PARAFAC Analysis. *Limnol. Oceanogr.* 50, 686–697. doi:10.4319/lo.2005.50.2.0686

Stedmon, C. A., and Markager, S. (2005b). Tracing the Production and Degradation of Autochthonous Fractions of Dissolved Organic Matter by Fluorescence Analysis. *Limnol. Oceanogr.* 50, 1415–1426. doi:10.4319/lo.2005.50.5.1415

Tareq, S. M., Rahaman, M., Rikta, S., Islam, S. N., and Sultana, M. S. (2013). Seasonal Variations in Water Quality of the Ganges and Brahmaputra River, Bangladesh. *Jahangirnagar Univ. Environ. Bull.* 2, 71–82. doi:10.3329/jueb.v2i0.16332

The Himalayan Climate and Water Atlas (2015). The Ganges River Basin. Available at: https://www.grida.no/resources/6685 (Accessed November 1, 2021).

Uddin, M. J., and Jeong, Y.-K. (2021). Urban River Pollution in Bangladesh during Last 40 years: Potential Public Health and Ecological Risk, Present Policy, and Future Prospects toward Smart Water Management. *Heliyon* 7, e06107. doi:10.1016/j.heliyon.2021.e06107

Ullah, H., Islam, M. N., and Malak, M. A. (2010). Charland Dynamics of the Brahmaputra-Jamuna River in Bangladesh. *Jahangirnagar Rev. Part II: Social Sci.* XXXIV, 167–184. doi:10.13140/RG.2.1.3324.3282

Wagner, S., Riedel, T., Niggemann, J., Vähätalo, A. V., Dittmar, T., and Jaffé, R. (2015). Linking the Molecular Signature of Heteroatomic Dissolved Organic Matter to Watershed Characteristics in World Rivers. *Environ. Sci. Technol.* 49, 13798–13806. doi:10.1021/acs.est.5b00525

WHO (2004). *Guidelines for Drinking-Water Quality*. 3rd. Geneva, Switzerland.

Wu, J., Zhang, H., He, P.-J., and Shao, L.-M. (2011). Insight into the Heavy Metal Binding Potential of Dissolved Organic Matter in MSW Leachate Using EEM Quenching Combined with PARAFAC Analysis. *Water Res.* 45, 1711–1719. doi:10.1016/j.watres.2010.11.022

Wünsch, U. J., and Murphy, K. (2021). A Simple Method to Isolate Fluorescence Spectra from Small Dissolved Organic Matter Datasets. *Water Res.* 190, 116730. doi:10.1016/j.watres.2020.116730

Yang, L., Chang, S.-W., Shin, H.-S., and Hur, J. (2015). Tracking the Evolution of Stream DOM Source during Storm Events Using End Member Mixing Analysis Based on DOM Quality. *J. Hydrology* 523, 333–341. doi:10.1016/j.jhydrol.2015.01.074

Yang, L., Zhang, J., and Yang, G.-P. (2021). Mixing Behavior, Biological and Photolytic Degradation of Dissolved Organic Matter in the East China Sea and the Yellow Sea. *Sci. Total Environ.* 762, 143164. doi:10.1016/j.scitotenv.2020.143164

Zhou, Y., Martin, P., and Müller, M. (2019). Composition and Cycling of Dissolved Organic Matter from Tropical Peatlands of Coastal Sarawak, Borneo, Revealed by Fluorescence Spectroscopy and Parallel Factor Analysis. *Biogeosciences* 16, 2733–2749. doi:10.5194/bg-16-2733-2019

Conflict of Interest: The authors declare that the research was conducted in the absence of any commercial or financial relationships that could be construed as a potential conflict of interest.

Publisher's Note: All claims expressed in this article are solely those of the authors and do not necessarily represent those of their affiliated organizations, or those of the publisher, the editors, and the reviewers. Any product that may be evaluated in this article, or claim that may be made by its manufacturer, is not guaranteed or endorsed by the publisher.

frontiers | Frontiers in Environmental Science

TYPE Original Research
PUBLISHED 11 August 2022
DOI 10.3389/fenvs.2022.778544

OPEN ACCESS

EDITED BY
Oladele Ogunseitan,
University of California, Irvine,
United States

REVIEWED BY
Bodrud-Doza,
International Centre for Climate Change and Development (ICCCAD),
Bangladesh
Md. Mahbubul Hoque,
Mawlana Bhashani Science and Technology University, Bangladesh

*CORRESPONDENCE
Mir Mohammad Ali,
mir.ali@sau.edu.bd
Md. Mostafizur Rahman,
rahmanmm@juniv.edu

SPECIALTY SECTION
This article was submitted to Toxicology, Pollution and the Environment,
a section of the journal
Frontiers in Environmental Science

RECEIVED 17 September 2021
ACCEPTED 12 July 2022
PUBLISHED 11 August 2022

CITATION
Kubra K, Mondol AH, Ali MM, Palash MAU, Islam MS, Ahmed ASS, Masuda MA, Islam ARMT, Bhuyan MS, Rahman MZ and Rahman MM (2022), Pollution level of trace metals (As, Pb, Cr and Cd) in the sediment of Rupsha River, Bangladesh: Assessment of ecological and human health risks.
Front. Environ. Sci. 10:778544.
doi: 10.3389/fenvs.2022.778544

Pollution level of trace metals (As, Pb, Cr and Cd) in the sediment of Rupsha River, Bangladesh: Assessment of ecological and human health risks

Khadijatul Kubra[1], Anwar Hossain Mondol[1], Mir Mohammad Ali[2]*, Md. Amin Ullah Palash[3], Md. Saiful Islam[4], A. S. Shafiuddin Ahmed[5], Mst Antara Masuda[6], Abu Reza Md. Towfiqul Islam[7], Md. Simul Bhuyan[8], Md. Zillur Rahman[9] and Md. Mostafizur Rahman[10]*

[1]Department of Aquaculture, Patuakhali Science and Technology University, Patuakhali, Bangladesh, [2]Department of Aquaculture, Sher-e-Bangla Agricultural University, Dhaka, Bangladesh, [3]Department of Marine Biology, King Abdulaziz University, Jeddah, Saudi Arabia, [4]Department of Soil Science, Patuakhali Science and Technology University, Patuakhali, Bangladesh, [5]Department of Fisheries and Marine Science, Noakhali Science and Technology University, Noakhali, Bangladesh, [6]Department of Environmental Science, Bangladesh Agricultural University, Mymensingh, Bangladesh, [7]Department of Disaster Management, Begum Rokeya University, Rangpur, Bangladesh, [8]Institute of Marine Sciences, Faculty of Marine Sciences and Fisheries, University of Chittagong, Chittagong, Bangladesh, [9]Quality Control Laboratory, Department of Fisheries, Khulna, Bangladesh, [10]Department of Environmental Sciences, Jahangirnagar University, Dhaka, Bangladesh

The study area was selected in the Rupsha river basin and the sediment samples were collected to determine trace metal concentrations of As, Pb, Cd, and Cr along with biological effects, and potential ecological and human health hazards for adults and children. The concentrations of trace metals were detected from sixty composite sediment samples using an Atomic Absorption Spectrophotometer (AAS) following some sequential analytical procedures. The mean concentrations of trace metals were organized in the descending order of chromium (Cr) (43.2 mg/kg) > lead (Pb) (29.21 mg/kg) > arsenic (As) (5.18 mg/kg) > cadmium (Cd) (1.8 mg/kg). The current study highlighted that metals were attributed to the riverine sediments from natural sources and other anthropogenic sources, particularly from various industries. Based on the effect-range classifications of threshold effect concentration (TEC) and probable effect concentration (PEC), the trace metal concentrations can impact on the sediment-dwelling organisms occasionally especially for Cr, Cd, and Pb. That is, the concentrations had negative biological consequences on aquatic creatures. The assessed potential ecological risk of Cd offers a significant risk to the aquatic ecosystem, whereas As, Cr, and Cd were in low-risk. Most of the sites of the study area were within the range of moderate risk, indicated by the risk index (RI) values. Furthermore, the applied sediment quality indices, geo-accumulation index (I_{geo}) indicated that sediment was contaminated by Cd whereas contamination factor (CF)

denoted that the sediment of the study area was moderately polluted by Pb. However, pollution load index (PLI) revealed that the study area was polluted for cumulative sence especially in winter season. The age-group risk index (HI) was much lower than the threshold limit of 1, showing that the pollution had no non-carcinogenic risk effect. Total carcinogenic risk (TCR) was less than one-tenth of a percentile. For the sake of human and environmental health, proper monitoring of metal element attribution and strict regulation are required to lessen trace metal pollution.

KEYWORDS

trace metals, biological effects, ecological risk, human health risk, rupsha river

Introduction

Because of the toxicity and persistence in the environment, heavy metal pollution has become a global, regional, and local concern (Ahmed et al., 2020; Islam A et al., 2020; Khan et al., 2020; Babu et al., 2021; Kumar et al., 2021; Ali et al., 2022). The aquatic ecology is effected by the various toxic trace metals as most of them are long-persistent, bio-accumulative character and non-biodegradable in nature (Bhuyan et al., 2017; Ali et al., 2018; Bhuyan et al., 2019). Many anthropogenic actions released heavy metals into the aquatic habitats directly or indirectly and these metals are carried *via* the water column, deposited in sediment, and biomagnified through the food chain (Kahal et al., 2020; Ali et al., 2022), resulting from a considerable risk to benthic invertebrates, fish and humans (Ali et al., 2016; Islam et al., 2016; Ali et al., 2018, Shen et al., 2019; Shaheen et al., 2019; Ali et al., 2020a, b).

In a riverine ecosystem, the concentration of HM in sediment is thought to be an indicator of monitoring the environmental conditions and pollution status (Han et al., 2018; Rahman et al., 2019; Hossain et al., 2021; Ali et al., 2022). As metals tend to accumulate in the bottom layers of riverine water bodies, heavy metals are much higher in sediment than in the water column (Bhuyan et al., 2017; Islam et al., 2021; Jolly et al., 2021). Heavy metals are not permanently attached to sediments, and they can be released into the water column due to the change in environmental circumstances such as temperature and pH, or other physical or biological disturbances (Agarwal et al., 2005). A lower concentration of HMs is necessary for organism survival, whereas higher concentrations are poisonous and adversely impact organisms (Fu and Wang 2011; Ahmed et al., 2020). Thus, the monitoring of sediment provides valuable information on a variety of pollution indicators.

Different sediment quality indicators can be used to determine the extent of contamination and the biological characteristics of sediment in any aquatic ecosystem (Ganugapenta et al., 2018). For pollution control, it is important to understand the origins of pollutants in sediments of the aquatic environments. Multivariate statistical approaches, such as Pearson correlation analysis, principal components analysis (PCA), and cluster analysis, are considered to be practical tools for identifying pollution sources and have been successfully used in several studies on heavy metal pollution in sediments (Larrose et al., 2010; Bai et al., 2011; Yi et al., 2011; Chabukdhara and Nema 2012). Analysis of toxic elements in riverine sediment is essential for environmental contamination assessment (Ali et al., 2018). Heavy metals in sediments pose distinct ecological risks to different receptors. The possible harmful impacts of heavy metals on sediment-dwelling organisms in freshwater systems have been assessed using the criteria in sediment quality guidelines (SQGs) (Persaud et al., 1993; Ingersoll et al., 1996; Smith et al., 1996; MacDonald et al., 2000). Few SQGs, on the other hand, have been conducted to assess the negative impacts of heavy metals in sediment on higher trophic levels (fish or other species) (Bhavsar et al., 2010). Hakanson (1980) proposed a prospective ecological risk index based on heavy metal concentrations in sediment, the simplest and most widely used method for ecological risk assessment of the sediment.

Metal contamination has become a major problem in many rapidly developing countries (Ali et al., 2016; Bhuyan et al., 2019; Jolly et al., 2021; Rahman et al., 2021). Especially, in developing country people like Bangladesh, human healths are suffering from various diseases due to the contact of the toxic metals (Islam et al., 2016; Rehman et al., 2018). Many industries dump their untreated agricultural and chemical effluents into rivers directly. The water from these rivers and their tributaries and distributaries is used to irrigate agricultural lands for crop production (Ali et al., 2016; Islam et al., 2016; Ali et al., 2020a). The Rupsha River is an ecologically and economically significant urban river. Since, Rupsha River is being considered as the most important river for fish production. Moreover, various native crops were cultivated near the river bank employing different agricultural chemicals and fertilizers. Still, the bio-magnifications of HMs in fish species from water and sediments of this river may cause harmful effects to humans. Moreover, some studies like Jiménez-Oyola et al. (2021), Islam et al. (2014), Ali et al. (2022), Duodu et al. (2016), Jiang et al. (2013) and Abdelhafez & Li. (2015) investigated metal concentration level along with the ecological, biological

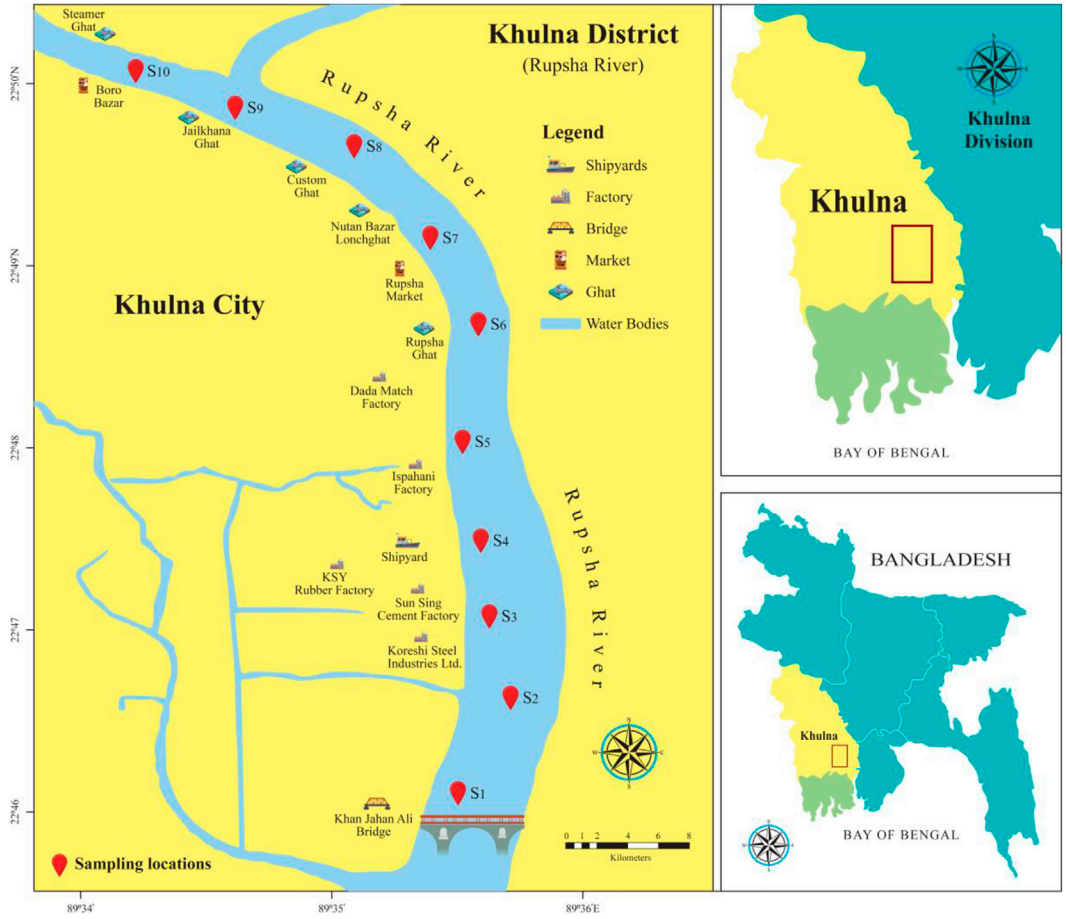

FIGURE 1
Map of the study area indicates the Rupsha River located south-western part of Bangladesh.

and provable human health risk near different river basins. Unfortunately, there is no critical information about the research area's including all the issues above due to the trace metal pollution has been determined. As a result, the current study focused on several crucial objectives, including determining the trace metals (As, Pb, Cr, and Cd) contamination in the sediment using several geochemical pollution indices and identifying the major sources of the specified metals. Finally, the potential ecological and biological consequences of these metals were assessed to determine the risks to adult's and children's health. The novel aspect of this work is that it is the inclusive investigation on riverine sediments pollution by heavy metals causing ecological and human health risks in the south-western area of Bangladesh. Also, the study will provide the relevant information which will help to introduce some actions plans regarding the surrounding environment of the Rupsha River.

Materials and methods

Study area

The present study was conducted in ten (10) sampling sites of the Rupsha River (Figure 1). Rupsha River is one of the important rivers in the South-west region of Bangladesh. It is formed as a result of the union of the Bhairab and Atrai rivers. Natural disasters like the destruction of spawning ground by ox-bow cutting (U-shaped lake that forms when a wide meander of a river is cut off, creating a free-standing body of water), massive quarry of sands from river bed illegally removed by a section of unscrupulous traders, pollution by industrial waste, unplanned construction sluice gates for irrigation purpose and indiscriminate catching and killing of the brood fishes have posed a serious threat to the biodiversity of Rupsha River.

Geographical layout

The Rupsha River is a Ganges distributary located in southwestern Bangladesh. It is formed when the Bhairab and Madhumati rivers meet and flow into the Pashur River. The tides have an impact on the entire length of it. It flows beside Khulna and links to the Bay of Bengal at Mongla channel *via* the Pashur River. It changes its name to Pashur River at Chalna and drains into the Bay of Bengal (Saran et al., 2018). This river has an average width of 486 m, with maximum and minimum widths of 650 and 322 m, respectively (Saran et al., 2018). This river's bank is home to many fisheries, dockyards, shipyards, and manufacturers. Many companies have sprouted near the Rupsha River. The Bangladeshi Department of Environment has designated this area as the country's most polluted hotspot (Department of Environment, 2001). Glass and plastic industries, chemical complexes, fish processing plants, steel mills, paper mill complexes, rayon mill complexes, cement factories, paint and dye manufacturing plants, several soaps and detergent factories, and many light industrial units, as well as wastes from brickyards and agricultural runoff, discharge untreated toxic effluent directly. Sewage and municipal wastes and undesirable residues mixed with $Fe_2O_3.2H_2O$ as a result of shipbreaking yard activities are released immediately. These enterprises dump around 4,500 m^3/ha of wastewater into the Rupsha River, which flows into the Sundarbans *via* the Bhairab-Rupsha River system (Department of Environment, 2001; Samad et al., 2015).

Sample collection and preservation

Sampling was carried out from August 2018 to February 2019, considering the winter and summer seasons by maintaining standard protocol (U.S Environmental Protection Agency [USEPA], 2001). The present study selected ten stations of the Rupsha River (Figure 1) based upon human activities such as fish farming, the geographical proximity of industrial and urban discharge of effluents, and dredging of the river for sand mining. Composite surface sediment samples were collected from different points of Rupsha River at a depth of 0–5 cm by Ekman dredge and kept in fresh plastic packets. Each sediment sample was taken at each sampling point by mixing randomly collected sediments (3 times) and sixty composite sediment samples were collected. After collection, sediment was placed in a separate cleaned with distilled water airtight polythene bag, sealed, labeled, packed, and transported to the Govt.-MoFL's Quality Control (QC) Laboratory in Khulna, Bangladesh laboratory testing. The samples were dried in an oven at 45°C for 48 h to gain constant weight (Islam et al., 2015b). The dried mass of each sample was then pulverized to fine powder using a mortar and pestle, sieved through 106 μm apertures and preserved in a plastic vial with the identification mark inside a desiccator (Islam et al., 2015b). Finally, a pellet maker used the homogeneous powder to prepare the pellet using 10-ton pressure (or elemental analysis (Hossain M. B. et al., 2020) using a tool, Specac, United Kingdom.

Sample digestion

In a 100 ml beaker, a 2 g sediment sample was placed, and 15 ml of ultrapure HNO_3 was added. The contents were cooked for 5 h at 130°C, or only 2–3 ml remained. Materials were passed through Whatman 41 filter paper after digestion (colorless or weak color of content), rinsed with 0.1 M HNO_3 solution, and produced up to 100 ml volume for metal analysis (Ali et al., 2021).

Analytical technique and accuracy check

An atomic absorption spectrophotometer (Model ZEEnit700P# 150Z7P0110, Analytikjena, Germany) was used to test all samples for As, Pb, Cr, and Cd. All of the procedures were validated in-house following EC567/2002 (Ali et al., 2022). ST 1 summarizes the analytical conditions for measuring heavy metals in samples using AAS. The instrument calibration standards were created using Sigma Aldrich's (Switzerland) diluting standard (1,000 ppm). Dry weight sediment data were recorded as mg/kg. Throughout the experiment, de-ionized ultrapure (0.05 s) water was used. Before usage, all glassware and containers were carefully cleaned with 20% nitric acid, then rinsed multiple times with De-ionized ultrapure water and oven-dried. DORM-4, a verified reference material, was used to check the analytical method. The National Research Council of Canada prepared and supplied these sediment samples. The certified and observed values were found to be in good agreement. As shown in ST 2, the standard deviations of the averages for the reported certified materials were 0.65–8%, and the percentage recovery was 89–99%.

Assessment of sediment contamination

The selection of background values is critical in the interpretation of geochemical data. As reference baselines, Olivares-Rieumont et al. (2005), Pekey (2006), and Singh et al. (2005) employed the average shale values or average crustal abundance data. The best alternative is to compare quantities between contaminated and uncontaminated sediments that are mineralogically and texturally comparable (Rubio et al., 2000; Sakan et al., 2009). Because no background concentrations for the analyzed Rupsha River sediment from nearby locations were available, the background values in this

TABLE 1 Classifications of the geoaccumulation index grade ro sediment quality assessment.

Classification	Contamination degree	References
$I_{geo} < 0$	Practically uncontaminated	Müller (1981)
$0 \leq I_{geo} < 1$	Uncontaminated to moderately contaminated	
$1 \leq I_{geo} < 2$	Moderately contaminated	
$2 \leq I_{geo} < 3$	Moderately to heavily contaminated	
$3 \leq I_{geo} < 4$	Heavily contaminated	
$4 \leq I_{geo} < 5$	Heavily to extremely contaminated	
$I_{geo} \geq 5$	Extremely contaminated	

paper were estimated using the mean heavy metal concentrations in uncontaminated sediments from the study area. The enrichment factor and Geo-accumulation index were employed to determine the degree of heavy metal pollution in Rupsha River sediments.

Sediment quality guidelines

This study employed consensus-based sediment-quality guidelines (SQGs) to assess the potential danger of heavy metal contamination in the study area's sediments (Ahmed et al., 2019a). The consensus-based SQGs were created using published sediment-quality criteria that were derived using many methods (Feng et al., 2011). A threshold effect concentration (TEC) below which harmful effects are unlikely to occur and a probable effect concentration (PEC) above which adverse effects are likely to occur more frequently than not are included in these synthesis guidelines (Long et al., 1995; MacDonald et al., 2000).

Geoaccumulation index (Igeo)

Geoaccumulation index (Igeo) is a quantitave measurement of the degree of contamination of sediment was introduced by Muller (1969) (Hossain et al., 2019). It is actually based on the background concentration of a particular metal element (Milićević et al., 2017) The following equation defines the geoaccumulation index (I_{geo}):

$$I_{geo} = Log_2\left[\frac{Cm}{1.5BAn}\right]$$

Where, Cn denotes the metal concentration in sediment samples and BAn denotes the metal's geochemical background concentration (n). Due to lithospheric influences, the background matrix correction factor is 1.5. Müller (1981) defined seven classifications in the geoaccumulation index (Table 1).

Contamination factor (CF) and pollution index (PLI)

To assess contamination in the study region, the contamination factor (CF) is used (Wang et al., 2007; Kadhum et al., 2016). PLI was used as a quick and simple means to determine the sediment quality in the research region (Jolly et al., 2021).

$$CF = Cn_{(Sample)} \Big/ Bn_{(Shale)}$$

$$\text{PLI} = (\text{CF1} \times \text{CF2} \times \text{CF3} \times \ldots \times \text{CFn})^{1/n}$$

Divide the concentration of each metal in sediments by the background level to get the CF value (Hakanson 1980; Ali et al., 2016). For PLI, 'n' is the total number of element. CF < 1: Low contamination; 1 ≤ CF < 3: Moderate contamination; 3 ≤ CF < 6: Considerable contamination, CF ≥ 6: Very high pollution (Turekian and Wedepohl 1961; Hakanson 1980; Loska et al., 1997) And PLI = 0: perfect quality, PLI < 1: No pollution; PLI > 1: Polluted.

Evaluation of potential ecological risk

Hakanson (1980) developed a system for assessing ecological risks in the context of heavy metals pollution. However, the assumption of an aquatic environment's sensitivity is dependent on its productivity, which may also be assessed using the approach. In addition, the possible ecological risk index (RI) was created to quantify the severity of sediment pollution (Liu et al., 2018). By combining ecological and environmental consequences with toxicological, the index allows for a more accurate assessment of heavy metal contamination's possible ecological risk factor (Bi et al., 2018). The employed formula is as follows:

$$E_r^i = T_r^i \times CF$$

$$C_f^i = C_n^i / C_o^i$$

$$RI = \sum_{i=1}^{n} E_r^i$$

Where, RI is the sum of all heavy metal risk aspects in sediment, E_r^i is the monomial potential ecological risk factor, T_r^i is the toxic response factor for selective elements that are responsible for the poisonous and sensitive requirement, and the values of As, Cr, Hg, and U correspond to 10, 2, 40, and 42, respectively (Yu et al., 2010); C_f^i is the monomial contamination factor; C_n^i is the metal subject in the sediment, and C_o^i is a background value of each element. The potential ecological risk index (RI) of the sediment can be divided into the following categories: $E_r^i < 30$, $R_I < 100$: Low risk; $30 \leq E_r^i < 50$, $100 \leq R_I < 150$: Moderate risk; $50 \leq E_r^i < 100$, $150 \leq R_I < 250$: Considerable risk; $100 \leq E_r^i < 150$, $200 \leq R_I < 350$: Very high risk; $E_r^i > 150$, $R_I > 350$: Disastrous risk (Hakanson 1980; Zhao et al., 2016; Kusin et al., 2018).

Human health risk assessment

Chronic daily intake (CDI) was used to assess the risk of human health from exposure to the trace metals found in the sediment as well as soil (Hu et al., 2017). CDIs can be evaluated for the following routes since humans can uptake metal contents through three methods (inhalation, cutaneous contact, and ingestion) (USEPA 2011; Kusin et al., 2018; Ali et al., 2020a, 2022):

$$CDI\ (for\ inhalation) = \frac{PM \times CS \times ET \times EF \times IR_{air} \times ED}{BW \times PEF \times AT}$$

$$CDI\ (for\ dermal\ contact) = \frac{CS \times SA \times AF \times EF \times ED \times ABS}{BW \times AT \times 10^6}$$

$$CDI\ (for\ ingestion) = \frac{CS \times EF \times ED \times IRS}{BW \times AT \times 10^6}$$

where CS is the trace metal concentration in the soil; PM is the ambient particulate material of the desired area (0.146 mg/kg) (Shen et al., 2019); ET is the exposure frequency of 24 h/d; EF is the exposure frequency 350 d/a (USEPA 2011); IR_{air} is the inhalation rate of air (20 m^3/d) (USEPA, 2002); ED is the exposure duration, which is 30 years (USEPA 2011); BW is body weight: 70 kg for adult and 15 kg for children (USEPA 2002); PEF is the particle emission factor 1.36×10^9 m^3/kg (USEPA 2002); AT is the average time for non-carcinogenic substance: 365× ED d (USEPA 2011); AT is the average time for carcinogen substance: 365× 70 d (USEPA 2011); SA is the skin surface area for soil contact exposure: 5,700 cm^2/d (adult) and 2,800 cm^2/d (child) (USEPA 2011); AF is the adherence factor of soil: 0.07 mg/cm^2 (adult), 0.2 mg/cm^2 (child) (USEPA 2011); 10^6 was used as a conversion factor to convert from kg to mg; ABS is a fraction of dermal absorption at 0.03 (for As) and 0.001 (for others) (USEPA 2011); and IRS is the ingestion rate: 100 mg/d (USEPA 2011; Liu et al., 2018).

Non-carcinogenic risk assessment

Due to varying exposures to an individual's metal contents, HQ was determined to determine HI as the non-carcinogenic risk for a given element. The ratio of CDI (mg/kg/d) to reference dose (mg/kg/day) was used to compute HQ (USEPA 1989). The HQ and HI assessment equations are as follows (USEPA 2000):

$$HQ = \frac{CDI}{RfD}$$

$$HI = \sum_{i=1}^{n} HQ_k = HQ_{inhalation} + HQ_{dermal} + HQ_{ingestion}$$

RfD values (mg/kg/day) for various elements, as well as their exposure pathways (USEPA 2011): As (3.00E-04), Pb (3.5E-03), Cr (3.00E-03), Cd (1.00E-03), and Hg (3.00E-04) (JECFA 1993) (3.00E-04). There is no way to mitigate the non-carcinogenic effect, the result of HI > 1 indicates that humans may be exposed to it (Saha et al., 2016; Zhao et al., 2018).

Carcinogenic risk assessment

The lifetime carcinogenic risk (CR) exposure for each pathway was calculated using the cancer risk factor (CSF) of the individual metal content (USEPA 2000; Fantke et al., 2012). CSFs of As, Cr, and Cd are 1.5 mg/kg/day (USEPA 2002), 0.5 mg/kg/day (Cancer IAfRo 2011), and 15 mg/kg/day (Cancer IAfRo 2011) respectively. The following equation can be used to calculate CR:

$$CR_i = CSF_i \times CDI_i$$

$$CR = \sum_{i=1}^{n} CR_i$$

The acceptable lifetime CR limit is between 10^{-6} and 10^{-4} (USEPA 2002; FAO 2014; Yin et al., 2015). A value greater than 10^{-5} indicates that an individual's cancer progression would be greater than 1 in 100,000 (Ahmed et al., 2019b; Traina et al., 2019).

Statistical analyses

To determine the data distribution, the Kolmogorov-Smirnov and Shapiro-Wilk tests were used to avoid difficulties like normal/non-normal data dispersion. Correlation analysis was used to evaluate relationships among the variables under consideration, with statistical significance set at $p \leq 0.05$. Cluster analysis (CA), an unsupervised pattern recognition technique, reveals the intrinsic structure of a data set without making a prior assumption about the data, allowing the system's objects to be classified or clusters based on their proximity or similarity (Varol and Sen 2009). Clusters are produced progressively by starting with the most similar pair of items and constructing higher clusters in a step-by-step method in hierarchical clustering, which is the most frequent approach. A "distance" can be expressed by the "difference" between analytical values from

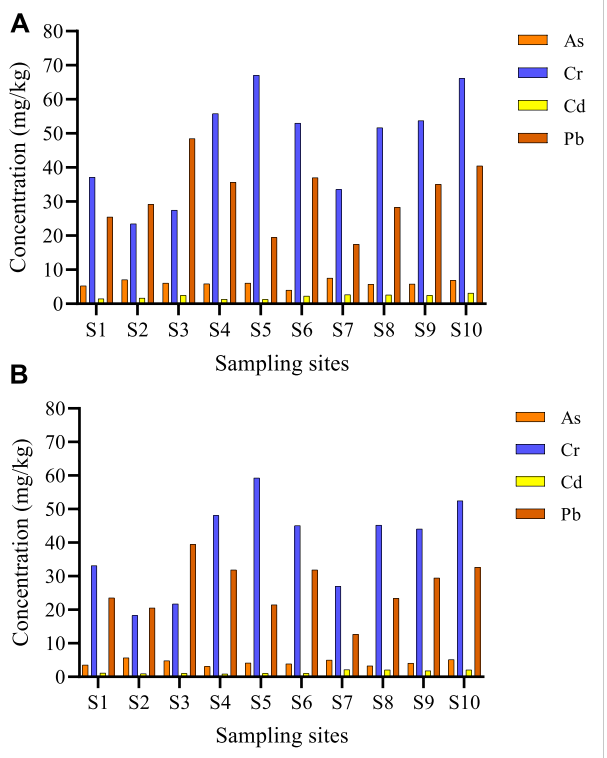

FIGURE 2
Heavy metals concentrations in sediment in the winter **(A)** and summer **(B)** seasons.

both samples, and the Euclidean distance usually gives similarities between two samples (Otto 1998). Using Ward's technique and Euclidean distances as a measure of similarity, hierarchical agglomerative CA was done on the normalized data set in this work (Ward, 1963). This method evaluates cluster distances using analysis of variance while seeking to minimize the sum of squares of any two clusters that can be constructed at each step. As a way to standardize the linkage distance represented on the *y*-axis, the linkage distance is reported as Dlink/Dmax, which means the quotient between the linkage distances for a particular case divided by the maximal distance, multiplied by 100 (Simeonov et al., 2000; Shrestha and Kazama 2007; Varol and Sen 2009).

Results and discussion

Charecterization of seasonal variation of heavy metals

In the summer and winter, heavy metals (As, Cr, Cd, and Pb) were measured in the Rupsha River's surface sediments and data are shown in Figures 2A,B. Metal concentrations in sediment were higher in the winter than in the summer due to lower water flow, presumably helping accumulate heavy metals in sediment (Bhuyan M. and Bakar M., 2017; Ali et al., 2020a; 2021; Islam M et al., 2020). In Bangladesh, there is no rainfall during the winter season is lower water flow in the river basin and the industrial operation is increased during the winter season. Meanwhile, higher industrial/agricultural activities cause excess levels of metals in river sediment. The average concentration of heavy metals in sediments was in the decreasing order of Cr > Pb > As > Cd for both the summer and winter seasons (Table 2).

Arsenic

Heavy metal concentrations and sources are being determined. As is a naturally occurring element in Bangladesh causes poisoning over a short period of exposure. Total arsenic concentrations in uncontaminated nearshore marine and estuarine sediments ranged from 5.0 to 15 mg/kg dry weight. The average concentration of arsenic in deep-sea sediments was found 40 mg/kg (Moore and Ramamoorthy 2012). Arsenic concentrations in river sediments in England and Wales ranged from 7 to 950 mg/kg (Langston 1980). Metal concentrations in sediments from estuaries receiving drainage from metal-mining areas could be much higher. It also has long-term effects on the human body, such as congenital disabilities, reproductive problems, and skin and vascular illnesses, all of which can lead to cancer (Bhuyan M. S. and Bakar M. A., 2017; Bhuyan et al., 2019; Ali et al., 2020a, 2022). The highest concentration of As was found 7.58 mg/kg and the lowest level was observed 3.12 mg/kg, respectively. The maximum concentration (7.58 mg/kg) was identified at site 7 during the winter, while the lowest concentration (3.12 mg/kg) was recorded at site 4 during the summer (Figure 3). At the Feni River Estuary, found 0.85 mg/kg (Table 2). This result is lower than that of the current study. Magesh et al. (2013) observed As levels 7.30, 5.06 and 5.69 mg/kg at Korampallam Creek, Punnakayal Estuary, and Kallar Estuary. The findings were likewise somewhat similar to those of the current study. Ali et al. (2018) found almost identical results in the Pasur River, Bangladesh (Table 2).

Chromium

Chromium (Cr) compounds are potent oxidizers that are irritating and corrosive, making them appear more dangerous (Rahman et al., 2012). In our study, Cr concentrations ranged from 18.67–67.12 mg/kg, with a mean value of 43.2 mg/kg. During the winter, the maximum level of 67.12 mg/kg was reported at site 5 (Figure 2A). During the summer, a minimum of 18.67 mg/kg was recorded at site 2 (Figure 2B). The metal concentration levels at all of the sites were higher than the WHO (2004), USEPA (1999, 2004), and Ayers and Westcot.

TABLE 2 Metal concentrations (mg/kg) in the estuary and coastal sediment from throughout the world are compared.

Location	As	Cr	Cd	Pb	Country	References
National						
Rupsha River	5.18	43.2	1.8	29.21	Bangladesh	**Present study**
Bhairab River	3.68	31.74	1.44	23.82	Bangladesh	Ali et al. (2022)
Kutubdia Channel	9.0	11.0	—	22.0	Bangladesh	Hossain et al. (2020b)
Feni River Estuary	0.85	35.28	—	6.47	Bangladesh	Islam et al. (2018)
Pasur River	3.15–19.9	20.67–83.7	0.39–3.17	7.34–55.32	Bangladesh	Ali et al. (2018)
Karnaphuli River	81.09	20.3	—	43.69	Bangladesh	Ali et al. (2016)
Karnaphuli River	—	0.76	0.24	4.96	Bangladesh	Islam et al. (2013)
Karnaphuli River	—	28.17	—	15.49	Bangladesh	Mamun et al., 2013
Karnaphuli River coast	—	-	0.43	26.7	Bangladesh	Siddique and Aktar, (2012)
Passur river	—	2.80–31.90	0.80–2.70	5.33–18.42	Bangladesh	Rahman et al. (2011)
Matamuhuri River	—	—	—	26.42	Bangladesh	Ashraful et al. (2009)
Moheshkhali River	—	—	—	49.22	Bangladesh	Ashraful et al. (2009)
Bakkhali River	—	—	—	3.12	Bangladesh	Ashraful et al. (2009)
International						
Yangtze River Estuary	—	34.4	0.13	25.8	China	Fan et al. (2020)
Yangtze River Estuary	—	69.5–103	0.037–0.212	13.7–23	China	Wang et al. (2020)
Kallar Estuary	7.30	10.12	3.61	29.11	India	Magesh et al. (2013)
Korampallam Creek	5.06	26.85	5.29	67.38	India	Magesh et al. (2013)
Punnakayal Estuary	5.69	9.34	10.40	28.13	India	Magesh et al. (2013)
Ennmore coast	—	148.6–243.2	4.6–7.5	24.9–40	India	Raj and Jayaprakash, (2008)
Vellar estuary	—	38	7	6	India	Ramanathan et al. (1999)
Pichavaram mangrove	—	141.2	6.60	11.2	India	Ramanathan et al. (1999)
Coleroon Estuary	—	49.6	8.60	4.60	India	Ramanathan et al. (1999)
Boston Harbor	—	231.5	—	135	United States	Bothner et al. (1998)
Tokyo Bay	—	77.3	0.996	50.68	Japan	Fukushima et al. (1992)
World Average		100		150		Venkatramanan et al. (2015)
Average Shale	13	90		20		Turekian and Wedepohl (1961)
Sediment Quality Guidelines (Effect range Low)	8.2	81		47		Long et al. (1995)
Sediment Quality Guidelines (Effect range medium)	70	370		220		Long et al. (1995)
Guideline						
USEPA (2006)	6	26	—	31		
USEPA (1999)	—	25	0.6	40		
WHO (2004)	—	25	6	—		
Ayers and Westcot. (1985)	—	0.1	—	5		

(1985) recommended levels (Table 2). At the Kutubdia Channel, Hossain M. B. et al. (2020) found a much lower level (11.0 mg/kg) (Table 2). In the Feni River Estuary, Karnaphuli River and Bhairab River, Islam et al. (2018), Ali et al. (2016, 2022), Islam et al. (2013), and Mamun et al. (2013) found lower levels of As. At the Yangtze River Estuary in China, Fan et al. (2020) found 34.4 mg/kg. At the Kallar Estuary, Korampallam Creek, and Punnakayal Estuary, Magesh et al. (2013) found 10.12 mg/kg, 26.85 mg/kg, and 9.34 mg/kg, respectively. The lower level of Cr in the Vellar estuary, India, was found by Ramanathan et al. (1999) (Table 2).

Cadmium

The average Cd concentration in the summer was 1.45 mg/kg, whereas 2.18 mg/kg in the winter (Figures 2A,B). The average concentration of Cd was 1.8 mg/kg on. The current findings are noted as exceeding the USEPA's (1999)

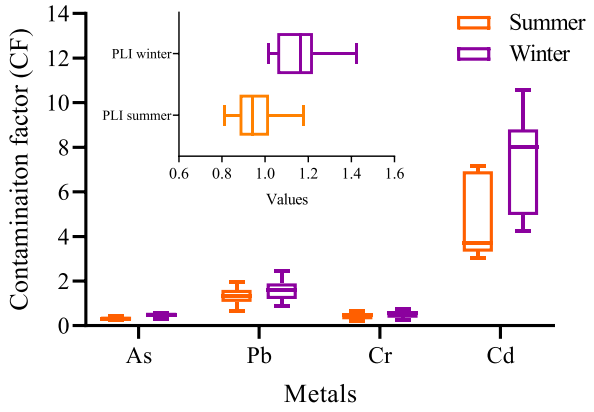

FIGURE 3
Contamination factor (CF) and pollution load index (PLI) in the sediment of the Rupsha River.

recommended limit. Cd concentrations were high throughout the winter, which could be linked to variations in water capacity in the study area, where restricted water flow caused Cd precipitation in sediment, elevating its concentration (Ali et al., 2016). In the Pasur River and Bhairab River, Ali et al. (2018) and Ali et al. (2022) found 0.39–3.17 and 1.41–1.92 mg/kg Cd respectively (Table 2). In the Karnaphuli River, Islam et al. (2013) and Siddique and Aktar (2012) found 0.24 mg/kg and 0.43 mg/kg Cd, respectively. Cd levels in the Passur river varied from 0.80 to 2.70 mg/kg, according to Rahman et al. (2011). In the Yangtze River Estuary, China, Fan et al. (2020) and Wang et al. (2020) found decreased levels of Cd. In Tokyo Bay, Japan, Fukushima et al. (1992) found 0.996 mg/kg Cd. Magesh et al. (2013) found greater levels of Cd than the current findings in the Kallar Estuary, Korampallam Creek, and Punnakayal Estuary. In India, Ramanathan et al. (1999) found high levels of Cd in the Vellar estuary, the Pichavaram mangrove, and the Coleroon Estuary (Table 2).

Lead

Lead (Pb) is a non-essential metal that causes neurotoxicity and nephrotoxicity in humans (Garca-Lestón et al., 2010). The mean Pb concentration was 29.21 mg/kg during the winter, with the maximum value being 48.52 mg/kg at site 3 (Figure 2A). The lowest concentration of 12.69 mg/kg was recorded during the summer season at site 7 (Figure 2B). In the Kutubdia Channel, Bangladesh, Hossain M. S. et al. (2020) found 22.0 mg/kg Pb. About 23.82 mg/kg, 6.47 mg/kg, 4.96 mg/kg, 15.49 mg/kg, 26.7 mg/kg, 26.42 mg/kg, and 3.12 mg/kg were found in the Bhairab River, Feni River Estuary, Karnaphuli River, Matamuhuri River, and Bakkhali River, respectively, by Ali et al. (2021), Islam et al. (2018), Islam et al. (2013), Mamun et al. (2013), Siddique and Aktar (2012), Ashraful et al. (2009). These results were lower than those found in the current study. In the Yangtze River Estuary, China, Fan et al. (2020) and Wang et al. (2020) reported decreased levels of Cd (Table 2). Magesh et al. (2013) found reduced Pb levels in the Kallar and Punnakayal Estuaries in India. The value of Cd observed in this study was higher than that found by Ramanathan et al. (1999) in India's Vellar estuary, Pichavaram mangrove, and Coleroon Estuary. Bothner et al. (1998) and Ali et al. (2016) found a greater concentration of Cd in Boston Harbor and Karnaphuli River than in the current research (Table 2).

Assessment of biological effect through SQGs

The ecotoxicological sensibility of the contaminants and the identification of metal components in an aquatic environment were assessed using sediment quality guidelines (SQGs) (Kumwimba et al., 2016). The SQGs were consensus-based assessments expressed in TEC, PEC, and ASV (Table 2). Cr metal had the highest TEC (43.40) while Pb had the highest level of PEC (128). The evaluation method, protection level connected to sediment characteristics such as TOC, pH, acid-volatile sulfide (AVS), and screening of important environmental elements are all aspects that contribute to the difference of findings in different sites (Chen et al., 2005; Ahmed et al., 2019a). These characteristics can make the usage of SQGs and their development more difficult (Gao et al., 2015). In our study area, 100% of the samples were below TEC limit for As in both summer and winter seasons. However, it was 60, 80, and 10% in summer and 60% 100%, and 30% in winter season for Cr, Cd, and Pb respectively, remained in the TEC-PEC range. Hence, the findings indicated tha the research area could be occasionally and directly influenced by anthropogenic activity. Furthermore, SQG evaluations revealed that pollutants in river sediment constitute major ecological harm to sediment-dwelling organisms. In comparison, our findings were similar to those of Wu et al. (2014). They observed that the sediment-dwelling organisms in the Baihua and Hongfeng reservoirs posed a moderate toxicological risk due to heavy metals exposure. However, to correctly assess the current condition of trace metal contamination, numerous developed geochemical indices must be evaluated (Siddique et al., 2020).

Geoaccumulation index (I_{geo})

I_{geo} is a critical ecological index for distinguishing between natural and human-caused metal sources and determining the level of contamination in sediment samples. The contamination of the HMs in the research region was delineated in the following order: Cd > Pb > Cr > As, based on average Igeo values. Cd (1.89), had the highest I_{geo} value, while Cr had the lowest (-1.96).

TABLE 3 I_{geo} values of the metal contents in the sediment of the Rupsha River, Bangladesh.

Sites	Summer				Winter			
	As	Pb	Cr	Cd	As	Pb	Cr	Cd
S1	−2.45	−0.35	−2.02	1.40	−1.88	−0.24	−1.86	1.76
S2	−1.78	−0.55	−2.89	1.08	−1.45	−0.04	−2.52	1.94
S3	−2.01	0.40	−2.63	1.19	−1.67	0.69	−2.29	2.48
S4	−2.64	0.09	−1.49	1.02	−1.72	0.25	−1.27	1.63
S5	−2.23	−0.48	−1.19	1.17	−1.67	−0.62	−1.01	1.51
S6	−2.33	0.09	−1.58	1.19	−2.26	0.30	−1.35	2.35
S7	−1.96	−1.24	−2.32	2.26	−1.36	−0.78	−2.01	2.60
S8	−2.55	−0.36	−1.58	2.20	−1.76	−0.08	−1.39	2.54
S9	−2.26	−0.02	−1.61	2.01	−1.74	0.23	−1.33	2.48
S10	−1.92	0.12	−1.36	2.22	−1.50	0.43	−1.03	2.82
Min	−2.64	−1.24	−2.89	1.02	−2.26	−0.78	−2.52	1.51
Max	−1.78	0.40	−1.19	2.26	−1.36	0.69	−1.01	2.82
Average	−2.21	−0.23	−1.87	1.57	−1.70	0.02	−1.61	2.21

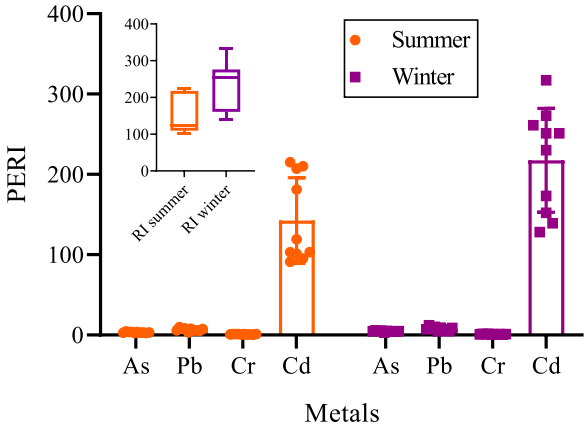

FIGURE 4
Potential ecological risk index (PERI) in the sediment of the Rupsha River.

Cd was found to be "moderately contaminated" at the sample site, while Pb, As, and Cr was found to be "least contaminated" (Table 3). Furthermore, a minor difference was observed among the metals in sampling sites due to the change of metal concentrations. All of the I_{geo} values of As, Pb, Cr, and Cd in the sampling area were found to be less contaminated, according to the findings. However, Ke et al. (2017) found that the I_{geo} values in the Liaohe River protected area were classified as highly contaminated. In addition, Mohiuddin et al. (2011) conducted a study on the Turag river, finding that I_{geo} values for Pb and Cu remained in the unpolluted category. The main explanation for this was that the attribution of metals in the Liaohe and Turag rivers was much higher than in our study sites.

Contamination factor and pollution load index

The CF values of the metals are shown in Figure 3, and they can be sorted in the following order: As varies from 0.33 to 0.45 (mean 0.39); Pb ranges from 1.34 to 1.59 (mean 1.47); Cr varies from 0.44 to 0.52 (mean 0.48), and Cd ranges from 4.75 to 7.25 (mean 6.0). The CF value of Cd indicated that there was significant contamination. According to the CF value, sediments of the study river were moderately polluted with Pb. CF values of As and Cr were found to be less than 1, indicating low contamination. The CF value was higher in the winter than in the summer. Islam et al. (2015a) and Ali et al. (2016, 2022) found similar results in a Bangladeshi urban river. According to the research, domestic wastewater drainage, industrial effluents, municipal runoffs, and atmospheric deposition are the main sources of the observed higher levels of metals in the surface sediment (Ali et al., 2020a). Hassan et al. (2015) conducted a study in the Meghna river, and their findings were identical to those of the current study.

The PLI can provide information about sediment quality to the general public. It also provides decision-makers with critical information on the state of pollution in the research area (Suresh et al., 2012). The pollution load index (PLI) values for metals in sediments are reported in Figure 3 (inside). If the PLI score is larger than one, the tested region is entirely polluted, according to. PLI values ranged from 1.01 to 1.42 at all sampling sites in the winter, indicating that the sediment in the study river was polluted (PLI > 1). Except at sites 8, 9, and 10, the PLI fell below 1 in the summer. In all sampling locations, PLI values are more than unity, owing to the impact of municipal and other industrial activity in these areas.

Potential ecological risk index

The PERI was assessed using a monomial ecological risk model and specific features that highlighted the cumulative ecological-toxicological effects of numerous contaminants in the aquatic environment (Karydas et al., 2015). In both the summer and winter seasons, Cd's monomial potential ecological risk assessment was determined at a higher level. At all of the sites, the PERI value for Cd exceeded the allowed limit. The PERI score ranged from 160 to 320, indicating a significant risk posed by Cd in the study area (Figure 4). Pb and Cr were determined to be in a low-risk status. Sites were organized in descending order based on the RI values for all cumulative metal concentrations: S4 > S2> S5 >S6 > S3 > S1 > S9 > S8 > S7 > S10 for the summer season, and S5 > S4 > S1 > S2 > S6 > S9 > S3 > S8 > S7 > S10 for the winter season. During the winter season, the highest value of RI (333.92)

TABLE 4 Value of different toxicity indexes in the sediment of the Rupsha River.

CDI				HQ			HI	TCR
Adults	**Dermal**	**Ingestion**	**Inhalation**	**Dermal**	**Ingestion**	**Inhalation**		
As	8.49E-07	7.09E-06	3.76E-09	2.83E-03	2.36E-02	1.25E-05	2.65E-02	1.19E-05
Pb	1.60E-07	4.00E-05	2.12E-08	4.56E-05	1.14E-02	6.06E-06	1.15E-02	
Cr	2.36E-07	5.92E-05	3.14E-08	7.87E-05	1.97E-02	1.05E-05	1.98E-02	2.97E-05
Cd	9.84E-09	2.47E-06	1.31E-09	9.84E-06	2.47E-03	1.31E-06	2.48E-03	3.72E-05
CDI				HQ			HI	TCR
Children	Dermal	Ingestion	Inhalation	Dermal	Ingestion	Inhalation		
As	5.56E-06	3.31E-05	1.75E-08	1.85E-02	1.10E-01	5.85E-05	1.29E-01	5.80E-05
Pb	1.05E-06	1.87E-04	9.90E-08	2.99E-04	5.34E-02	2.83E-05	5.37E-02	
Cr	1.55E-06	2.76E-04	1.46E-07	5.15E-04	9.20E-02	4.88E-05	9.26E-02	1.39E-04
Cd	6.44E-08	1.15E-05	6.10E-09	6.44E-05	1.15E-02	6.10E-06	1.16E-02	1.74E-04

was recorded at site 10. During the summer season, the lowest reading of 102.45 was observed at site 4 (Figure 4). The majority of the research region was found to be at a moderate risk to the aquatic ecology. Because industry and urbanization are quickly developing in our study area, more environmental elements should be carefully monitored to assess sediment quality and investigated new sources of metal content (Ali et al., 2022).

Human health risk assessment of the sediment

The local people surrounding the river basin were directly involved in various seasonal growing crops, therefore the human health risk was explored. The majority of the residents exploited the riverbank sediment for their agricultural plots. Sometimes river bed sediments are brought to the house for preparing household stuff. The local farmers also applied the river bed sediment to the agriculture fields to supplement organic matter. As a result, they have to be in direct touch with the sediment to grow seasonal vegetables. One of the significant characterizations and critical tools for understanding unfavorable human health impacts and environmental hazard exposures is risk assessment (Chonokhuu et al., 2019; El-Alfy et al., 2020). The following processes were followed to assess the danger to human health for three significant pathways:

Estimation of chronic daily intake

The metals' CDIs from the investigated sites were analyzed for adults and children, as shown in Table 4. CDIs were higher in children than in adults, according to the data, due to pathways that were grouped in decreasing order: ingestion > dermal > inhalation. For the targeted groups of people exposed through the exposure pathways, As had a higher CDI value than the other metals (Table 4). Through the dermal method, a child's concentration was observed to be 5.56E-06, while an adult's concentration was determined to be 8.49E-07. As consumption in children (3.31E-05) is higher than in adults (7.09E-06). Through all of the processes, Pb and Cr levels were shown to be higher in children than in adults. The intake of Cd was lower than the other metals in both children and adults (Table 4). Ali et al. (2022) found similar results where the CDIs were higher in children than adults.

THQ assessment (non-carcinogenic risk)

The average CDI values were used to assess the non-carcinogenic risk. In both age groups, Table 4 showed the maximum HQ value for the As metal content *via* the ingestion method (adult: 2.36E-02, children: 1.10E-01). In addition, metal As had a greater HQ attribution *via* the inhalation method, whereas As demonstrated a leadership position for all types of persons (Table 4). The overall results of HQ for all the pathways of the nearby local community were observed in the following order: As > Cr > Pb > Cd. The measurement of HQ was used to assess HI. Children were found to be more sensitive than adults as a result of the total HI of five components (Table 4). The overall results of 1 suggested that there was no substantial non-carcinogenic risk effect in the research area. A similar conclusion was made

TABLE 5 Correlation matrix of heavy metals in sediment of Rupsha River, Bangladesh.

Summer correlation in sediment					Winter correlation in sediment				
	As	Cr	Cd	Pb		As	Cr	Cd	Pb
As	1				As	1			
Cr	−0.513	1			Cr	−0.274	1		
Cd	0.126	0.135	1		Cd	0.230	0.024	1	
Pb	−0.158	0.148	−0.298	1	Pb	−0.265	−0.015	0.357	1

in the Yangtze River (Hu et al., 2017), where residents were safe from exceeding the worrying level (HI < 1). Ahmed et al. (2020) and Ali et al. (2022) found similar results in Bangladesh's Gomti river and Bhairab River respectively.

Carcinogenic risk evaluation

Because the USEPA did not give a carcinogen slope factor for Pb, the carcinogenic risk (CR) for the other elements, As, Pb, and Cr was approximated. Table 1 showed the results of the CR. For both adults and children, ingestion exposure was the most common among the three exposure routes. The CRs of different metals for different age groups, for example, may differ dramatically (Table 4). Children were shown to have higher CR values than adults (Table 2). Furthermore, children were exposed to higher CR in terms of As (5.80E-05) and Cd (1.74E-04) with a stronger effect than any other element through the ingestion channel. All As, Cr, and Cd risk values were found to be above 1×10^{-5}, indicating that the explored research region was not devoid of the detrimental effects of CR in both children and adults (Table 4). In contrast, El-Alfy et al. (2020) observed that consuming metals from the Burullus Lake silt exposed children rather than adults to the carcinogenic risk.

Source identification of heavy metals in sediment

Results from Kolmogorov-Smirnov and Shapiro-Wilk revealed that elements were generally distributed in the sediments of the study river. Other statistical analyses were concerned to provide some prospects which delivered some correlated possibilities using CM, PCA, and cluster analysis (CA).

Correlation matrix

The interrelationship between the metals was depicted in the correlation matrix. Pb and Cr (r = 0.148) and Cd and Cr (r = 0.135) had a weak positive connection in the summer. Cr Vs. was identified to have a moderately negative relationship (−0.513). Weak negative associations between Pb and Cd (r = −0.298) and Pb and As (r = −0.158) were investigated (Table 2). Pb Vs. Cd (r = 0.357), Cd Vs. Cr (r = 0.024), and Cd Vs. As (r = 0.230) all showed a positive weak linear relationship in the winter. Between Cr Vs. As (r = −0.274) and Pb Vs. As (r = −0.265), there was a negative linear connection (Table 5).

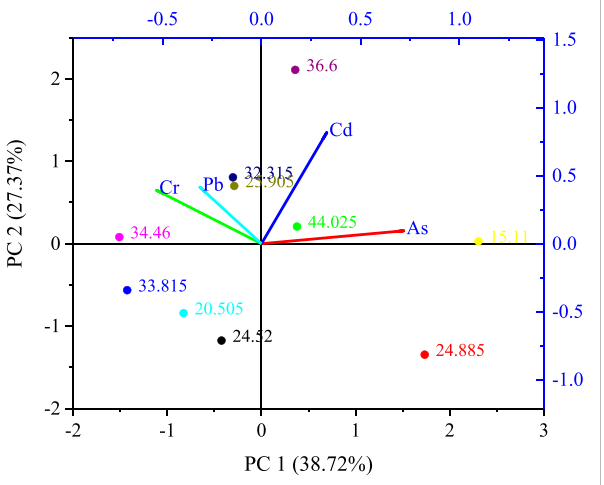

FIGURE 5
PCA among the metals in the sediment of the Rupsha River.

Principal component analysis

PCA was used to analyze the clustering behavior of several features qualitatively. Figure 5 shows the PCA findings for each factor with an eigenvalue greater than 1, a variance of 100%, and the cumulative variance. With a total variance of 89.90%, the PCA investigated the three grouping components. Due to the significant loadings of As, PC1 contributed 38.72% of the total variation (0.718). PC1 was shown to come from both geogenic and anthropogenic sources, such as manufacturing companies and refineries, according to the findings (Shikazono et al., 2012). PC2 accounted for 27.37% of the entire variance in the high Cd loading (0.816), which was attributed to battery manufacturing and other industrial concerns.

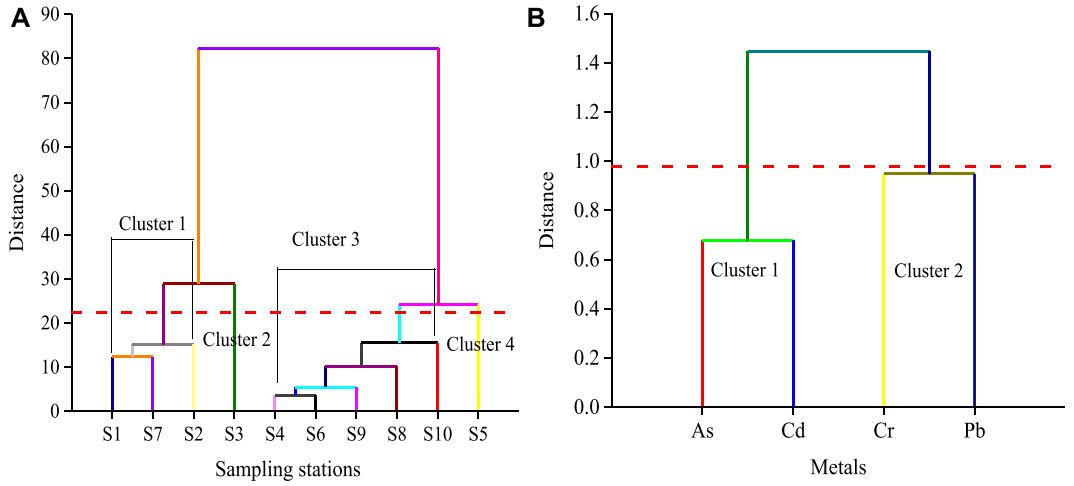

FIGURE 6
(A) Hierarchical cluster (dendrogram) of heavy metals in terms of sites. **(B)** Hierarchical cluster (dendrogram) of heavy metals in terms of metals.

Cluster analysis

A comparable set of sites was displayed in one group of the cluster, while a different group of sites was displayed in another group to pinpoint specific contamination locations (Yang et al., 2009; Sundaray et al., 2011). The cluster was explored using Ward Linkage and Euclidean distance. The dendrogram produced by the cluster analysis revealed a major cluster at (Dlink/Dmax)×100 < 30 and four prominent clusters: cluster 1, cluster 2, cluster 3, and cluster 4. Cluster 1 was possessed by S1, S7, and S2; cluster 2 was possessed by S4, S6, S9, and S8; while cluster 3 was possessed by S10. Finally, S5 was found in cluster 3. (Figure 6A). A similar strategy was used in the cluster analysis at (Dlink/Dmax)× 100 < 1 to determine the relationship between the studied metals and possible sources (Chung et al., 2011). Cluster 1 included As and Cd, while Cluster 2 comprised Cr and Pb (Figure 6B).

Conclusion

Heavy metals such as As, Cr, Cd, and Pb were examined in the Rupsha River sediment to estimate the contamination level as these contents are now available in the sediment throughout the world. We observed that Cr exhibited the highest concentration followed by Pb, As, and Cd. In the current study, Cd exceeded various standard limits among the metals examined. SQGs revealed that metals like Cd, Cr, and Pb had negative biological as well as ecological effects on the sediment-dwelling organisms. After measuring the river's sediment quality, we can conclude that according to Igeo, the river's sediment was moderately contaminated for Cd. CFs revealed that the study area was polluted especially for Cd whilst PLI indicated that investigated area was polluted in the winter season as it was > 1. The study region was located within the moderate-risk line, which can adversely influence the river's aquatic creatures, according to the possible ecological risk index and the risk index along with the sites. Multivariate analysis revealed that the metals were attributed to the river by diverse anthropogenic activities, largely from industries and municipal trash. Nonetheless, constant monitoring should be conducted, and appropriate rules should be put in place to limit any invasive anthropogenic activity across the river. This study suggested that the chemical fractionation of sediments should be considered to provide a more accurate appraisal of trace metals' risk and their distribution pathways in the riverine ecosystems.

Data availability statement

The original contributions presented in the study are included in the article/Supplementary Material, further inquiries can be directed to the corresponding authors.

Author contributions

All authors listed have made a substantial, direct, and intellectual contribution to the work and approved it for publication.

Funding

This manuscript is part of the master's thesis of KK from the Dept. of Aquaculture, Faculty of Fisheries, Patuakhali Science and Technology University, Bangladesh.

Acknowledgments

We are thankful to Muhammad Abdur Razzak, Dept. of Aquaculture, and other faculty members. The authors would like to express their gratefulness and sincerest thanks to the authority and staff members of the Quality Control (QC) Laboratory, Khulna, Bangladesh, for providing laboratory facilities.

Conflict of interest

The authors declare that the research was conducted in the absence of any commercial or financial relationships that could be construed as a potential conflict of interest.

Publisher's note

All claims expressed in this article are solely those of the authors and do not necessarily represent those of their affiliated organizations, or those of the publisher, the editors and the reviewers. Any product that may be evaluated in this article, or claim that may be made by its manufacturer, is not guaranteed or endorsed by the publisher.

Supplementary material

The Supplementary Material for this article can be found online at: https://www.frontiersin.org/articles/10.3389/fenvs.2022.778544/full#supplementary-material

References

Abdelhafez, A. A., and Li, J. (2015). Environmental monitoring of heavy metal status and human health risk assessment in the agricultural soils of the Jinxi River area, China. *Hum. Ecol. Risk Assess. An Int. J.* 21 (4), 952–971. doi:10.1080/10807039.2014.947851

Agarwal, A., Singh, R. D., Mishra, S. K., and Bhunya, P. K. (2005). ANN-based sediment yield river basin models for Vamsadhara (India). *Water sa.* 31 (1), 95–100. doi:10.4314/wsa.v31i1.5125

Ahmed, A. S., Rahman, M., Sultana, S., Babu, S. O. F., and Sarker, M. S. I. (2019a). Bioaccumulation and heavy metal concentration in tissues of some commercial fishes from the Meghna River Estuary in Bangladesh and human health implications. *Mar. Pollut. Bull.* 145, 436–447. doi:10.1016/j.marpolbul.2019.06.035

Ahmed, A. S. S., Hossain, M. B., Semme, S. A., Babu, S. M. O. F., Hossain, K., Moniruzzaman, M., et al. (2020). Accumulation of trace elements in selected fish and shellfish species from the largest natural carp fish breeding basin in asia: A probabilistic human health risk implication. *Environ. Sci. Pollut. Res.* 27 (30), 37852–37865. doi:10.1007/s11356-020-09766-1

Ahmed, A. S., Sultana, S., Habib, A., Ullah, H., Musa, N., Hossain, M. B., et al. (2019b). Bioaccumulation of heavy metals in some commercially important fishes from a tropical river estuary suggests higher potential health risk in children than adults. *Plos one* 14 (10), e0219336. doi:10.1371/journal.pone.0219336

Ali, M. M., Ali, M. L., Islam, M. S., and Rahman, M. Z. (2018). Assessment of toxic metals in water and sediment of Pasur River in Bangladesh. *Water Sci. Technol.* 77 (5), 1418–1430. doi:10.2166/wst.2018.016

Ali, M. M., Ali, M. L., Islam, M. S., and Rahman, M. Z. (2016). Preliminary assessment of heavy metals in water and sediment of Karnaphuli River, Bangladesh. *Environ. Nanotechnol. Monit. Manag.* 5, 27–35. doi:10.1016/j.enmm.2016.01.002

Ali, M. M., Ali, M. L., Proshad, R., Islam, S., Rahman, Z., Kormoker, T., et al. (2020b). Assessment of trace elements in the demersal fishes of a coastal river in Bangladesh: A public health concern. *Thalassas.* 36 (2), 641–655. doi:10.1007/s41208-020-00227-7

Ali, M. M., Ali, M. L., Proshad, R., Islam, S., Rahman, Z., Tusher, T. R., et al. (2020a). Heavy metal concentrations in commercially valuable fishes with health hazard inference from Karnaphuli river, Bangladesh. *Hum. Ecol. risk Assess. Int. J.* 26 (10), 2646–2662. doi:10.1080/10807039.2019.1676635

Ali, M. M., Rahman, S., Islam, M. S., Rakib, M. R. J., Hossen, S., Rahman, M. Z., et al. (2022). Distribution of heavy metals in water and sediment of an urban river in a developing country: A probabilistic risk assessment. *Int. J. Sediment Res.* 37 (2), 173–187. doi:10.1016/j.ijsrc.2021.09.002

Ashraful, M. A. K., Assim, Z. B., and Ismail, N. (2009). Monitoring and assessment of heavy metals levels in littoral sediments from the north eastern part of the Bay of Bengal coast, Bangladesh. *J. Industrial Pollut. Control* 25 (2), 105–111.

Ayers, R. S., and Westcot, D. W. (1985). *Water quality for agriculture*. Rome: FAO. Irrigation and Drainage Paper No. 29: Rev.1.

Babu, S. M., Hossain, M. B., Rahman, M. S., Rahman, M., Ahmed, A. S., Hasan, M., et al. (2021). Phytoremediation of toxic metals: A sustainable green solution for clean environment. *Appl. Sci.* 11 (21), 10348. doi:10.3390/app112110348

Bai, J., Cui, B., Chen, B., Zhang, K., Deng, W., Gao, H., et al. (2011). Spatial distribution and ecological risk assessment of heavy metals in surface sediments from a typical plateau lake wetland, China. *Ecol. Model.* 222 (2), 301–306. doi:10.1016/j.ecolmodel.2009.12.002

Bhavsar, S. P., Gewurtz, S. B., Helm, P. A., Labencki, T. L., Marvin, C. H., Fletcher, R., et al. (2010). Estimating sediment quality thresholds to prevent restrictions on fish consumption: Application to polychlorinated biphenyls and dioxins–furans in the Canadian Great Lakes. *Integr. Environ. Assess. Manag.* 6 (4), 641–652. doi:10.1002/ieam.102

Bhuyan, M., and Bakar, M. (2017b). Assessment of water quality in Halda River (the Major carp breeding ground) of Bangladesh. *Pollution* 3 (3), 429–441. doi:10.7508/pj.2017.03

Bhuyan, M. S., Bakar, M. A., Akhtar, A., Hossain, M. B., Ali, M. M., Islam, M. S., et al. (2017). Heavy metal contamination in surface water and sediment of the Meghna River, Bangladesh. *Environ. Nanotechnol. Monit. Manag.* 8, 273–279. doi:10.1016/j.enmm.2017.10.003

Bhuyan, M. S., Bakar, M. A., Rashed-Un-Nabi, M., Senapathi, V., Chung, S. Y., Islam, M. S., et al. (2019). Monitoring and assessment of heavy metal contamination in surface water and sediment of the Old Brahmaputra River, Bangladesh. *Appl. Water Sci.* 9 (5), 125. doi:10.1007/s13201-019-1004-y

Bhuyan, M. S., and Bakar, M. A. (2017a). Seasonal variation of heavy metals in water and sediments in the Halda River, Chittagong, Bangladesh. *Environ. Sci. Pollut. Res.* 24 (35), 27587–27600. doi:10.1007/s11356-017-0204-y

Bi, B., Liu, X., Guo, X., and Lu, S. (2018). Occurrence and risk assessment of heavy metals in water, sediment, and fish from Dongting Lake, China. *Environ. Sci. Pollut. Res.* 25 (34), 34076–34090. doi:10.1007/s11356-018-3329-8

Boström, K., and Valdes, S. (1969). Arsenic in ocean floors. *Lithos* 2 (4), 351–360. doi:10.1016/s0024-4937(69)80041-1

Bothner, M. H., Ten Brink, M. B., and Manheim, F. T. (1998). Metal concentrations in surface sediments of Boston Harbor-changes with time. *Mar. Environ. Res.* 45 (2), 127–155. doi:10.1016/s0141-1136(97)00027-5

Cancer IAfRo (2011). *Agents classified by the IARC monographs. IARC monographs on the evaluation of carcinogenic risks to humans*. Lyon, France: IARC).

Chabukdhara, M., and Nema, A. K. (2012). Assessment of heavy metal contamination in hindon river Sediments: A chemometric and geochemical approach. *Chemosphere* 87 (8), 945–953. doi:10.1016/j.chemosphere.2012.01.055

Chen, Y. Z., Yang, H., Zhang, Z. K., and Qin, M. (2005). The difference and cause analyses of freshwater sediment quality guidelines. *J. Lake Sci.* 3.

Chonokhuu, S., Batbold, C., Chuluunpurev, B., Battsengel, E., Dorjsuren, B., Byambaa, B., et al. (2019). Contamination and health risk assessment of heavy metals in the soil of major cities in Mongolia. *Int. J. Environ. Res. Public Health* 16 (14), 2552. doi:10.3390/ijerph16142552

Chung, C. Y., Chen, J. J., Lee, C. G., Chiu, C. Y., Lai, W. L., Liao, S. W., et al. (2011). Integrated estuary management for diffused sediment pollution in Dapeng Bay and neighboring rivers (Taiwan). *Environ. Monit. Assess.* 173 (1-4), 499–517. doi:10.1007/s10661-010-1401-z

Covelli, S., and Fontolan, G. (1997). Application of a normalization procedure in determining regional geochemical baselines. *Environ. Geol.* 30 (1-2), 34–45. doi:10.1007/s002540050130

Department of Environment (DoE) (2001). *Water quality data of rivers buriganga, Meghna, balu, shitalakhya and jamuna*. Dhaka, Bangladesh: Department of Environment.

Duodu, G. O., Goonetilleke, A., and Ayoko, G. A. (2016). Comparison of pollution indices for the assessment of heavy metal in Brisbane River sediment. *Environ. Pollut.* 219, 1077–1091. doi:10.1016/j.envpol.2016.09.008

El-Alfy, M. A., Darwish, D. H., and El-Amier, Y. A. (2020). Land use Land cover of the Burullus Lake shoreline (Egypt) and health risk assessment of metal-contaminated sediments. *Hum. Ecol. Risk Assess. An Int. J.* 27, 898–920. doi:10.1080/10807039.2020.1786667

Fan, H., Chen, S., Li, Z., Liu, P., Xu, C., Yang, X., et al. (2020). Assessment of heavy metals in water, sediment and shellfish organisms in typical areas of the Yangtze River Estuary, China. *Mar. Pollut. Bull.* 151, 110864. doi:10.1016/j.marpolbul.2019.110864

Fantke, P., Friedrich, R., and Jolliet, O. (2012). Health impact and damage cost assessment of pesticides in Europe. *Environ. Int.* 49, 9–17. doi:10.1016/j.envint.2012.08.001

FAO (2014). *The state of the world fisheries and aquaculture*. Rome, Italy: FAO Fisheries and Aquaculture Department.

Feng, H., Jiang, H., Gao, W., Weinstein, M. P., Zhang, Q., Zhang, W., et al. (2011). Metal contamination in sediments of the Western Bohai Bay and adjacent estuaries, China. *J. Environ. Manag.* 92 (4), 1185–1197. doi:10.1016/j.jenvman.2010.11.020

Fu, F., and Wang, Q. (2011). Removal of heavy metal ions from wastewaters: A review. *J. Environ. Manag.* 92 (3), 407–418. doi:10.1016/j.jenvman.2010.11.011

Fukushima, K., Saino, T., and Kodama, Y. (1992). Trace metal contamination in Tokyo Bay, Japan. *Sci. total Environ.* 125, 373–389. doi:10.1016/0048-9697(92)90402-e

Ganugapenta, S., Nadimikeri, J., Chinnapolla, S. R. R. B., Ballari, L., Madiga, R., Nirmala, K., et al. (2018). Assessment of heavy metal pollution from the sediment of Tupilipalem Coast, southeast coast of India. *Int. J. Sediment Res.* 33 (3), 294–302. doi:10.1016/j.ijsrc.2018.02.004

Gao, L., Gao, B., Wei, X., Zhou, H., Xu, D., Wang, Y., et al. (2015). Assessment of metal toxicity and development of sediment quality guidelines using the equilibrium partitioning model for the Three Gorges Reservoir, China. *Environ. Sci. Pollut. Res.* 22 (22), 17577–17585. doi:10.1007/s11356-015-4959-8

García-Lestón, J., Méndez, J., Pásaro, E., and Laffon, B. (2010). Genotoxic effects of lead: An updated review. *Environ. Int.* 36 (6), 623–636. doi:10.1016/j.envint.2010.04.011

Hakanson, L. (1980). An ecological risk index for aquatic pollution control. A sedimentological approach. *Water Res.* 14 (8), 975–1001. doi:10.1016/0043-1354(80)90143-8

Han, L., Gao, B., Hao, H., Zhou, H., Lu, J., Sun, K., et al. (2018). Lead contamination in sediments in the past 20 years: A challenge for China. *Sci. Total Environ.* 640, 746–756. doi:10.1016/j.scitotenv.2018.05.330

Hassan, M., Rahman, M. A. T., Saha, B., and Kamal, A. K. I. (2015). Status of heavy metals in water and sediment of the Meghna River, Bangladesh. *Am. J. Environ. Sci.* 11 (6), 427–439. doi:10.3844/ajessp.2015.427.439

Hossain, M. B., Habib, S. B., Hossain, M. S., Jolly, Y. N., Kamal, A. H. M., Idris, M. H., et al. (2020a). Data set on trace metals in surface sediment and water from a sub-tropical estuarine system, Bay of Bengal, Bangladesh. *Data brief* 31, 105911. doi:10.1016/j.dib.2020.105911

Hossain, M. B., Semme, S. A., Ahmed, A. S. S., Hossain, M. K., Porag, G. S., Parvin, A., et al. (2021). Contamination levels and ecological risk of heavy metals in sediments from the tidal river Halda, Bangladesh. *Arab. J. Geosci.* 14 (3), 158. doi:10.1007/s12517-021-06477-w

Hossain, M. B., Shanta, T. B., Ahmed, A. S., Hossain, M. K., and Semme, S. A. (2019). Baseline study of heavy metal contamination in the Sangu River estuary, Chattogram, Bangladesh. *Mar. Pollut. Bull.* 140, 255–261. doi:10.1016/j.marpolbul.2019.01.058

Hossain, M. S., Ahmed, M. K., Sarker, S., and Rahman, M. S. (2020b). Seasonal variations of trace metals from water and sediment samples in the northern Bay of Bengal. *Ecotoxicol. Environ. Saf.* 193, 110347. doi:10.1016/j.ecoenv.2020.110347

Hu, B., Jia, X., Hu, J., Xu, D., Xia, F., Li, Y., et al. (2017). Assessment of heavy metal pollution and health risks in the soil-plant-human system in the Yangtze River Delta, China. *Int. J. Environ. Res. Public Health* 14 (9), 1042. doi:10.3390/ijerph14091042

Ingersoll, C. G., Haverland, P. S., Brunson, E. L., Canfield, T. J., Dwyer, F. J., Henke, C. E., et al. (1996). Calculation and evaluation of sediment effect concentrations for the amphipod Hyalella azteca and the midge Chironomus riparius. *J. Gt. Lakes. Res.* 22 (3), 602–623. doi:10.1016/s0380-1330(96)70984-x

Islam, A. R. M. T., Hasanuzzaman, M., Islam, H. M. T., Mia, M. U., Khan, R., Habib, M. A., et al. (2020). Quantifying source apportionment, Co-occurrence, and ecotoxicological risk of metals from upstream, lower midstream, and downstream river segments, Bangladesh. *Environ. Toxicol. Chem.* 39 (10), 2041–2054. doi:10.1002/etc.4814

Islam, F., Rahman, M., Khan, S. S. A., Ahmed, B., Bakar, A., and Halder, M. (2013). Heavy metals in water, sediment and some fishes of Karnofuly River, Bangladesh. *Pollut. Res.* 32 (4), 715–721.

Islam, M. A., Das, B., Quraishi, S. B., Khan, R., Naher, K., Hossain, S. M., et al. (2020). Heavy metal contamination and ecological risk assessment in water and sediments of the halda river, Bangladesh: A natural fish breeding ground. *Mar. Pollut. Bull.* 160, 111649. doi:10.1016/j.marpolbul.2020.111649

Islam, M. M., Rahman, S. L., Ahmed, S. U., and Haque, M. K. I. (2014). Biochemical characteristics and accumulation of heavy metals in fishes, water and sediments of the river Buriganga and Shitalakhya of Bangladesh. *J. Asian Sci. Res.* 4 (6), 270.

Islam, M. S., Ahmed, M. K., Habibullah-Al-Mamun, M., and Hoque, M. F. (2015a). Preliminary assessment of heavy metal contamination in surface sediments from a river in Bangladesh. *Environ. Earth Sci.* 73 (4), 1837–1848. doi:10.1007/s12665-014-3538-5

Islam, M. S., Ahmed, M. K., Habibullah-Al-Mamun, M., Raknuzzaman, M., Ali, M. M., Eaton, D. W., et al. (2016). Health risk assessment due to heavy metal exposure from commonly consumed fish and vegetables. *Environ. Syst. Decis.* 36 (3), 253–265. doi:10.1007/s10669-016-9592-7

Islam, M. S., Ahmed, M. K., Raknuzzaman, M., Habibullah-Al-Mamun, M., and Islam, M. K. (2015b). Heavy metal pollution in surface water and sediment: A preliminary assessment of an urban river in a developing country. *Ecol. Indic.* 48, 282–291. doi:10.1016/j.ecolind.2014.08.016

Islam, M. S., Hossain, M. B., Matin, A., and Sarker, M. S. I. (2018). Assessment of heavy metal pollution, distribution and source apportionment in the sediment from Feni River estuary, Bangladesh. *Chemosphere* 202, 25–32. doi:10.1016/j.chemosphere.2018.03.077

Islam, M. S., Idris, A. M., Islam, A. R. M. T., Ali, M. M., and Rakib, M. R. J. (2021). Hydrological distribution of physicochemical parameters and heavy metals in surface water and their ecotoxicological implications in the Bay of Bengal coast of Bangladesh. *Environ. Sci. Polluttion* 28 (48), 68585–68599. doi:10.1007/s11356-021-15353-9

Jiang, M., Zeng, G., Zhang, C., Ma, X., Chen, M., Zhang, J., et al. (2013). Assessment of heavy metal contamination in the surrounding soils and surface sediments in Xiawangang River, Qingshuitang District. *PloS one* 8 (8), e71176. doi:10.1371/journal.pone.0071176

Jiménez-Oyola, S., García-Martínez, M. J., Ortega, M. F., Chavez, E., Romero, P., García-Garizabal, I., et al. (2021). Ecological and probabilistic human health risk assessment of heavy metal (loid) s in river sediments affected by mining activities in Ecuador. *Environ. Geochem. Health* 43, 4459–4474. doi:10.1007/s10653-021-00935-w

Jolly, Y. N., Rakib, M. R. J., Islam, M. S., Akter, S., Idris, A. M., Phoungthong, K., et al. (2021). Potential toxic elements in sediment and fishes of an important fish breeding river in Bangladesh: A preliminary study for ecological and health risks assessment. *Toxin Rev.*, 1–14. doi:10.1080/15569543.2021.1965624

Kadhum, S. A., Ishak, M. Y., and Zulkifli, S. Z. (2016). Evaluation and assessment of baseline metal contamination in surface sediments from the Bernam River, Malaysia. *Environ. Sci. Pollut. Res.* 23 (7), 6312–6321. doi:10.1007/s11356-015-5853-0

Kahal, A., El-Sorogy, A. S., Qaysi, S., Almadani, S., Kassem, O. M., Al-Dossari, A., et al. (2020). Contamination and ecological risk assessment of the Red Sea coastal sediments, southwest Saudi Arabia. *Mar. Pollut. Bull.* 154, 111125. doi:10.1016/j.marpolbul.2020.111125

Karydas, C. G., Tzoraki, O., and Panagos, P. (2015). A new spatiotemporal risk index for heavy metals: Application in Cyprus. *Water* 7 (8), 4323–4342. doi:10.3390/w7084323

Ke, X., Gui, S., Huang, H., Zhang, H., Wang, C., Guo, W., et al. (2017). Ecological risk assessment and source identification for heavy metals in surface sediment from the Liaohe River protected area, China. *Chemosphere* 175, 473–481. doi:10.1016/j.chemosphere.2017.02.029

Khan, R., Islam, M. S., Tareq, A. R. M., Naher, K., Islam, A. R. M. T., Habib, M. A., et al. (2020). Distribution, sources and ecological risk of trace elements and polycyclic aromatic hydrocarbons in sediments from a polluted urban river in central Bangladesh. *Environ. Nanotechnol. Monit. Manag.* 14, 100318. doi:10.1016/j.enmm.2020.100318

Kumar, S., Islam, A. R. M. T., Hasanuzzaman, M., Roquia, S., Khan, R., Islam, M. S., et al. (2021). Preliminary assessment of heavy metals in surface water and sediment in Nakuvadra-Rakiraki River, Fiji using indexical and chemometric approaches. *J. Environ. Manag.* 298, 113517. doi:10.1016/j.jenvman.2021.113517

Kumwimba, M. N., Zhu, B., Wang, T., and Muyembe, D. K. (2016). Distribution and risk assessment of metals and arsenic contamination in man-made ditch sediments with different land use types. *Environ. Sci. Pollut. Res.* 23 (24), 24808–24823. doi:10.1007/s11356-016-7690-1

Kusin, F. M., Azani, N. N. M., Hasan, S. N. M., and Sulong, N. A. (2018). Distribution of heavy metals and metalloid in surface sediments of heavily-mined area for bauxite ore in Pengerang, Malaysia and associated risk assessment. *Catena* 165, 454–464. doi:10.1016/j.catena.2018.02.029

Langston, W. J. (1980). Arsenic in UK estuarine sediments and its availability to benthic organisms. *J. Mar. Biol. Assoc. U. K.* 60 (4), 869–881. doi:10.1017/s0025315400041953

Larrose, A., Coynel, A., Schäfer, J., Blanc, G., Massé, L., Maneux, E., et al. (2010). Assessing the current state of the Gironde Estuary by mapping priority contaminant distribution and risk potential in surface sediment. *Appl. Geochem.* 25 (12), 1912–1923. doi:10.1016/j.apgeochem.2010.10.007

Liu, X., Jiang, J., Yan, Y., Dai, Y., Deng, B., Ding, S., et al. (2018). Distribution and risk assessment of metals in water, sediments, and wild fish from Jinjiang River in Chengdu, China. *Chemosphere* 196, 45–52. doi:10.1016/j.chemosphere.2017.12.135

Long, E. R., MacDonald, D. D., Smith, S. L., and Calder, F. D. (1995). Incidence of adverse biological effects within ranges of chemical concentrations in marine and estuarine sediments. *Environ. Manag.* 19 (1), 81–97. doi:10.1007/bf02472006

Loska, K., Cebula, J., Pelczar, J., Wiechuła, D., and Kwapuliński, J. (1997). Use of enrichment, and contamination factors together with geoaccumulation indexes to evaluate the content of Cd, Cu, and Ni in the Rybnik water reservoir in Poland. *Water Air Soil Pollut.* 93 (1-4), 347–365. doi:10.1007/bf02404766

MacDonald, D. D., Ingersoll, C. G., and Berger, T. A. (2000). Development and evaluation of consensus-based sediment quality guidelines for freshwater ecosystems. *Archives Environ. Contam. Toxicol.* 39 (1), 20–31. doi:10.1007/s002440010075

Magesh, N. S., Chandrasekar, N., Kumar, S. K., and Glory, M. (2013). Trace element contamination in the estuarine sediments along Tuticorin coast–Gulf of Mannar, southeast coast of India. *Mar. Pollut. Bull.* 73 (1), 355–361. doi:10.1016/j.marpolbul.2013.05.041

Mamun, A., Sumon, K. A., Sukhan, Z. P., Hoq, E., Alam, M. W., Haq, M. S., et al. (2013). "Heavy metal contamination in water and sediments of the river Karnafuli from south-east coast of Bangladesh," in *Conference paper, 4th the international conference on environmental aspects of Bangladesh* (Japan: Fukuoka), 113–116.

Milićević, T., Relić, D., Škrivanj, S., Tešić, Ž., and Popović, A. (2017). Assessment of major and trace element bioavailability in vineyard soil applying different single extraction procedures and pseudo-total digestion. *Chemosphere* 171, 284–293. doi:10.1016/j.chemosphere.2016.12.090

Mohiuddin, K. M., Ogawa, Y., Zakir, H. M., Otomo, K., and Shikazono, N. (2011). Heavy metals contamination in water and sediments of an urban river in a developing country. *Int. J. Environ. Sci. Technol. (Tehran).* 8 (4), 723–736. doi:10.1007/bf03326257

Moore, J. W., and Ramamoorthy, S. (2012). *Heavy metals in natural waters: Applied monitoring and impact assessment*. Berlin, Germany: Springer Science & Business Media.

Müller, G. (1981). Die schwermetallbelstung der sedimente des neckars und seiner nebenflusse: Eine bestandsaufnahme. *Chemiker-Zeitung* 105, 157–164.

Muller, G. (1969). [Limb fitting for thigh amputees]. *Hefte Unfallheilkd.* 2, 108–110.

Olivares-Rieumont, S., De la Rosa, D., Lima, L., Graham, D. W., Katia, D., Borroto, J., et al. (2005). Assessment of heavy metal levels in Almendares River sediments-Havana City, Cuba. *Water Res.* 39 (16), 3945–3953. doi:10.1016/j.watres.2005.07.011

Otto, M. (1998). "Multivariate methods," in *WIDMER, HM.* Analytical chemistry. Editors R. KELLNER, J. M. MERMET, and M. OTTO (Weinheim: Wiley VCH).

Pandey, J., and Singh, R. (2017). Heavy metals in sediments of ganga river: Up- and downstream urban influences. *Appl. Water Sci.* 7 (4), 1669–1678. doi:10.1007/s13201-015-0334-7

Pekey, H. (2006). The distribution and sources of heavy metals in Izmit Bay surface sediments affected by a polluted stream. *Mar. Pollut. Bull.* 52 (10), 1197–1208. doi:10.1016/j.marpolbul.2006.02.012

Persaud, D., Jaagumagi, R., and Hayton, A. (1993). *Guidelines for the protection and management of aquatic sediment quality in Ontario*. Ontario: Ministry of Environment and Energy.

Rahman, M. S., Ahmed, A. S., Rahman, M. M., Babu, S. O. F., Sultana, S., Sarker, S. I., et al. (2021). Temporal assessment of heavy metal concentration and surface water quality representing the public health evaluation from the Meghna River estuary, Bangladesh. *Appl. Water Sci.* 11 (7), 121. doi:10.1007/s13201-021-01455-9

Rahman, M. S., Hossain, M. B., Babu, S. O. F., Rahman, M., Ahmed, A. S., Jolly, Y. N., et al. (2019). Source of metal contamination in sediment, their ecological risk, and phytoremediation ability of the studied mangrove plants in ship breaking area, Bangladesh. *Mar. Pollut. Bull.* 141, 137–146. doi:10.1016/j.marpolbul.2019.02.032

Rahman, M. S., Molla, A. H., Saha, N., and Rahman, A. (2012). Study on heavy metals levels and its risk assessment in some edible fishes from Bangshi River, Savar, Dhaka, Bangladesh. *Food Chem.* 134 (4), 1847–1854. doi:10.1016/j.foodchem.2012.03.099

Rahman, M. T., Rahman, M. S., Quraishi, S. B., Ahmad, J. U., Choudhury, T. R., and Mottaleb, M. A. (2011). Distribution of heavy metals in water and sediments in Passur river, sundarban mangrove forest. *Bangladesh. J. Int. Environ. Appl. Sci.* 6 (4), 537.

Raj, S. M., and Jayaprakash, M. (2008). Distribution and enrichment of trace metals in marine sediments of Bay of Bengal, off Ennore, south-east coast of India. *Environ. Geol.* 56 (1), 207–217. doi:10.1007/s00254-007-1156-1

Ramanathan, A. L., Subramanian, V., Ramesh, R., Chidambaram, S., and James, A. (1999). Environmental geochemistry of the Pichavaram mangrove ecosystem (tropical), southeast coast of India. *Environ. Geol.* 37 (3), 223–233. doi:10.1007/s002540050380

Rehman, K., Fatima, F., Waheed, I., and Akash, M. S. H. (2018). Prevalence of exposure of heavy metals and their impact on health consequences. *J. Cell. Biochem.* 119 (1), 157–184. doi:10.1002/jcb.26234

Rubio, B., Nombela, M. A., and Vilas, F. (2000). Geochemistry of major and trace elements in sediments of the ria de Vigo (NW Spain): An assessment of metal pollution. *Mar. Pollut. Bull.* 40 (11), 968–980. doi:10.1016/s0025-326x(00)00039-4

Saha, N., Mollah, M. Z. I., Alam, M. F., and Rahman, M. S. (2016). Seasonal investigation of heavy metals in marine fishes captured from the Bay of Bengal and the implications for human health risk assessment. *Food control.* 70, 110–118. doi:10.1016/j.foodcont.2016.05.040

Saha, P. K., and Hossain, M. D. (2011). "Assessment of heavy metal contamination and sediment quality in the Buriganga River, Bangladesh," in *Proceeding: 2nd international conference on environmental science and Technology* (Singapore: IPCBEE), 6, 384–388.

Sakan, S. M., Đorđević, D. S., Manojlović, D. D., and Predrag, P. S. (2009). Assessment of heavy metal pollutants accumulation in the Tisza River sediments. *J. Environ. Manag.* 90 (11), 3382–3390. doi:10.1016/j.jenvman.2009.05.013

Samad, M. A., Mahmud, Y., Adhikary, R. K., Rahman, S. B. M., Haq, M. S., and Rashid, H. (2015). Chemical profile and heavy metal concentration in water and freshwater species of Rupsha River, Bangladesh. *Am. J. Environ. Prot.* 3 (6), 180–186.

Saran, S. H., Rahman, A., and Yunus, A. (2018). Comparative analysis on flow and salinity of Rupsha-Passur river system of Bangladesh. *J. Mod. Sci. Technol.* 6 (2), 19–31.

Shaheen, S. M., Abdelrazek, M. A., Elthoth, M., Moghanm, F. S., Mohamed, R., Hamza, A., et al. (2019). Potentially toxic elements in saltmarsh sediments and common reed (phragmites australis) of Burullus coastal lagoon at north nile delta, Egypt: A survey and risk assessment. *Sci. Total Environ.* 649, 1237–1249. doi:10.1016/j.scitotenv.2018.08.359

Shen, F., Mao, L., Sun, R., Du, J., Tan, Z., Ding, M., et al. (2019). Contamination evaluation and source identification of heavy metals in the sediments from the Lishui River Watershed, Southern China. *Int. J. Environ. Res. Public Health* 16 (3), 336. doi:10.3390/ijerph16030336

Shikazono, N., Tatewaki, K., Mohiuddin, K. M., Nakano, T., and Zakir, H. M. (2012). Sources, spatial variation, and speciation of heavy metals in sediments of the Tamagawa River in Central Japan. *Environ. Geochem. Health* 34 (1), 13–26. doi:10.1007/s10653-011-9409-z

Shrestha, S., and Kazama, F. (2007). Assessment of surface water quality using multivariate statistical techniques: A case study of the fuji river basin, Japan. *Environ. Model. Softw.* 22 (4), 464–475. doi:10.1016/j.envsoft.2006.02.001

Siddique, M. A. M., and Aktar, M. (2012). Heavy metals in salt marsh sediments of porteresia bed along the Karnafully River coast, Chittagong. *Soil &. Water Res.* 7 (3), 117–123. doi:10.17221/7/2012-swr

Siddique, M. A. M., Rahman, M., Rahman, S. M. A., Hassan, M. R., Fardous, Z., Chowdhury, M. A. Z., et al. (2020). Assessment of heavy metal contamination in the surficial sediments from the lower Meghna River estuary, Noakhali coast, Bangladesh. *Int. J. Sediment Res.* 36 (3), 384–391. doi:10.1016/j.ijsrc.2020.10.010

Simeonov, V., Massart, D. L., Andreev, G., and Tsakovski, S. (2000). Assessment of metal pollution based on multivariate statistical modeling of 'hot spot'sediments from the Black Sea. *Chemosphere* 41 (9), 1411–1417. doi:10.1016/s0045-6535(99)00540-8

Singh, K. P., Mohan, D., Singh, V. K., and Malik, A. (2005). Studies on distribution and fractionation of heavy metals in Gomti river sediments-a tributary of the Ganges, India. *J. hydrology* 312 (1-4), 14–27. doi:10.1016/j.jhydrol.2005.01.021

Smith, S. L., MacDonald, D. D., Keenleyside, K. A., Ingersoll, C. G., and Field, L. J. (1996). A preliminary evaluation of sediment quality assessment values for freshwater ecosystems. *J. Gt. Lakes. Res.* 22 (3), 624–638. doi:10.1016/s0380-1330(96)70985-1

Sundaray, S. K., Nayak, B. B., Lin, S., and Bhatta, D. (2011). Geochemical speciation and risk assessment of heavy metals in the river estuarine sediments-a case study: Mahanadi basin, India. *J. Hazard. Mater.* 186 (2-3), 1837–1846. doi:10.1016/j.jhazmat.2010.12.081

Suresh, G., Sutharsan, P., Ramasamy, V., and Venkatachalapathy, R. (2012). Assessment of spatial distribution and potential ecological risk of the heavy metals in relation to granulometric contents of Veeranam lake sediments, India. *Ecotoxicol. Environ. Saf.* 84, 117–124. doi:10.1016/j.ecoenv.2012.06.027

Traina, A., Bono, G., Bonsignore, M., Falco, F., Giuga, M., Quinci, E. M., et al. (2019). Heavy metals concentrations in some commercially key species from Sicilian coasts (Mediterranean Sea): Potential human health risk estimation. *Ecotoxicol. Environ. Saf.* 168, 466–478. doi:10.1016/j.ecoenv.2018.10.056

Turekian, K. K., and Wedepohl, K. H. (1961). Distribution of the elements in some major units of the earth's crust. *Geol. Soc. Am. Bull.* 72 (2), 175. doi:10.1130/0016-7606(1961)72[175:doteis]2.0.co;2

USEPA (2011). Exposure factors handbook 2011 edition (Final). Retrieved from: http://cfpub.epa.gov/.

USEPA (2001). *Methods for collection, storage and manipulation of sediments for chemical and toxicological analyses*. Washington, DC: Office of Water. Technical Manual, EPA-823-B-01-002.

USEPA (2006). *National recommended water quality criteria*. Washington, D.C.: United States Environmental Protection Agency. Office of Water, Office of Science and Technology.

USEPA (1989). *Risk assessment guidance for Superfund. Human health evaluation manual.* Washington, DC: Office of emergency and remedial response.

USEPA (2000). *Risk-based concentration table*. Washington, DC: USEPA.

USEPA (2002). *Supplemental guidance for developing soil screening levels for superfund sites OSWER 9355*. Washington, DC, USA, 4–24.

USEPA (1999). US environmental protection agency: Screening level ecological risk assessment protocol for hazardous waste combustion facilities. *Append. E Toxic. Ref. Values* 3.

Varol, M., and Şen, B. (2009). Assessment of surface water quality using multivariate statistical techniques: A case study of behrimaz stream, Turkey. *Environ. Monit. Assess.* 159 (1), 543–553. doi:10.1007/s10661-008-0650-6

Venkatramanan, S., Chung, S. Y., Ramkumar, T., and Selvam, S. (2015). Environmental monitoring and assessment of heavy metals in surface sediments at Coleroon River Estuary in Tamil Nadu, India. *Environ. Monit. Assess.* 187 (8), 505. doi:10.1007/s10661-015-4709-x

Wang, X. C., Feng, H., and Ma, H. Q. (2007). Assessment of metal contamination in surface sediments of Jiaozhou Bay, Qingdao, China. *Clean. Soil Air Water* 35 (1), 62–70. doi:10.1002/clen.200600022

Wang, X., Liu, B., and Zhang, W. (2020). Distribution and risk analysis of heavy metals in sediments from the Yangtze River Estuary, China. *Environ. Sci. Pollut. Res.* 27 (10), 10802–10810. doi:10.1007/s11356-019-07581-x

Ward, J. H., Jr. (1963). Hierarchical grouping to optimize an objective function. *J. Am. Stat. Assoc.* 58 (301), 236–244. doi:10.1080/01621459.1963.10500845

Who (2004). *Guidelines for drinking water. Quality*. 3rd Edition. Geneva, Switzerland: World Health Organization, 515.

Word, J. Q., Albrecht, B. B., Anghera, M. L., Baudo, R., Bay, S. M., Di Toro, D. M., et al. (2005). *Predictive ability of sediment quality guidelines. Use of sediment quality guidelines and related tools for the assessment of contaminated sediments*. Pensacola (Florida): Society of Environmental Toxicology and Chemistry, 121–161.

Wu, B., Wang, G., Wu, J., Fu, Q., and Liu, C. (2014). Sources of heavy metals in surface sediments and an ecological risk assessment from two adjacent plateau reservoirs. *PLoS One* 9 (7), e102101. doi:10.1371/journal.pone.0102101

Yang, Z., Wang, Y., Shen, Z., Niu, J., and Tang, Z. (2009). Distribution and speciation of heavy metals in sediments from the mainstream, tributaries, and lakes of the Yangtze River catchment of Wuhan, China. *J. Hazard. Mater.* 166 (2-3), 1186–1194. doi:10.1016/j.jhazmat.2008.12.034

Yi, Y., Yang, Z., and Zhang, S. (2011). Ecological risk assessment of heavy metals in sediment and human health risk assessment of heavy metals in fishes in the middle and lower reaches of the Yangtze River basin. *Environ. Pollut.* 159 (10), 2575–2585. doi:10.1016/j.envpol.2011.06.011

Yin, S., Feng, C., Li, Y., Yin, L., and Shen, Z. (2015). Heavy metal pollution in the surface water of the Yangtze estuary: A 5-year follow-up study. *Chemosphere* 138, 718–725. doi:10.1016/j.chemosphere.2015.07.060

Yu, X., Yan, Y., and Wang, W. X. (2010). The distribution and speciation of trace metals in surface sediments from the Pearl River Estuary and the Daya Bay, Southern China. *Mar. Pollut. Bull.* 60 (8), 1364–1371. doi:10.1016/j.marpolbul.2010.05.012

Zhao, G., Lu, Q., Ye, S., Yuan, H., Ding, X., Wang, J., et al. (2016). Assessment of heavy metal contamination in surface sediments of the west Guangdong coastal region, China. *Mar. Pollut. Bull.* 108 (1-2), 268–274. doi:10.1016/j.marpolbul.2016.04.057

Zhao, X. M., Yao, L. A., Ma, Q. L., Zhou, G. J., Wang, L., Fang, Q. L., et al. (2018). Distribution and ecological risk assessment of cadmium in water and sediment in Longjiang River, China: Implication on water quality management after pollution accident. *Chemosphere* 194, 107–116. doi:10.1016/j.chemosphere.2017.11.127

frontiers | Frontiers in Earth Science

TYPE Original Research
PUBLISHED 28 March 2023
DOI 10.3389/feart.2023.1060312

OPEN ACCESS

EDITED BY
Youhei Yamashita,
Hokkaido University, Japan

REVIEWED BY
Bernhard Wehrli,
ETH Zürich, Switzerland
Takeshi Yoshimura,
Hokkaido University, Japan
Richard James Cooper,
University of East Anglia, United Kingdom

*CORRESPONDENCE
Yu Umezawa,
umezawa@me.tuat.ac.jp

SPECIALTY SECTION
This article was submitted to Hydrosphere, a section of the journal Frontiers in Earth Science

RECEIVED 03 October 2022
ACCEPTED 16 March 2023
PUBLISHED 28 March 2023

CITATION
Kozyrev R, Umezawa Y and Yoh M (2023), Total phosphorus and phosphorus forms change in sediments along the Tone River.
Front. Earth Sci. 11:1060312.
doi: 10.3389/feart.2023.1060312

Total phosphorus and phosphorus forms change in sediments along the Tone River

Roman Kozyrev[1], Yu Umezawa[2]* and Muneoki Yoh[2]

[1]United Graduate School of Agricultural Science, Tokyo University of Agriculture and Technology, Fuchu, Japan, [2]Department of Environmental Science on Biosphere, Tokyo University of Agriculture and Technology, Fuchu, Japan

Phosphorus (P) is an essential element for the metabolism, growth, and development of living organisms, and it often limits primary production in freshwater ecosystems. During flood events, rivers can transport considerable amounts of particulate organic P (org-P) and inorganic P from the basin to the ocean. Understanding the transport mechanisms and changes in P distribution from upstream to downstream areas of rivers is crucial to estimate its flux to the ocean. However, the processes involved in P transformation and cycling among different forms in rivers are not well understood. To better understand P transformation and total P (TP) concentrations in river basins, this study examined various P forms in bottom sediments, river bank sediments, parent rock material, and soil samples along the Tone River, Japan. P forms such as org-P, Ca-bound phosphorus (apatite, Ca-P), P bound with iron oxides/hydroxides (Fe-P), bio unavailable non-apatite inorganic P (NAIP), and TP were analyzed. The results showed an increase in TP concentration in bottom and bank sediment samples along the course of the Tone River. This change in TP was mostly due to the increases in Fe-P and bioavailable org-P, while Ca-P and NAIP decreased toward the downstream area. Analysis of parent rock in three main mountain group areas (Mount Tanigawa, Mount Akagi, and Mount Tsukuba) showed their downstream impacts on TP and the distribution of P forms. Sediment grain size distribution analysis suggested that Fe-P and org-P fractions increased with decreasing sediment particle size, while Ca-P and NAIP were relatively evenly distributed among all grain sizes. The data revealed the transformation of P forms in sediments of the largest river in the Kanto region, Japan, which influence its flux to the Pacific Ocean. The results suggest that Fe-P and org-P may play a more significant role in P transport from river basins to the ocean than previously thought. The findings of this study can be useful for estimating P fluxes to the ocean and for the management of freshwater ecosystems.

KEYWORDS

phosphorus, surface sediments, parent rock, sediment transport, grain size

1 Introduction

Phosphorus (P) is an essential and sometimes limiting nutrient in aquatic systems, controlling the growth rate of algae and aquatic plants. Photosynthesis (primary production) in aquatic ecosystems and the oceanic carbon cycle are also strongly dependent on nutrient elements, such as nitrogen (N) and P (Holland, 1984). In the

eastern Mediterranean Sea (Krom et al., 1991; Krom et al., 2010; Lazarri et al., 2015) and other coastal areas (Fisher et al., 1992; Hayashi et al., 2000; Kubo et al., 2019), P is the limiting nutrient for primary production due to high N:P values in all external nutrient inputs. Therefore, understanding the process by which P is supplied to the terrestrial and aquatic ecosystems is an important issue.

In soils, Ca-bound phosphorus (apatite, Ca-P) is the dominant P-bearing primary mineral (Nezat et al., 2008). P mainly originates as apatite in bedrock or in uplifted sedimentary deposits. Several studies have been conducted on the dominant P form (apatite) in many parent materials (Williams, 1969; Kohler et al., 2005), but there has been little research regarding the characterization of P forms. Parent materials differ in P concentration, which may influence P availability across the whole area of a river basin. Furthermore, P weathering, leaching, and other processes are strictly dependent on the origin of P source in parent rocks, meaning that P flux is likely to differ in different geological systems (Hartmann et al., 2014). As with silicate minerals, the solubility of apatite is higher under acidic conditions, and it has been reported that the concentration of phosphate in stream water is higher in areas where the surface geology is andesite or basalt (Wakamatsu et al., 2006). Once P is released from apatite, dissolved phosphate ions can be transported *via* natural waters to the ocean. Along this path, P can be adsorbed onto inorganic particles or incorporated into various metabolic reactions and pathways (Ruttenberg, 2004).

In aquatic systems, P occurs in a number of basic forms, including dissolved inorganic P (IP, readily reactive P, which is immediately bioavailable), dissolved organic P (org-P), particulate organic P (detritus and living biomass), and particulate inorganic P (mostly represented by Fe/Al-bound P). The availability of P in water is influenced by various physical and chemical transformations as well as biological processes. The adsorption of P onto sediment particles plays a key role in P cycling, especially in streams and rivers affected by agricultural land use (Withers and Jarvie, 2008; Weigelhofer et al., 2018). Particle-bound P settles in retention zones of rivers, such as pools, floodplain lakes, and impounded sections, and can then be released into the water column. The amount of P in the sediments is strongly dependent on grain size, and is highest in mud (<63 μm) and fine sand (63–250 μm) and decreases with increasing grain size (Reddy et al., 1999; Mainstone and Parr, 2002; Peng et al., 2021). Therefore, it is necessary to gain an understanding of the changes in P forms and grain sizes from upstream to downstream areas of the rivers.

Phosphorus speciation in sediment provides useful information on the reactivity and potential bioavailability of P in the aquatic ecosystem. However, most experimental studies on phosphate release from sediments have focused on static release in lakes or estuaries, but there are not many studies about P in river sediments. There is a need for more research on the interactions between different forms of P, its spatial variability and other chemical, and physical factors in the river sediments and water column.

This study was performed to determine the spatial variability of P in bottom sediment and bank sediment along the Tone River, Japan, to understand grain size changes from the upstream to downstream areas of the Tone River, and to identify and compare different P forms and their interactions, and changes in the sediment, with reference to its tributary zones with different surface geology.

2 Materials and methods

2.1 Study site

A field survey was conducted along the Tone River, the largest river in the Kanto region, which includes Tokyo, Japan. The river is 322 km long and has a drainage area of 16,840 km^2. The mean annual discharge of the Tone River varies depending on the year and the season, however, the long-term average annual discharge is approximately 20.5 × 10^9 m^3/year.

The land in the Tone River basin consists of about 62% mountainous land mostly covered with forest, 23% agricultural land, such as rice paddies and fields, around 7% is urban land, such as residential land, and 8% of water surfaces, mainly represented by the Lake Kasumigaura (Ministry of Land, Infrastructure, Transport, and Tourism, 2011). Therefore, the supply of P-bearing parent rock is important over a wide area, in addition to the supply of phosphate and org-P through treated sewage water as possible local sources of P. As of 1 October 2022, the estimated total population of prefectures within the Tone River basin is approximately 15.9 million people (Ministry of Internal Affairs and Communications, Japan).

The upper reaches of the Tone River basin are mostly represented by two groups of parent rock material, i.e., dacite and rhyolite with relatively low P concentrations, and andesite group rocks with high P concentrations (Figure 1). Mount Tanigawa is mainly represented by relatively low-P rhyolite and dacite (mean P concentration is 14.2 and 27.2 μmol/g respectively), while Mount Akagi, located to the southwest, consists almost entirely of andesite and basaltic-andesite rocks with mean P content of 37.1 and 50.1 μmol/g respectively (National Institute of Advanced Industrial Science and Technology Geological Survey of Japan, GeomapNavi, 2018).

The downstream area is represented by plains covered by tablelands consisting of unconsolidated agglomerates of shallow marine sediments (Okamoto and Ikeda, 2000). River valley lowlands separate the hills and tablelands into independent sections. While upstream reaches of the valleys are gravelly and rather dry, the middle- and downstream portions become deltaic, wet, and swampy. Decomposed red-brown volcanic ash soil, called Kanto loam, covers the flat-topped tablelands. Mount Tsukuba, one of the sources of P in the lower reaches of the Tone River basin, is located to the north of the downstream area of the Tone River and northwest of Lake Kasumigaura. Mount Tsukuba consists of granitic and gabbroic rocks (mean P concentration is 31.1 and 26.1 μmol/g respectively), which have relatively high P contents. Data from whole-rock analyses obtained from the EarthChem website (www.earthchem.org).

2.2 Sampling

Samples of sediments were taken at 23 sampling sites in the Tone River basin (Supplementary Table S1). Sampling sites 1–3 represent

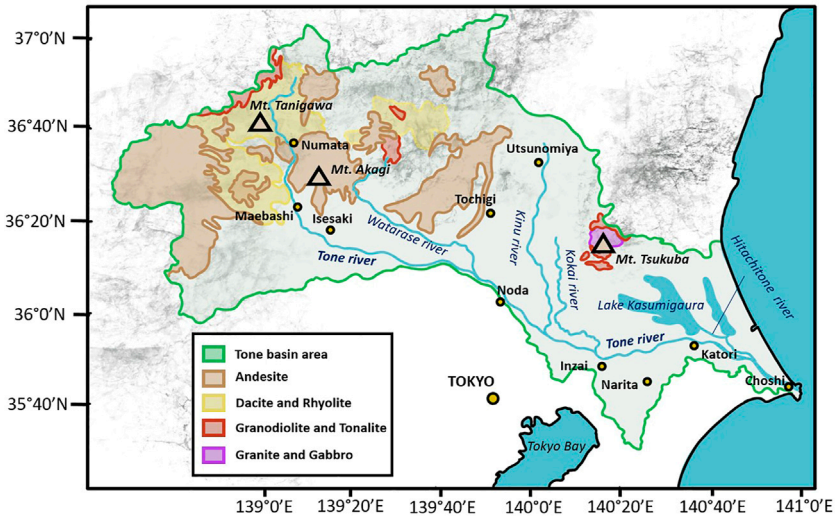

FIGURE 1
Geological map of the Tone River basin.

upstream areas; sites 1 and 2 are located at Mount Tanigawa, site 3 is located in the Tone River area close to Maebashi City, and sites 3-2 and 3-3 are located at Mount Akagi. Sample 3-2 was taken in the western part of Mount Akagi at the Akagishirakawa River. Sample 3-3 was taken southeast of Mount Akagi, at the Kasugawa River. Both the Akagishirakawa River and Kasugawa River join the Tone River *via* the Watarase River. The middle-stream area is represented by sampling sites 4–6. Sites 4 and 5 are located downstream from Isesaki City. Site 6 is located after the mixing of the Tone River and Watarase River. The downstream area is represented by sampling sites 7–9. Site 7 is located after the Kinugawa River merges with the Tone River, site 8 after the Kokai River, and site 9 is located close to Katori City. Sampling areas 10–12 represent a mixing zone of the Tone River that is influenced by the salty water from the Pacific Ocean with salinity ranging from 6.5 at site 10–9.1 at site 9. Sampling site 10 is located downstream of the mixing of the Tone River and Hitachitone River, site 11 is approximately 10 km from the estuary, and site 12 is about 5 km from the estuary. Four samples (K1–K4) of bottom sediment (0–10 cm depth) from Lake Kasumigaura were collected using an Ekman grab from a boat with the help of the National Institute for Environment Studies. Sample K5 was also taken using Ekman grab at the Hitachitone River, which connects Lake Kasumigaura and the Tone River.

Stream bank erosion is one of the main sources of suspended sediments in stream water, and may be a source of P during flood periods (Rahutomo et al., 2019). Therefore, nine bank sediment samples—six from the Tone River (1, 2, 4–7), three from tributaries of the Tone River (3-2, 3-3, and K5) —were collected by hand from single point of surficial material, representing only modern depositional surfaces. After collection, bottom sediment and bank sediment samples were transported in cooling boxes to the laboratory and frozen until analysis. Similar to bank sediments, soil sediment samples were taken from four sites as potential P sources. T1 represents Mount Tsukuba, AL-1 and AL-2 are soil samples from agricultural lands located to the southwest of the main body of Lake Kasumigaura in the downstream area of the Tone River, and soil sample K3-2 was taken from one of the bays of Lake Kasumigaura. These samples were collected by hand.

The three largest mountain groups along the river course were sampled for parent rock material, consisting of one sampling site at Mount Tanigawa (R1–R3), two sampling sites at Mount Akagi close to the Akagishirakawa River (R4) and Kasugawa River (R5), and one site at Mount Tsukuba (R6 and R7), which is one of the main P sources in the Kasumigaura area connected to the Tone River by the Hitachitone River. Locations of sampling sites are shown on the map in Figure 2.

2.3 Analytical methods

Bottom sediment, bank sediment, soil, and parent rock samples were dried for 3 days at 105°C and then ground using a tungsten mortar and pestle. These samples were divided into four subsamples, and different forms of P were quantified as P bound with Fe oxides/hydroxides (Fe-P), apatite P (Ca-P, $CaCO_3$-P and possibly some residual of Fe-, Al-, Mn-bound P), and non-apatite inorganic P (NAIP), representing some hardly extractable P and silica-bound P. The first subsample was extracted with citrate-dithionite-bicarbonate solution at pH 7.6; this fraction represents Fe-P. The second subsample was ashed for 6 h at 550°C and then extracted with 1 M HCl. The difference between subsample 1 and 2 represented the apatite P fraction. The third subsample was also extracted with 1 M HCl but without ashing. The difference between these two subsamples (2 and 3) represented the org-P fraction (Ruttenberg, 1992). Subsample 4, was extracted with hydrogen fluoride (HF) digestion with HNO_3 and $HClO_4$ pretreatment, and represents total P (TP). The difference between hydrogen fluoride and HCl 550°C subsamples represented NAIP. Phosphate in solution, after filtration, was analyzed by the standard molybdate-blue spectrophotometric method using a spectrophotometer (U-1500; Hitachi, Tokyo, Japan).

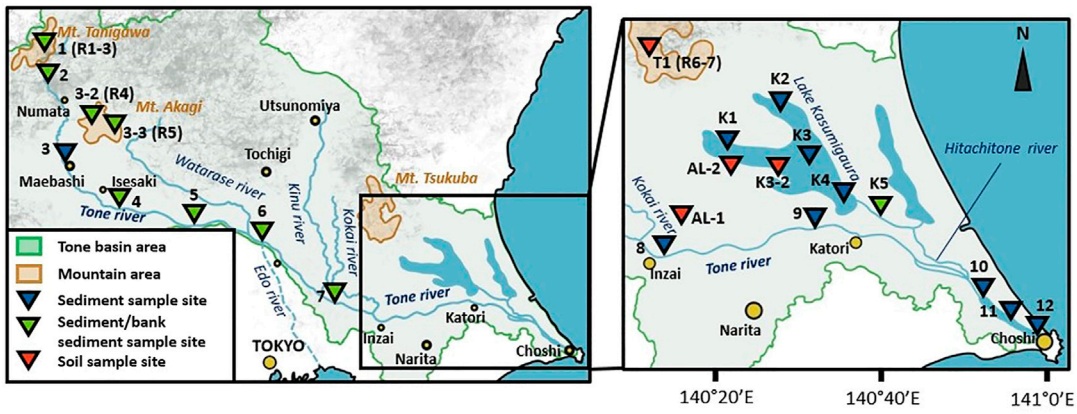

FIGURE 2
Locations of sampling sites in the Tone River basin. R1–R7 indicate the locations of parent rock sampling sites.

Although the SEDEX method (Ruttenberg, 1992) was originally developed for use with marine sediments, this method is often used for sequential extraction of P from freshwater sediments (Filippelli et al., 2006; Wang L. et al., 2013; Simon et al., 2009). For example, Liu et al. (2018) and Zheng et al. (2016) used a modified method with higher acid concentrations and longer extraction times. The reason for using higher acid concentrations (or stronger acids) is that river sediments can contain more mineral phases, such as iron and aluminum oxides/hydroxides, and apatite-P, that can adsorb or precipitate phosphorus, making it less available for extraction with original Ruttenberg's method. Using a stronger acid can help dissolve these mineral phases and release the P that can bind with them. Therefore, in this study, an additional phase of HF digestion was performed. The standard deviation of replicate measurements for each P form was less than 10% of the mean.

The non-ground subsample was used for grain size analyses. First, subsamples were weighed and put into a sieving machine (MVS-1; AS ONE, Osaka, Japan) with four sieves with mesh sizes ranging from 4 mm to 250 μm to separate the gravel and coarse sand fractions. All fractions were then weighed and the fraction with grain size <250 μm was put into a separate container for further laser analysis using a laser diffraction particle size analyzer (SALD-2300; Shimadzu, Kyoto, Japan). The sieved fraction was put into a glass container with purified water and left to stabilize with stirring for 5 min before analysis. The obtained data were tabulated with data for other grain sizes from the first step, and the overall grain size distribution was calculated with weight-based method.

3 Results

3.1 Grain size distribution in the bottom sediments along the Tone River

The upstream portion of the Tone River was mainly represented by gravel sediment: 91.4% at sampling site 1, 72.7% at site 2, and 58.8% at site 3. Approaching the middle-stream region of the Tone River, sediment grain size changed from gravel to sand. Sediments at sites 4–6 were composed mainly of the middle fraction of sand (1,000–500 μm), at around 73%, and contained only about 9% and 8% coarse sand and fine sand fractions, respectively. In the downstream area (sites 7–9), sediments were composed mainly of the middle sand fraction (59.7% on average), and contained 1% coarse sand and 36.8% fine sand. Among downstream samples, site 8 had the highest proportion of the middle sand fraction, while site 9 had the highest proportion of coarse sand. The mixing zone showed the most rapid change in sediment grain size stratification. While site 10 (mixing area of the Tone and Hitachitone rivers) mostly consisted of fine sand (grain size: 63–250 μm; 75.1%), site 11 had only 36.6% fine sand and 51% middle sand and 10.8% mud (grain size: <63 μm, i.e., silt and clay). Among mixing zone sites, site 12, the closest to the ocean, had the highest percentage of mud (26.8%), although fine sand was the main fraction (53.8%); the middle sand fraction was lowest at this site (17%) (Figure 3; Supplementary Table S2).

3.2 Changes in TP concentration in the Tone River basin

An notable increase in P concentration was observed between Mount Tanigawa (sites 1 and 2) and Mount Akagi (sites 3–5), resulting in an elevation of TP content in the bottom sediment from the upper reaches of the Tone River to the downstream area. The mean TP in the Tanigawa and Akagi areas were 9.7 and 14.5 μmol/g, respectively, representing an almost 5 μmol/g increase in TP in the latter (Figure 4A). From the middle-stream area, TP continued to increase smoothly by about 1.5–2.5 μmol/g among sampling sites. A decrease in total phosphorus (TP) content of 7 μmol/g was observed at site 9 compared to site 8, and a decrease of almost 10 μmol/g was observed at site 9 compared to site 10. On the other hand, the sampling sites in the mixing zone, including sites 10, 11, and 12, exhibited the highest TP contents, measuring 22.6, 25.7, and 26.6 μmol/g respectively.

Bottom sediment samples from the Lake Kasumigaura (K1–K5) showed a slight increase in TP concentration at sampling sites K1–K3, with an increase from 26.5 μmol/g to 30.3 μmol/g (a 3.8 μmol/g increase). Subsequently, there was a marked decrease

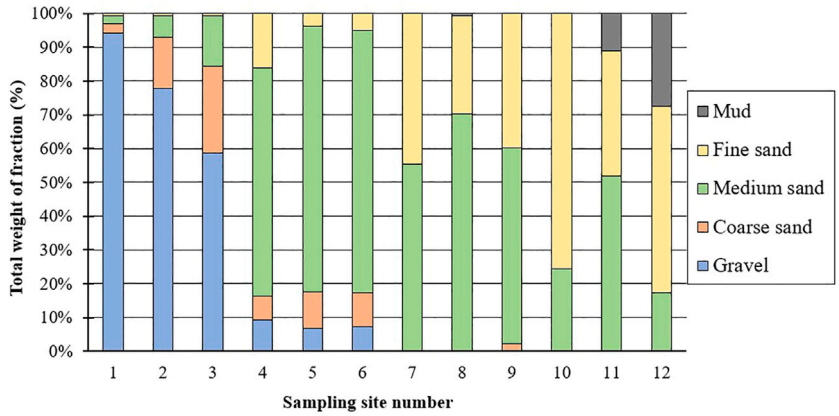

FIGURE 3
Grain size distribution in the bottom sediments of the Tone River.

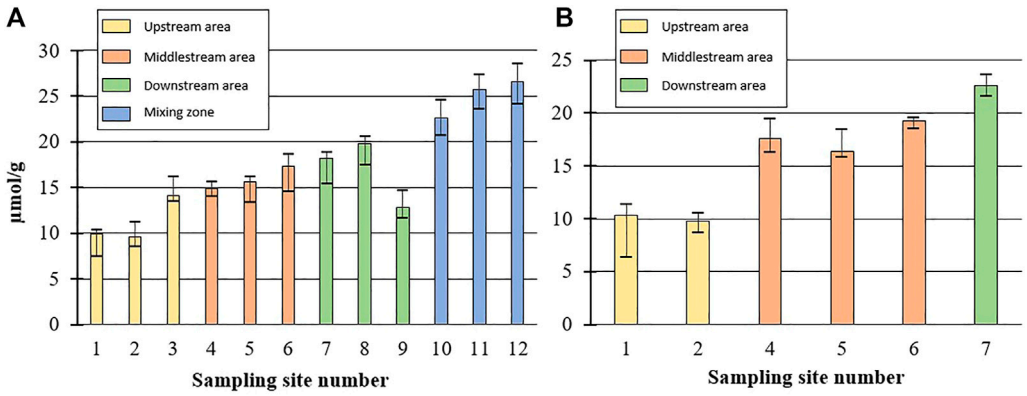

FIGURE 4
(A) TP changes in bottom sediments of Tone River. **(B)** TP changes in bank sediments of Tone River.

TABLE 1 TP contents in parent rocks in the Tone River basin.

Area	Sample Number	TP content (pmol/g)			Rock type
		Min	Mean	Max	
Tanigawa	R1	10.4	12.7	13.2	Rhyolite
	R2	16.7	22.7	23.9	Dacite
	R3	11.6	13.8	14.7	Rhyolite
Akagi	R4	30.5	35.7	37.4	Andesite
	R5	33.1	36.2	36.7	Andesite
Tsukuba	R6	25.5	27.9	28.8	Granodiolite
	R7	23.1	23.6	24.6	Granodiolite

in TP concentration towards sites K4–K5 (15.9 and 15.1 μmol/g respectively; Supplementary Figure S1A). Interestingly, site K3 also showed the greatest sediment thickness among all sites (about 100 cm) (GSI, 2021; Supplementary Figure S1B).

Similar to the bottom sediment samples, bank sediment TP showed notable increases between Mount Tanigawa and Mount Akagi (average of sites 1 and 2: 10.9 μmol/g; average of sites 4–6: 17 μmol/g) (Figure 4B). Parent rocks also showed differences in TP levels from

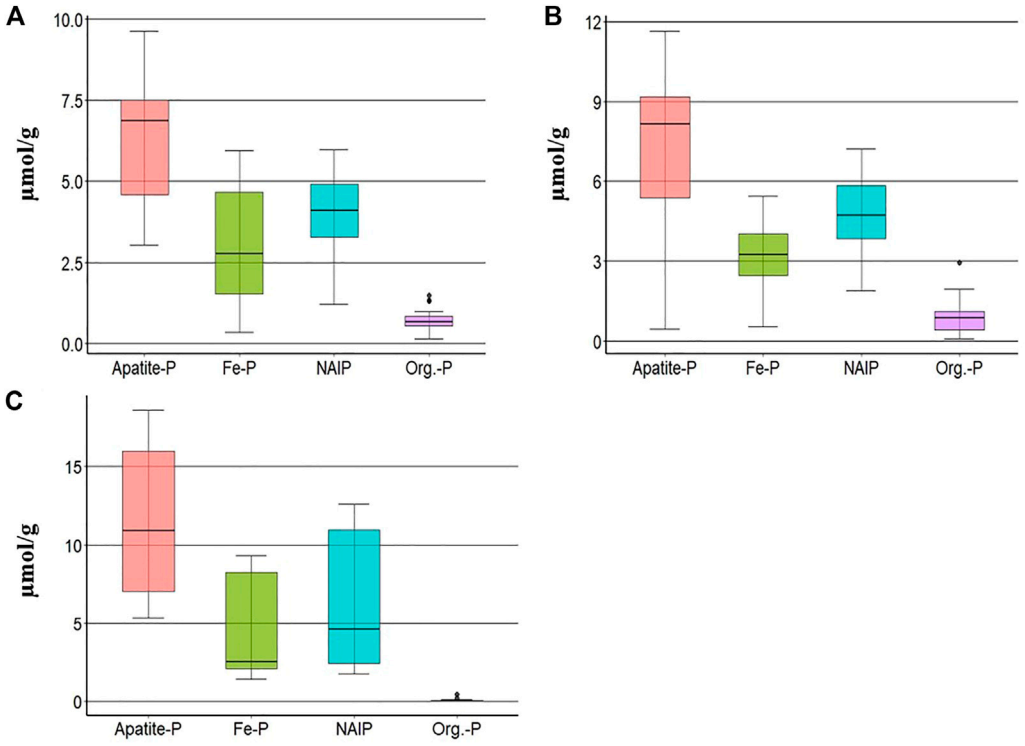

FIGURE 5
Mean concentrations (range) of different forms of P in **(A)** bottom sediments (n = 54), **(B)** bank sediments (n = 27), and **(C)** parent rocks (n = 21), where n = number of samples.

Mount Tanigawa to Mount Akagi and Mount Tsukuba. The mean TP concentrations at Mount Tanigawa (samples R1–R3) were in the range of 12.7–22.7 µmol/g, with a maximum TP concentration of 23.9 µmol/g in dacite rocks. The mean TP at Mount Akagi (R4–R5) showed higher P contents compared to both Mount Tanigawa and Mount Tsukuba (35.7 and 36.2 µmol/g, respectively), with a maximum TP content of 37.4 µmol/g at site R5, which also corresponded to the mean TP content in andesite rocks. The mean TP concentration in parent rock samples of Mount Tsukuba was 25.8 µmol/g (range: 23.1–28.2 µmol/g) (Table 1). The TP concentration in soil samples varied markedly over the course of the river, with the minimum concentration observed at site K3-2 (14.2 µmol/g) and the maximum at site AL-1, representing agricultural land (32.4 µmol/g).

3.3 Changes in P forms in the Tone River basin

TP was dominated by inorganic forms (apatite-P, NAIP, and Fe-P), which represented about 90% of the TP in the sediment samples of the Tone River. The mean concentrations of Apatite-P (Ca-P), Fe-P, NAIP, and org-P in bottom sediments along the course of the Tone River were 5.2, 3.7, 4.1 and 1.4 µmol/g, respectively. This P form distribution was also observed in parent rocks and bank sediments, where the most dominant form was apatite-P, followed in order by NAIP, Fe-P, and org-P (Figure 5).

Upper and lower error bars represent the largest value within 1.5 times interquartile range above 75th percentile and the smallest value below 25th percentile. Top and bottom of the boxplot stand for 75th and 25th percentile respectively. 50th percentile (median) shown as the horizontal bold line inside of the boxplot.

The percentage of Ca-P decreased from the upper reaches of the Tone River (46%) toward the downstream area (4% at site 12); similarly, NAIP decreased from about 29% to only 3%, except at sites 9 and 10 in the downstream area, where the proportion of NAIP increased to around 37%. In the mixing zone, NAIP showed the lowest concentration and continued to decrease toward site 12, where it reached a minimum of 0.2% of total IP. Meanwhile, Fe-P and org-P showed increasing trends, from 12% in the upper reaches to 37% in the mixing zone for Fe-P, and from 7% to almost 50% in the mixing zone for org-P (Figure 6).

Comparison of P concentrations in the bottom sediment between the mixing zone and other areas of the river showed that the increase in TP was due to the increases in Fe-P (7.3 µmol/g increase) and org-P (4.2 µmol/g increase) (Figure 7A). In contrast to the increases in Fe-P and org-P, the Ca-P fraction in the mixing zone was 2.8 µmol/g less than that in river bottom sediments. NAIP was relatively stable and did not show a marked change (0.3 µmol/g increase in the mixing zone).

There were small increases in all P forms in the bank sediments compared to bottom sediment samples, and the TP increase was mostly due to the inorganic forms (Figure 7B).

Soil samples collected in the downstream area of the Tone River showed relatively high org-P concentrations compared to the bottom and bank sediments along the entire course of the river (4.9 µmol/g on average, with lowest org-P of 3.2 µmol/g at site K3-2 and highest of 5.5 µmol/g at T1). Fe-P and Ca-P fractions varied significantly among soil samples. Fe-P concentrations were 3.6, 15.2, 8.2, and 4.1 µmol/g for

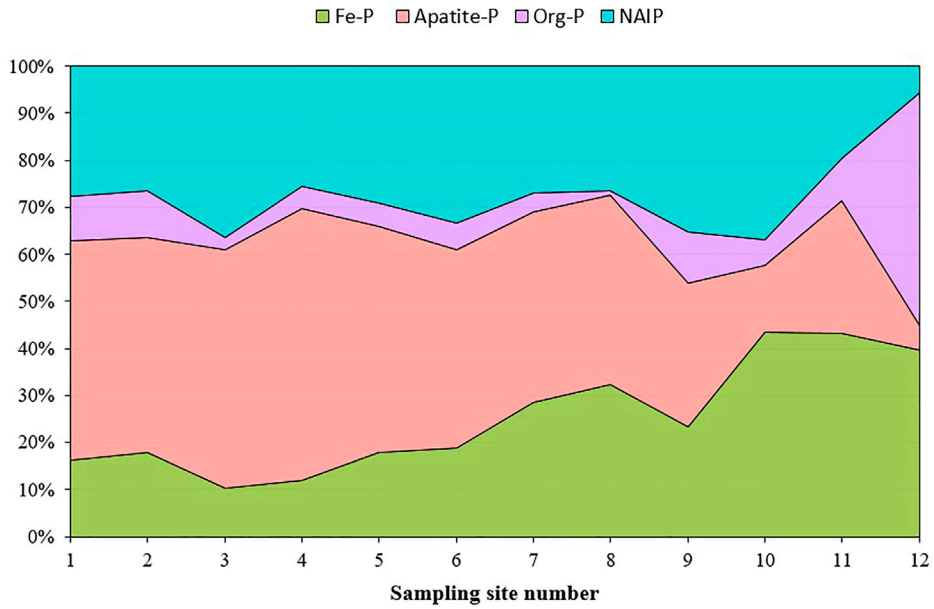

FIGURE 6
Stacked area plot of the percent change of different types of phosphorus within the Tone River flow.

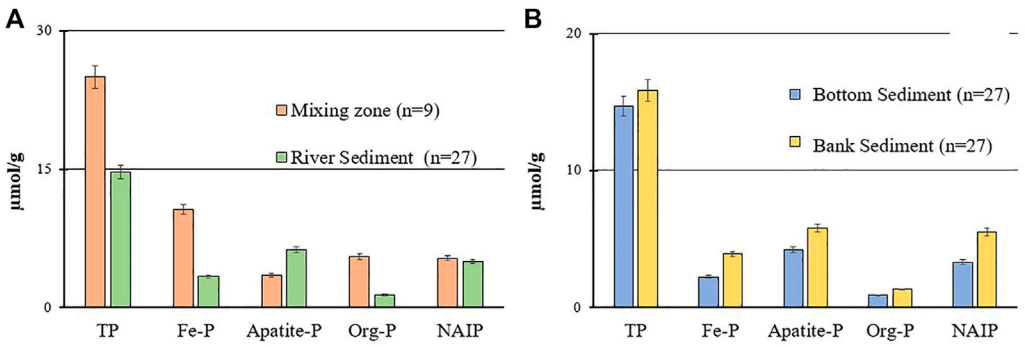

FIGURE 7
(A) Comparison of the mean concentrations of different P forms between the river bottom sediment samples and sediments deposited in the mixing zone area of the Tone River. **(B)** Comparison of the mean concentrations of different forms of P between Tone River sediment samples and riverbank samples (only sampling sites where both bottom and bank sediments samples were collected), where *n* = number of samples.

sites T1, AL-1, AL-2, and K3-2, respectively. Ca-P ranged from 1.9 μmol/g at K3-2 to 10.6 μmol/g at AL-1, with a mean concentration of 5.2 μmol/g. NAIP was mostly stable across all soil samples, with a mean concentration of 5.5 μmol/g.

4 Discussion

4.1 Influence of parent rock type on TP concentration in Tone River sediments

The TP concentration in parent rock material in the Tone River basin ranged from 9.7 μmol/g at Mount Tanigawa to a maximum of 38.9 μmol/g at Mount Akagi. These values were consistent with previous reports that average P concentration ranges between 7.2 and 55 μmol/g in igneous basaltic rocks, and between 0.9 and 27 μmol/g in sedimentary rocks (Reinmann and de Caritas, 1998). One reason for the increase of 5 μmol/g in TP from Mount Tanigawa to Mount Akagi in bottom sediments could be the different origins of the parent rocks in these areas. The bottom sediments in sites downstream of Mount Akagi showed higher overall IP concentrations than sites 1 and 2, resulting in an increase in TP. Furthermore, parent rock samples and bottom sediments showed similar Ca-P and NAIP distributions. For the Mount Tanigawa area, the mean Ca-P/IP ratios in bottom sediments and parent rock material were 51.1% and 51.7%, respectively, and the mean NAIP/IP ratios were 28.4% and 26.5%, respectively. For Mount Akagi, the mean Ca-P/IP ratios in bottom sediments and parent rocks were 49.6% and 45.9%, respectively,

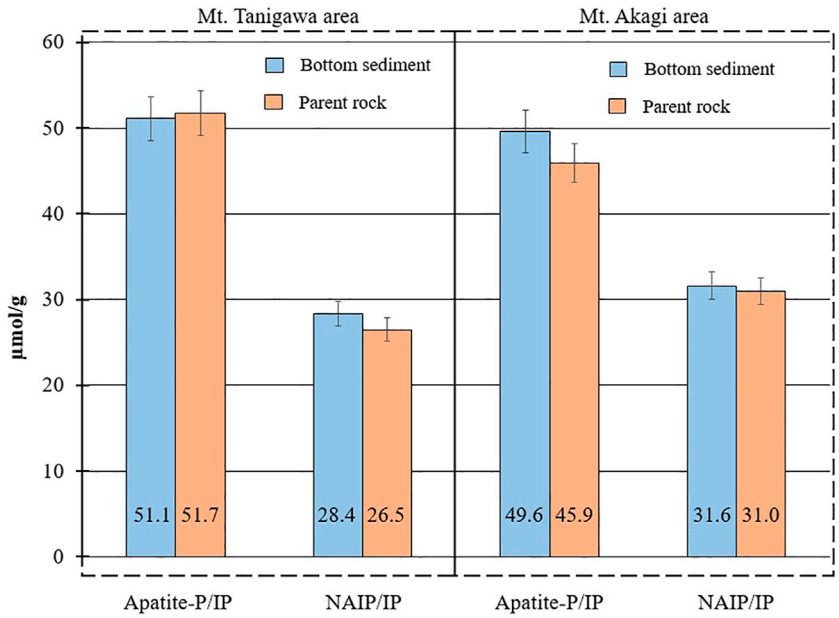

FIGURE 8
Ca-P and NAIP distributions in the bottom sediments and parent rock material in Mount Tanigawa and Mount Akagi areas.

and the mean NAIP/IP ratios were 31.6% and 30.9%, respectively (Figure 8). These data suggest that the P in parent rock can impact TP and P form distribution in sediments located downstream of the mountains (Wakamatsu et al., 2006).

4.2 Changes in P forms and dependence on grain size

Phosphate rocks are the main natural source of P, where it mostly exists as insoluble Ca-P, also known as apatite. In this study, the mean percentage of Ca-P contained in the bed sediments from the upper to the lower reaches of the Tone River was about 45%, and that in the bank sediments was 38%. The Ca-P/Fe-P ratio in the Tone River bottom sediments showed a negative correlation ($r^2 = 0.81$) (Figure 9). Although the sum of Fe-P and Ca-P showed no significant changes, the percentage ratio of the sum (Fe-P and Ca-P) to IP in the bottom sediment samples of the Tone River ranged from 57% to 64%. Ca-P seemed to be controlled by chemisorption on colloidal ferric and aluminum oxides/hydroxides adsorbed on the surface of the Ca-containing particles. The pH-dependent Ca-P variations were reflected by the Fe-P fraction (Oxmann et al., 2008; Oxmann et al., 2010; Golterman, 2001). Similar to this study, Oxmann et al. (2008) showed that Al/Fe-P mirrored Ca-P in the pH range 4–8, and the sum of these fractions remained mostly unchanged.

Several studies have examined the relationships of different forms of inorganic P to sediment grain size (Andrieux-Loyer and Aminot, 2001; Rao and Berner, 1997), and the Al/Fe-P form was shown to be related to fine-grained sediments. In this study, Al/Fe-bound P was also closely related to fine-grained particles (Table 2); therefore, the concentrations in the upstream and middle-stream areas, where the sediments were mostly represented by gravels (grain size: 4–16 mm), were the lowest compared to the downstream area of the Tone River where the range of the Fe-P form was between 0.3 and 10.9 µmol/g. In contrast to Fe-P, Ca-P was relatively evenly distributed among different grain size classes (Andrieux-Loyer and Aminot, 2001), leading to relatively smooth spread of Ca-P.

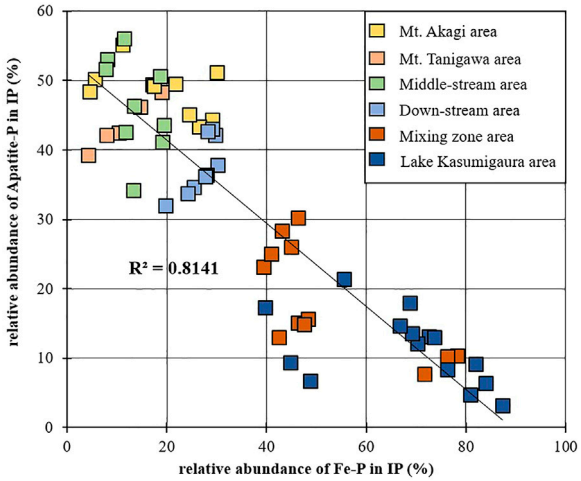

FIGURE 9
Correlation between the relative abundance of Fe-P and Apatite-P in IP (%) within the bottom sediments of the Tone River basin.

The NAIP fraction was relatively stable throughout all of the samples and sampling sites from upstream to downstream areas of the Tone River. The ratio of NAIP to total IP (NAIP/IP) was in the range of 14%–38%. This fraction did not show any significant correlation to any other P form or grain size.

TABLE 2 Correlation matrix for grain size and P species in bottom sediments of the Tone River.

Parameters	Fe-P	Org-P	Apat-P	NAIP	TP	Gravel (%)	Sand (%)	Mud (%)
Fe-P	1							
Org-P	0.72**	1						
Apat-P	−0.11	−0.47	1					
NAIP	0.03	−0.43	0.60*	1				
TP	0.74**	0.41	0.51	0.44	1			
Gravel (%)	−0.55	−0.24	0.02	−0.36	−0.67*	1		
Sand (%)	0.41	0.02	0.08	0.49	0.52	−0.97**	1	
Mud (%)	0.65*	0.91**	−0.40	−0.43	0.69*	−0.24	0.01	1

The statistical significance for following levels: * $p<0.05$ and ** $p<0.01$.

Despite the paucity of studies on the relationships between org-P and sediment grain size, some reports have agreed that organic matter is preferentially adsorbed in muddy sediments (Turner et al., 1994; Vilas et al., 2005). Sediments of smaller grain sizes have relatively large specific surface area, which can enhance the adsorption of metals, organic matter, and other contaminants (Turner et al., 1994). Moreover, some portion of mud-sized sediment is thought to be derived from bacterial and phytoplankton remains, which are rich in organic carbon and org-P (Coppola et al., 2005; Coppola et al., 2007). Org-P is often the dominant component of the TP content in silt and clay fractions (i.e., mud), while in sandy fractions the org-P/TP ratio varies significantly (Makarov et al., 2002). Finer sediments are normally localized to areas with lower hydrodynamic forcing, such as the deepest points of estuaries. Similar results were obtained in this study; the org-P/TP ratio increased toward the mixing zone of the Tone River, where the sediment grain size was smaller, from around 5% to around 50% at sampling site 12, which was high in silty sediments.

4.3 Phosphorus forms change mechanisms in sediments along the Tone River flow

The Tone River is one of the major river systems in Japan that plays a critical role in the transport of nutrients, including phosphorus. P is often the rate-limiting element for primary production, especially in freshwater ecosystems compared to marine ecosystems (Doering et al., 1995). Therefore, it is important to understand the supply of phosphate to the water column and the underlying mechanisms. As water flows downstream, the P concentration and binding forms in the bottom sediments may undergo significant changes due to various biogeochemical processes. There are several studies conducted on temperature, pH, salinity, and dissolved oxygen (DO) effect on release of phosphate from sediments into the water column (Bidle et al., 2002; Zhang et al., 2012; Koriyama et al., 2013; Muta et al., 2019). However, not many researches are conducted on spatial distribution and changes of P forms in the river bodies. The distribution of P in the river bottom sediments can change from the up-stream to the down-stream due to various natural and anthropogenic factors. This study focused on understanding the longitudinal changes in the total concentration and binding forms of phosphorus (apatite-P, Fe-P, NAIP and org-P) in the bottom sediments of the Tone River.

In the upper reaches of the Tone River, phosphorus in the sediments is typically dominated by mineral-bound P forms, such as apatite and iron-bound P, which are less bioavailable to aquatic organisms. This is due to the geology of the watershed, which is dominated by granitic and metamorphic rocks (dacite, rhyolite) that are relatively low in organic matter and P. The total P concentration in the sediments is also relatively low, reflecting low inputs from anthropogenic sources. This study showed that TP concentration in the river bottom sediments in the up-stream area is almost fully depending on the geological condition of the area (net concentration of apatite-P in the parent rocks).

In the mid-lower reaches of the Tone River, the sediment P forms content is shifting from apatite-P dominated towards Fe- and Al-bound P (in this study Fe-P). This is due to the presence of iron and aluminum-rich soils in the watershed, as well as inputs from wastewater treatment plants and other point sources. Another reason for this shift is that apatite-P can be converted to iron-bound P through several steps (diagenesis). In general, this process involves the dissolution of apatite particles, which releases the P, followed by the precipitation of iron oxide/hydroxide minerals that bind the P (Palmer-Felgate et al., 2011). The dissolution of apatite particles can be influenced by a number of factors, including pH, temperature, and the concentration of other ions in the water (Yang et al., 2017; Shi et al., 2020). The surface area-to-volume ratio of the river bottom sediment particles can also play an important role in the dissolution process. Finer sediment particles have a greater surface area per unit volume than coarser sediment particles, which means that they can potentially dissolve more apatite particles and release more P into the water (Green et al., 2014; Liao et al., 2015; Zhou et al., 2019), this was also observed in this study.

As the Tone River flows downstream towards the estuary, inputs of organic matter and nutrients from agricultural and urban sources lead to an increase in the organic- P fraction in the sediments. While the bottom sediments in the up-, middle- and downstream of the Tone River were dominated by inorganic P forms, the mixing zone was dominated by org-P form. This change occurs due to a variety of factors. Water chemistry can influence the transformation of P forms. Changes in pH, redox potential, and the concentration of other ions, such as iron and aluminium can affect the solubility and reactivity of P compounds. For example, under reducing conditions, iron-bound phosphorus (Fe-P) can be converted to organic phosphorus (Org-P) through microbial processes such as microbial degradation of organic matter and/or microbial reduction of Fe(III) to Fe(II). The microbial processes

result in the formation of organic molecules that incorporate phosphorus in their structure and contribute to the build-up of organic phosphorus in soils and sediments (Reddy and DeLaune, 2008; Chen et al., 2017; Liu et al., 2021). Sedimentation processes can also play a role in the transformation of P forms. The accumulation of organic matter and other sediment components can create anoxic conditions that promote the conversion of inorganic P to organic P. Land use and management practices can have a significant impact on P transformation in aquatic systems. Human activities such as agriculture, urbanization, and wastewater treatment can introduce organic matter and nutrients to aquatic systems, which can promote the formation of organic P (Sharpley et al., 2000; Schindler et al., 2008).

Lake Kasumigaura is also an important source of P to the Tone River. Several studies have shown that Lake Kasumigaura is a major source of dissolved reactive phosphorus (DRP) to the Tone River. The DRP inputs from Lake Kasumigaura can have a significant impact on downstream P dynamics, especially during periods of high flow and low dilution capacity in the river (Fujimoto et al., 2017; Nagano et al., 2020). This study showed that in addition to DRP, Lake Kasumigaura can also be a source of particulate phosphorus (PP) to the Tone River. PP is a less bioavailable form of P that is bound to sediment particles and can be transported downstream during high-flow events. While PP is generally considered to be less of a concern for eutrophication than DRP, it can still contribute to sediment accumulation and enhance P forms change in the downstream portion of the Tone River.

In summary, understanding the changes in phosphorus forms in the Tone River is critical for managing its water quality and the associated ecological impacts. This study highlights the importance of considering natural factors, such as geology and sediment particle size, as well as anthropogenic factors, such as land use and wastewater inputs, in understanding the distribution and transformation of phosphorus forms in the river. This knowledge can help inform effective management strategies to reduce nutrient pollution and maintain the health of the river ecosystem.

Data availability statement

The raw data supporting the conclusion of this article will be made available by the authors, without undue reservation.

Author contributions

RK designed the study, generated and analyzed the datasets, and wrote the manuscript. YU and MY designed the study, joined field surveys, and revised the manuscript.

Funding

This work was supported by JSPS KAKENHI project (22A402), MacroCoast (Macro coastal oceanography: integrated simulation for the material dynamics from the land through the open ocean).

Acknowledgments

We express our gratitude to Y. Arata for the assistance provided with sediment grain size analysis, and to Captain Hidaka for facilitating the collection of river sediments. We are also grateful to Y. Tashiro, M. Inada, R. Ueba for supporting field research and sample analyses in the laboratory. Furthermore, we would like to thank Editor and Reviewers for their valuable contribution towards enhancing the quality of this manuscript.

Conflict of interest

The authors declare that the research was conducted in the absence of any commercial or financial relationships that could be construed as a potential conflict of interest.

Publisher's note

Supplementary material

The Supplementary Material for this article can be found online at: https://www.frontiersin.org/articles/10.3389/feart.2023.1060312/full#supplementary-material

SUPPLEMENTARY TABLE S1
Sampling site information.

SUPPLEMENTARY TABLE S2
Grain size distribution in bottom sediments of the Tone River.

SUPPLEMENTARY FIGURE S1
(A) TP changes in Lake Kasumigaura. **(B)** Lake Kasumigaura sediment accumulation.

References

Andrieux-Loyer, F., and Aminot, A. (2001). Phosphorus forms related to sediment grain size and geochemical characteristics in French coastal areas. *Estuar. Coast. Shelf Sci.* 52, 617–629. doi:10.1006/ecss.2001.0766

Bidle, K. D., Manganelli, M., and Azam, F. (2002). Regulation of Oceanic silicon and carbon preservation by temperature control on bacteria. *Science* 298, 1980–1984. doi:10.1126/science.1076076

Chen, C., Huang, C., Wong, M. H., Wong, J. T. F., and Sun, W. (2017). Microbial conversion of inorganic phosphorus to organic forms in soils: Progress and prospects. *Chemosphere* 184, 594–600. doi:10.1016/j.chemosphere.2017.06.025

Coppola, L., Gustafsson, O., Andersson, P., and Axelsson, P. (2005). Fractionation of surface sediment fines based on a coupled sieve-SPLITT (split flow thin cell) method. *Water Res.* 39, 1935–1945. doi:10.1016/j.watres.2005.04.005

Coppola, L., Gustafsson, O., Andersson, P., Eglinton, T. I., Uchida, M., and Dickens, A. F. (2007). The importance of ultrafine particles as a control on the distribution of

organic carbon in Washington Margin and Cascadia Basin sediments. *Chem. Geol.* 243, 142–156. doi:10.1016/j.chemgeo.2007.05.020

Doering, P. H., Oviatt, C. A., Nowicki, B. L., Klos, E. G., and Reed, L. W. (1995). Phosphorus and nitrogen limitation of primary production in a simulated estuarine gradient. *Mar. Ecol. Prog. Ser.* 124, 271–287. doi:10.3354/meps124271

Filippelli, G. M., Souch, C., Menounos, B., Slater-Atwater, S., Jull, A. J. T., and andSlaymaker, O. (2006). Alpine lake sediment records of the impact of glaciation and climate change on the biogeochemical cycling of soil nutrients. *Quat. Res.* 66, 158–166. doi:10.1016/j.yqres.2006.03.009

Fisher, T. R., Peele, E. R., Ammerman, J. W., and Harding, L. W. (1992). Nutrient limitation of phytoplankton in chesapeake bay. *Mar. Ecol. Prog. Ser.* 82, 51–63. doi:10.3354/meps082051

Fujimoto, K., Ito, S., Otsuka, S., and Nakamura, T. (2017). Spatial and temporal variations in the phosphorus distribution in the Tone River basin, Japan. *J. Hydro-environment Res.* 16, 1–16. doi:10.1007/s11356-017-9361-1

Golterman, H. L. (2001). Phosphate release from anoxic sediments or 'What did Mortimer really write? *Hydrobiologia* 450, 99–106. doi:10.1023/a:1017559903404

Green, S. A., Stott, A. W., Ritsema, C. J., and Geissen, V. (2014). The dissolution of apatite in soils: A review of mechanisms, modelling approaches and controlling factors. *Earth-Science Rev.* 139, 47–58. doi:10.1016/j.earscirev.2014.09.001

GSI (2021). Geospatial information authority of Japan. Available at: https://www.gsi.go.jp/kankyochiri/kanto-kasumigaura.html (Accessed December, 2021).

Hartmann, J., Moosdorf, N., Leuerwald, R., Hinderer, M., and West, A. J. (2014). Global chemical weathering and associated p-release — The role of lithology, temperature and soil properties. *Chem. Geol.* 363, 145–163. doi:10.1016/j.chemgeo.2013.10.025

Hayashi, M., Yanagi, T., and Hashimoto, T. (2000). Standing stock ratios of nitrogen and phosphorus in the Seto Inland Sea. *Oceanogr. Jpn.* 9, 83–89. doi:10.5928/kaiyou.9.83

Holland, H. D. (1984). *The chemical evolution of the atmosphere and oceans*. Princeton, New Jersey, United States: Princeton University Press.

Kohler, J., Hilt, S., Adrian, R., Nicklisch, A., Kozerski, H. P., and Walz, N. (2005). Long-term response of a shallow, moderately flushed lake to reduced external phosphorus and nitrogen loading. *Freshw. Biol.* 50, 1639–1650. doi:10.1111/j.1365-2427.2005.01430.x

Koriyama, M., Hayami, Y., Koga, A., Yamamoto, K., Insasetyo, A., Hamada, T., et al. (2013). Seasonal variations of water column nutrients in the inner area of Ariake Bay, Japan: The role of muddy sediments. *Environ. Monit. Assess.* 185, 6831–6846. doi:10.1007/s10661-013-3068-8

Krom, M. D., Brenner, S., Kress, N., and Gordon, L. I. (1991). Phosphorus limitation of primary productivity in the eastern Mediterranean Sea. *Limnol. Oceanogr.* 36, 424–432. doi:10.4319/lo.1991.36.3.0424

Krom, M. D., Emeis, K. C., and Van Cappellen, P. (2010). Why is the Eastern Mediterranean phosphorus limited? *Prog. Oceanogr.* 85, 236–244. doi:10.1016/j.pocean.2010.03.003

Kubo, A., Hashihama, F., Kanda, J., Horimoto-Miyazaki, N., and Ishimaru, T. (2019). Long-term variability of nutrient and dissolved organic matter concentrations in Tokyo Bay between 1989 and 2015. *Limnol. Oceanogr.* 64, 209–222. doi:10.1002/lno.10796

Lazarri, P., Solidoro, C., Salon, S., and Bolzon, G. (2015). Spatial variability of phosphate and nitrate in the Mediterranean Sea: A modeling approach. *Deep Sea Res. Part I Oceanogr. Res. Pap.* 108, 39–52. doi:10.1016/j.dsr.2015.12.006

Liao, Q., Xie, X., and Huang, Q. (2015). Effects of sediment grain size on the characteristics of phosphorus release from sediments in a eutrophic lake. *Environ. Sci. Pollut. Res.* 22 (13), 10027–10035. doi:10.1007/s11356-015-4347-x

Liu, B., Gao, C., Zeng, Q., and Huang, Q. (2021). The role of microorganisms in the transformation of iron-bound phosphorus in paddy soils: A review. *J. Soils Sediments* 21 (6), 2496–2509. doi:10.1007/s11368-020-02607-2

Liu, S., Wang, X., Zhang, L., Zhang, Y., and Yang, Y. (2018). Effects of extraction conditions on different forms of phosphorus in sediments of three Chinese shallow lakes. *J. Soils Sediments* 18 (1), 283–291. doi:10.1007/s11368-017-1754-4

Mainstone, C., and Parr, W. (2002). Phosphorus in rivers – ecology and management. *Sci. Total Environ.* 282, 25–47. doi:10.1016/S0048-9697(01)00937-8

Makarov, M. I., Haumaier, L., and Zech, W. (2002). Nature of soil organic phosphorus: An assessment of peak assignments in the diester region of 31P NMR spectra. *Soil Biol. Biochem.* 34, 1467–1477. doi:10.1016/S0038-0717(02)00091-3

Muta, N., Umezawa, Y., Yamaguchi, A., Suzaki, H., Wada, M., Nakata, H., et al. (2019). Estimation of spatiotemporal variations in nutrient fluxes from sediments in the seasonally hypoxic Omura Bay, Japan. *Limnology* 21, 341–356. doi:10.1007/s10201-019-00591-1

Nagano, M., Yoshimura, C., Hayashi, K., and Tsuda, R. (2020). Importance of Lake Kasumigaura as a phosphorus source to the Tone River during baseflow conditions. *Limnology* 21 (1), 67–77. doi:10.1007/s10201-019-00617-6

Nezat, C. A., Blum, J. D., Yanai, R. D., and Park, B. B. (2008). Mineral sources of calcium and phosphorus in soils of the northeastern United States. *Soil Sci. Soc. Am. J.* 72, 1786–1794. doi:10.2136/sssaj2007.0344

Okamoto, T., and Ikeda, H. (2000). Origins of the silt bed section at the down-stream area of the Tone river. *Bull. Terr. Environ. Res. Cent. Univ. Tsukuba* 1, 35–41.

Oxmann, J. F., Pham, Q. H., and Lara, R. J. (2008). Quantification of individual phosphorus species in sediment: A sequential conversion and extraction method. *Eur. J. Soil Sci.* 59, 1177–1190. doi:10.1111/j.1365-2389.2008.01062.x

Oxmann, J. F., Pham, Q. H., Schwendenmann, L., Stellman, J. M., and Lara, R. J. (2010). Mangrove reforestation in Vietnam: The effect of sediment physicochemical properties on nutrient cycling. *Plant Soil* 326, 225–241. doi:10.1007/s11104-009-0003-4

Palmer-Felgate, E. J., Bowes, M. J., Stratford, C., Neal, C., and MacKenzie, S. (2011). Phosphorus release from sediments in a treatment wetland: Contrast between DET and EPC0 methodologies. *Ecol. Eng.* 37, 826–832. doi:10.1016/j.ecoleng.2010.12.024

Peng, H., Jiang, A., and Wang, H. (2021). Adsorption and desorption characteristics of phosphorus on sediments in Panzhihua section of Jinsha River, China. *IOP Conf. Ser. Earth Environ. Sci.* 651, 042059. doi:10.1088/1755-1315/651/4/042059

Rahutomo, S., Kovar, J. L., and Thompson, M. L. (2019). Phosphorus transformations in stream bank sediments in Iowa, USA, at varying redox potentials. *J. Soils Sediments* 19, 1029–1039. doi:10.1007/s11368-018-2139-4

Rao, Ji-L., and Berner, R. A. (1997). Time variations of phosphorus and sources of sediments beneath the chang jiang (yangtze river). *Mar. Geol.* 139, 95–108. doi:10.1016/s0025-3227(96)00100-4

Reddy, K. R., Kadlec, R. H., Flaig, E., and Gale, P. M. (1999). Phosphorus retention in streams and wetlands: A review. *Crit. Rev. Environ. Sci. Technol.* 29, 83–146. doi:10.1080/10643389991259182

Reddy, K. R., and DeLaune, R. D. (2008). *Biogeochemistry of wetlands: Science and applications*. Boca Raton, Florida, United States: CRC Press. ISBN: 9781420053521.

Reimann, C., and de Caritas, P. (1998). *Chemical elements in the environment*. Berlin-Heidelberg: Springer-Verlag, 398.

Ruttenberg, K. C. (1992). Development of a sequential extraction method for different forms of phosphorus in marine sediments. *Limnol. Oceanogr.* 37, 1460–1482. doi:10.4319/lo.1992.37.7.1460

Ruttenberg, K. C. (2004). The global phosphorus cycle. *Treatise Geochem.* 8, 585–643. doi:10.1016/B0-08-043751-6/08114-0

Schindler, D. W., Hecky, R. E., Findlay, D. L., Stainton, M. P., Parker, B. R., Paterson, M. J., et al. (2008). Eutrophication of lakes cannot be controlled by reducing nitrogen input: Results of a 37-year whole-ecosystem experiment. *Proc. Natl. Acad. Sci.* 105 (32), 11254–11258. doi:10.1073/pnas.0805108105

Sharpley, A., Metcalf, J. A., and Withers, P. J. A. (2000). Phosphorus inputs and eutrophication of receiving waters: A review. *J. Environ. Qual.* 29 (1), 28–36. doi:10.2134/jeq2000.00472425002900010005x

Shi, L., Wang, D., Qian, L., Hellio, C., Fauchon, M., Trepos, R., et al. (2020). Reduction of potential ennoblement of stainless steel in natural seawater by an ecofriendly biopolymer. *J. Environ. Chem. Eng.* 8 (1), 103609. doi:10.1016/j.jece.2019.103609

Simon, N. S., Lynch, D., and Gallaher, T. N. (2009). Phosphorus fractionation in sediment cores collected in 2005 before and after onset of an Aphanizomenon flos-aquae bloom in upper Klamath Lake, OR, USA. *Water Air Soil Pollut.* 204, 139–153. doi:10.1007/s11270-009-0033-9

Turner, S. J., Flindell, P. A., Hendri, D., Hardjana, I., Lauricella, P. F., Lindsay, R. P., et al. (1994). Sediment-hosted gold mineralisation in the ratatotok district, north sulawesi, Indonesia. *J. Geochem. Explor.* 50, 317–336. doi:10.1016/0375-6742(94)90029-9

Vilas, F., Bernabeu, A. M., and Mendez, G. (2005). Sediment distribution pattern in the rias baixas (NW Spain): Main facies and hydrodynamic dependence. *J. Mar. Syst.* 54, 261–276. doi:10.1016/j.jmarsys.2004.07.016

Wakamatsu, T., Konohira, E., Shindo, J., Yoshioka, T., Okamoto, K., Itaya, A., et al. (2006). Dissolved inorganic phosphate concentration in stream water in Japan and factors controlling the concentration. *J. Jpn. Soc. Water Environ.* 29, 679–686. doi:10.2965/jswe.29.679

Wang, L., Ye, M., Li, Q., Zou, H., and Zhou, Y. (2013). Phosphorus speciation in wetland sediments of Zhujiang (Pearl) river estuary, China. *Chin. Geogr. Sci.* 23, 574–583. doi:10.1007/s11769-013-0627-4

Weigelhofer, G., Hein, T., and Bondar-Kunze, E. (2018). Phosphorus and nitrogen dynamics in riverine systems: Human impacts and management options. Riverine ecosystem management. *Aquat. Ecol. Ser.* 8, 187–202. doi:10.1007/978-3-319-73250-3_10

Williams, P. M. (1969). Organic and inorganic constituents of the amazon river. *Nature* 218, 937–938. doi:10.1038/218937a0

Withers, P., and Jarvie, H. (2008). Delivery and cycling of phosphorus in rivers: A review. *Sci. Total Environ.* 400, 379–395. doi:10.1016/j.scitotenv.2008.08.002

Yang, J., Li, J., Li, M., and Zhou, Q. (2017). The effect of pH and temperature on the dissolution of hydroxyapatite nanoparticles in aqueous solution. *J. Environ. Sci.* 51, 109–118. doi:10.1016/j.jes.2016.06.018

Zhang, K., Cheng, P., Zhong, B., and Wang, D. (2012). Total phosphorus release from bottom sediments in flowing water. *J. Hydrodynamics, Ser. B* 24, 589–594. doi:10.1016/S1001-6058(11)60281-3

Zheng, M., Zhu, B., Han, X., and Morgenroth, E. (2016). Formation of aerobic granules for the treatment of real and low-strength municipal wastewater using a sequencing batch reactor operated at constant volume. *Water Res.* 106, 341–350. doi:10.1016/j.watres.2016.09.007

Zhou, S., Zhao, X., Wang, Y., Xu, X., and Liu, Y. (2019). An emerging environmental concern: Biochar-induced dust emissions and their potentially toxic properties. *Sci. Total Environ.* 687, 813–820. doi:10.1016/j.scitotenv.2019.05.007

frontiers | Frontiers in Earth Science

TYPE Original Research
PUBLISHED 09 May 2023
DOI 10.3389/feart.2023.1067744

OPEN ACCESS

EDITED BY
Mashura Shammi,
Jahangirnagar University, Bangladesh

REVIEWED BY
Jeffrey E. Richey,
University of Washington, United States
Lishan Ran,
The University of Hong Kong, Hong Kong SAR, China
Yuanbi Yi,
Hong Kong University of Science and Technology, Hong Kong SAR, China
Selvaraj Kandasamy,
Xiamen University, China

*CORRESPONDENCE
Sanjeev Kumar,
sanjeev@prl.res.in

RECEIVED 12 October 2022
ACCEPTED 11 April 2023
PUBLISHED 09 May 2023

CITATION
Sarkar S, Verma S, Begum MS, Park J-H and Kumar S (2023), Sources, supply, and seasonality of total suspended matter and associated organic carbon and total nitrogen in three large Asian rivers—Ganges, Mekong, and Yellow. *Front. Earth Sci.* 11:1067744. doi: 10.3389/feart.2023.1067744

Sources, supply, and seasonality of total suspended matter and associated organic carbon and total nitrogen in three large Asian rivers—Ganges, Mekong, and Yellow

Siddhartha Sarkar[1,2], Sangeeta Verma[1], Most Shirina Begum[3], Ji-Hyung Park[3] and Sanjeev Kumar[1]*

[1]Geosciences Division, Physical Research Laboratory, Ahmedabad, India, [2]Indian Institute of Technology, Gandhinagar, India, [3]Department of Environmental Science and Engineering, Ewha Womans University, Seoul, Republic of Korea

Asian rivers, covering ~29% of the global river surface area, account for ~35% of the global freshwater discharge and transport a disproportionately large flux (~70%) of total suspended matter to the oceans. With recent anthropogenic and climate-induced changes in the flow regimes, it is challenging to constrain the fluxes and elemental signatures of the suspended organic matter in rivers. This study aimed to understand seasonal changes in the characteristics of total suspended matter (TSM) associated organic carbon (C) and total nitrogen (N) during high and low flow periods in three large Asian rivers (Ganges, Mekong, and Yellow). By measuring organic C and total N contents and their isotopic compositions at multiple locations along the studied rivers, distinct seasonality in the sources of organic matter was observed. Allochthonous sources dominated the organic matter pool during the high flow condition, whereas autochthonous organic matter derived from enhanced phytoplankton production appeared to have dominated during low flow. C/N ratio showed positive correlation with altitude during wet period, which reversed during dry, supporting the transition of sediment dominated high flow riverine system into relatively clear and productive low flow system. Generally, organic matter content in TSM was higher during the low flow with signatures of potential N_2 fixation. Temporal analysis based on present and earlier estimates of fluxes and yields of TSM indicated manifold decrease in TSM load and associated C and N fluxes over decades in the three river systems largely attributed to reduction in river discharge. Wastewater dominated locations showed similar C and N contents and isotopic signatures as those of productive river waters during low flow, indicating a possible interference in the interpretation of biogeochemical information.

KEYWORDS

rivers, total suspended matter, particulate organic matter, carbon, nitrogen, Ganges, Yellow, Mekong

1 Introduction

Inland waters cover less than 4% of the surface of the Earth and play a disproportionately large role in the global biogeochemical cycles, especially for carbon (C) and nitrogen (N) (Cole et al., 2007; Tranvik et al., 2009; Downing, 2010; Verpoorter et al., 2014). Annually, around 50% (~2.7 billion metric tons) of C removed from the atmosphere via terrestrial sink winds up in the inland waters, which then has a huge potential to process and eventually either bury or emit the C in forms of organic/inorganic matter and greenhouse gases (GHGs: CO_2 and CH_4) respectively (Battin et al., 2009; Aufdenkampe et al., 2011; Bastviken et al., 2011; Raymond et al., 2013). Rivers act as active conduits for the transport of C and N from the terrestrial to the marine system. Annually ~0.9 and 0.046 Pg of C and N, respectively, get exported to the global oceans (Hope et al., 1994; Mackenzie et al., 2002; McKee, 2003; Suchet et al., 2003; Cole et al., 2007; Biddanda, 2017). This flux of C, if not constrained, could disturb the elemental budgets and offset our climate predictions to a large extent. Nitrogen is closely connected to C in the global biogeochemical cycle and often acts as a limiting nutrient, thereby making its flow vital along the land ocean continuum. With increasing human perturbations to the biosphere and a changing climate, the movement and fluxes of C and N along the river continuum has been largely altered over the past decades.

Stable isotopes of C (^{12}C and ^{13}C) and N (^{14}N and ^{15}N) have proven to be robust tools for tracking the organic matter sources and identifying the biogeochemical processes in aquatic environments (Meybeck, 1982; Pocklington and Tan, 1987; Louchouarn et al., 1997; Louchouarn et al., 1999; Hopkinson et al., 1998). Isotope analysis also provides information regarding the watershed, especially the dominant vegetation, and the level of anthropogenic developments (Hedges et al., 1986; Lambert et al., 2017). Terrestrial plants can largely be classified into C3 and C4 plants depending on their photosynthetic pathways and each have distinct isotopic signatures (C3: $\delta^{13}C$ −32‰ to −22‰, C4: $\delta^{13}C$ −14‰ to −9‰) (Ehleringer, 1978; Ehleringer and Pearcy, 1983). Similarly, the C isotopic signatures of freshwater macrophytes and plankton range between −28‰ to −18‰ and −42‰ to −24‰, respectively (Kendall et al., 2001). The isotopic signatures of soil organic matter (SOM) reflect that of the dominant vegetation over the region (Boutton, 1996). The N isotopic signatures of SOM in most soils varies between +2‰ and +5‰, with cultivated soils showing lower values (Broadbent et al., 1980). The relative abundance of these end members along with various biogeochemical processes, both physiochemical and microbial, determine the concentrations and isotopic signatures of total suspended matter (TSM) in rivers. Intense weathering and fluvial control on the TSM in rivers result in a TSM with dominant allochthonous inputs and therefore represent the isotopic signatures of SOM and litter of the catchment (Lloret et al., 2011; Tamooh et al., 2012). Increased productivity, on the other hand, increases the relative contribution of planktons to the particulate organic matter (POM) fraction of TSM and therefore lowers its C isotopic composition ($\delta^{13}C_{TSM}$). Similarly, N isotopic signatures of TSM ($\delta^{15}N_{TSM}$) integrate processes like dinitrogen fixation, denitrification, and mineralization. Over the years, stable isotopes of C and N in organic matter have been widely used for source apportionment of river—estuarine suspended matter and sediments (Thornton and McManus, 1994; Prasad et al., 2017; Gawade et al., 2018; Wang et al., 2018; Huang et al., 2020), paleoclimate reconstructions (Rahman et al., 2020), and to decipher the biogeochemical processes driving their concentrations and signatures.

Among the world's rivers, those originating from the Tibetan Plateau carry ~70% of the global suspended sediments to the oceans (Milliman and Meade, 1983; Ran et al., 2013). Tropical monsoonal rivers such as the Ganges and Mekong, originating from the Himalayan highland, have high sediment yields as well (Lu et al., 2010). The suspended matter load in rivers represents an aggregation of minerals and organic matter, which acts as a substrate for several microbially mediated processes that often releases CO_2, CH_4, and N_2O as by-products. Understanding the sources and fate of organic matter is therefore vital to constrain the loss processes of C and N from these systems. Furthermore, with increasing urbanisation and human induced changes in the flow regimes of world rivers, it is essential to revisit the export fluxes of TSM and associated C and N from the rivers. In this study, an attempt has been made to understand the dynamics of C and N in TSM of three large Asian river systems, i.e., Ganges, Mekong, and Yellow. The specific aims of the study were to understand i) seasonal and spatial variations in C and N in TSM along the river continuum across the altitudinal gradient, ii) the effect of seasonality on their concentrations and isotopic compositions along with underlying processes, and iii) the export fluxes of C and N from these rivers and potential long-term changes compared to previous studies.

2 Materials and methods

2.1 Study area

The Ganges, Mekong, and Yellow River originate from the Himalayan mountains and the Tibetan plateau (Figure 1). The source of the Ganges is the Gangotri Glacier in the Garhwal Himalaya. With headwaters at the elevation of 3,800 m (Gaumukh), the mainstem of the Ganges forms later at Devprayag with the confluence of the Alaknanda and Bhagirathi Rivers (Singh, 2007). Thereafter, the river descends down into the plains and traverses a journey of ~2,700 Kilometer (km), with a catchment of 1,260,000 km^2 (Parua, 2010). Once the river enters the Gangetic plains, it passes through major cities like Kanpur, Prayagraj, Varanasi, and Patna. A major tributary of the Ganges (i.e., the Yamuna) passes through Delhi and joins the mainstem near Prayagraj. The river supports large human population along its banks, providing water for irrigation and drinking purposes. Two bifurcated distributaries of Ganges, Hooghly and Padma, flow through India and Bangladesh, respectively. The Padma River confluence with two major rivers in Bangladesh, i.e., Brahmaputra and Meghna, before discharging into the Bay of Bengal (Parua, 2010).

Rising at an altitude of 5,000–6,000 m at the source in the Tibetan Plateau, the Yellow River covers around 5,464 km, draining a catchment of 753,000 km^2 to finally discharge into the Bohai Sea near Shandong Province, China (Xu and Ma, 2009; Peng et al., 2010; Miao et al., 2011; Ran et al., 2013). In terms of the channel length, the Yellow River is the second largest in Asia and

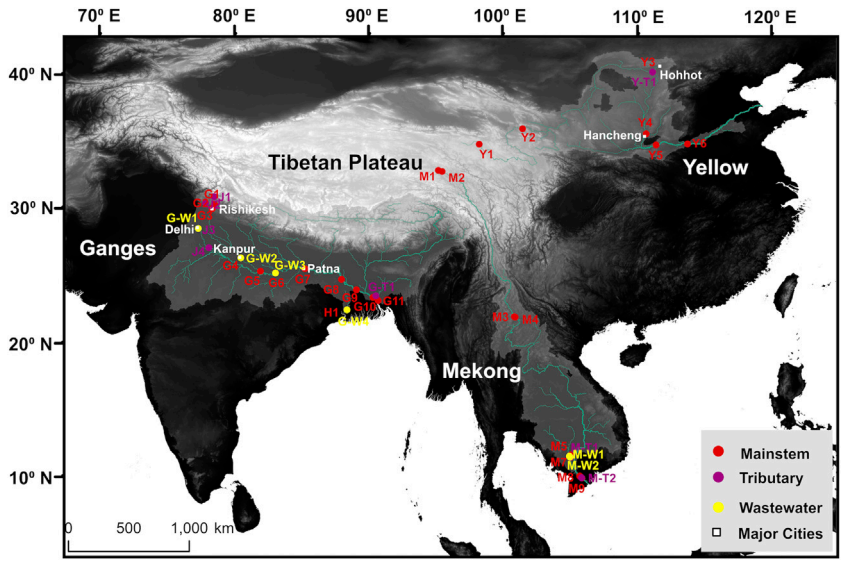

FIGURE 1
Map showing sampling locations on the Ganges, Mekong, and Yellow River Basins (shaded).

seventh in the world. It is followed by the Mekong and Ganges-Brahmaputra at third and sixth place, respectively. The upper reaches of the Yellow River are predominantly an arid setting with complex geological structures, mainly comprising of old metamorphosed rocks, carbonates and modern fluvio-lacustrine sediments (Wang et al., 2012; Ran et al., 2013). In the middle reaches, the river drains the loess plateau, with abundant Quaternary loess deposits (Zhang et al., 1995; Chen et al., 2005; Wu et al., 2005). Finally, the lower reaches reflect a flat alluvial plain. The lower reaches have extensive man-made levees along its banks giving the perched riverbed an elevation of 3–4 m higher than the surrounding floodplains (Bulletin of Chinese River Sediment (BCRS), 2000; Peng et al., 2010).

The Mekong River originates at an elevation of 4,968 m in the Tibetan Plateau and flows southwards through several countries (China, Myanmar, Thailand, Lao PDR, Cambodia, and Vietnam) to drain into the South China Sea. The channel length of the river is around 4,800 km and the drainage basin area is 795,000 km^2. The upper reaches of the river are confined to narrow deep gorges with high energy, resulting in largescale transport of sediments to the lower reaches (Hori, 2000; Gupta, 2005; MRC, 2005). Only at the very lower stages, near Kratie, Cambodia, the Mekong River has been observed to drain flat terrains and flood plains where there is scope for sedimentation (Gupta et al., 2002; Wang et al., 2011). The Ganges, Mekong, and Yellow River support around 400, 70, and 107 million people in its basins (Parua, 2010; Gao et al., 2017; Park et al., 2018; MRC: Mekong River Commission, 2019).

2.2 Basin characteristics of the Ganges, Mekong, and Yellow river

Based on the amount of fluvial runoff (discharge/surface area), Milliman and Farnsworth (2011) classified the Yellow River basin as arid (<100 mm y^{-1} runoff) and the Ganges and Mekong River basins as humid basins (250–750 mm y^{-1}). But within each of these river basins there is large spatial heterogeneity of the hydrological parameters. For instance, the northern catchments of the Ganges River basin receive heavier rainfall as compared to the southern parts, which leads to an increased annual runoff (750 mm y^{-1}) from the northern tributaries as compared to the low runoff (300 mm y^{-1}) in the rivers draining the southern basin (Parua, 2010). Seasonal distribution of rainfall over the Ganges, Mekong, and Yellow River basins clearly shows the rainfall rates to be minimum in the Yellow River basin as compared to the Ganges and the Mekong River Basin (Figures 2A–F). The northern parts of the Ganges River basin and the central and southern regions in the Mekong River basin receive relatively more precipitation as compared to the other regions over these basins. Normalized differential vegetation index (NDVI), which is widely used for vegetation classification and crop monitoring, revealed that among the three basins, Mekong was the most densely vegetated followed by the Ganges and Yellow River basins (Figures 2G–I). The Yellow River basin seemed to be dominantly arid with scarce vegetation in the upstream reaches with dominant ecosystem being alpine meadows (Weiguo et al., 2003; Ran et al., 2013). The average soil organic carbon (SOC) in the three basins were below 300 t ha^{-1} (Figures 2J–L). Among the three river basins, the Ganges had most of its region with poor SOC content followed by the Yellow River, which had high SOC contents only in the upstream reaches of the basin. The upstream reaches of the Yellow River basin have been reported to have SOC content ~1.5%–39% whereas the loess plateau has SOC below 0.8% (Ran et al., 2013). The Mekong River basin had relatively large SOC contents in the soils with higher contents in the middle reaches (Figure 2L).

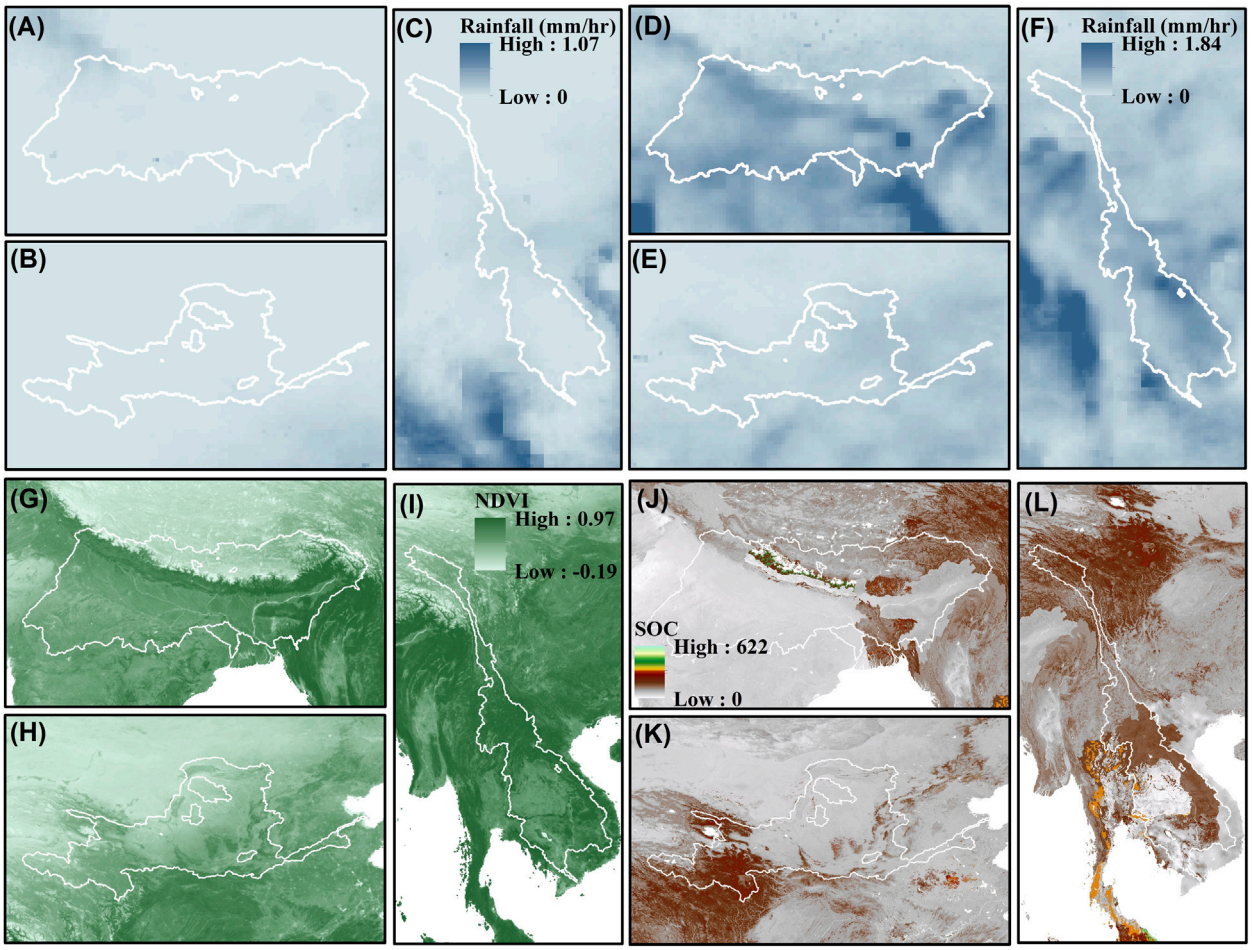

FIGURE 2
Time average rainfall over the river basins (Ganges, Mekong, and Yellow) for the dry [**(A–C)**: January–May] and wet [**(D–F)**: July–October] seasons during 2016–2018. Normalized differential vegetation index (NDVI) showing the distribution of vegetated land cover across the **(G)** Ganges, **(H)** Mekong, and **(I)** Yellow River Basin. Briefly, higher NDVI values indicate hardwood trees and dense forest canopy, whereas low values represent scarce vegetation, shrubland, and arid deserts. Soil organic carbon contents in the surficial soils of the **(J)** Ganges, **(K)** Mekong, and **(L)** Yellow River Basin. Data source: Global Soil Organic Carbon Map (GSOC map), published and maintained by Food and Agriculture Organisation (FAO) of the United Nations (*http://54.229.242.119/GSOCmap/*).

2.3 Sample collection and laboratory analysis

The sampling for the present study was carried out as a part of a larger project aimed at assessing the dynamics of GHGs in these anthropogenically modified Asian river systems (Begum et al., 2021). Sampling campaigns were carried out along mainstem reaches of the Ganges, Mekong, and Yellow River along with few tributaries and wastewater drains between August 2016 and July 2019. The mainstems were divided in upper, middle and lower reaches. Wastewater samples were collected at outlets of natural streams or constructed drains used for discharging urban sewage (Supplementary Table S1; Begum et al., 2021). Sampling was conducted during the wet (July–September; Ganges: n = 21, Mekong: n = 11 and Yellow: n = 7) and the dry (January–May; Ganges: n = 9, Mekong: n = 9 and Yellow: n = 2) seasons to capture the high and low flow conditions (Figure 1). Briefly, water samples were collected at 10–20 cm below the surface using polycarbonate bottles or a portable water sampler (Masterflex E/S, Cole-Parmer, United States). *In situ* water quality parameters were measured using a portable multiparameter probe (Orion 5-Star Portable, Thermo Scientific, United States). Samples were frozen within 12 h and shipped to the laboratory wherein thawed water was filtered through pre-combusted (4 h at 400°C) and pre weighed glass fibre filters (Whatman GF/F, 0.7 µm pore size) for TSM. The filters were dried at 60°C for 48 h and weighed gravimetrically for estimating the TSM load. Filters for particulate organic carbon (POC) concentration and its stable isotopic composition ($\delta^{13}C_{TSM}$) were fumigated in HCl vapours to remove any inorganic C and analysed using an EA-IRMS (Flash 2000 connected to a Delta V, Thermo Fisher Scientific, Germany). Filters for particulate nitrogen (PN) concentrations and isotopic composition ($\delta^{15}N_{TSM}$) were not treated with HCl vapours. IAEA standards of cellulose (IAEA-CH-3; $\delta^{13}C$ =−24.72‰; C content = 44.4%) and ammonium sulphate (IAEA-N-2; $\delta^{15}N$ = 20.3‰; N content = 21.2%) were used as laboratory standards for C and N contents and isotopic analysis. The analytical precision for C and N isotopic composition for repeat measurement of standards were better than 0.1‰ and 0.3‰, respectively. The precision for C and N contents were better than 10%.

TABLE 1 Length, basin area, and annual discharge of the Ganges, Mekong, and the Yellow River systems.

River	Length (km)	Basin area ($\times 10^3$ km^2)	Discharge (km^3 yr^{-1})	References
Ganges	2,700	1,260	1,270*	Parua (2010), Milliman and Farnsworth (2011)
Mekong	4,800	880	550	MRC: Mekong River Commission (2019)
				Milliman and Farnsworth (2011)
Yellow	5,500	753	15	Milliman and Farnsworth (2011)

(* at the confluence of Ganges and Meghna, downstream of Ganges-Brahmaputra confluence.).

2.4 Statistical analysis

Shapiro-Wilk test was applied to check the normality in the distribution of the data using SigmaPlot (Systat, United States). To analyze significant difference in measured parameters across seasons and basins, a one-way ANOVA on ranks using the Kruskal-Wallis's method, followed by Dunn's test was performed (for the data not normally distributed). Spearman rank correlation and Pearson's correlation among parameters were performed in R. Isotope mixing model was used to identify the source of organic matter in these river systems. Briefly, the isotopic signature of the source was obtained from the slope of the regression between the C concentration of the pool of interest and the product of $\delta^{13}C$ and C concentrations (Miller and Tans, 2003). This method is based on the principle of conservation of mass and mixing of C sources with distinct isotopic signatures. This method was further extended for the source identification of N in TSM. Mixing models have been widely used in related studies around riverine DIC and GHGs (Campeau et al., 2017; O'Dwyer et al., 2020; Begum et al., 2021). We attempted to use this model to distinguish the source isotopic signatures across basins and across seasons.

2.5 Estimation of export fluxes and yields

The fluxes and yields of organic matter were calculated based on the following equations:

$$F_{TSM} = Q \times TSM \quad (1)$$

$$F_{POC_{(or\,PN)}} = F_{(TSM)} \times [\%\,OC\ (or\ \%\,N)_{TSM}] \quad (2)$$

$$Y_{POC} = F_{POC} / A \quad (3)$$

here, TSM is the median TSM concentration at the lower sampling sites (i.e., outlet), Q is the annual discharge, F_{TSM} is the annual flux of TSM, F_{POC} is the annual flux of organic C, F_{PN} is the annual flux of N, A is the catchment surface area and Y_{POC} is the annual yield of POC from the catchment. The discharge data were taken from the existing literature (Table 1) and the concentration values used for flux calculation are shown in Table 2.

3 Results

3.1 Total suspended matter

Total suspended matter (TSM) concentration was high during the monsoon season in the mainstem of all the three river systems (Ganges: 263.5 ± 232.9 mg L^{-1}; Mekong: 136.3 ± 106.4 mg L^{-1}; Yellow: 707.4 ± 944.2 mg L^{-1}1; Figures 3A, D, G). In the Ganges basin, high TSM was observed in the Yamuna (a major tributary of Ganges) near Dakpatthar Barrage (1,940.6 mg L^{-1}), Delhi (254.4 mg L^{-1}) and at several sites in the Ganges mainstem along major cities (393 mg L^{-1} near Rishikesh; 341.3 mg L^{-1} near Kanpur; 416.9 mg L^{-1} near Patna; 828.2 mg L^{-1} at Hardinge Bridge near Kushtia, and 416.6 mg L^{-1} at the confluence of Ganges and Brahmaputra near Mawa) (Supplementary Table S1). TSM in the Mekong mainstem was the highest in the upstream reaches (128.5 ± 64.1 mg L^{-1}), followed by the middle reaches (82.4 ± 26.3 mg L^{-1}) and tributaries (54.7 ± 2.7 mg L^{-1}) (Figure 3D). In the Yellow River, very high TSM were observed at two downstream sites near the outlet of loess plateau (1941.6 mg L^{-1}) and upstream of Sanmenxia Dam, Hancheng (1909.2 ± 64.1 mg L^{-1}) (Figure 3G; Supplementary Table S1). During the dry season, TSM was low in the Ganges (53.9 ± 34.9 mg L^{-1}) and Mekong (20.7 ± 6.0 mg L^{-1}), whereas high TSM load was observed at the sites along the middle reaches of the Yellow River (1,656.4 mg L^{-1}) (Figures 3A, D, G). Wastewater TSM concentrations were around 116.2 ± 36.4 mg L^{-1} in the Ganges and 111.7 ± 54.7 mg L^{-1} in the Mekong (Supplementary Table S1).

3.2 Particulate organic carbon

During monsoon, POC concentrations varied significantly along the mainstem of the Ganges (average ~2.58 ± 1.50 mg L^{-1}) with low values near the headwaters (1.01 ± 0.27 mg L^{-1}), which increased towards the middle (3.12 ± 1.07 mg L^{-1}) and downstream reaches (3.09 ± 1.85 mg L^{-1}) (Figure 3B). The highest POC concentration (~39.47 mg L^{-1}) was observed in the wastewater draining into the Ganges (Supplementary Table S1). The Yamuna also followed a similar trend with increasing POC from the headwaters (0.52 mg L^{-1}) to urban location near Delhi (8.39 mg L^{-1}) (Supplementary Table S1). In general, the mean POC in the Ganges mainstem declined from monsoon to dry season (Figure 3B); however, the station on the Yamuna near Delhi showed an increase in the POC (~16.89 mg L^{-1}). Compared to the Ganges, the average concentration of POC in the Mekong was relatively low during monsoon (1.57 ± 0.65 mg L^{-1}), with 1.84 mg L^{-1} in the upstream reach, later falling to 0.62 mg L^{-1} and steadily increasing to 2.83 mg L^{-1} in the middle reach (Figure 3E). Downstream reaches of the Mekong River had POC ~1.55 ± 0.26 mg L^{-1} with even lesser concentration (1.21 ± 0.17 mg L^{-1}) at the lower reaches where two tributaries join. During the dry season, Mekong had very low POC (downstream: 0.69 ± 0.12 mg L^{-1}, tributaries: 0.79 ± 0.24 mg L^{-1}) (Figure 3E).

TABLE 2 Concentrations, annual fluxes, and yields of suspended particulate carbon and nitrogen in some Asian rivers. TSM, POC and PN values shown from the present study represent median concentrations of selected downstream locations [Ganges (Dry): G9 and G12; Ganges (Wet): G8, G9, G10 and G11; Mekong (Dry and Wet): M8 and M9; and Yellow (Wet): Y6], which have been used for flux and yield calculations during this study. Complete dataset from the present study have been provided in Supplementary Table S1.

River	TSM (mg L^{-1})	POC (mg L^{-1})	PN (mg L^{-1})	F_{POC} ($\times10^8$ kg y^{-1})	Y_{POC} ($\times10^2$ kg km^{-2} y^{-1})	F_{PN} ($\times10^6$ kg y^{-1})	Y_{PN} (kg km^{-2} y^{-1})	References
Ganges (Dry)	44	0.528	0.007	24	19	34	27	This study
Ganges (Wet)	274.3	3.292	0.046					
Mekong (Dry)	17.5	0.209	0.003	2.8	3.5	3.9	4.9	This study
Mekong (Wet)	67.5	0.810	0.011					
Yellow (Dry) (At Tongguan)	1,656.4	19.900	0.278	0.44	0.59	0.62	0.83	This study
Yellow (Wet)	161.2	1.934	0.027					
Yellow Lijin	3,589	13.279	2.512	4.1	5.45*	69	91.63*	Ran et al. (2013)
Yellow Lijin	2,522	11.679	5.411	3.89	5.17*	134	177.96*	Wang et al. (2012)
Mekong	80.8	2.010	0.188	16.7	18.98*	150	170.46*	Ellis et al. (2012)
Rivers draining Western Ghats (India)	83	2.860	NA	7.9	70.3	NA	NA	Reddy et al. (2021)

(*recalculated from the fluxes from the respective studies and the basin area from Table 1).

Similar to that in the Ganges, the highest POC in the Mekong River basin was observed at the wastewater discharge site (~4.71 mg L^{-1} in monsoon and 21.28 ± 21.87 mg L^{-1} during the dry season). The Yellow River had a wide range of POC along its mainstem (4.15 ± 3.99 mg L^{-1}) with lower concentration in the upstream reach (0.75 ± 0.03 mg L^{-1}) to increase in the middle (5.85 ± 3.86 mg L^{-1}) (Figure 3H). Surprisingly DaHeiHe tributary had the highest POC (~15.78 mg L^{-1}). During the dry season, two sites sampled showed 7.86 mg L^{-1} POC in the middle reach and 4.10 mg L^{-1} in the DaHeiHe tributary (Supplementary Table S1).

3.3 Particulate nitrogen

During monsoon, particulate nitrogen in the Ganges mainstem varied between 0.08 and 1.46 mg L^{-1} (mean: 0.60 ± 0.40) (Figure 3C). Similar to POC, the upstream reach had low PN (0.12 ± 0.06 mg L^{-1}) as compared to the middle (0.76 ± 0.40 mg L^{-1}) and downstream reach (0.64 ± 0.36 mg L^{-1}). The highest PN was observed in the wastewaters (2.75 ± 3.20 mg L^{-1}) followed by that in the Yamuna (1.24 ± 0.86 mg L^{-1}). PN was low during the dry season (0.25 ± 0.13 mg L^{-1}) except for the site in Yamuna near Delhi (~2.60 mg L^{-1}) (Figure 3C; Supplementary Table S1). PN in the Mekong during monsoon had a low range (0.20 ± 0.11 mg L^{-1}) with the upstream site having PN at 0.24 mg L^{-1}. PN showed a wide range in the middle (0.21 ± 0.18 mg L^{-1}) and downstream reaches (0.19 ± 0.07 mg L^{-1}) with low values for tributaries (0.13 ± 0.02 mg L^{-1}) (Figure 3F; Supplementary Table S1). PN decreased during the dry season with average concentration ~0.06 ± 0.03 mg L^{-1} in the downstream reaches and ~0.09 ± 0.04 mg L^{-1} in the tributaries (Figure 3F; Supplementary Table S1). In the Yellow River, PN showed a wide range (0.84 ± 1.05 mg L^{-1}) with low concentrations in the upstream region (0.08 ± 0.03 mg L^{-1}) and higher concentrations with wider range (1.22 ± 1.12) mg L^{-1} in the middle reaches (Figure 3I). The PN was high in the Yellow River during the dry period with concentration ~1.51 mg L^{-1}. In all the river basins, the highest PN concentrations were observed in the wastewaters (Ganges: 2.75 ± 3.20 mg L^{-1} in monsoon and 2.40 mg L^{-1} in dry period; Mekong: 1.00 mg L^{-1} in monsoon and 2.01 ± 1.58 mg L^{-1} in dry period) (Supplementary Table S1).

In the Ganges and the Mekong, C/N ratio in TSM were lower during the wet period. In the Ganges, the C/N ratio near the headwaters were ~8.1 ± 1.7, and dropped near the middle (4.3 ± 0.6) and lower reaches (4.7 ± 1.2) (Figure 3A). In the Mekong the C/N ratio remained similar along the mainstem during the wet period (8.1 ± 1.5) (Figure 3D). Similar to the Ganges, the Yellow River witnessed a fall in C/N ratio during the wet period from the upper (9.7 ± 2.9) to the middle (6.5 ± 3.9) and lower (4.5) reaches (Figure 3G). During the dry period, C/N ratios were relatively higher in the Ganges mainstem (5.7 ± 0.9) and downstream reaches of the Mekong (11.7 ± 2.4) (Figures 3A, D).

3.4 Isotopic composition of total suspended matter

$\delta^{13}C_{TSM}$ did not show much variation along the whole continuum of the Ganges River (monsoon: −25.4‰ ± 2.2‰; dry: −28.7‰ ± 1.4‰) (Figure 3B). However, during monsoon, the $\delta^{15}N_{TSM}$ was high in the middle reaches (11.4‰ ± 2.4‰) as

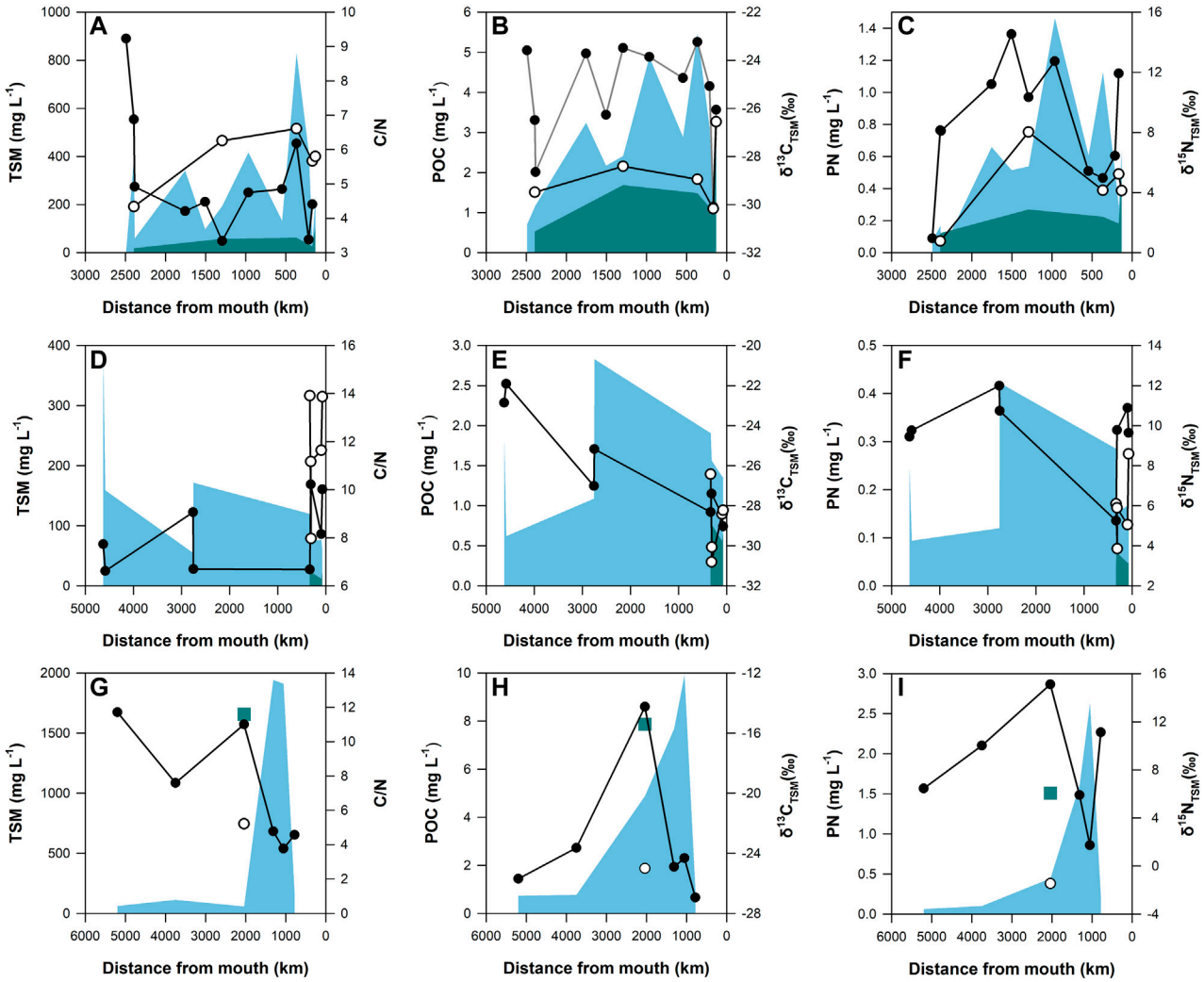

FIGURE 3
Variation of TSM, C/N, POC, $\delta^{13}C_{TSM}$, PN and $\delta^{15}N_{TSM}$ along the mainstem of Ganges **(A–C)**, Mekong **(D–F)** and Yellow River **(G–I)**. Shaded area represents TSM, POC and PN in wet (blue) and dry (dark green) seasons. Circles connected by solid lines represent C/N, $\delta^{13}C_{TSM}$ and $^{15}N_{TSM}$ in wet (black circles) and dry (white circles) seasons. In Yellow river, dry seasons data is represented by scatter plot (dark green square and white circle).

compared to the other sections (mainstem mean: 8.6‰ ± 4.0‰; upstream: 4.0‰ ± 4.6‰; downstream: 7.19‰ ± 3.21‰; Figure 3C). The Yamuna had the lowest $\delta^{15}N_{TSM}$ with average value ~2.0‰ ± 1.4‰. In the Ganges, the average $\delta^{15}N_{TSM}$ decreased during the dry season to 4.5‰ ± 2.6‰. The Mekong River showed similar range as the Ganges for $\delta^{13}C_{TSM}$ (Monsoon: −26.3‰ ± 2.7‰; Dry: −28.8‰ ± 1.7‰) and $\delta^{15}N_{TSM}$ (Monsoon: 9.7‰ ± 2.0‰; Dry: 5.9‰ ± 1.7‰) (Figures 3E, F). The $\delta^{13}C_{TSM}$ was highest in the Yellow River (Monsoon: −23.3‰ ± 4.6‰; Dry: −25.0‰) (Figure 3H). $\delta^{15}N_{TSM}$ was high in the Yellow River during monsoon (8.4‰ ± 4.7‰) and surprisingly showed negative value during the dry period (- 1.5‰) (Figure 3I). Overall, we also observed consistently higher $\delta^{13}C_{TSM}$ during monsoon in the three rivers. The wastewater isotopic signatures for $\delta^{13}C_{TSM}$ and $\delta^{15}N_{TSM}$ in the Ganges were −25.8‰ ± 0.4‰ and 3.5‰ ± 3.8‰, respectively. The same for the Mekong were −25.8‰ ± 0.7‰ and 2.5‰ ± 1.6‰, respectively (Supplementary Table S1).

4 Discussion

4.1 Total suspended matter along the river continuum

Overall, TSM varied over a broad range along the continuum of the studied rivers with relatively higher concentrations near major urban areas. In the Ganges, for example, high TSM were observed near major urban clusters like Rishikesh, Kanpur and Patna. This is generally attributed to different levels of anthropogenic activities, including agricultural practices, which play a significant role in mobilizing the surface soils and subsequent loading into the river (Asselman et al., 2003; Walling and Fang, 2003; Hunter and Walton, 2008). Furthermore, higher TSM near major cities could be a result of wastewater inputs. The Mekong River had lower TSM concentrations compared to the Ganges with decreasing concentrations from upstream to downstream. Along the

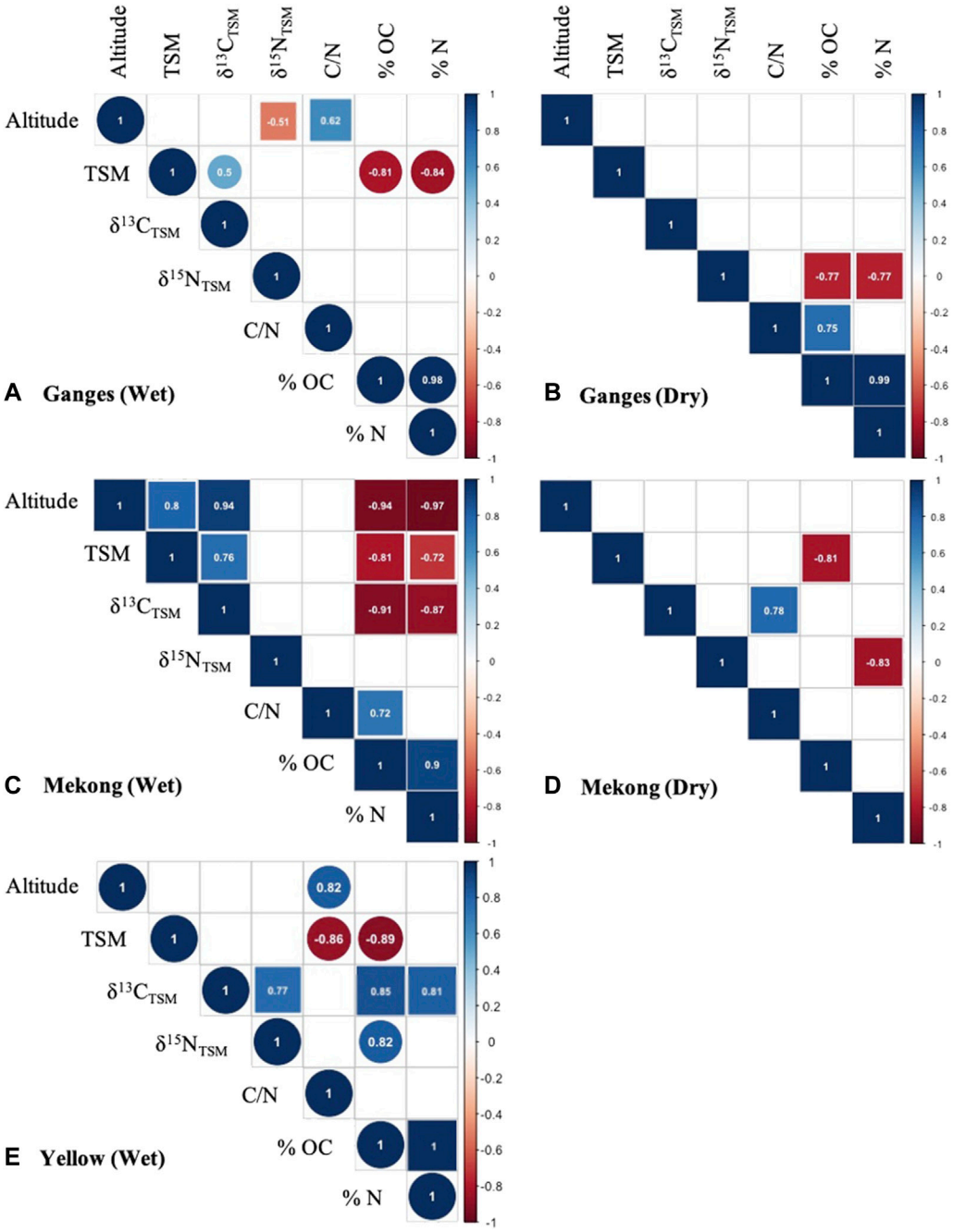

FIGURE 4
Correlation plots between measured parameters in **(A)** Ganges (Wet), **(B)** Ganges (Dry), **(C)** Mekong (Wet), **(D)** Mekong (Dry), and **(E)** Yellow (Wet). The coefficient of correlation was derived from Spearman rank correlation (Circles) and Pearson's correlation (Squares). The coefficient of correlation (R) is shown in the figure ($p < 0.05$).

continuum, abruptly low TSM was observed downstream of Jinghong Dam, Yunnan, which could be attributed to enhanced sedimentation upstream of the dam. During the dry periods, only the downstream sites were sampled and they showed low TSM concentrations, typical of clear waters. All sites in the Yellow River except for those within the loess plateau region during the wet periods, and Hohhot during the dry months, had TSM below 500 mg L^{-1}. The high TSM load near the middle reaches of Yellow River was potentially due to the high soil erosion in the loess plateau region. Intensive rainfall in the middle reaches (the loess plateau) has been attributed as the causal factor for high discharge and TSM as compared to upstream and downstream sites (Ran et al., 2013). Earlier studies have also recognized the loess plateau to supply 90% of the sediments in the Yellow River (Zhang et al., 1990; Milliman and Syvitski, 1992; Chen et al., 2005; Wang et al., 2010; Wang et al., 2016; Wang et al., 2017; Yu et al., 2013).

The increase in TSM in the middle reaches of the Yellow River basin was accompanied by an abrupt increase in $\delta^{13}C_{TSM}$ and $\delta^{15}N_{TSM}$. A similar increase in $\delta^{15}N_{TSM}$ was observed in the

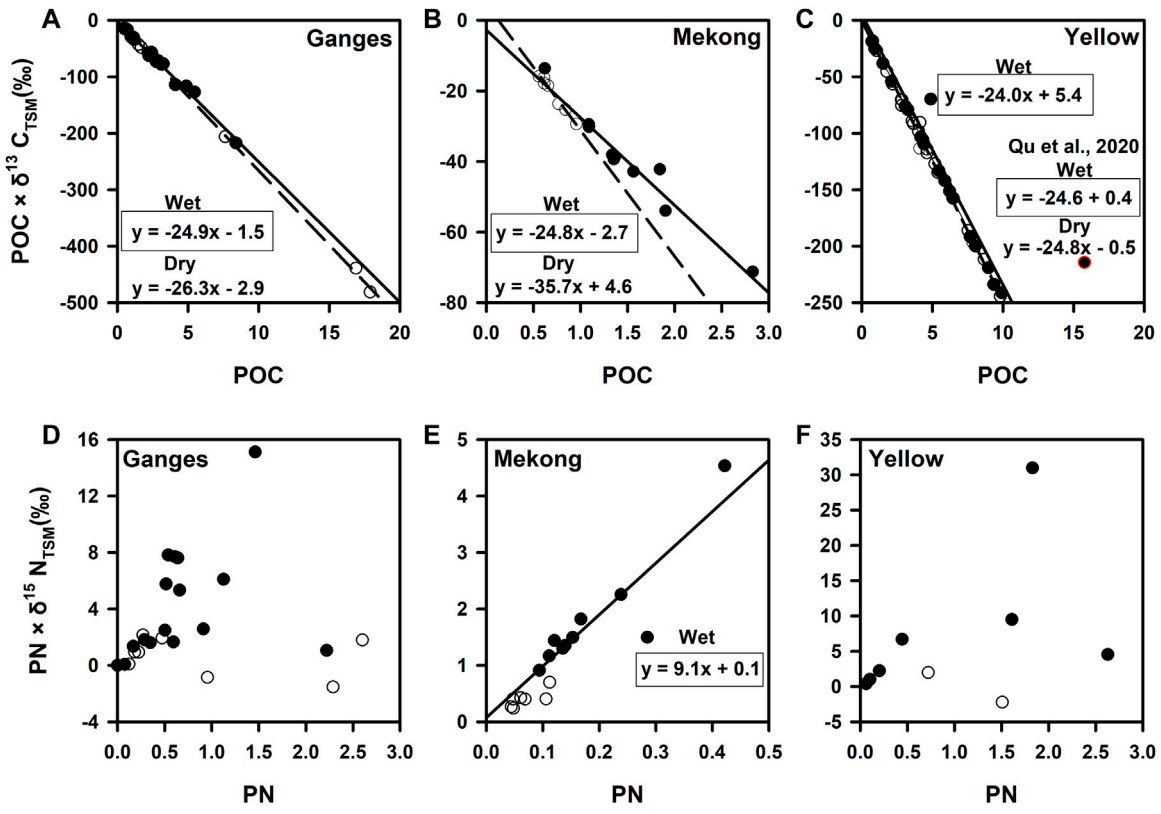

FIGURE 5
Graphical mixing model for tracking the sources of OC and N in TSM. Significant regressions obtained for OC in the **(A)** Ganges, **(B)** Mekong, and **(C)** Yellow River. Source organic matter isotopic signatures are shown by the slope of the regression. The regressions for wet seasons are bounded by a rectangular box. For the Yellow River, due to low sample size in the dry seasons, we used the data from Qu et al. (2020) for seasonal comparison. This graphical mixing model failed to distinguish the source signature of N in **(D)** Ganges and **(F)** Yellow but obtained a strong regression for **(E)** Mekong during the wet season (source $\delta^{15}N_{TSM}$ = 9.1‰).

Ganges with decrease in altitude (Figure 4A). This increase in isotopic signatures of TSM can either be a result of inputs of organic matter with enriched isotopic signatures or in-stream processes altering the isotopic composition of TSM. It was also observed that the altitude exercised a significant control on C/N ratios of TSM in the river basins (Figures 4A, E) which was quite obvious in the Ganges but not conclusive in the Mekong and Yellow, particularly due to lower sample size. During the wet season, with decrease in altitude, the C/N ratios started to fall (r = 0.35, $p < 0.05$; Pearson), reflecting the dominance of allochthonous organic matter inputs in the upstream reaches mainly consisting of plant litter having high C/N. In contrast, the C/N ratios were negatively correlated with altitude during the dry periods (r =–0.85, $p < 0.05$; Spearman), which suggested organic matter inputs of high C/N ratios into the rivers as the river order increased.

Apart from the above-mentioned control of terrain on TSM across the three rivers, the Mekong River also displayed significant positive relationship between altitude and TSM loading (Figure 4C). With decreasing altitude, the TSM concentrations in the Mekong fell consistently accompanied by an increase in its organic C and N contents. This relationship between TSM and its organic contents to altitude provides an insight into the effect of damming and changes in flow regime of the river on its TSM dynamics. The upstream reaches of the Mekong showed the signatures of intense weathering and erosion with high TSM load and low organic content, whereas the lower reaches displayed decrease in TSM loading and increase in organic content, characteristic of productive waters.

4.2 Sources of riverine carbon and nitrogen

The TSM in rivers is a derivative of *in situ* primary producers, plant litter, and soil (Ittekkot, 1988; Hillebrand et al., 2018). Different environmental and hydrological factors (precipitation, runoff, catchment land cover, discharge, etc.) control the relative dominance of each source. For instance, rivers with high discharge generally have high turbidity due of excessive sediment loading, which prevents light penetration, thereby decreasing primary production. Such rivers have a dominant allochthonous sources of organic matter. On the other hand, low discharge rivers with relatively low TSM loads are favorable for *in situ* productivity (Leithold et al., 2006; Ran et al., 2013).

In the present study, isotope mixing model did not clearly distinguish among the prospective organic matter sources such as C3 plants, C4 plants, SOM, and *in situ* phytoplankton. However, the source of organic matter was significantly enriched in ^{13}C during the wet seasons compared to the dry season (by 1.4‰ in the Ganges and 10.9‰ in Mekong) (Figure 5). Except for Mekong during the wet seasons (source $\delta^{15}N_{TSM}$ = 9.1‰), the mixing

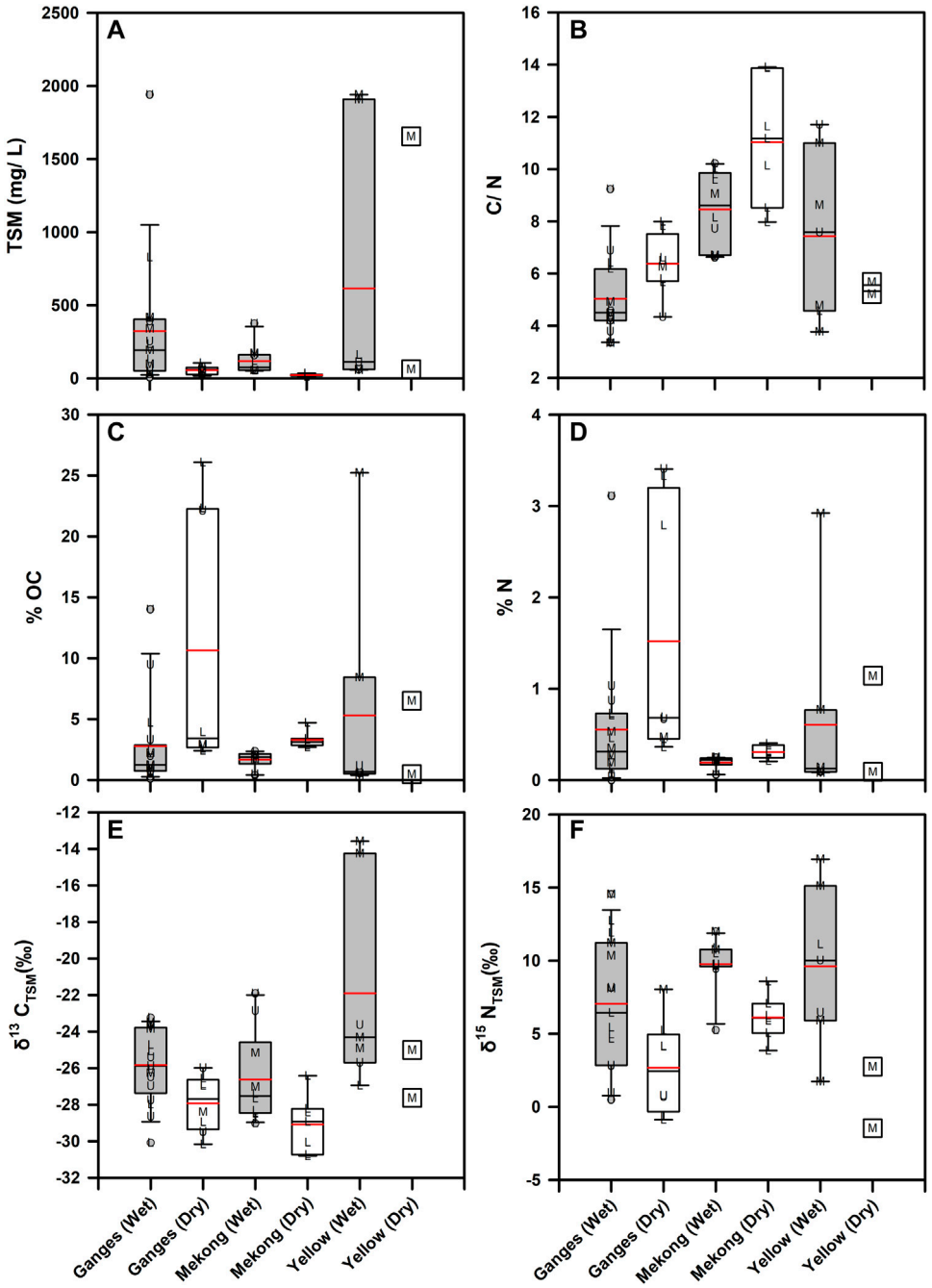

FIGURE 6
Box-whiskers plots showing seasonal variation in **(A)** TSM, **(B)** C/N ratios, **(C)** % OC, **(D)** % N, **(E)** $\delta^{13}C_{TSM}$ and **(F)** $\delta^{15}N_{TSM}$. Red lines shows mean values. Significant difference ($p < 0.001$) between the median TSM values were observed across seasons and river basins. The whole range of TSM were significantly different ($p < 0.05$) among Mekong (Dry) and Mekong (Wet). Similarly, median C/N were significantly different among different sample classes ($p < 0.001$). During each season, the whole range of C/N values were higher for the Mekong as compared to the Ganges ($p < 0.05$). Median values were significantly different in **(C)** with $p < 0.005$ and **(D)** $p < 0.05$. Median $\delta^{13}C_{TSM}$ and $\delta^{15}N_{TSM}$ were significantly different among each class ($p < 0.005$). The letters L, M and U represents sites from the lower, middle and upper reaches respectively.

models did not clearly identify the N sources as a strong linear regression was not achieved (Figure 5). The lack of correlation could be attributed to point source N pollution along the river continuum, prevalent in urbanized river systems (Zhang et al., 2015). The relationship between TSM concentrations and its organic C and N contents provide insight into vegetation versus soil contributions. If organic C and N contents increase with TSM, it suggests contribution from *in situ* phytoplankton or terrestrial litter (C3 and C4). We observed significant negative relationships between TSM and organic C and N contents in the Ganges and Mekong (Figures 4A, C), whereas with only organic C during the wet season was observed in the Yellow River (Figure 4E). Such relationships indicated inputs from soil organic matter with low C and N contents to TSM (Meybeck

and Ragu, 1995; Ludwig et al., 1996). This observation was further supported by positive correlations between TSM and $\delta^{13}C_{TSM}$ in the Ganges and Mekong during the wet period (Figures 4A, C), as soil organic matter is generally associated with high $\delta^{13}C$. Similarly, a decrease in C/N ratio with increase in TSM in the Yellow River during the wet period indicated SOM as the dominant source of organic matter, which is consistent with high sediment load derived from the loess plateau. Previous studies have also reported the middle reaches of the Yellow River to be rich in highly decomposed loess deposits which have high $\delta^{13}C$ signatures (Zhang et al., 1990; 1992; Chen et al., 2005). During the dry season, N contents showed significant negative relationship with $\delta^{15}N_{TSM}$ (Figures 4B, D) indicating association of increase in productivity with enhanced N_2 fixation by phytoplankton.

4.3 Seasonality in total suspended matter as inferred from elemental biogeochemistry

The Asian rivers are subjected to high seasonality in their hydrological regime, which in turn governs the *in situ* elemental biogeochemistry. The TSM is usually a function of the discharge and also reflects the level of anthropogenic disturbances within the watershed (Li et al., 2008; Chang et al., 2021). Higher TSM concentrations were observed during the wet season than in the dry period in all the three rivers (Figure 6A), which is in agreement with studies elsewhere (Dunne and Ongweny, 1976; Kitheka et al., 2005; Tamooh et al., 2012). The low C/N that accompanied the high TSM during the wet season indicated terrestrial inputs of SOM having low C/N (Figure 6B). The TSM and C/N ratio obey an inverse relationship in an environmental setting prone to aeolian and fluvial erosion (Weiguo et al., 2003; Boix-Fayos et al., 2015). Generally, the surficial soil of the catchment holding the remains of parent plant material with high C/N is likely to be removed first leaving behind SOM with relatively low C/N. With successive erosion events, the rivers draining such terrain would receive this organic matter resulting in higher TSM with low C/N (Weiguo et al., 2003). Contrary to the general observations of low C/N during low flow conditions, representing fine algal materials and phytoplankton (C/N: 4.6 to 7.5, Bordowskiy, 1965; Muller, 1977; Meybeck, 1982; Balakrishna and Probst, 2005; Ellis et al., 2012), we observed relatively higher C/N ratio during the dry season. This might be due to high growth period, wherein competition for nutrients likely resulted in higher C uptake relative to N by phytoplankton resulting in higher C/N of TSM. As such productivity increases during the low flow conditions under reduced turbidity which is favorable for algal growth (Beusen et al., 2005). Possible increase in productivity during the dry period is also reflected on higher organic C and N contents in TSM (Figures 6C, D). In contrast, organic C in TSM decreased during the high flow condition (Figure 6C), reflecting the C content of SOM (Giresse and Maley, 1998; Coynel et al., 2005). Although decomposition of organic matter during high flow conditions might also result in lower organic carbon in TSM and associated increase in $\delta^{13}C_{TSM}$, the negative relationship observed between TSM and % OC and % N (Figures 4A, C, E) indicates addition of TSM with low organic matter content. Similar negative relationship between organic matter and TSM have been reported in the Yellow River basin during high flow periods (Beusen et al., 2005; Ellis et al., 2012).

Generally, C/N ratios, when used solely, do not convincingly distinguish the sources and relative contributions (autochthonous versus allochthonous) of organic matter to riverine systems (C/N for phytoplankton: 4.6 to 7.5, aquatic plants: 4 to 12, degraded SOM: low C/N; Bordowskiy, 1965; Meybeck, 1982; Muller, 1977) as these systems have large catchments and several biogeochemical processes simultaneously regulate the elemental ratios (Milliman et al., 1984; Meyers, 1997). However, in conjunction with stable isotopes, they can be a robust tool to study aquatic elemental biogeochemistry. In this study, relatively lower $\delta^{13}C_{TSM}$ (Figure 6E) in all the river basins during the dry season was observed, which possibly indicated increased *in situ* primary production, which has a general range between −40‰ and −22‰ (Kendall et al., 2001). As described earlier, low flow conditions with clear and less turbid water are favourable for primary productivity and algal growth. Phytoplankton in such an environmental setting, i.e., well oxygenated and non-eutrophic, can have isotopically depleted organic C signatures (Leng et al., 2006). Yu et al. (2019) employed dual isotopic ($\delta^{13}C$ and $\Delta^{14}C$) source apportionment and observed similar signatures of enhanced primary production in the Yellow River due to less turbidity and suitable water temperature during spring and summer. Furthermore, higher $\delta^{13}C_{TSM}$ during the wet season showed signatures of terrestrial inputs, with higher C4 contribution, in the Yellow River. Unlike earlier observations of a lack of seasonality in the isotopic composition of POM in the Mekong River (Ellis et al., 2012), our results showed significant increase in the C and N isotopic signatures during the wet seasons. Similar to C, relatively higher $\delta^{15}N_{TSM}$ during the wet season is indicative of SOM and the low $\delta^{15}N_{TSM}$ during the dry season is indicative of *in situ* production with the low (~0‰) signatures representing N_2 fixation during high growth phase (Figure 6F).

4.4 Yield and export fluxes of particulate organic carbon and nitrogen

Assuming a catchment area of 980×10^3 km^2, annual sediment load and yield for the Ganges have been reported to be ~$1,060 \times 10^9$ kg y^{-1} and $1,340 \times 10^3$ kg km^{-2} y^{-1}, respectively (Milliman and Farnsworth, 2011). Similarly, for the Yellow and the Mekong Rivers, the sediment load (yield) has been estimated at 1,100 (1,500) and 150×10^9 kg y^{-1} (190×10^3 kg km^{-2} y^{-1}), respectively (Milliman and Farnsworth, 2011). Estimates of C and N fluxes from the Ganges River system is scarce and only one study reported organic C flux to be 6×10^9 kg y^{-1} (Aucour et al., 2006). For the Ganges, our estimates for the annual TSM export flux was 202×10^9 kg y^{-1}, which indicated significant decrease in the suspended load and its C content (at present $F_{POC} = 2.4 \times 10^9$ kg y^{-1}; Table 2) over the years. TSM flux from the Yellow River has been known to reduce drastically over the decades. Milliman and Farnsworth (2011) reported ~10 times reduction of TSM export from the Yellow River in recent decades, from 1,100 Mt y^{-1} (Qian and Dai, 1980) to <100 Mt y^{-1} (Wang et al., 2016), attributing the major cause of this decline to be excessive water consumption and droughts. For the Yellow River, the early export flux of organic C was estimated to be 6.1×10^9 kg y^{-1} in 1987 (Zhang et al., 1992). Later, a reduction by a factor of 15 by the year 2009 was observed (Wang et al., 2012). The estimates

calculated based on the wet season data from the present study showed further reduction by a factor of 10 since Wang et al. (2012). Paucity of dry season observation from the Yellow River during the present study restricted us from providing a well constrained annual flux estimate. This high reduction in POC flux in the Yellow River within a decade is not surprising, considering the steady fall in river discharge and associated sediment load over the last 60 years (Wang et al., 2016). Apart from the construction of dams and landscape engineering, large scale vegetation restoration projects and associated reduction in soil erosion rates have been identified as the causal factors for the decline in sediment load in the Yellow River (Wang et al., 2016). In the last decade, a large fall in the export fluxes were observed in the Mekong River basin as well. Ellis et al. (2012) reported an annual flux of 76.3×10^9 kg y^{-1} and 1.67×10^9 kg y^{-1} for TSM and organic C, respectively, during the year 2006. Our results indicated ~6 times decrease in organic C flux for the Mekong River.

Transport of N in rivers are generally assumed to be dominantly in the form of dissolved inorganic ions. However, Ittekkot and Zhang (1989) highlighted the global significance of the movement of particulate N within river corridors. They estimated a net global riverine flux of $\sim 33 \times 10^9$ kg N y^{-1} in the form of PN among which ~80% was supposedly delivered by large river systems like the Ganges, Mekong, and Yellow River. Following the work by Ittekkot and Zhang (1989), studies on PN fluxes and yields are still limited from the Asian rivers systems. Our flux calculations showed the Ganges with the highest PN flux followed by the Mekong and the Yellow Rivers (Table 2). Similar to organic C, significant reduction in PN flux was also observed for three studied river basins (Table 2).

4.5 Wastewater input: an underrepresented source of organic matter

With rapid urbanization and population bloom, large quantities of sewage are being generated by metropolises across the globe. Most of these cities are situated alongside river channels and therefore dumps all the wastes into the flowing water, most of which remains poorly treated or otherwise untreated. The Ganges and the Yellow Rivers are known to receive around $1{,}186 \times 10^9$ and 45×10^9 kg y^{-1} of wastewater, respectively (CPCB, 2013; Dutta et al., 2020; Qi et al., 2020; Zhao et al., 2020). Taking the wastewater discharge from the earlier studies (CPCB, 2013; Dutta et al., 2020) and using our TSM data, we estimated a total flux of $(123.2 \pm 43.3) \times 10^6$ kg y^{-1} of $TSM_{wastewater}$ into the Ganges. Paucity of wastewater discharge information from the Mekong Basin and $TSM_{wastewater}$ from the Yellow river makes it difficult to estimate the $TSM_{wastewater}$ flux for these systems in our study. There are studies where wastewater have been found to play a significant role in the inorganic C dynamics (Yang et al., 2018; Li et al., 2019). Wastewaters usually have a high concentration of DIC accompanied by low $\delta^{13}C_{DIC}$ (Yang et al., 2018). In terms of organic C content, wastewater have high concentration of DOC, which further acts as substrates for methanogenesis leading to enhanced GHGs emissions (Begum et al., 2021). The TSM in the wastewater from our sampled sites were rich in organic matter (~17% organic C and ~2% N). Such high organic matter content is usually characteristic of autochthonous productivity in rivers. Therefore, it is possible that overlooking the contributions from wastewater inputs, while interpreting TSM data in rivers may be misleading.

5 Conclusion

The present study attempted to compare the flow of C and N in its particulate form (POC and PN) between dry and wet periods among three large Asian river systems. Given the global implication in constraining their fluxes and isotopic signatures, this study deciphered the effect of seasonality on the POC and PN fluxes and the associated biogeochemical processes that might have a significant control over their process dynamics. In the three studied river systems, altitude seemed to have a strong control over the C/N ratios and C isotopic signatures of TSM. Furthermore, in the Yellow River basin, the loess plateau was the major driver of suspended matter dynamics. Application of a mixing model revealed an enriched C isotopic signature of the source organic matter in the Ganges and Mekong during the wet seasons which was attributed to allochthonous inputs (soil organic matter and C4 vegetation). Using the same model for N source identification, the $\delta^{15}N_{TSM\ (Source)}$ for the Mekong River was also constrained. Primary production dominated in all the three river systems during the dry seasons with evidences of N_2 fixation as well. The high C/N ratios that accompanied the high growth phase during this study disagreed with the general understanding of low C/N during low flow conditions, indicating that competition for nutrients can shoot up the C/N ratios of POM beyond the known range of values. The fluxes and yields of C and N estimated in this study showed drastic reduction over the decades in these river basins and also provided a modest number that could be used in models for global budgeting. Finally, the potential role of wastewater inputs in the elemental biogeochemistry of riverine system was indicated by similar C/N ratios and isotopic composition of wastewater and productive river POM, which suggest that they might cause biases while investigating river processes.

Data availability statement

The original contributions presented in the study are included in the article/Supplementary Material, further inquiries can be directed to the corresponding author.

Author contributions

MB and J-HP collected the samples, SV and SK analyzed the samples, SS analyzed the data and wrote the draft with contributions from all the co-authors.

Funding

The funding for sampling towards this work was supported by the Asia-Pacific Network for Global Change Research (CRRP 2016-01MY-Park) and the National Research Foundation of Korea funded by the Korean Government (NRF-2017R1D1A1B06035179). The funding for

sample analysis was provided by the Department of Space, Govt. of India.

Acknowledgments

The authors thank the project members and students of Jahangirnagar University, Royal University of Phnom Penh, Cantho University, and University of Inner Mongolia for their assistance with sampling.

Conflict of interest

The authors declare that the research was conducted in the absence of any commercial or financial relationships that could be construed as a potential conflict of interest.

Publisher's note

All claims expressed in this article are solely those of the authors and do not necessarily represent those of their affiliated organizations, or those of the publisher, the editors and the reviewers. Any product that may be evaluated in this article, or claim that may be made by its manufacturer, is not guaranteed or endorsed by the publisher.

Supplementary material

The Supplementary Material for this article can be found online at: https://www.frontiersin.org/articles/10.3389/feart.2023.1067744/full#supplementary-material

References

Asselman, N. E., Middelkoop, H., and Van Dijk, P. M. (2003). The impact of changes in climate and land use on soil erosion, transport and deposition of suspended sediment in the River Rhine. *Hydrol. Process.* 17 (16), 3225–3244. doi:10.1002/hyp.1384

Aucour, A. M., France-Lanord, C., Pedoja, K., Pierson-Wickmann, A. C., and Sheppard, S. M. (2006). Fluxes and sources of particulate organic carbon in the Ganga-Brahmaputra river system. *Glob. Biogeochem. Cycles* 20 (2). doi:10.1029/2004gb002324

Aufdenkampe, A. K., Mayorga, E., Raymond, P. A., Melack, J. M., Doney, S. C., Alin, S. R., et al. (2011). Riverine coupling of biogeochemical cycles between land, oceans, and atmosphere. *Front. Ecol. Environ.* 9 (1), 53–60. doi:10.1890/100014

Balakrishna, K., and Probst, J. L. (2005). Organic carbon transport and C/N ratio variations in a large tropical river: Godavari as a case study, India. *Biogeochemistry* 73 (3), 457–473. doi:10.1007/s10533-004-0879-2

Bastviken, D., Tranvik, L. J., Downing, J. A., Crill, P. M., and Enrich-Prast, A. (2011). Freshwater methane emissions offset the continental carbon sink. *Science* 331 (6013), 50. doi:10.1126/science.1196808

Battin, T. J., Luyssaert, S., Kaplan, L. A., Aufdenkampe, A. K., Richter, A., and Tranvik, L. J. (2009). The boundless carbon cycle. *Nat. Geosci.* 2 (9), 598–600. doi:10.1038/ngeo618

Begum, M. S., Bogard, M. J., Butman, D. E., Chea, E., Kumar, S., Lu, X., et al. (2021). Localized pollution impacts on greenhouse gas dynamics in three anthropogenically modified Asian river systems. *J. Geophys. Res. Biogeosciences* 126, e2020JG006124. doi:10.1029/2020jg006124

Beusen, A. H. W., Dekkers, A. L. M., Bouwman, A. F., Ludwig, W., and Harrison, J. (2005). Estimation of global river transport of sediments and associated particulate C, N, and P. *Glob. Biogeochem. Cycles* 19 (4). doi:10.1029/2005gb002453

Biddanda, B. A. (2017). *Global significance of the changing freshwater carbon cycle.* Eos, 98. doi:10.1029/2017EO069751

Boix-Fayos, C., Nadeu, E., Quiñonero, J. M., Martínez-Mena, M., Almagro, M., and De Vente, J. (2015). Sediment flow paths and associated organic carbon dynamics across a Mediterranean catchment. *Hydrology Earth Syst. Sci.* 19 (3), 1209–1223. doi:10.5194/hess-19-1209-2015

Bordowskiy, O. K. (1965). Sources of organic matter in marine basins. *Mar. Geol.* 3, 5–31. doi:10.1016/0025-3227(65)90003-4

Boutton, T. W. (1996). Stable carbon isotope ratios of soil organic matter and their use as indicators of vegetation and climate change. *Mass Spectrom. soils*, 47–82.

Broadbent, F. E., Rauschkolb, R. S., Lewis, K. A., and Chang, G. Y. (1980). Spatial variability of nitrogen-15 and total nitrogen in some virgin and cultivated soils. *Soil Sci. Soc. Am. J.* 44 (3), 524–527. doi:10.2136/sssaj1980.03615995004400030017x

Bulletin of Chinese River Sediment (BCRS) (2000). *Ministry of Water Resources Conservancy*. Beijing, China. Available at: http://www.mwr.gov.cn/xygb/hlnsgb/index.aspx. (in Chinese).

Campeau, A., Wallin, M. B., Giesler, R., Löfgren, S., Mörth, C. M., Schiff, S., et al. (2017). Multiple sources and sinks of dissolved inorganic carbon across Swedish streams, refocusing the lens of stable C isotopes. *Sci. Rep.* 7 (1), 9158. doi:10.1038/s41598-017-09049-9

Central Pollution Control Board (CPCB) (2013). *Pollution assessment: River Ganga*. CPCB. Available at: https://cpcb.nic.in.

Chang, H., Makido, Y., and Foster, E. (2021). Effects of land use change, wetland fragmentation, and best management practices on total suspended solids concentrations in an urbanizing Oregon watershed, USA. *J. Environ. Manag.* 282, 111962. doi:10.1016/j.jenvman.2021.111962

Chen, J., Wang, F., Meybeck, M., He, D., Xia, X., and Zhang, L. (2005). Spatial and temporal analysis of water chemistry records (1958–2000) in the Huanghe (Yellow River) basin. *Glob. Biogeochem. cycles* 19 (3). doi:10.1029/2004gb002325

Cole, J. J., Prairie, Y. T., Caraco, N. F., McDowell, W. H., Tranvik, L. J., Striegl, R. G., et al. (2007). Plumbing the global carbon cycle: Integrating inland waters into the terrestrial carbon budget. *Ecosystems* 10 (1), 172–185. doi:10.1007/s10021-006-9013-8

Coynel, A., Seyler, P., Etcheber, H., Meybeck, M., and Orange, D. (2005). Spatial and seasonal dynamics of total suspended sediment and organic carbon species in the Congo River. *Glob. Biogeochem. cycles* 19 (4). doi:10.1029/2004gb002335

Downing, J. A. (2010). Emerging global role of small lakes and ponds: Little things mean a lot. *Limnetica* 29 (1), 0009–0024. doi:10.23818/limn.29.02

Dunne, T., and Ongweny, G. S. O. (1976). A new estimate of sedimentation rates on the upper Tana River. *Kenyan Geogr.* 2 (2), 26–109.

Dutta, V., Dubey, D., and Kumar, S. (2020). Cleaning the River Ganga: Impact of lockdown on water quality and future implications on river rejuvenation strategies. *Sci. Total Environ.* 743, 140756. doi:10.1016/j.scitotenv.2020.140756

Ehleringer, J. R. (1978). Implications of quantum yield differences on the distributions of C3 and C4 grasses. *Oecologia* 31 (3), 255–267. doi:10.1007/bf00346246

Ehleringer, J., and Pearcy, R. W. (1983). Variation in quantum yield for CO_2 uptake among C3 and C4 plants. *Plant Physiol.* 73 (3), 555–559. doi:10.1104/pp.73.3.555

Ellis, E. E., Keil, R. G., Ingalls, A. E., Richey, J. E., and Alin, S. R. (2012). Seasonal variability in the sources of particulate organic matter of the Mekong River as discerned by elemental and lignin analyses. *J. Geophys. Res. Biogeosciences* 117 (G1). doi:10.1029/2011jg001816

Gao, X., Shi, Y., Han, Z., Wang, M., Wu, J., Zhang, D., et al. (2017). Performance of RegCM4 over major river basins in China. *Adv. Atmos. Sci.* 34 (4), 441–455. doi:10.1007/s00376-016-6179-7

Gawade, L., Krishna, M. S., Sarma, V. V. S. S., Hemalatha, K. P. J., and Rao, Y. V. (2018). Spatio-temporal variability in the sources of particulate organic carbon and nitrogen in a tropical Godavari estuary. *Estuar. Coast. Shelf Sci.* 215, 20–29. doi:10.1016/j.ecss.2018.10.004

Giresse, P., and Maley, J. (1998). The dynamic of organic carbon in South Cameroon: Fluxes in a tropical River system and a lake system as a varying sink on a glacial–interglacial time scale. *Glob. Planet. Change* 16, 53–74. doi:10.1016/s0921-8181(98)00007-1

Gupta, A., Hock, L., Xiaojing, H., and Ping, C. (2002). Evaluation of part of the Mekong River using satellite imagery. *Geomorphology* 44 (3-4), 221–239. doi:10.1016/s0169-555x(01)00176-3

Gupta, A. (Editor) (2005). *The physical geography of Southeast Asia(Vol. 4)* (Oxford University Press on Demand).

Hedges, J. I., Ertel, J. R., Quay, P. D., Grootes, P. M., Richey, J. E., Devol, A. H., et al. (1986). Organic carbon-14 in the amazon River system. *Science* 231 (4742), 1129–1131. doi:10.1126/science.231.4742.1129

Hillebrand, G., Hardenbicker, P., Fischer, H., Otto, W., and Vollmer, S. (2018). Dynamics of total suspended matter and phytoplankton loads in the river Elbe. *J. Soils Sediments* 18 (10), 3104–3113. doi:10.1007/s11368-018-1943-1

Hope, D., Billett, M. F., and Cresser, M. S. (1994). A review of the export of carbon in river water: Fluxes and processes. *Environ. Pollut.* 84 (3), 301–324. doi:10.1016/0269-7491(94)90142-2

Hopkinson, C. S., Buffam, I., Hobbie, J., Vallino, J., Perdue, M., Eversmeyer, B., et al. (1998). Terrestrial inputs of organic matter to coastal ecosystems: An intercomparison of chemical characteristics and bioavailability. *Biogeochemistry* 43 (3), 211–234. doi:10.1023/a:1006016030299

Hori, H. (2000). *The Mekong: Environment and development*. Tokyo: United Nations University.

Huang, C., Chen, F., Zhang, S., Chen, C., Meng, Y., Zhu, Q., et al. (2020). Carbon and nitrogen isotopic composition of particulate organic matter in the Pearl River Estuary and the adjacent shelf. *Estuar. Coast. Shelf Sci.* 246, 107003. doi:10.1016/j.ecss.2020.107003

Hunter, H. M., and Walton, R. S. (2008). Land-use effects on fluxes of suspended sediment, nitrogen and phosphorus from a river catchment of the Great Barrier Reef, Australia. *J. hydrology* 356 (1-2), 131–146. doi:10.1016/j.jhydrol.2008.04.003

Ittekkot, V., and Zhang, S. (1989). Pattern of particulate nitrogen transport in world rivers. *Glob. Biogeochem. Cycles* 3 (4), 383–391. doi:10.1029/gb003i004p00383

Ittekkot, V. (1988). Global trends in the nature of organic matter in river suspensions. *Nature* 332 (6163), 436–438. doi:10.1038/332436a0

Kendall, C., Silva, S. R., and Kelly, V. J. (2001). Carbon and nitrogen isotopic compositions of particulate organic matter in four large river systems across the United States. *Hydrol. Process.* 15 (7), 1301–1346. doi:10.1002/hyp.216

Kitheka, J. U., Obiero, M., and Nthenge, P. (2005). River discharge, sediment transport and exchange in the Tana Estuary, Kenya. *Estuar. Coast. Shelf Sci.* 63 (3), 455–468. doi:10.1016/j.ecss.2004.11.011

Lambert, T., Bouillon, S., Darchambeau, F., Morana, C., Roland, F. A., Descy, J. P., et al. (2017). Effects of human land use on the terrestrial and aquatic sources of fluvial organic matter in a temperate river basin (The Meuse River, Belgium). *Biogeochemistry* 136 (2), 191–211. doi:10.1007/s10533-017-0387-9

Leithold, E. L., Blair, N. E., and Perkey, D. W. (2006). Geomorphologic controls on the age of particulate organic carbon from small mountainous and upland rivers. *Glob. Biogeochem. Cycles* 20 (3). doi:10.1029/2005gb002677

Leng, M. J., Lamb, A. L., Heaton, T. H., Marshall, J. D., Wolfe, B. B., Jones, M. D., et al. (2006). "Isotopes in lake sediments," in *Isotopes in palaeoenvironmental research* (Dordrecht: Springer), 147–184.

Li, S., Gu, S., Liu, W., Han, H., and Zhang, Q. (2008). Water quality in relation to land use and land cover in the upper Han River Basin, China. *Catena* 75 (2), 216–222. doi:10.1016/j.catena.2008.06.005

Li, X., Han, G., Liu, M., Song, C., Zhang, Q., Yang, K., et al. (2019). Hydrochemistry and dissolved inorganic carbon (DIC) cycling in a tropical agricultural river, Mun River Basin, Northeast Thailand. *Int. J. Environ. Res. public health* 16 (18), 3410. doi:10.3390/ijerph16183410

Lloret, E., Dessert, C., Gaillardet, J., Albéric, P., Crispi, O., Chaduteau, C., et al. (2011). Comparison of dissolved inorganic and organic carbon yields and fluxes in the watersheds of tropical volcanic islands, examples from Guadeloupe (French West Indies). *Chem. Geol.* 280 (1-2), 65–78. doi:10.1016/j.chemgeo.2010.10.016

Louchouarn, P., Lucotte, M., Canuel, R., Gagné, J. P., and Richard, L. F. (1997). Sources and early diagenesis of lignin and bulk organic matter in the sediments of the Lower St. Lawrence Estuary and the Saguenay Fjord. *Mar. Chem.* 58 (1-2), 3–26. doi:10.1016/s0304-4203(97)00022-4

Louchouarn, P., Lucotte, M., and Farella, N. (1999). Historical and geographical variations of sources and transport of terrigenous organic matter within a large-scale coastal environment. *Org. Geochem.* 30 (7), 675–699. doi:10.1016/s0146-6380(99)00019-4

Lu, X. X., Zhang, S., and Xu, J. (2010). Climate change and sediment flux from the Roof of the World. *Earth Surf. Process. Landforms J. Br. Geomorphol. Res. Group* 35 (6), 732–735. doi:10.1002/esp.1924

Ludwig, W., Probst, J. L., and Kempe, S. (1996). Predicting the oceanic input of organic carbon by continental erosion. *Glob. Biogeochem. Cycles* 10 (1), 23–41. doi:10.1029/95gb02925

Mackenzie, F. T., Ver, L. M., and Lerman, A. (2022). Century-scale nitrogen and phosphorus controls of the carbon cycle. *Chem. Geol.* 190 (1–4), 13–32. doi:10.1016/S0009-2541(02)00108-0

McKee, B. A. (2023). RiOMar: The transport, transformation and fate of carbon in river-dominated ocean margins: a report of the RioMar community workshop. New Orleans, LA: Tulane University. (Accessed November 1–3, 2001).

Mekong River Commission (2005). *Overview of the hydrology of the Mekong Basin*. Vientiane: Mekong River Commission, 82.

Meybeck, M., and Ragu, A. (1995). *River discharges to oceans: An assessment of suspended solids, major ions and nutrients, report*. Nairobi: UN Environ.Programme.

Meybeck, M. (1982). Carbon, nitrogen, and phosphorus transport by world rivers. *Am. J. Sci.* 282 (4), 401–450. doi:10.2475/ajs.282.4.401

Meyers, P. A. (1997). Organic geochemical proxies of paleoceanographic, paleolimnologic, and paleoclimatic processes. *Org. Geochem.* 27 (5-6), 213–250. doi:10.1016/s0146-6380(97)00049-1

Miao, C., Ni, J., Borthwick, A. G., and Yang, L. (2011). A preliminary estimate of human and natural contributions to the changes in water discharge and sediment load in the Yellow River. *Glob. Planet. Change* 76 (3-4), 196–205. doi:10.1016/j.gloplacha.2011.01.008

Miller, J.B., and Tans, P. P. (2003). Calculating isotopic fractionation from atmospheric measurements at various scales. *Tellus B Chem. Phys. Meteorol.* 55 (2), 207–214. doi:10.1034/j.1600-0889.2003.00020.x

Milliman, J. D., and Farnsworth, K. L. (2011). *River discharge to the coastal ocean: A global synthesis*. Cambridge University Press. doi:10.1017/CBO9780511781247

Milliman, J. D., and Meade, R. H. (1983). World-wide delivery of river sediment to the oceans. *J. Geol.* 91 (1), 1–21. doi:10.1086/628741

Milliman, J. D., and Syvitski, J. P. (1992). Geomorphic/tectonic control of sediment discharge to the ocean: The importance of small mountainous rivers. *J. Geol.* 100 (5), 525–544. doi:10.1086/629606

Milliman, J. D., Qinchun, X., and Zuosheng, Y. (1984). Transfer of particulate organic carbon and nitrogen from the Yangtze River to the ocean. *Am. J. Sci.* 284 (7), 824–834. doi:10.2475/ajs.284.7.824

MRC: Mekong River Commission (2019). State of the basin report 2018. Vientiane, Lao PDR.

Müller, P. J. (1977). Ratios in Pacific deep-sea sediments: Effect of inorganic ammonium and organic nitrogen compounds sorbed by clays. *Geochimica Cosmochimica Acta* 41 (6), 765–776. doi:10.1016/0016-7037(77)90047-3

O'Dwyer, M., Butman, D. E., Striegl, R. G., Dornblaser, M. M., Wickland, K. P., Kuhn, C. D., et al. (2020). Patterns and isotopic composition of greenhouse gases under ice in lakes of interior Alaska. *Environ. Res. Lett.* 15 (10), 105016. doi:10.1088/1748-932=6/abb493

Park, J. H., Nayna, O. K., Begum, M. S., Chea, E., Hartmann, J., Keil, R. G., et al. (2018). Reviews and syntheses: Anthropogenic perturbations to carbon fluxes in Asian river systems–concepts, emerging trends, and research challenges. *Biogeosciences* 15 (9), 3049–3069. doi:10.5194/bg-15-3049-2018

Parua, P. K. (2010). *The Ganga: Water use in the Indian subcontinent(vol 64)*. Springer Science & Business Media.

Peng, J., Chen, S., and Dong, P. (2010). Temporal variation of sediment load in the Yellow River basin, China, and its impacts on the lower reaches and the river delta. *Catena* 83 (2-3), 135–147. doi:10.1016/j.catena.2010.08.006

Pocklington, R., and Tan, F. C. (1987). Seasonal and annual variations in the organic matter contributed by the st lawrence River to the gulf of st. Lawrence. *Geochimica Cosmochimica Acta* 51 (9), 2579–2586. doi:10.1016/0016-7037(87)90308-5

Prasad, M., Kumar, A., Ramanathan, A. L., and Datta, D. K. (2017). Sources and dynamics of sedimentary organic matter in Sundarban mangrove estuary from Indo-Gangetic delta. *Ecol. Process.* 6 (1), 8–15. doi:10.1186/s13717-017-0076-6

Qi, M., Yang, Y., Zhang, X., Zhang, X., Wang, M., Zhang, W., et al. (2020). Pollution reduction and operating cost analysis of municipal wastewater treatment in China and implication for future wastewater management. *J. Clean. Prod.* 253, 120003. doi:10.1016/j.jclepro.2020.120003

Qian, N., and Dai, D. Z. (1980). "The problems of river sedimentation and the present status of its research in China," in Proceedings of the International Symposium on River Sedimentation. Guanghue Press 24 (29), 19–39.

Qu, Y., Jin, Z., Wang, J., Wang, Y., Xiao, J., Gou, L. F., et al. (2020). The sources and seasonal fluxes of particulate organic carbon in the Yellow River. *Earth Surf. Process. Landforms* 45 (9), 2004–2019. doi:10.1002/esp.4861

Rahman, A., Sarkar, S., and Kumar, S. (2020). Paleoenvironment of the Central Himalaya during late MIS 3 using stable isotopic compositions of lacustrine organic matter occluded in diatoms and sediments. *Quat. Int.* 558, 1–9. doi:10.1016/j.quaint.2020.08.024

Ran, L., Lu, X. X., Sun, H., Han, J., Li, R., and Zhang, J. (2013). Spatial and seasonal variability of organic carbon transport in the Yellow River, China. *J. Hydrology* 498, 76–88. doi:10.1016/j.jhydrol.2013.06.018

Raymond, P. A., Hartmann, J., Lauerwald, R., Sobek, S., McDonald, C., Hoover, M., et al. (2013). Global carbon dioxide emissions from inland waters. *Nature* 503 (7476), 355–359. doi:10.1038/nature12760

Reddy, S. K. K., Gupta, H., Badimela, U., Reddy, D. V., Kurakalva, R. M., and Kumar, D. (2021). Export of particulate organic carbon by the mountainous tropical rivers of Western Ghats, India: Variations and controls. *Sci. Total Environ.* 751, 142115. doi:10.1016/j.scitotenv.2020.142115

Singh, I. B. (2007). "The Ganga river," in *Large rivers: Geomorphology and management* (Chichester: Wiley), 347–371.

Suchet, P. A., Probst, J. L., and Ludwig, W. (2003). Worldwide distribution of continental rock lithology: Implications for the atmospheric/soil CO2 uptake by continental weathering and alkalinity river transport to the oceans. *Glob. Biogeochem. cycles* 17 (2), 7–1. doi:10.1029/2002GB001891

Tamooh, F., Van den Meersche, K., Meysman, F., Marwick, T. R., Borges, A. V., Merckx, R., et al. (2012). Distribution and origin of suspended matter and organic carbon pools in the Tana River Basin, Kenya. *Biogeosciences* 9 (8), 2905–2920. doi:10.5194/bg-9-2905-2012

Thornton, S. F., and McManus, J. (1994). Application of organic carbon and nitrogen stable isotope and C/N ratios as source indicators of organic matter provenance in estuarine systems: Evidence from the tay estuary, scotland. *Estuar. Coast. Shelf Sci.* 38 (3), 219–233. doi:10.1006/ecss.1994.1015

Tranvik, L. J., Downing, J. A., Cotner, J. B., Loiselle, S. A., Striegl, R. G., Ballatore, T. J., et al. (2009). Lakes and reservoirs as regulators of carbon cycling and climate. *Limnol. Oceanogr.* 54, 2298–2314. doi:10.4319/lo.2009.54.6_part_2.2298

Verpoorter, C., Kutser, T., Seekell, D. A., and Tranvik, L. J. (2014). A global inventory of lakes based on high-resolution satellite imagery. *Geophys. Res. Lett.* 41 (18), 6396–6402. doi:10.1002/2014gl060641

Walling, D. E., and Fang, D. (2003). Recent trends in the suspended sediment loads of the world's rivers. *Glob. Planet. change* 39 (1-2), 111–126. doi:10.1016/s0921-8181(03)00020-1

Wang, H., Bi, N., Saito, Y., Wang, Y., Sun, X., Zhang, J., et al. (2010). Recent changes in sediment delivery by the huanghe (Yellow River) to the sea: Causes and environmental implications in its estuary. *J. Hydrology* 391 (3-4), 302–313. doi:10.1016/j.jhydrol.2010.07.030

Wang, J. J., Lu, X. X., and Kummu, M. (2011). Sediment load estimates and variations in the lower Mekong River. *River Res. Appl.* 27 (1), 33–46. doi:10.1002/rra.1337

Wang, X., Ma, H., Li, R., Song, Z., and Wu, J. (2012). Seasonal fluxes and source variation of organic carbon transported by two major Chinese Rivers: The Yellow River and Changjiang (Yangtze) River. *Glob. Biogeochem. Cycles* 26 (2). doi:10.1029/2011gb004130

Wang, S., Fu, B., Piao, S., Lü, Y., Ciais, P., Feng, X., et al. (2016). Reduced sediment transport in the Yellow River due to anthropogenic changes. *Nat. Geosci.* 9 (1), 38–41. doi:10.1038/ngeo2602

Wang, S., Fu, B., Liang, W., Liu, Y., and Wang, Y. (2017). Driving forces of changes in the water and sediment relationship in the Yellow River. *Sci. Total Environ.* 576, 453–461. doi:10.1016/j.scitotenv.2016.10.124

Wang, C., Lv, Y., and Li, Y. (2018). Riverine input of organic carbon and nitrogen in water-sediment system from the Yellow River estuary reach to the coastal zone of Bohai Sea, China. *Cont. Shelf Res.* 157, 1–9. doi:10.1016/j.csr.2018.02.004

Weiguo, L., Zisheng, A., Weijian, Z., Head, M. J., and Delin, C. (2003). Carbon isotope and C/N ratios of suspended matter in rivers: An indicator of seasonal change in C4/C3 vegetation. *Appl. Geochem.* 18 (8), 1241–1249. doi:10.1016/s0883-2927(02)00249-4

Wu, L., Huh, Y., Qin, J., Du, G., and van Der Lee, S. (2005). Chemical weathering in the upper Huang He (Yellow River) draining the eastern Qinghai-Tibet plateau. *Geochimica Cosmochimica Acta* 69 (22), 5279–5294. doi:10.1016/j.gca.2005.07.001

Xu, J., and Ma, Y. (2009). Response of the hydrological regime of the Yellow River to the changing monsoon intensity and human activity. *Hydrological Sci. J.* 54 (1), 90–100. doi:10.1623/hysj.54.1.90

Yang, X., Xue, L., Li, Y., Han, P., Liu, X., Zhang, L., et al. (2018). Treated wastewater changes the export of dissolved inorganic carbon and its isotopic composition and leads to acidification in coastal oceans. *Environ. Sci. Technol.* 52 (10), 5590–5599. doi:10.1021/acs.est.8b00273

Yu, Y., Wang, H., Shi, X., Ran, X., Cui, T., Qiao, S., et al. (2013). New discharge regime of the Huanghe (Yellow River): Causes and implications. *Cont. Shelf Res.* 69, 62–72. doi:10.1016/j.csr.2013.09.013

Yu, M., Eglinton, T. I., Haghipour, N., Montluçon, D. B., Wacker, L., Hou, P., et al. (2019). Impacts of natural and human-induced hydrological variability on particulate organic carbon dynamics in the Yellow River. *Environ. Sci. Technol.* 53 (3), 1119–1129. doi:10.1021/acs.est.8b04705

Zhang, J., Huang, W. W., and Shi, M. C. (1990). Huanghe (Yellow River) and its estuary: sediment origin, transport and deposition. *J. Hydrology* 120 (1-4), 203–223. doi:10.1016/0022-1694(90)90150-v

Zhang, S., Gan, W. B., and Ittekkot, V. (1992). Organic matter in large turbid rivers: the Huanghe and its estuary. *Mar. Chem.* 38 (1-2), 53–68. doi:10.1016/0304-4203(92)90067-k

Zhang, J., Huang, W. W., Letolle, R., and Jusserand, C. (1995). Major element chemistry of the Huanghe (Yellow River), China-weathering processes and chemical fluxes. *J. Hydrology* 168 (1-4), 173–203. doi:10.1016/0022-1694(94)02635-o

Zhang, X., Wu, Y., and Gu, B. (2015). Urban rivers as hotspots of regional nitrogen pollution. *Environ. Pollut.* 205, 139–144. doi:10.1016/j.envpol.2015.05.031

Zhao, M. M., Wang, S. M., Chen, Y. P., Wu, J. H., Xue, L. G., and Fan, T. T. (2020). Pollution status of the Yellow River tributaries in middle and lower reaches. *Sci. Total Environ.* 722, 137861. doi:10.1016/j.scitotenv.2020.137861

Frontiers in Earth Science

Investigates the processes operating within the major spheres of our planet

Advances our understanding across the earth sciences, providing a theoretical background for better use of our planet's resources and equipping us to face major environmental challenges.

Discover the latest Research Topics

See more →

Frontiers

Avenue du Tribunal-Fédéral 34
1005 Lausanne, Switzerland
frontiersin.org

Contact us

+41 (0)21 510 17 00
frontiersin.org/about/contact